CDF Study Report
FIRI
Far Infrared Interferometer

FRONT COVER

FIRI spacecraft in front of the Red Spider Nebula
(Image: ESA/ISO)

Further information and/or additional copies of the report can be requested from:

A. Lyngvi
ESA/ESTEC/SCI-AM
Postbus 299
2200 AG Noordwijk
The Netherlands
Tel: +31-(0)71-5656588
Fax: +31-(0)71-5654690
Aleksander.Lyngvi@esa.int

For further information on the Concurrent Design Facility please contact:

M. Bandecchi
ESA/ESTEC/TEC-SYE
Postbus 299
2200 AG Noordwijk
The Netherlands
Tel: +31-(0)71-5653701
Fax: +31-(0)71-5656024
Massimo.Bandecchi@esa.int

This Page Intentionally Blank

TABLE OF CONTENTS

This Page Intentionally Blank

1 INTRODUCTION

1.1 Background

The ESA Concurrent Design Facility (CDF) was requested and financed by ESA/ESTEC/SCI-AM to carry out the assessment study of a Far-InfraRed Interferometer Technology Reference Study (FIRI). The main science objective is to perform measurements at significantly improved angular resolution obtainable with today's IR telescopes (i.e. sub-arcsec resolution) by using space Interferometry. The overall mission goals were to study the following:

- Formation and evolution of stars
- Formation of planetary systems and planet detection
- Formation and evolution of galaxies.

1.2 Scope

The objectives of the study were to assess the feasibility of a Far-InfraRed Michelson Interferometer mission and the identification of the critical technology in order to define a Technology Development Plan with particular emphasis on the following:

- To assess the feasibility of a far-infrared Michelson interferometer based on a single spacecraft
- To design the mission
- To identify the critical technologies and define their development plan
- To make cost, risk and programmatics analysis for the mission and for the technology development plan.

1.3 Document Structure

The layout of this report of the study results can be seen in the Table of Contents. The Executive Summary chapter provides an overview of the study; details of each domain addressed in the study are contained in specific chapters.

Due to the different distribution requirements, the costing information is published in a separate document CDF-49(B)

The identification of the critical technologies and the needed development plan has been edited as a separate document FIRI Technology Development Plan CDF-49(C) and contains for the most critical technologies the following:

- Description of the technology
- Whether it is critical or mission enhancing
- Maturity level
- Required specifications of an end-product
- Required demonstration and/or technology development
- Current state of the art in EU and in USA, Japan or other countries
- Identification of potential companies
- ROM cost estimate of the development

- ROM schedule estimate
- Risk estimate, back-up solution.

2 EXECUTIVE SUMMARY

2.1 Study Flow

The study consisted of eight half day sessions, starting with a kick-off on the 31st of May 2006 and finishing with an Internal Final Presentation on the 28th of June 2006.

2.2 Requirements and Design Drivers

The following requirements Table 2-1 are typical science requirements for a future FIR mission. It is clear that performing the required measurements a sufficient number of times is too ambitious for the FIRI mission

Requirement ID (Prefix-#)	Requirement Level	Title	STATEMENT (Defines a REQUIREMENT, unless specified as a GOAL or LIMIT value.)	Rationale and/or Comments
SR - Science Requirements SR.BAS - Baseline Science Requirements				
SR.BAS-1	1-Drivers	Star formation through collapsing of the prostellar core	Obtain spectral maps of protostars enabling internal chemical structure evaluation.	*The protostars differs from a greybody at 60-100 microns and for luminosity and temperature determinations it is therefore required to be in the band between ~50μm and ~500μm (it would also be important to get line maps of the excited H2 line emission at 28μm)*
SR.BAS-2	1-Drivers	Star formation in clusters	Obtain spectral maps of protostars enabling internal chemical structure evaluation.	*Typical cluster forming regions have a diameter of about 1 pc with surface density of 2000 stars per pc. A star formation condensation in such a cluster would have size of about 5000 AU*
SR.BAS-3	1-Drivers	Binary star formation	Obtain spectral maps of protostars enabling internal chemical structure evaluation.	*Three different types of multiple systems have been identified; seperate envelope with separations larger than 6000 AU, common envelope with separation between 100-3000 AU and common disk with separation less than 100 AU.*
SR.BAS-4	1-Drivers	Formation of planetary systems	Be able to image the warmer dust that is not accessible from ground measurements	*Imaging of the same star formation regions as described in SR.BAS-1, of particular interest are H2O, CO and H2 lines*
SR.BAS-5	1-Drivers	Planet detection	Be able to detect a series of new extra solar planets and be able to image the warmer dust that is not accessible from ground measurements	*Imaging can detect the dust in the protoplanetary disk. Depending on the number of planets, their size their orbit etc. the debris disk will obtain different resonant structures. The imaging of warmer dust will help to better understand the relationship between planets and the extrasolar analogs of the kuiper belt*
SR.BAS-6	1-Drivers	Formation of early stars, 10<z<20	Observation of star-forming clouds	*The current estimation of when the first star formation took place is at a redshift of z~10-20, yielding observation wavelengths between 170-560μm for H2-lines at 17μm and 28μm. The line strength at these wavelengths might be as low as E-23-E-24 W/m2*
SR.BAS-7	1-Drivers	Resolving the cosmic infrared background (CIB)	Resolve most of the CIB (>90%)	*The CIB peaks at about 160 μm. Faint sources will need to be investigated - observing in the solar system ecliptic plane gives a large foreground flux resulting from the zodiacal dust emission. Hence, survey of the CIB will benefit greatly from taking place in the planes out of the ecliptic. To resolve most of the background (i.e. >90%), a sensitivity of ~10 mJy would allow detection of galaxies well be low luminosities of E11 Lv*
SR.BAS-8	1-Drivers	Star Formation at 1<z<5	Studying HII regions and supernovae remnants in a massive star formation area(?) in a large sample of galaxies	*Star formation rate for 1<z<5 can be measured through high sensitivity imaging from ~30-100μm. To understand the star formation rate in distance galaxies investigations of the spectrum of the incoming emission are needed, of particular interest is the CII line at 158 μm. Performing line measurements would also allow estimating the redshift of the different objects.*

Table 2-1: FIRI Science Requirements

Table 2-2 provides the programmatic requirements for FIRI.

Requirement ID (Prefix-#)	Requirement Level	Title	STATEMENT (Defines a REQUIREMENT, unless specified as a GOAL or LIMIT value.)	Rationale and/or Comments
PM - Programmatic Requirements PM.SCH Schedule and Budget				
PM.SCH-1	1-Drivers	Schedule	Launch in 2020-2025	*Study assumption*
PM.SCH-2	1-Drivers	Design life	The design life shall be 5 years	
PM.SCH-3		Technology Readiness	Only technologies with a TRL of 5 by start of Phase-B shall be used.	
PM.SCH-4	1-Drivers	Launch Vehicle Selection	Launch Vehicle shall be Soyuz-Fregat or Ariane 5	*If Soyuz is too constraining Ariane-5 shall be used.*

Table 2-2: FIRI Programmatic Requirements

The requirements specific to the interferometer are shown in Table 2-3.

Requirement ID (Prefix-#)	Requirement Level	Title	STATEMENT (Defines a REQUIREMENT, unless specified as a GOAL or LIMIT value.)	Rationale and/or Comments
IR - Interferometer Requirements IR.GEN - General Interferometer Requirements				
IR.GEN-1	3-Subsystem	Type	A Michelson interferometer using direct detection is required	*Because of the required spectral resolution.*
IR.GEN-2	3-Subsystem	Wavelength range	The wavelength range shall be 25-300μm, 25-500μm (goal)	
IR.GEN-3	3-Subsystem	Angular Resolution	The angular resolution shall be 0.25" @ 30μm and 2.5" @ 300μm	
IR.GEN-4	3-Subsystem	Field of view (FOV)	1' FOV (Disc)	
IR.GEN-5	3-Subsystem	Line sensitivity	1E-21W/m2 Line sensitivty	*This is a stringent requirement and some relaxation of this requirement is possible*
IR.GEN-6	3-Subsystem	Spectral resolution	The spectral resolution is to be about 3 for photometry, about 20 to provide SEDs, about 300 for extra galactic measurements and about 3000 for resolving lines in star formation regions	$\frac{\lambda}{\Delta\lambda}$

Table 2-3: FIRI Interferometer Requirements

2.3 Mission

Table 2-4 provides a schematic summary of the FIRI mission and spacecraft design. For further details, see relevant chapters in the report.

Mission Objectives	Three main goals: 1. Formation and evolution of stars • Obtain spectral maps of protostars enabling internal chemical structure evaluation 2. Formation of planetary systems and planet detection • Be able to image the warmer dust that is not accessible from ground measurements and be able to detect a series of new extra solar planets 3. Formation and evolution of galaxies • Observing formation of early stars and stars at 1<z<5 and resolving the cosmic infrared background	
Launch	Launcher	Ariane 5
	Launch date	End of 2024

Orbit	Orbit type	L2 (wide Lissajous)
	Amplitude	800,000 km
	Eclipse	None
Operations	Ground station	Cebreros
	Mission operations centre	ESA/ESOC
	Science operations centre	ESA
	Visibility	Mean 8.4 h per day (4.7 min, 10.7 max)
Spacecraft Design	Design lifetime	5 years
	Launch mass (incl. adapter)	5377 kg
	Dimensions (adapter)	Cylinder 0.9 m (height) x 2.6 m (diam)
	Dimensions (hub)	SM: Box 2.3 m x 2.3 m x 0.9 m (height) PLM: Box 1.9 m x 1.9 m x 1.9 m (height)
	Dimensions (telescopes)	Cylinder 2.4 m (height) x 1.6 m (diam)
	Dimensions (booms)	Support Beam Telescope: 0.3 m x 0.3 m x 14.0 m (length) with guiding rails
	AOCS	Three-axis stabilised with reaction wheels (of which 2 magnetic bearing RWs), 6 DOF
	Communications	• TC, HKTM, Ranging in X-band (2 omni-directional LGAs) • Science TM at 26 GHz (1 HGA, dual feed)
	Data handling	• 1.28 Tbit mass memory • 1+1 redundant IPPM in Hub and in each telescope (Total: 3+3) • Wireless data transmission from telescopes to hub
	Power	• Three independent power systems • Hub o 50 V bus o AsGa MJ solar cells, 6.90 m^2 o Li Ion battery of 864 Wh BOL / 5A • Per telescope o 50 V bus o AsGa MJ solar cells, 0.39 m^2 o Li Ion battery of 250 Wh BOL / 5A
	Programmatics	Proto-flight approach, TRL 5 reached for all subsystem in 2015, except detectors (2018)

	Propulsion	Monopropellant Hydrazine system, twelve 10 N thrusters, 429 kg of propellant
	Thermal	Passive control
	Thermal (cryogenics)	Sorption cooler (5 K) in telescopes, Sorption cooler + solid H-cooler (5 K) + ADR for detector (50 mK) in hub
	Detector	Direct detection with TES and SQUID readout for all bands

	Mechanisms	Payload mechanisms:
		• Rolling element bearing + drive unit for the telescope carriers
		• 5 DoF positioning mechanism for the telescopes
		• Inside telescope (all mechanisms with very low power dissipation):
		  • 2 DoF FPA tip/tilt mechanism for field separator
		  • Refocusing mechanism
		• Inside Hub (all mechanisms with very low power dissipation, 2 – 15 mW):
		  • FPA 2 DoF mechanism for internal metrology alignment
		  • FPA 2 DoF mechanism pupil conditioner
		  • Science ODL
		  • Common ODL
		Service module mechanisms include:
		Hinges; HDRMs for antenna, sunshields, booms and telescope carriers; antenna deployment and pointing mechanism; beam jettison mechanism; telescope carrier mechanism; telescope 5 DOF positioning mechanism

	Optics	• Observation band split in 4 sub-bands • Two telescopes, main reflector 1.02 m diameter • One science Michelson Fourier Transform interferometer • One calibration Michelson Fourier Transform interferometer • Calibration with two black bodies • Redundant detection chains

Table 2-4: FIRI Mission and Spacecraft Design Characteristics

3 MISSION OBJECTIVES

3.1 Background

In October 2004 the Astronomy Working Group (AWG) of the Science Directorate recommended further study of a far infrared mission in preparation for the Cosmic Vision programme. This mission, if selected, could be the next European far-infrared telescope after Herschel. To investigate the feasibility of such a far infrared mission the Science Payload & advanced concepts office (SCI-A) have started a technology reference study (TRS) that would allow investigation of critical aspects of such a project.

On the basis of the existing programmatic constraints, it has been decided to study a Far InfraRed Interferometer (FIRI) based on a single spacecraft rather than an interferometer consisting of several separate platforms. The single spacecraft approach allows a thorough investigation of large deployable structures as an alternative to the more expensive formation flying configurations.

3.2 Mission Justification

Far infrared measurements are limited by the obtainable angular resolution. The long wavelength makes imaging at high angular resolutions impossible without using interferometry due to the unrealistic diameter required for a single telescope approach. Interferometry is regularly used on ground. However a very important portion of the infrared range (i.e. ~30-300 microns) is not accessible from ground due to absorption in the atmosphere. In this band, only low resolution imaging has been done , and with the launch of Herschel, which is a large step forward from current missions, the resolution will still only be about 7" (@ 100 microns).

A future infrared mission would therefore strongly focus on obtaining a better angular resolution, thereby facilitating a range of interesting scientific measurements. For a far infrared interferometer typical scientific areas would be to better understand the birth and evolution of galaxies, in particular at high red-shifts, and to improve the understanding of the formation of stars and planetary systems.

FIRI will be a very challenging mission, in which particular areas such as the cryogenics, the mechanisms, the optical chain and the detectors with the related readout will need considerable attention. Creative solutions within these areas will need to be investigated in order to obtain a feasible baseline that can be studied in the CDF. The experience and knowledge acquired will allow the Agency to enrich its technology development plans as well as to have a more informed position on possible future science missions.

3.3 Science Objectives and Requirements

The science topics of FIRI fall into the three main categories shown in Table 3-1. These three overall mission goals can be subdivided into the science requirements found in Table 3-2. The Parent Requirements, found in Table 3-1, have been indicated in the rightmost column. The requirement levels are explained in the Systems Chapter. For more information regarding the science topics see RD[1].

Requirement ID (Prefix-#)	Requirement Level	Title	STATEMENT (Defines a REQUIREMENT, unless specified as a GOAL or LIMIT value.)
MG - Overall Mission Goals			
MG.XXX-1	1-Drivers	Formation and evolution of stars	Obtain spectral maps of protostars enabling internal chemical structure evaluation.
MG.XXX-2	1-Drivers	Formation of planetary systems and planet detection	Be able to image the warmer dust that is not accessible from ground measurements and be able to detect a series of new extra solar planets.
MG.XXX-3	1-Drivers	Formation and evolution of galaxies	Observing formation of early stars and stars at 1<z<5 and resolving the cosmic infrared background.

Table 3-1: FIRI Science Objectives

Requirement ID (Prefix-#)	Requirement Level	Title	STATEMENT (Defines a REQUIREMENT, unless specified as a GOAL or LIMIT value.)	Rationale and/or Comments	Parent ID (Prefix-#)
SR - Science Requirements SR.BAS - Baseline Science Requirements					
SR.BAS-1	1-Drivers	Star formation through collapsing of the prostellar core	Obtain spectral maps of protostars enabling internal chemical structure evaluation.	*The protostars differs from a greybody at 60-100 microns and for luminosity and temperature determinations it is therefore required to be in the band between ~50µm and ~500µm (it would also be important to get line maps of the excited H2 line emission at 28µm)*	MG.XXX-1
SR.BAS-2	1-Drivers	Star formation in clusters	Obtain spectral maps of protostars enabling internal chemical structure evaluation.	*Typical cluster forming regions have a diameter of about 1 pc with surface density of 2000 stars per pc. A star formation condensation in such a cluster would have size of about 5000 AU*	MG.XXX-1
SR.BAS-3	1-Drivers	Binary star formation	Obtain spectral maps of protostars enabling internal chemical structure evaluation.	*Three different types of multiple systems have been identified; seperate envelope with separations larger than 6000 AU, common envelope with separation between 100-3000 AU and common disk with separation less than 100 AU.*	MG.XXX-1
SR.BAS-4	1-Drivers	Formation of planetary systems	Be able to image the warmer dust that is not accessible from ground measurements	*Imaging of the same star formation regions as described in SR.BAS-1, of particular interest are H2O, CO and H2 lines*	MG.XXX-2
SR.BAS-5	1-Drivers	Planet detection	Be able to detect a series of new extra solar planets and be able to image the warmer dust that is not accessible from ground measurements	*Imaging can detect the dust in the protoplanetary disk. Depending on the number of planets, their size their orbit etc. the debris disk will obtain different resonant structures. The imaging of warmer dust will help to better understand the relationship between planets and the extrasolar analogs of the kuiper belt*	MG.XXX-2
SR.BAS-6	1-Drivers	Formation of early stars, 10<z<20	Observation of star-forming clouds	*The current estimation of when the first star formation took place is at a redshift of z~10-20, yielding observation wavelengths between 170-560µm for H2-lines at 17µm and 28µm. The line strength at these wavelengths might be as low as E-23-E-24 W/m2*	MG.XXX-3
SR.BAS-7	1-Drivers	Resolving the cosmic infrared background (CIB)	Resolve most of the CIB (>90%)	*The CIB peaks at about 160 µm. Faint sources will need to be investigated - observing in the solar system ecliptic plane gives a large foreground flux resulting from the zodiacal dust emission. Hence, survey of the CIB will benefit greatly from taking place in the planes out of the ecliptic. To resolve most of the background (i.e. >90%), a sensitivity of ~10 mJy would allow detection of galaxies well be low luminosities of E11 Lv*	MG.XXX-3
SR.BAS-8	1-Drivers	Star Formation at 1<z<5	Studying HII regions and supernovae remnants in a massive star formation area(?) in a large sample of galaxies	*Star formation rate for 1<z<5 can be measured through high sensitivity imaging from ~30-100µm. To understand the star formation rate in distance galaxies investigations of the spectrum of the incoming emission are needed, of particular interest is the CII line at 158 µm. Performing line measurements would also allow estimating the redshift of the different objects.*	MG.XXX-3

Table 3-2: FIRI Science Requirements

In order to meet the scientific requirements both photometry and spectroscopy is required. The spectral resolution ($\lambda/\Delta\lambda$) would typically need to be about 3 for photometry, about 20 to provide SEDs, about 300 for extra galactic measurements and about 3000 for resolving lines in star formation regions. To meet the sensitivity requirement, an interferometer using direct detection is required.

As the mission would need to measure star formation at very high redshifts, very good line sensitivity of about 10^{-22} W/m^2 (TBC) is required, although this will need to be consolidated based on the optical design and the available technology. It is currently assumed that an interferometer with two cryogenically cooled (~4 K to 5 K) ~1 m (TBC) diameter mirrors, would be able to provide this sensitivity. The actual mirror size will need to be further consolidated based on cost, radiometric performance, accommodation in the launcher etc. Suitable detectors with related read out electronics and data processing will also need to be identified. The very high sensitivity required is likely to require detectors cooled down to below 50 mK.

For the instrument it is also clear that a large dynamic range is required. Both within the same image and between measurements, the actual requirement is still TBD but it shall be as large as possible.

The field of view should be designed for a goal of 1 arcmin (disc). However, the FOV shall not be the driving requirement on the instrument side.

FIRI will need to do imaging in order to meet the scientific objectives and therefore a very good uv-coverage is required. Having a good uv-coverage implies that the mirrors will need to be able to move radially in order to change the Inter-Telescope Distance (ITD) and that the spacecraft would need to rotate in order to fill the uv-plane.

Operationally, the area in which the spacecraft would be able to point is also of great scientific interest. For instance, for cosmology surveys imaging in the north or south ecliptic pole is of benefit to avoid disturbance from the zodiacal light. However, for star and planetary system formation the need for observing out of the ecliptic is of less importance. In Table 3-3, some targets that could be of interest are listed. The list is not exhaustive and should therefore only be taken as a guideline as to the location of the targets.

Target	**Ecliptic Coordinates**	
	Longitude	**Latitude**
Star formation		
Rho Ophiuchi Cloud	249.18	-2.75
Taurus molecular Cloud	72.26	+3.64
Orion B	84.95	-25.26
Great Orion Nebula	82.99	-28.68
Chamaleon 1 Cloud	237.94	-66.23
Lupus Region	246.29	-17.04
Corona Australis Cloud	282.69	-14.22

Target	Ecliptic Coordinates	
	Longitude	Latitude
Cosmology		
Lockman Hole	137.13	45.17
North Galactic Pole	180.02	29.81
Hubble Deep Field	148.36	57.29
Deep GSS 162-7875	180.00	59.61
Cosmos 5975	211.57	-21.11
XMM-LSS	32.29	-17.82
Hubble Ultra Deep Field	41.19	-45.19
QSO B1623+268A	238.05	47.6

Table 3-3: Preliminary List of Targets

Based on Table 3-3 FIRI shall be able to observe at an angle at least about 25 degrees out of the ecliptic with a goal of observing about 45 degrees out of the ecliptic. Figure 3-1 shows the observation sphere following from this requirement.

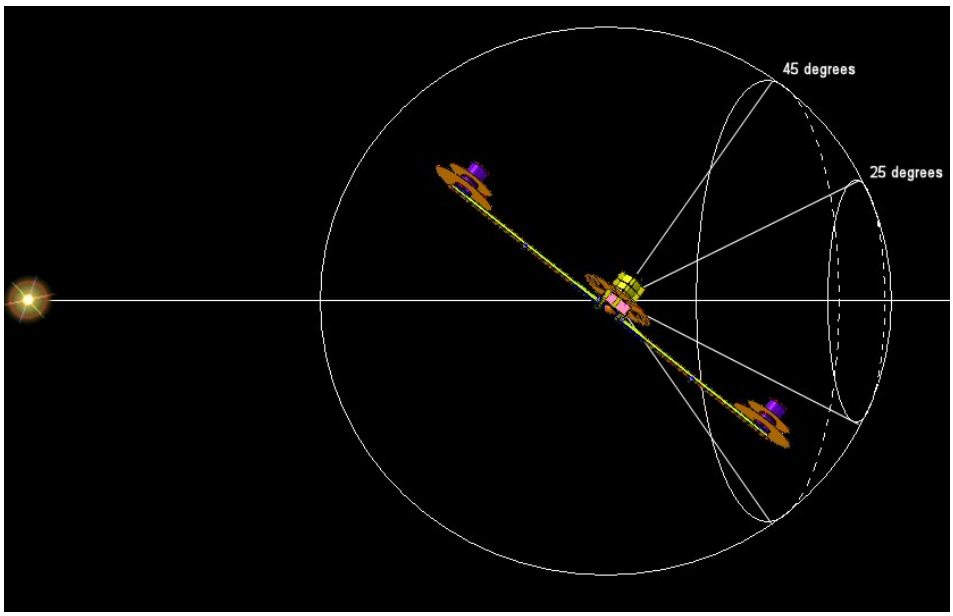

Figure 3-1: FIRI Observation Sphere

The science requirements described in the above section have been translated into system and subsystem requirements that can be found in the Systems Chapter.

3.4 Mission Requirements

FIRI shall keep within the Cosmic Vision constraints regarding budget and timeframe. Therefore the cost of the mission is not to exceed the cost cap for a large Cosmic Vision 2015-2025 mission, and launch is envisaged in 2020 to 2025. The launch date infers a constraint on the

technology development for the mission – Technologies used shall be at Technology Readiness Level (TRL) 5 in 2015.

FIRI shall be designed for a mission duration of 5 years, and areas that need attention in case of a mission prolongation shall be addressed.

The above programmatic requirements are summarised in Table 3-4.

Requirement ID (Prefix-#)	Requirement Level	Title	STATEMENT (Defines a REQUIREMENT, unless specified as a GOAL or LIMIT value.)	Rationale and/or Comments
PM - Programmatic Requirements PM.SCH Schedule and Budget				
PM.SCH-1	1-Drivers	Schedule	Launch in 2020-2025	*Study assumption*
PM.SCH-2	1-Drivers	Design life	The design life shall be 5 years	
PM.SCH-3		Technology Readiness	Only technologies with a TRL of 5 by start of Phase-B shall be used.	
PM.SCH-4	1-Drivers	Launch Vehicle Selection	Launch Vehicle shall be Soyuz-Fregat or Ariane 5	*If Soyuz is too constraining Ariane-5 shall be used.*

Table 3-4: FIRI Programmatic Requirements

This Page Intentionally Blank

4 MISSION ANALYSIS

The mission analysis work in the context of the CDF study was concerned with the selection of a FIRI operational orbit that is consistent with the scientific, payload and communications requirements, the analysis of the launcher performance, transfer strategy, stationkeeping cost, orbital geometry and ground station visibility conditions.

4.1 Requirements and Design Drivers

The following requirements and design drivers are relevant to the mission analysis process:

4.1.1 Target Orbit

The baseline orbit has been selected (see 5.2.2) as an orbit around the Earth-Sun L2 point that can be reached with maximized payload mass, i.e. without deep space manoeuvres. Typically this leads to a large-amplitude Lissajous or Halo.

4.1.2 Ground Stations

The ESA ground stations to be regarded in the analysis are:

- Cebreros (Lon: 4.367 deg W, Lat: 40.455 deg N, Alt: 789 m)
- New Norcia (Lon: 116.192 deg E, Lat: 31.048 deg S, Alt: 224 m)

4.1.3 Launch Vehicle

With a launch mass of the spacecraft of ~5400 kg, the launch vehicle has been selected (see 5.2.1) as an Ariane 5 ECA, launched from Kourou. For this vehicle, a dedicated launch shall be assumed.

4.2 Assumptions and Trade-Offs

4.2.1 Target Orbit

In addition to the baseline large-amplitude Lissajous orbit around the L2 point, a trade-off shall be performed with the following alternatives:

- A reduced-amplitude Lissajous orbit, where the Sun-Spacecraft-Earth angle is constrained to below 15 deg, as for the Gaia mission
- A heliocentric orbit trailing the Earth, as for the NASA IR space telescope Spitzer.

4.2.2 Launch Vehicle

As a launch alternative, a shared launch with Ariane 5 ECA into GTO using the standard midnight launch window shall be regarded.

4.3 Baseline Design

4.3.1 Launch Vehicle Performance

The worst-case payload performance of the Ariane 5 ECA launcher into a wide Lissajous orbit is taken from RD[3], where it is cited as 6273 kg, including adapters. This value constitutes a

reduction from earlier predictions and takes into account modifications implemented after the December 2002 launch failure. In view of future improvements, this figure may be conservative.

4.3.2 Large-Amplitude Lissajous Orbit Around Lagrange Point L2

The Lagrange point L2 in the Sun-Earth system is one of the locations specific to the three-body problem. Near the L2 point, which is "beyond" the Earth, as seen from the sun, at a distance of around 1.5 million km, the combined gravitational effect of Earth and Sun is such that a body located there will travel around the Sun with a period of one year, so it will maintain approximately the same distance and location relative to the Earth if displayed in a coordinate frame that rotates around the Sun with the Earth. Normally, a spacecraft at a larger distance from the Sun would move more slowly than the Earth, quickly drifting away.

A spacecraft will never be located directly in the L2 point (apart from being physically impracticable, this would also place the spacecraft eternally inside the Earth penumbra). It will orbit around the L2 location on a wide loop with a period of 6 months. Two classes of such "orbits" exist:

- Halo orbits are typically very wide, they trace approximately the same path in the sky as seen from the Earth, and they are eclipse-free.
- Lissajous curves can have large or small amplitudes, they do not trace the same figure over and over again and they may pass through the Earth penumbra cone. Lissajous curves with very large amplitudes may have properties similar to Halos. Typically, reaching a large-amplitude Lissajous curve can be achieved without any DSMs, while reaching a narrow Lissajous requires a DSM, the size of which depends on the amplitude reduction to be performed.

All such orbits require stationkeeping. The cost depends on the residual uncertainties in the perturbation model and also on the frequency of the correction manoeuvres. A major source of such uncertainties is the acceleration induced by solar radiation pressure, which cannot be modelled with absolute accuracy. A typical value for the Stationkeeping cost is 2 m/s/year.

On a low-amplitude Lissajous curve, eclipse avoidance manoeuvres may have to be performed in regular intervals to prevent the trajectory from intersecting the Earth penumbra cone. Additionally, the spacecraft may pass through the Moon penumbra cone, which can reduce the available sunlight by up to about 13%.

4.3.2.1 Operational orbit

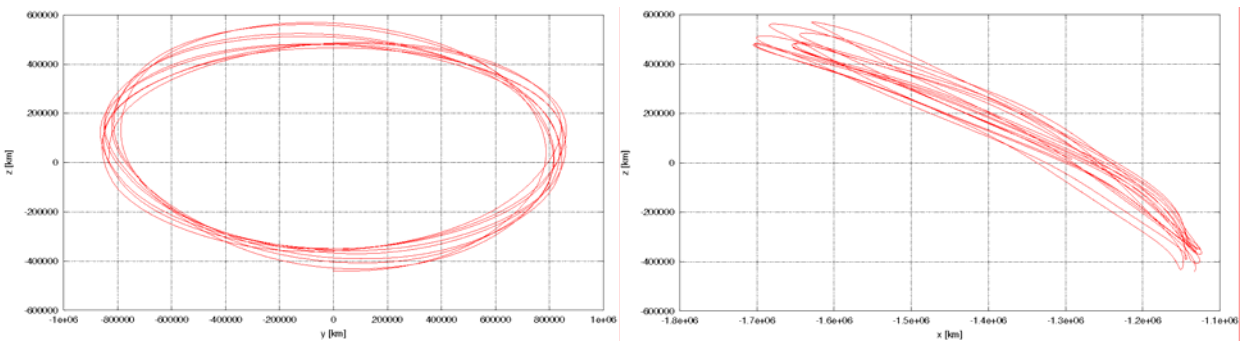

Figure 4-1: y-z (left) and x-z (right) Views of the FIRI Baseline Operational Orbit

Figure 4-1 shows the trajectory curve for the operational orbit, in the y-z-view (left hand diagram), as it would appear when looking from the Earth into the anti-sun direction, and in the x-z-view (right-hand diagram), x denoting the anti-sun-axis and z the out-of-ecliptic direction. The figure shows the large excursions of more than 600,000 km and 800,000 km in the z- and y-directions. Also, there is a large variation in the x-direction, which varies between 1.13 million and 1.7 million km. The period on the ellipse-like curve is 6 months.

The large amplitudes in the orbit lead to the variations in Earth range and Sun-Spacecraft-Earth-Angle (SSEA) shown in Figure 4-2. The range varies between 1.2 and 1.8 million km, the SSEA between 16 and 33 deg. The range is an important input for the design of the communications system, the SSEA impinges on the telescope and baffle design. At no point do eclipse conditions occur.

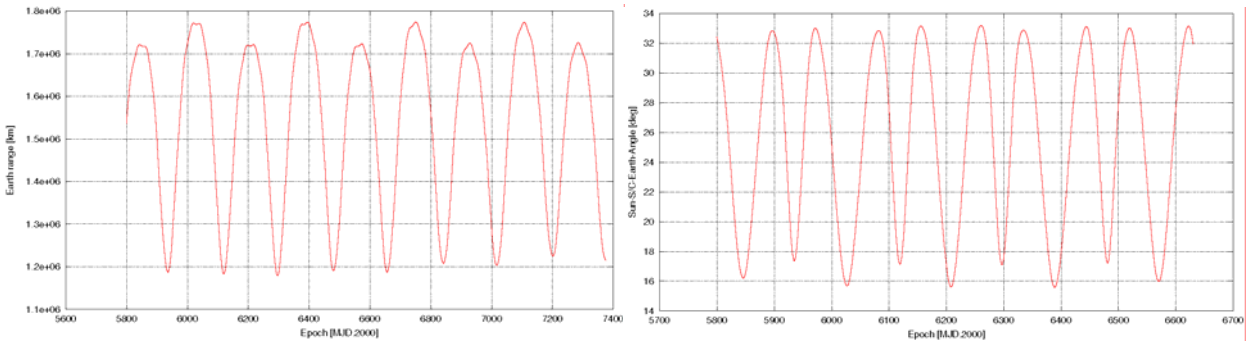

Figure 4-2: Earth Range and SSEA on FIRI Baseline Operational Orbit

4.3.2.2 Coverage on the baseline operational orbit

Ground station coverage conditions for the two regarded ground station locations also show a strong variation with time due to the spacecraft motion on the orbit around L2. The period of the variation is 6 months.

Min. el. [deg]	Pass dur. [h]	Cebreros	New Norcia
	Minimum	8.3	9.2
5	Mean	11.3	10.9
	Maximum	13.5	12.9
	Minimum	7.2	8.4
10	Mean	10.3	10.1
	Maximum	12.5	12.1
	Minimum	4.7	6.5
20	Mean	8.4	8.4
	Maximum	10.7	10.5

Table 4-1: Ground Station Coverage on FIRI Baseline Operational Orbit

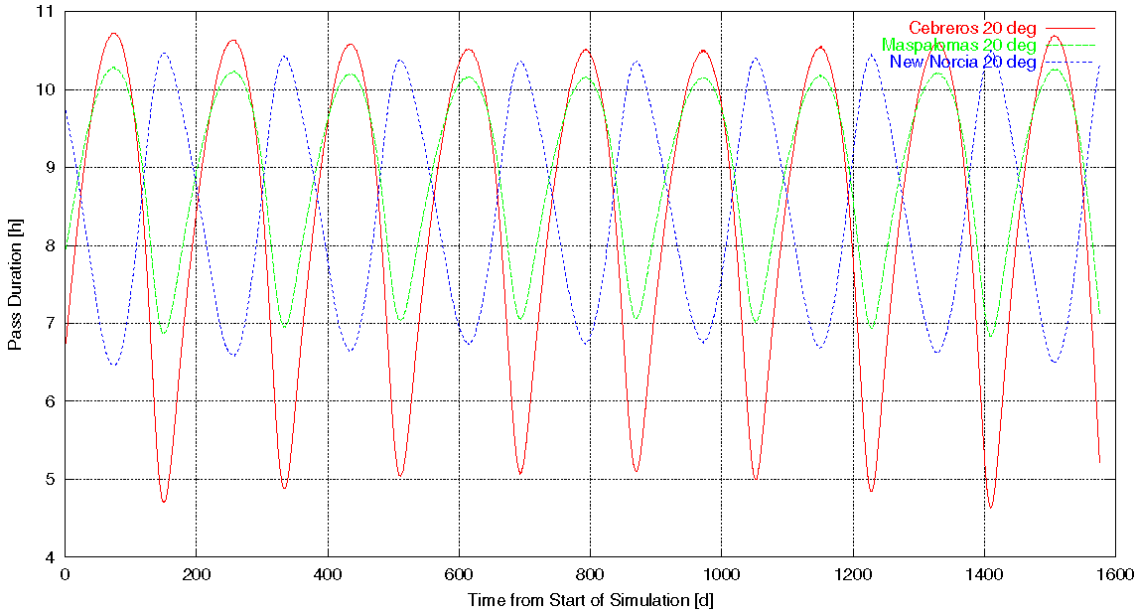

Figure 4-3: Coverage Evolution for FIRI Baseline Orbit, 20 deg Min. Elevation

The dependency of minimum, mean and maximum duration of the daily coverage passes on the epoch is shown in Table 4-1, which also highlights the influence of the minimum elevation over the local horizon for each ground station location. The most favourable ground station, with the least variations and the highest mean value is Maspalomas, due to its location close to the equator.

4.3.2.3 Transfer orbit

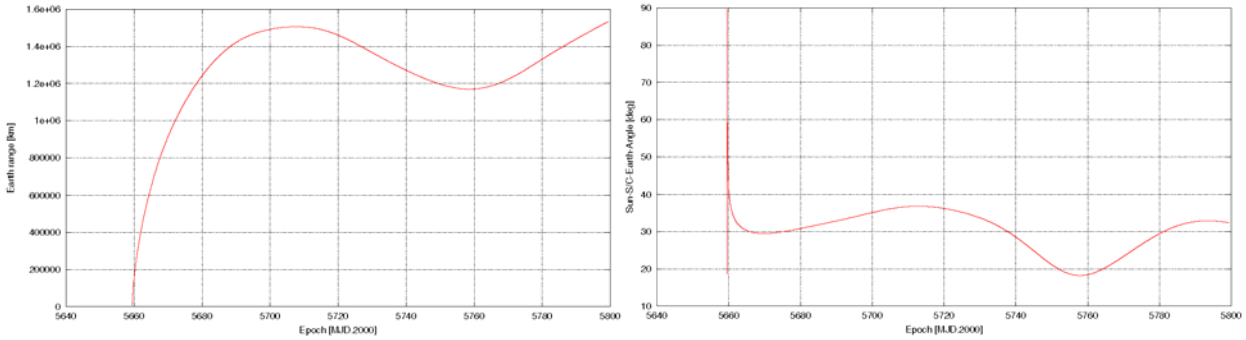

Figure 4-4: Earth Range and SSEA for Transfer to FIRI Baseline Orbit

There is no clear separation between transfer and operational orbit due to the absence of an insertion manoeuvre. The range increases sharply at first, reaching 1 million km only 11 days after departure from LEO. There are no eclipses and the SSEA remains below 37 deg, only slightly larger than the maximum of 33 deg achieved during the operational orbit. The transfer phase can be seen as over around 40-50 days after departure, but the experiment hardware can be commissioned earlier than that.

4.4 Options

4.4.1 Shared Launch with Ariane 5 ECA into Standard GTO

A possible alternative to a dedicated Ariane 5 ECA launch is a shared commercial launch. The most common type of launch for the Ariane 5 family is into GTO, mostly using the midnight launch window. For such a launch, the apogee would be oriented towards the sun direction, which would be useful for launch into the L1 point.

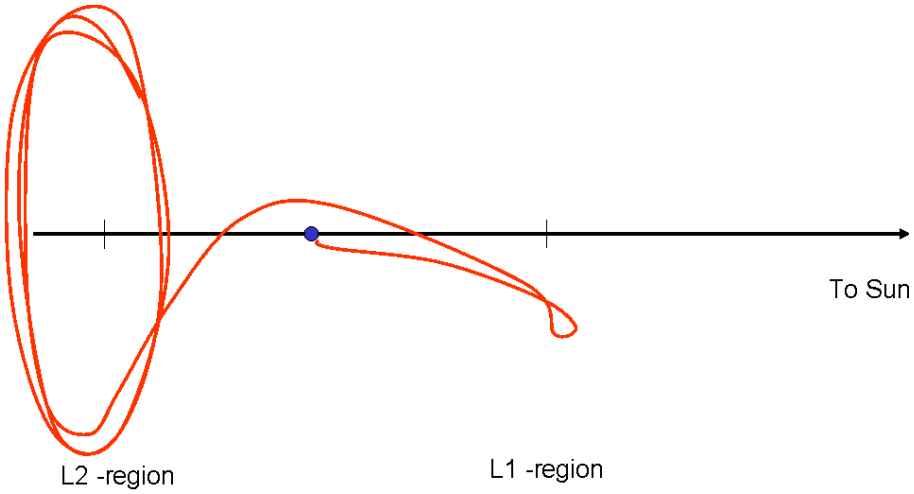

Figure 4-5: Qualitative Example of Transfer to L2 via L1

However, detailed numerical analysis performed by M. Hechler of ESOC Mission Analysis RD[4] showed that it is possible to reach an orbit around L2 by inserting first into the WSB at L1. The transfer trajectory is very sensitive and requires careful control, but the feasibility has been demonstrated. The impulsive manoeuvre cost is around 755 m/s starting out from GTO and the transfer duration is 100 – 200 days. Typically, the spacecraft moves out to the L1 WSB, then returns to the Earth, performing one or several wide loops, before ending up in an orbit around L2. An example of such a transfer is shown in Figure 4-5.

4.4.2 Soyuz-Fregat Launch Performance

The Soyuz performance into a wide Lissajous orbit is 2090 kg, including the adapter mass. For a transfer including a moon swingby, the performance is 2260 kg, also including the adapter. The payload capability of this rocket is not sufficient for the purposes of FIRI. This option has been discarded.

4.4.3 Reduced-Amplitude Lissajous Orbit Around L2

As described in Section 4.3.2.1, the baseline operational orbit, reachable without DSMs, features large amplitudes and leads to an SSEA of up to 33 deg. Limiting SSEA to less than 15 deg requires a considerable reduction of the amplitudes. The transfer will then incorporate a sizeable DSM with a magnitude of 120-160 m/s, as Gaia analysis has shown RD[2].

Furthermore, for the Gaia mission, eclipse avoidance is required every 6 years. One eclipse avoidance manoeuvre costs 15 m/s. It might be possible to perform the entire FIRI mission including extension within an eclipse-free period, if the initial phase can be chosen just right,

which will constrain the launch date. Otherwise, 15 m/s have to be budgeted on top of the DSM and the Stationkeeping cost.

4.4.4 Trailing Orbit

The trailing orbit was initially regarded for FIRI but later discarded due to link budget reasons. The characteristics of this option are however included here for the sake of completeness.

The NASA IR telescope Spitzer was launched into an Earth trailing orbit, i.e., a heliocentric orbit that slowly drifts away from the Earth but remains at a heliocentric range of approximately 1 AU. Spitzer's drift rate is around 0.1 AU/year.

The way to achieve a drift orbit is to insert the spacecraft into a slightly hyperbolic orbit (C_3 ca. 0.4 km^2/s^2), aiming at the anti-sun direction. The spacecraft will then initially be in the immediate vicinity of the Earth. As the Earth will still exert considerable gravitational perturbations, the spacecraft orbit will gain energy and thus increase. The increase in orbital energy corresponds to an increase in the semi-major axis. The orbit also becomes slightly eccentric, making it loop away from the Earth. The drift rate initially increases strongly, then becomes quasi-constant.

C_3 for escape [km^2/s^2]	0.4
Earth range [km / AU]	
After 1 year	7.2 million / 0.05
After 2 years	22.9 million / 0.15
After 5 years	76 million / 0.5
Maximum sun range [km / AU]	158 million / 1.06
Minimum sun range [km / AU]	144 million / 0.96
Launch mass w/adapter [kg]	2020 kg

Table 4-2: Properties of Trailing Orbit

Table 4-2 summarizes the salient characteristics of the trailing orbit. The payload mass is slightly lower than for L2 orbits, and the Earth range is much larger and increases with time. The benefits are:

- The spacecraft never experiences an eclipse pass
- There are no DSMs and no need for stationkeeping. Also, it is not necessary to correct the dispersion in the ΔV imparted by the Fregat stage. Therefore, the spacecraft does not require an onboard orbit control system. This benefit alone leads to savings that outweigh the slightly lower launch mass.
- In the present analysis, launch in March was assumed. For this launch date, the New Norcia ground station has 12 hours of coverage every day, except for the first two months of the mission, when the daily pass duration is slightly shorter.

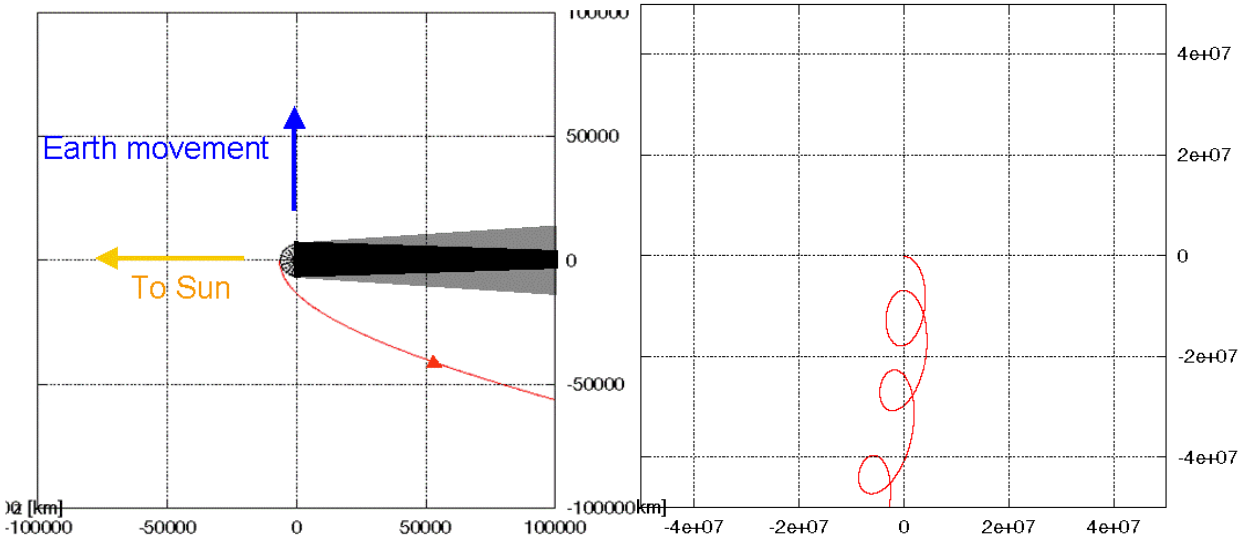

Figure 4-6: Close-up and Pan View of Trailing Orbit Trajectory

Figure 4-6 shows a close-up of the trajectory at escape and a panned view of the orbit as it drifts away from the Earth in loops. In both cases, a rotating coordinate frame is chosen, with the Sun constantly in the –x-direction and the Earth moving in the +y-direction. It can be seen how the spacecraft remains well clear of the eclipse cone and how the trajectory evolves with time.

Figure 4-7 shows the Earth and sun distance as function of time for a period of 5 years. Note how the Earth perturbations have a strong initial effect, increasing the drift rate. With time, the drift rate becomes constant.

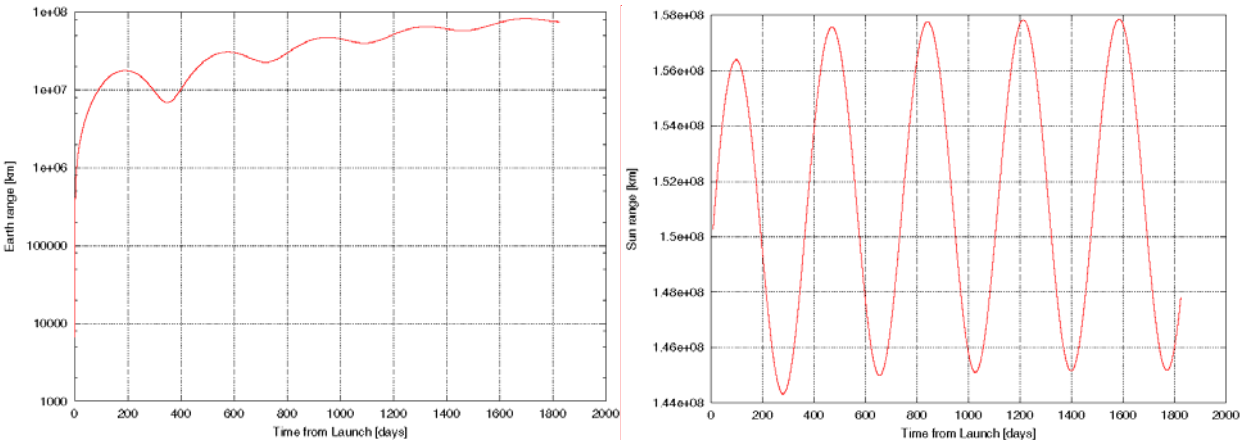

Figure 4-7: Earth and Sun Range on Trailing Orbit

This Page Intentionally Blank

5 SYSTEMS

5.1 System Requirements and Design Drivers

The requirements have been divided into three levels:

1. Drivers
2. Systems
3. Subsystem.

The drivers are presented in Chapter 3 Mission Objectives and the systems and subsystem level requirements will be presented in this chapter. For clarity the system level requirements have been split into two parts; space and ground segment. The requirements have been given an ID to simplify the traceability and the parent requirement, if any, is indicated in the rightmost column of the following tables.

The mission system requirements presented in Table 5-1 have been based on the science requirements provided in the Mission Objectives Chapter.

Requirement ID (Prefix-#)	Requirement Level	Title	STATEMENT (Defines a REQUIREMENT, unless specified as a GOAL or LIMIT value.)	Rationale and/or Comments	Parent ID (Prefix-#)
MS - Mission Systems Requirements					
MS.OBS Observation Strategy					
MS.OBS-1	2-Space Segment	Observation angles	Observe at an angle at least ~25 degrees out of the ecliptic, with a goal of observing ~45 degrees out of the ecliptic.	*For cosmology surveys imaging needs to be done in the north or south ecliptic pole directions, to avoid disturbance from the zodiacal light. However, for star and planetary system formation the need for observing out of the ecliptic is of less importance.*	
MS.OBS-2	2-Space Segment	uv-coverage	Coverage needed is still TBD, but the spacecraft should have the possibility to obtain as close to 100% coverage as possible.	*Operationally this implies that the mirrors will need to be able to obtain a 2-dimensional movement filling the uv plane sufficiently.*	
MS.OBS-3	2-Space Segment	Geometric resolution	The ITD shall change with 1m in between measurements, corresponding to a geometric resolution of 0.5	*To cover the uv-plane*	MS.OBS-2
MS.OBS-4	2-Space Segment	uv-coverage strategy	The uv-plane shall be covered with a strategy having an overlap consistent with the geometric resolution	*To cover the uv-plane*	MS.OBS-2
MS.LOP Launch and Orbit Parameters					
MS.LOP-1	2-Space Segment/Ground Segment	Orbit	A thermally stable orbit shall be chosen		
MS.LOP-2	2-Space Segment/Ground Segment	Orbit-Visibility	The orbit visibility shall be sufficient to provide a downlink window large enough for the Science and Housekeeping data		
MS.GSO Ground Station and Operations					
MS.GSO-1	2-Ground Segment	Data collection, S/C monitoring and control	The Ground Segment shall ensure the collection on ground of the data generated by the satellite (payload and platform), as well as the monitoring and control of the spacecraft		
MS.GSO-2	2-Ground Segment	Data delivery	The ground segment shall deliver the payload data to the Science Operations Centre and the HKTM to the Mission Operations Centre		
MS.GSO-3	2-Ground Segment	Data reliability and delivery timeliness	The ground segment shall satisfy the requirements imposed by the FIRI Project on scientific data reliability and availability as well as on science data delivery timeliness		

Table 5-1: Mission Systems Requirements

The spacecraft system requirements, presented in Table 5-2, have been based on the mission requirements in the Mission Objectives Chapter and on CDF margin philosophy.

Requirement ID (Prefix-#)	Requirement Level	Title	STATEMENT (Defines a REQUIREMENT, unless specified as a GOAL or LIMIT value.)	Rationale and/or Comments	Parent ID (Prefix-#)
SS - Spacecraft System Requirements					
SS.GEN - Spacecraft General Requirements					
SS.GEN-1	2-Space segment	Height	The FIRI Total spacecraft length (including telescope, SVM) shall fit within the Soyuz ST fairing - less than 5070 mm at max diam.	*Changes to 7455mm at max diameter with Ariane 5 launch(Medium fairing)*	PM.SCH-5
SS.GEN-2	2-Space segment	Diameter	The FIRI Total spacecraft diameter (including telescope, SVM) shall be less than 3800 mm.	*Changes to 4570mm with Ariane 5 launch*	PM.SCH-5
SS.GEN-3	2-Space segment	Launch Frequencies	The FIRI spacecraft fundamental frequencies shall be >= 15 Hz lateral and >= 35 Hz longitudinal	*Changes to >= 8 Hz lateral and >= 27 Hz longitudinal with Ariane 5 launch*	PM.SCH-5
SS.MAR - Spacecraft Margin Philosophy					
SS.MAR-1	2-Space segment	Link Budget	A 3dB margin shall be applied in calculating the link budget		
SS.MAR-2	2-Space segment	System margin	A system margin of 20% shall be added to the dry mass which is calculated as a sum of all the components including maturity margin		
SS.MAR-3	2-Space segment	Maturity margin	Technology maturity margins of 5, 10 or 20% shall be added.		
SS.MAR-4	2-Space segment	Power margin	A 20% margin shall be applied at system level to the overall budget		
SS.MAR-5	2-Space segment	Propellant margin	A propellant margin of 2% shall be added to any calculations for manoeuvres		
SS.MAR-6	2-Space segment	AOCS impulse	A margin of 100% shall be added to the AOCS total impulse calculation for the nominal mission lifetime		

Table 5-2: Spacecraft System Requirements

The science and system level requirements have been translated into subsystem requirements. Table 5-3 provides general requirements for the interferometer and requirements on the optics and detector.

Requirement ID (Prefix-#)	Requirement Level	Title	STATEMENT (Defines a REQUIREMENT, unless specified as a GOAL or LIMIT value.)	Rationale and/or Comments	Parent ID (Prefix-#)
IR - Interferometer Requirements					
IR.GEN - General Interferometer Requirements					
IR.GEN-1	3-Subsystem	Type	A Michelson interferometer using direct detection is required		IR.GEN-6
IR.GEN-2	3-Subsystem	Wavelength range	The wavelength range shall be 25-300µm, 25-500µm (goal)		
IR.GEN-3	3-Subsystem	Angular Resolution	The angular resolution shall be 0.25" @ 30µm and 2.5" @ 300µm		
IR.GEN-4	3-Subsystem	Field of view (FOV)	1' FOV (Disc)		
IR.GEN-5	3-Subsystem	Line sensitivity	1E-21W/m2 Line sensitivty		
IR.GEN-6	3-Subsystem	Spectral resolution	The spectral resolution is to be about 3 for photometry, about 20 to provide SEDs, about 300 for extra galactic measurements and about 3000 for resolving lines in star formation regions	$\frac{\lambda}{\Delta\lambda}$	
IR.OPT - Optics Requirements					
IR.OPT-1	3-Subsystem	Size	The mirrors shall have a diameter of 1m	*To cope with sensitivity requirements*	IR.GEN-5
IR.OPT-2	3-Subsystem	Temperature	The mirrors shall be kept at ~5K	*To cope with sensitivity requirements*	IR.GEN-5
IR.DFR - Detector and Filter Requirements					
IR.DFR-1	3-Subsystem	Detector temperature	The detectors need to be cooled down to a temperature that complies with sensitivity requirements	*<100 mK for the selected detectors with a bath temperature below.*	IR.GEN-5
IR.DFR-2	3-Subsystem	Sensitivity	The confusion limit needs to comply with sensitivity requirements	*~10 mJy for the selected detectors*	IR.GEN-5
IR.DFR-3	3-Subsystem	NEP photometry	1E-18W/√Hz Sensitivity in Noise Equivalent Power (NEP) during photometry		
IR.DFR-4	3-Subsystem	NEP spectroscopy	GOAL: 1E-20W/√Hz Sensitivity in NEP during spectroscopy		

Table 5-3: Interferometer Requirements

The requirements specific to the boom are presented in Table 5-4.

Requirement ID (Prefix-#)	Requirement Level	Title	STATEMENT (Defines a REQUIREMENT, unless specified as a GOAL or LIMIT value.)	Rationale and/or Comments	Parent ID (Prefix-#)
BR - Boom Requirements					
BR.GEN - Boom Structural Requirements					
BR.STR-1	3-Subsystem	Boom length	The mirrors need to be separated by a distance of at least 30m.	*To comply with the angular resolution requirements.*	IR.GEN-3

Table 5-4: Boom requirements

The subsystem requirements for the service module are shown in Table 5-5, and for the payload module in Table 5-6. In Baseline design section, the split between service and payload module is explained.

Requirement ID (Prefix-#)	Requirement Level	Title	STATEMENT (Defines a REQUIREMENT, unless specified as a GOAL or LIMIT value.)	Rationale and/or Comments	Parent ID (Prefix-#)
SC - Service Module Requirements					
SC.ACS - Spacecraft AOCS Requirements					
SC.ACS-1	3-Subsystem	APE	The FIRI Absolute Pointing Error shall be less than or equal to 13 arcsec		
SC.ACS-2	3-Subsystem	AME	The FIRI Absolute Measurement Error shall be less than or equal to 0.017 arcsec		
SC.DHS - Spacecraft DHS Requirements					
SC.DHS-1	3-Subsystem	Data Storage	The mass memory shall provide data storage for P/L compressed data and S/C housekeeping data	*Need to accommodate 2 uv-planes*	
SC.COM - Spacecraft Communications Requirements					
SC.COM-1	3-Subsystem	Frequency band	The baseline frequency band shall be Ka 26 GHz		
SC.COM-2	3-Subsystem	Freq band option	GOAL: X-band option using ESA DSN should be considered		
SC.POW - Spacecraft Power Requirements					
SC.POW-1	3-Subsystem		The power s/s shall supply power to the S/C		
SC.THE - Spacecraft Thermal Requirements					
SC.THE-1	3-Subsystem		The Thermal s/s shall maintain equipment within its specified temperature limits		
SC.STR - Spacecraft Structure Requirements					
SC.STR-1	3-Subsystem		The structure s/s shall comply with stiffness and strength requirements	*From launcher and other subsystems*	
SC.MEC - Mechanism Requirements					
SC.MEC-1	3-Subsystem	Telescope carrier mechanism	The mirrors need to be translated on the boom to a position with 1cm accuracy.	*To comply with the Optics requirements.*	

Table 5-5: Service Module Requirements

Requirement ID (Prefix-#)	Requirement Level	Title	Required		Achieved	Compliance (Y/N)	Rationale and/or Comments
PL - Payload Module Requirements							
PL.THE - Spacecraft Thermal Requirements							
PL.THE-1	3-Subsystem	Mirror Temperature		5K	4K	Y	
PL.THE-2	3-Subsystem	Detector temperature		<100mK	50mK	Y	

Table 5-6: Payload Module Requirements

5.2 System Trade-Offs and Options

Several trades were carried out at system level for the FIRI study.

5.2.1 Launcher Selection

Two main options have been considered for this study, Ariane 5 ECA and Soyuz Fregat, both of them launching from Kourou. The main characteristics of these two launchers can be found in Table 5-7:

Launcher	Ariane 5 ECA	Soyuz
Mass to L2 [kg]	6273	2090
Fairing length [m]	5770-10004	5070
Fairing diameter [m]	4570	3800
Axial load [g]	5.90	4.50
Lateral load [g]	2	0.4
Axial frequency [Hz]	31	35
Lateral frequency [Hz]	10	15

Table 5-7: Launcher characteristics

A preliminary mass budget was computed for the FIRI spacecraft, showing early in the study that in terms of mass, it would be extremely challenging to fit in Soyuz.

No detailed configuration work was carried out to check the suitability of Soyuz fairing at this stage, although it was identified as a critical area for this launcher.

Therefore, Ariane 5 ECA was retained as the only European option.

5.2.2 Orbit Selection

Two main orbit options were identified as suitable for the mission:

- Earth trailing orbit, heliocentric orbit following the one of the Earth, drifting away from it
- Lisajous orbit around L2 point of the Earth Sun system (800000km amplitude).

The main advantages of an Earth trailing orbit are that no propulsion system is required to perform any orbit insertion manoeuvre and that no orbit maintenance is required. The disadvantage is that the distance with respect to the Earth increases in a continuous way with time, imposing severe constraints in the communication subsystem after a couple of years.

In Table 5-8 the main differences among the proposed orbits can be seen.

Orbit	Earth trailing	L2 800000 km
Ariane 5 ECA mass to orbit	7140	6273
Launcher dispersion [m/s]	0	30
ΔV for orbit insertion [m/s]	0	0
Maintenance ΔV [m/s per year]	0	2
Eclipse	no	no
Thermal environment	constant	constant
Earth range	up to 75 million km	~ 1.5 million km
Maximum data rate (with 15 watt 0.3 m HGA, 26 GHz) [Mbps]	0.006	15

Table 5-8: Orbit selection

An orbit around the L2 point was selected. It allows a high return data rate throughout the mission lifetime. The disadvantage of the orbit maintenance manoeuvres was assessed to be small.

5.2.3 Sun Shield

In order to achieve the scientific objectives of this mission, the optics have to be kept below 4K. For this reason, the solar radiation input has to be minimised, using passive methods as much as possible. A configuration making use of sun shields was found to be the most effective one. Two possible configurations were analysed at system level:

- Attached to the telescope, dedicated sun shields under the hub and the telescopes (and therefore mobile together with the telescopes)
- Below the boom, long fixed sun shield along the boom, covering both the hub and the telescopes

Attached to the telescope Below the boom

Figure 5-1: Sun shield configurations

Table 5-9 shows the main characteristics of each option.

Sun Shield	Attached to the telescope	Below the boom
Thermal environment	Possibility of using grooves for telescopes Extra shield needed for boom ΔT on boom 100K	DT on boom < 100K Lower temperature on the boom Higher temperature on the outer part of telescopes (no grooves), more straylight Lower temperature for the telescope carrier mechanisms located on the boom making the development more challenging
Sun shield stowage/deployment	Deployment mechanism needed, but smaller sun shield, can be accomodated around the telescopes and the hub	Deployment mechanism needed, complex strategy due to size of the shield and fairing constraints
Complexity of the mechanism	Based on Gaia	New development
Pointing constraints/perturbances rejection		Bigger cross section wrt the sun, more SRP torque to be rejected
Minimum intertelescope distance	Limited by baffle/sun shield (8 m)	Limited by baffle (4 m, TBC)
Acomodation inside fairing	Driven by booms and telescopes	More complex, driven by sun shield folding around the boom and telescopes
AIT		More complex, need to test the shield deployment on ground
Mass		Extra mass due to bigger shield and mechanisms

Table 5-9: Sun shield configuration

The main advantages of the sun shield below the boom would be to reduce the minimum inter telescope distance to 4 m and to reduce the thermal gradients on the boom itself. However, this configuration presents some problems due to the impossibility of using grooves to help in the passive thermal design of the telescopes themselves, therefore their external part will be warmer and problems with straylight may rise (TBC).

Furthermore, the sunshield itself presents problems in the stowed configuration and for the deployment mechanisms and sequence. Around 210 m^2 of sun shield are required in this configuration, which also implies an increase in the total mass of the system. No easy solution was found during the course of the study.

Finally, it would imply a technology development (in the case of dedicated sun shields for the telescopes some heritage exist from GAIA) and a more complex AIT, as the deployment mechanism will have to be tested on ground.

Therefore, the option of sun shields attached to the telescopes and the hub was selected as baseline.

5.2.4 Power (and data system)

The baseline design of the FIRI spacecraft consists of a central hub containing the beam combiner and the service module to which a fixed boom is attached. The telescopes will move along the boom to modify the inter telescope distance.

In order to simplify the interfaces between the telescopes and the rest of the spacecraft, the possibility of eliminating the power and data harness in between them was analysed.

With regards to the power subsystems, two main options were analysed:

- Distributed power system, one power system (solar panels, battery and control and distribution units) for the hub plus another two independent power systems for the telescopes
- Centralised power system with power distribution lines along the booms

Figure 5-2: Power system configuration options

Table 5-10 shows the main differences between the two systems.

	3 EPS	1 EPS
Power	No harness required (req. wireless data handling)	Less Modules - Easier development/ procurement & Monitoring simplified onboard
	No mechanical element for the harness required	Less power dissipation in the telescopes modules
	PCDU total mass expected to increase	Higher Harness mass
	SA total area required expected to be higher (worst case for each EPS might not be simultaneous + redundant string required)	PCU and SA designs might increase due to voltage drop in harness
	More power dissipation in telescopes	More power dissipation at hub level
Thermal	Increase in complexity (Can be solved with MLI etc)	
Configuration	Accomodation of SA not a big issue	Solar Array can be accommodated on the Hub (50% of the available clearance in the fairing)
		Harness accomodation TBD
Units	3 x PCU	1 x PCU
	3 x PDU	3 x PDU
	No harness	Harness
	Solar Array: 1.52m2 per Telescope 4.45m2 at Hub (7.48m2 in total)	Solar Array: 7.71m2 at Hub
	Battery Telescopes & Hub	Battery Hub
Mass [kg]	64	59
Cost [k€]	8400	7930

Table 5-10: Power system characteristics for the two options

Both options are similar in terms of total mass required as well as in the solar array surface (no accommodation problems in either of the options). Cost is also similar in both cases, as well as the technology used for the different units.

Some small differences exist in the thermal design, as in the case of the distributed power system, the dissipation in the telescopes will increase. But this was found not to be a problem for the design.

The main difference resides in the power distribution. A centralised power system needs to distribute the power from the central hub to the telescopes. This requires harnesses to be extended along the booms and interfaced with the telescopes. Several problems arise in this area, as the telescopes are moving parts along the boom. The harness will have to be constrained in

some way so that it does not interfere with the telescopes, i.e. it will have to be rolled in and out when the telescopes move. No space qualified technology exists at the moment to overcome this problem, and therefore a technology development plan should be proposed.

Therefore a distributed power system was selected due to its simplicity of interfaces, while keeping the total mass and cost at the same level as a centralised system.

Therefore, it was decided to use wireless data transmission (TM/TC) in between the telescope and the hub (see DHS Chapter 8.5 for more details).

5.2.5 Boom

It was proposed to investigate a new concept for supporting and moving the telescopes with respect to the central hub. So far all the missions studied have relied on standard fixed booms along which the telescopes will move. In the course of this study, the idea of using articulated booms, simplified versions of a robotic arm was analysed.

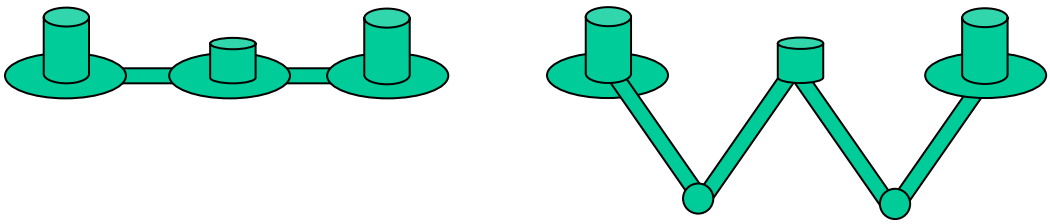

Figure 5-3: Boom options

Table 5-11 shows the main differences between the two options.

Boom	Deployable boom	Articulated boom
Total mass of the system [kg]	860	550 (estimation)
Structure	222	
Mechanisms	535	
Harness	102	
Power consumption [W]	Only 2 driving mechanisms	High power consumption due to number of driving mechanisms
Harness routing	Extra guiding system required	Inside the boom
Heat shield deployment	No problem	Possible interference with the arm in the hub
Thermal environment for telescope	Dedicated sun shield	
Thermal environment for hub	Sun shield available	Depending on hub heat sun shield
Thermal environment for light beam	Baffles are required to reduce the view of the boom	Boom sight can be avoided and baffles reduced
Thermal environment for mechanisms	Warmer environment available	Around 100 K
Stowed configuration	Feasible inside Ariane 5 medium fairing	To be investigated in detail, position of telescopes for launch not clear
Vibration damping	TBD	TBD
Pointing accuracy	Initial error on hinge deployment, constant with time. Possibility of implementing a fine pointing mechanism for the telescope in the carrier. Vibrations dumped with time	Accuracy of hinges is 1 arcmin, new mechanism to be develop to avoid back lash
Control complexity	Only 1 dof to be controlled at boom level	5 dof
Number of driving mechanism	1 to 2 per boom	At least 4 per boom
Number of hinges	2	3
Number of latch mechanisms	2	0
Duty cycle of driving mechanisms	~10000	~10000
Number of single point failure	2	4
Development	Similar structures have flown (ISS), standard qualification programme	3 years of development time plus extensive qualification progamme
Testing procedures	A section of the boom may be enough	Lifetime testing is an issue
Cost	TBD	TBD

Table 5-11: Boom characteristics for the two options

An articulated boom would have a lower mass than the standard deployable booms plus will simplify the harness problem. It would also reduce the size of the straylight baffles required in between the telescopes and the hub, as the boom will not be in the way.

However, articulated booms cause major problems to arise in the pointing of the telescopes, as the state of the art for robotic arm mechanisms can only ensure a pointing accuracy in the order of one arcmin. Therefore, a technology development should be carried out, including intense qualification programme (including lifetime tests). Furthermore, the launch configuration is not clear.

Therefore, the use of a standard deployable boom was selected as baseline.

5.2.6 Other Trade Offs

Several other trade offs were carried out during the course of the study, especially in the area of optics for the telescopes and thermal design. For further details on these trade offs refer to chapter 7.1 and 7.6

5.3 System Baseline Design and Architecture

FIRI mission consists of a Michelson interferometer for the Far Infrared. The main elements of the interferometer are a central hub housing the beam combiner and the service module plus two telescopes that move along the boom attached to the hub.

The maximum distance between the telescopes (inter telescope distance, ITD) is 30 m, while the minimum distance will be 8 m. The wavelength is from 25 to 300µm, with a spectral resolution of 3000 at 150µm and a minimum of 1.7. The field of view is 1' circular, with an angular resolution of 0.25" at 30µm and 2.5" at 300µm.

Figure 5-4 shows the product tree of the system:

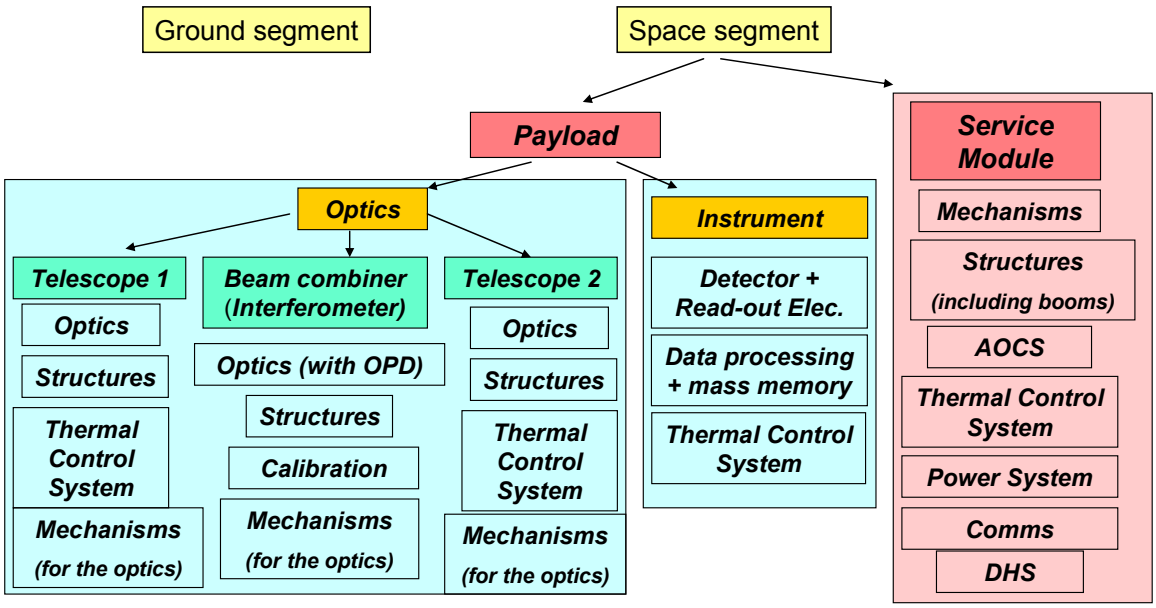

Figure 5-4: FIRI product tree

5.3.1 Payload Module Design

5.3.1.1 Telescope design

The telescopes consist of a series of four mirrors with a magnification factor of 5. The diameter of the primary mirror, M1, is 1.02 m, and the last mirror in the system, M4, is a tip tilt mirror. All the optics will be kept at a temperature of 5 K using JT sorption coolers (He and H2) plus a sun shield with grooves attached to the telescope. Finally, hollow reflectors are added to the system for metrology.

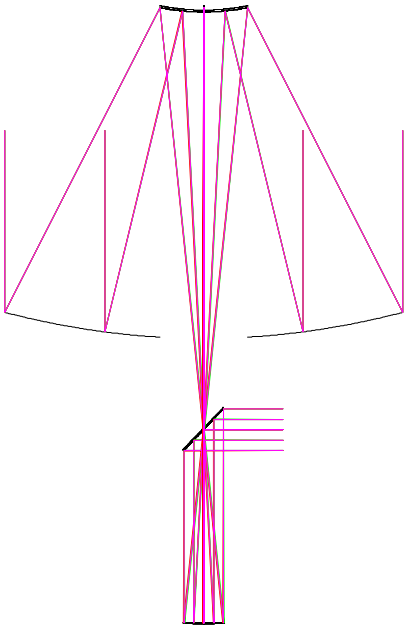

Figure 5-5: Sketch of the optics in the telescope

5.3.1.2 Beam combiner (interferometer) design

The payload module houses the beam combiner and sits on top of the service module in the central hub. It comprises two interferometers, the first one for fringe tracking and the second one to gather the scientific data. It also includes the fine pointing sensor and the internal metrology system.

The optics in the beam combiner are also kept at 5 K thanks to a four stages thermal design, using a cryostat, JT coolers and an ADR to get the detector down to 50 mK (with a lower bath temperature). Finally there is also a sun shield attached to the hub to help in the thermal design.

5.3.1.3 Detection

CMOS detectors (1+1 for redundancy) are used for fringe tracking at 50 K. For the science detectors, TES low G legs technology is used. Redundancy is also provided by duplicating the detection chain. The complete wavelength band is divided into 4 bands:

- 25.00 - 46.53 μm

- 46.53 - 86.60 μm
- 86.60 - 161.19 μm
- 161.19 – 300 μm

5.3.2 Service Module Design

The service module comprises the two deployable booms plus the service part of the central hub. Both booms are 7m long and are fabricated in CFRP, with a squared cross section of 300mm (2 mm wall thickness). Each boom is folded in two parts in the launch configuration and later on deployed thanks to two hinges. Finally, rails are attached to the boom to guide the movement of the telescopes.

The telescopes move along the booms thanks to a telescope carrier, a supporting structure equipped with three pairs of preloaded ball bearing roller assemblies. The movement is provided by a driving mechanism with rotary actuators. The movement of the carrier is helped out by solid lubrication.

The thermal design of the service module is completely passive, making use of radiators plus a sun shield using the deployment mechanisms of GAIA.

The power system is based on a distributed design, comprising three independent power systems, one in the central hub and one in each telescope. Solar arrays make use of AsGa TJ cells, requiring 8.3 m^2 in the central hub and 0.7 m^2 in the telescopes. Li-Ion batteries are used by the three systems, plus dedicated Power Distribution Conditioning Units (PDCUs). No power harness is required in between the telescopes and the hub.

The data handling system is composed of four computers, one per telescope plus one for the payload module and one for the service module. 6 x 256 Gbit memory cards are used to store the scientific data, including redundancy. Finally, wireless communication between telescopes and hub is used, and therefore, no data harness is required in between the telescopes and the hub.

The communications system makes use of two bands. The science data link uses 26 GHz frequency to download the data to earth at a data rate of 50 Mbps, making use of a 45 cm High Gain Antenna (HGA) and 15 W transmitted power. Data rate could be increased with little impact on the system and up to a level that would not cause further complexity on the GS. Configuration allows for up to 70 cm antenna. An X band link is also included for TM/TC and ranging. It makes use of the same antenna plus two Low Gain Antenna (LGA), transmitting 5 W.

The attitude control system makes use of the fringe tracking for fine pointing, plus an assembly of 3 star trackers, sun sensors and accelerometers. As actuators, a reaction wheel assembly is used, plus twelve 10N hydrazine thrusters.

The propulsion system is in charge of performing the orbit maintenance plus the correction of the launch errors. A monopropellant blow down system is used. A total of 420 kg of propellant are required, 100 kg for launcher dispersion corrections and orbit maintenance, plus 320 kg for AOCS manoeuvres SRP disturbance corrections.

5.3.3 Configuration

The FIRI spacecraft is composed mainly of a central hub to which two booms are attached plus two telescopes that move along the booms. The total length of the spacecraft is 30 m once the

booms are deployed, with a height of 3 m for the central hub and 2.5 m for the telescopes. Sun shields are placed under the telescopes and the hub, with a diameter of 6m.

For the launch configuration the booms will be folded in two parts and the telescopes placed on top of the hub. A supporting structure is required for the telescopes in the launch configuration (see Figure 5-7 for details).

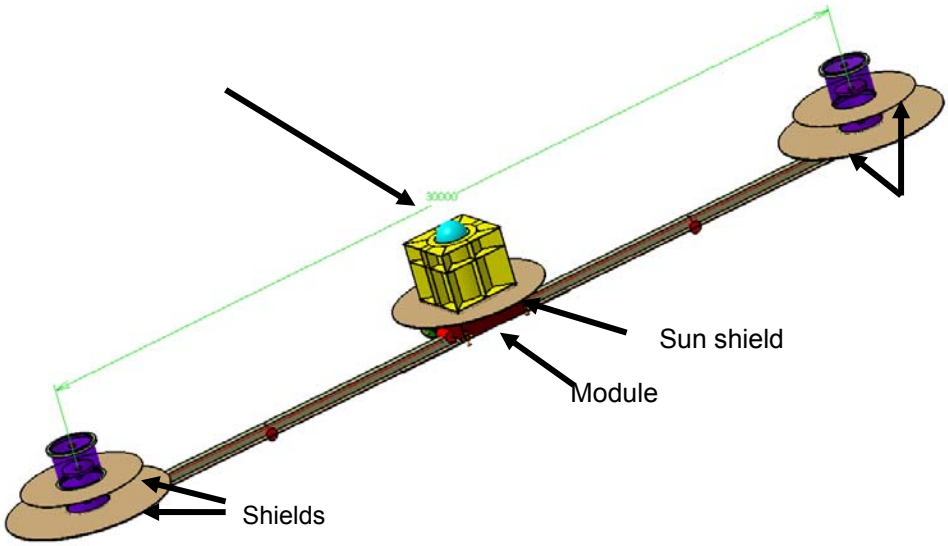

Figure 5-6: FIRI spacecraft configuration

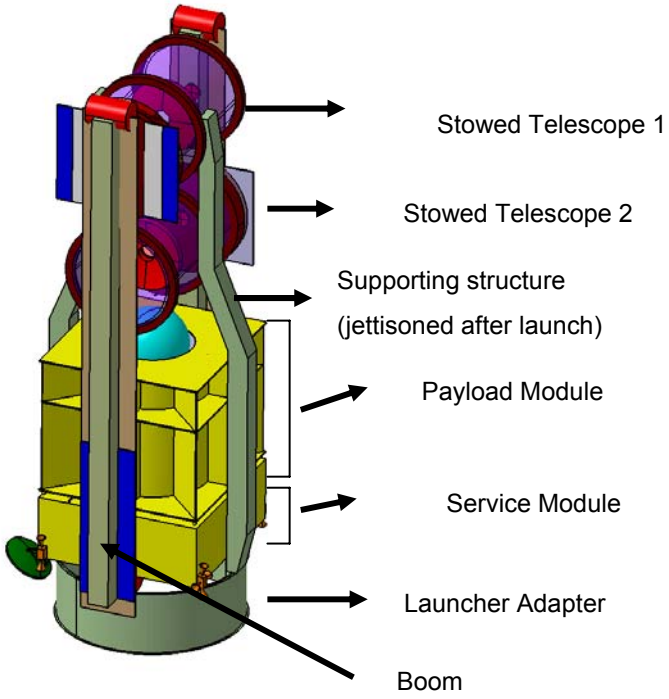

Figure 5-7: FIRI spacecraft stowed configuration

5.3.4 Mission Design

A Lissajous orbit around the L2 point of the Earth-Sun system has been selected. The amplitude of the orbit is 800,000 km, while the average range from Earth is 1.5×10^6 km.

The launch will be carried out by an Ariane 5 ECA launcher from Kourou. The total lift-off mass capability is 6273 kg, which provides enough margin for the baseline design, 5400kg, 16% margin. In case a higher capability is required, some improvements can be achieved by constraining the launch window (around 10% improvement) possibly more mass with smaller launch window

For the ground segment the Cebreros station is selected with its 35 m antenna. It has 8 hours of visibility per day for 5 hours required. The flight operations centre will be located at ESOC.

5.3.5 Other Design Issues

5.3.5.1 Contamination

Contamination issues were not analysed during the CDF study. Only a preliminary list of contaminants sources was elaborated:

- AIV
- Outgassing
- Creation of particles during the move of the telescope carrier along the boom (solid lubricant)
- Hydrazine coming from AOCS
- Hydrogen gas ejected from the cryostat of the Hub.

5.3.5.2 Lifetime

The nominal mission lifetime is 5 years. A possible extension of the operational lifetime to 10 years could be achieved, bearing in mind that:

Cryostat: the actual design is 800 litres, containing enough Hydrogen for 5 years of operation. Modifications to the design are required to increase the volume and therefore mass of Hydrogen.

Mechanisms cycles: some of the mechanisms are already extensively used during the mission, i.e. the ODL. If longer lifetime is expected, it should be specified in the technology development plan. In other cases like the telescope carrier, the number of cycles is in the order of 10000, which was considered not to be an issue.

AOCS consumables: the actual design carries the required propellant for 5 years plus a 100 percent margin for the AOCS functions. An increase in AOCS propellant of 50% without margins should typically be expected in the case of 10 years lifetime requirement.

Solar array: degradation over time of the solar cells has already been taken into account for a lifetime of 5 years. An increase of the SA size should be expected in case the lifetime is extended, but there is enough room for this change in the actual design.

5.3.6 System Budgets

5.3.6.1 Mass budget

The total launch-mass of the FIRI spacecraft is 5377 kg, including 20% system margin, launch vehicle adapter and 430 kg of propellant.

Total Dry(excl.adapter)			**3965.38 kg**
System margin (excl.adapter)	**20.00**	**%**	**793.08 kg**
Total Dry with margin (excl.adapter)			**4758.46 kg**
Total wet mass (excl.adapter)			**5187.01 kg**
Launch mass (including adapter)			**5377.01 kg**

Table 5-12: System mass

Service Module					
	Without Margin	**Margin**		**Total**	**% of Total**
Dry mass contributions		**%**	**kg**	**kg**	
Structure	**332.86 kg**	**20.00**	66.57	**399.43**	14.19
Thermal Control	**136.62 kg**	**9.96**	13.60	**150.23**	5.34
Mechanisms	**774.00 kg**	**16.12**	124.80	**898.80**	31.94
Communications	**32.80 kg**	**15.52**	5.09	**37.89**	1.35
Data Handling	**25.64 kg**	**8.75**	2.24	**27.88**	0.99
AOCS	**73.90 kg**	**6.83**	5.05	**78.95**	2.81
Propulsion	**62.20 kg**	**5.00**	3.11	**65.31**	2.32
Power	**62.78 kg**	**10.00**	6.28	**69.06**	2.45
Harness	**85.13 kg**	**20.00**	17.03	**102.15**	3.63
Total Dry(excl.adapter)	**1585.93**			**1829.70 kg**	
System margin (excl.adapter)		**20.00**	**%**	**365.94 kg**	
Total Dry with margin (excl.adapter)				**2195.64 kg**	
Other contributions					
Wet mass contributions					
Propellant	**420.15 kg**	**2.00**	8.40	**428.56**	15.23
Adapter mass (including sep. mech.), kg	**190.00 kg**	**0.00**	0.00	**190.00**	0.07
Total wet mass (excl.adapter)				**2624.20 kg**	
Launch mass (including adapter)				**2814.20 kg**	

Table 5-13: Service module mass budget

Payload Module					
	Without Margin	**Margin**		**Total**	**% of Total**
Dry mass contributions		**%**	**kg**	**kg**	
Structure	**457.98 kg**	**20.00**	91.60	**549.58**	21.44
Thermal Control	**749.26 kg**	**15.18**	113.71	**862.97**	33.67
Mechanisms	**250.00 kg**	**20.00**	50.00	**300.00**	11.71
Data Handling	**75.78 kg**	**5.48**	4.15	**79.93**	3.12
Harness	**119.18 kg**	**20.00**	23.84	**143.01**	5.58
Optics	**171.35 kg**	**10.35**	17.74	**189.09**	7.38
Detector	**10.55 kg**	**5.26**	0.56	**11.11**	0.43
Total Dry(excl.adapter)	**1834.10**			**2135.68 kg**	
System margin (excl.adapter)		**20.00**	**%**	**427.14 kg**	
Total Dry with margin (excl.adapter)				**2562.82 kg**	
Other contributions					
Wet mass contributions					
Adapter mass (including sep. mech.), kg	**0.00 kg**	**0.00**	0.00	**0.00**	0.00
Total wet mass (excl.adapter)				**2562.82 kg**	
Launch mass (including adapter)				**2562.82 kg**	

Table 5-14: Payload module mass budget

Table 5-15 shows the mass breakdown for the FIRI modules. The service module has been split into telescopes, hub and booms and the payload module into telescopes and instrument (located in the hub).

Element 1 - Service Module - Telescopes					580.12
FUNCTIONAL SUBSYSTEM	nr	Total Mass (kg)	Margin (%)	Margin (kg)	Mass (kg) with Margin
Structure		22.68	20.00	4.54	27.22
Thermal		51.76	9.01	4.66	56.42
Mechanisms		368.00	14.95	55.00	423.00
Communications		4.00	20.00	0.80	4.80
Power		21.51	10.00	2.15	23.67
Harness		37.51	20.00	7.50	45.02

Element 1 - Service Module - Hub					719.60
FUNCTIONAL SUBSYSTEM	nr	Total Mass (kg)	Margin (%)	Margin (kg)	Mass (kg) with Margin
Structure		200.10	20.00	40.02	240.12
Thermal Control		63.35	10.99	6.96	70.31
Mechanisms		89.00	13.93	12.40	101.40
Communications		28.80	14.90	4.29	33.09
Data Handling		25.64	8.75	2.24	27.88
AOCS		73.90	6.83	5.05	78.95
Propulsion		62.20	5.00	3.11	65.31
Power		41.27	10.00	4.13	45.40
Harness		47.61	20.00	9.52	57.13
Propellant					428.56

Element 1 - Service Module - Booms					529.98
FUNCTIONAL SUBSYSTEM	nr	Total Mass (kg)	Margin (%)	Margin (kg)	Mass (kg) with Margin
Structure		110.07	20.00	22.01	132.09
Thermal Control		21.52	9.18	1.98	23.49
Mechanisms		317.00	18.11	57.40	374.40

Element 2 - Payload Module - Telescopes					578.29
FUNCTIONAL SUBSYSTEM	nr	Total Mass (kg)	Margin (%)	Margin (kg)	Mass (kg) with Margin
Structure		143.82	20.00	28.76	172.59
Thermal Control		202.56	11.66	23.63	226.19
Mechanisms		10.00	20.00	2.00	12.00
Data Handling		4.68	9.27	0.43	5.11
Optics		91.92	10.00	9.19	101.11
Harness		51.08	20.00	10.22	61.29

Element 2 - Payload Module - Instrument					1557.39
FUNCTIONAL SUBSYSTEM	nr	Total Mass (kg)	Margin (%)	Margin (kg)	Mass (kg) with Margin
Structure		314.16	20.00	62.83	376.99
Thermal Control		546.70	16.48	90.08	636.78
Mechanisms		240.00	20.00	48.00	288.00
Data Handling		71.10	5.23	3.72	74.82
Optics		79.44	10.76	8.54	87.98
Detector		10.55	5.26	0.56	11.11
Harness		68.10	20.00	13.62	81.72

Table 5-15: Mass Breakdown for the FIRI Modules

The total weight with and without system margin, including both service and payload modules, for the telescopes, hub and booms is presented in Table 5-16.

TOTAL			
Telescopes	1158.41	1390.10	(696kg per telescope)
Hub	2276.99	2732.38	
Booms	529.98	635.98	(318kg per boom)
S/C Dry Tot:	3965.38	4758.46	

Table 5-16: Total weight for the telescopes, hub and booms

5.3.6.2 Power budget

The main part of the power required is in the hub, with a continuous demand of 1.2 kW with peaks of 2 kW. In the telescopes the power demand has been reduced to around 100 W continuous with peaks of almost 200 W.

Central Module							
		Stand By / Comms		Observation		Retargeting Mode	
Max Continuous Power	S/S	Max Continuous Power	Peak Power (incl. transients)	Max Continuous Power	Peak Power (incl. transients)	Max Continuous Power	Peak Power (incl. transients)
Service Module	Thermal	100 W	200 W	241 W	481 W	149 W	297 W
Instrument	Thermal	70 W	140 W	70 W	140 W	70 W	140 W
Array + SQUID Read Out	instruments	0 W	0 W	0 W	0 W	0 W	0 W
FPGA	instruments	0 W	0 W	10 W	20 W	0 W	0 W
AOCS	AOCS	20 W	20 W	100 W	200 W	100 W	200 W
Central Module Mechanisms	mechanisms	40 W	80 W	175 W	263 W	0 W	0 W
Communications	Communications	89 W	135 W	15 W	23 W	16 W	24 W
DHS Service Module	Data Handling	36 W	56 W	56 W	56 W	49 W	56 W
DHS Instrument	Data Handling	132 W	132 W	132 W	132 W	80 W	132 W
Metrology	Optics	0 W	0 W	59 W	89 W	59 W	89 W
Total		**487 W**	**762 W**	**857 W**	**1402 W**	**522 W**	**937 W**
Maturity Margin	20%	97 W	152 W	171 W	280 W	104 W	187 W
Total		**584 W**	**915 W**	**1029 W**	**1683 W**	**627 W**	**1125 W**

Table 5-17: Central Hub power budget

Telescopes (Both telescopes)							
		Stand By / Comms		Observation		Retargeting Mode	
Max Continuous Power	S/S	Max Continuous Power	Peak Power (incl. transients)	Max Continuous Power	Peak Power (incl. transients)	Max Continuous Power	Peak Power (incl. transients)
Cryostat+JT coolers	Thermal	40 W	80 W	40 W	80 W	40 W	80 W
Telescopes Mechanisms	mechanisms	0 W	0 W	0 W	0 W	0 W	0 W
DHS	Data Handling	30 W	45 W	30 W	45 W	30 W	45 W
Wireless Tranceiver	Communications	0 W	0 W	5 W	8 W	3 W	5 W
Total		**70 W**	**125 W**	**75 W**	**133 W**	**73 W**	**130 W**
Maturity Margin	20%	14 W	25 W	15 W	27 W	15 W	26 W
Total		**84 W**	**150 W**	**90 W**	**159 W**	**88 W**	**155 W**

Table 5-18: Telescopes power budget

5.3.7 Spacecraft Modes

Table 5-19 shows the operational modes of the FIRI spacecraft.

Number	Mode Name	Definition	Acronym	Duration (min)
1	Launch Mode	***Lift off to separation*** All subsys are off except for essential equipment Battery fully charged	LM	20
2	Initialisation Mode	***Satellite initialisation-trajectory insertion*** An automatic switch is used at separation to activate the equipment (incl. Transmitter) start-up sequence Coarse sun pointing provided by upper stage at separation Satellite capable of receiving and executing telecommands TT&C by LGA. Attitude acquisition in Sun Pointing Mode (SPM) SA operational, Sun shield to be deployed? Launch dispertion correction and bbq mode	IN	60
3	Cruise Mode	***Trajectory adjustment - up to "orbit insertion"*** Service Module Commissioning - all s/s in nominal working status Trajectory determinations and corrections Data communication S/C - Earth Power generation (SA; battery as backup) and distribution to all S/S with instruments in stand-by mode Payload initialisation?	CM	1440
4	Orbit insertion/Orbit maintenance	***Orbit insertion and possible orbit maintenance manoeuvres*** Mode similar to the cruise mode Propulsion system active to perform manoeuvres Orbit determinations and corrections attitude) Power generation (SA; battery as backup) and distribution to all S/S with instruments in stand-by mode Deployment	OIOM	120
5	Stand By/Comms	***Stand By Mode - up to rendezvous with DSC*** Mode similar to the cruise mode - the only difference is that the MSC is now in a halo orbit Orbit determinations and corrections attitude) Power generation (SA; battery as backup) and distribution to all S/S with instruments in stand-by mode Payload inactive Thermal control active?	SBC	1440
6	Observation	***Obsevation mode, target tracking and data collection*** Payload active and collecting data Mechanismas operated to change ITD and orientation AOCS actively tracking target, pointing and stabilising platform Power generation (SA; battery as backup) and distribution to all S/S with instruments in stand-by mode Comms?	OBS	1440
7	Retargeting Mode	***Manoeuvre to obtain a different target to scan*** The MSC receives an attitude profile from GS for the slew maneuver towards a new target star The MSC performs an open loop slew maneuver Settling phase (cancelling rates) and switch to closed loop attitude lock	RTM	1440
8	Safe Mode	***Hibernation and Failure Recovery mode:*** The spacecraft is kept SUN pointing. Accuracy determined by power system. Instruments are put on standby or switched off. Non-essential functions are halted. reconfiguration. TT&C by LGA. Failure detection and recovery are executed by the ground. ***Emergency Sun Acquisition Maneuver***	SA	1440

Table 5-19: Operational modes

5.4 Observation Strategy

The requirement to have a uv-coverage as close to 100% as possible as well as the desire to cover as many targets as possible drives the observation strategy. The main parameters defining the strategy are:

- ODL scanning procedure (spectral resolution and detector integration time), see 5.4.1
- uv-plane scanning procedure, see 5.4.2
- Retargeting manoeuvres, see 5.4.3
- Communications, see 5.4.4

The uv-plane is defined in 7.1.2.1.

There were no strict requirements on the desired number of targets, or the scan strategy given in the beginning of the study. The scan strategy could for example be to first scan a target with only one uv-line and if it is scientifically interesting a full uv-plane scan would be performed. In order to aid the work with the observation strategy a tool was therefore created in the System WB (see snapshot of one of the sheets in Figure 5-8), and later refined in a self-standing tool provided to the Customer. This tool gives the flexibility to vary the input parameters and see the response in the observation time, and will aid the development of a final observation scheme.

Inputs:

Inter-telescope distance (ITD)	30.00	m
Diameter of inner circle	8.00	m
Telescope diameter (d)	1.00	m
λmin	25.00	μm
λmax	300.00	μm
Spectral resolution	3000.00	
Geometric resolution (GR)	0.50	
Sky view	1.00	arcmin
	60.00	arcsec
Integration time	0.10	ms
Nr of ODL fold	2.00	
Req. ODL movement band1	58.15	mm
Req. ODL movement band2	52.17	mm
Req. ODL movement band3	47.59	mm
Req. ODL movement band4	43.80	mm
Nr of ODL points band1	13007	
Nr of ODL points band2	12541	
Nr of ODL points band3	12291	
Nr of ODL points band4	12157	
Telescope movement time (radial+angular, including stabilisation)	1800	s
S/C retargeting time (including stabilisation)	1800	s

Outputs:

Observation strategy: Circles

Observation time per uv-plane point	23.26	s
Nr of points in uv-plane	1373.00	
Nr of circles	23	

Observation time

Tot observation time (uv&mov)	**0.83**	days
Tot observation time (uv&sky&mov)	36.01	days
Theoretical (no movements included)		
Tot observation time (uv)	0.37	days
Tot observation time (uv&sky)	33.63	days

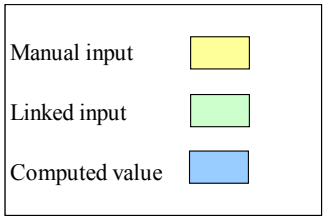

Figure 5-8: Snapshot of the Observation Strategy Tool in the Systems Workbook

5.4.1 ODL Scanning Procedure

The main objective is to get the required spectral resolution without blurring the image. To satisfy this requirement the optical displacement of the ODL over the integration time shall be below 0.5 mm. Two ODL scanning strategies are proposed:

- Continuous movement of the ODL, with maximum speed dictated by the blurring of the image and the minimum speed by the mechanism
- Scanning in steps, where the ODL speed is mainly dependant on the time required to go from one step to the next (can be faster than continuous movement), but this option has a higher power dissipation

The two strategies are illustrated in Figure 5-9.

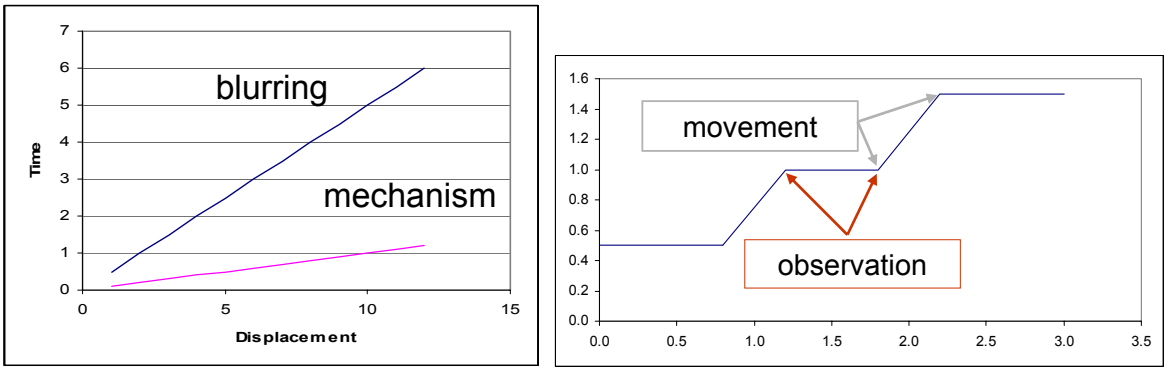

Figure 5-9: The two different ODL scanning principles

The continuous moving of the ODL has been chosen as baseline because of the lower power consumption.

5.4.2 UV-Plane Scanning Procedure

To cover the uv-plane the telescopes need to be translated on the booms and the spacecraft needs to spin around the observation axis. These movements can either be done in steps or continuously, yielding different scanning procedures. The following three were analysed in the CDF:

1) Step by step

   Starting from a stabilised position of the spacecraft the telescopes are moved along the boom to scan a line. Then the spacecraft is rotated slightly and the next line is scanned, and so on.

2) Concentric semicircles

   The spacecraft is spun and the scan is done for 180°, covering the full 360° because of the two telescopes. Then the spinning is stopped and the ITD is decreased and the resulting smaller circle is scanned, and so on.

3) Spiral.

   The spacecraft is spun and the ITD is slowly decreased at the same time.

In Figure 5-10 the three scanning strategies are shown. The green coloured circles represent one telescope and the light blue the other.

The overlap of the translation movement is determined by the geometric resolution, which was required to be 0.5, meaning that with a 1 m telescope the movement between two points should not be more than 0.5 m.

Having this overlap for the largest ITD in the first approach will result in oversampling for the shortest ITD. This approach is also very time-consuming since the spacecraft needs to be stabilised in between the scans.

In the second approach only 23 movements are needed. The manoeuvres will include decrease of the ITD, stabilisation and correction of the spin rate in order to have correct overlap.

In the third approach the spinning of the spacecraft results in complex movement and control laws and the gain in time was not substantial.

Based on the above discussion the second approach was chosen as baseline. It might still be interesting to scan targets with only one or two uv-lines, and therefore the budgets for this has also been calculated, see 5.4.5.

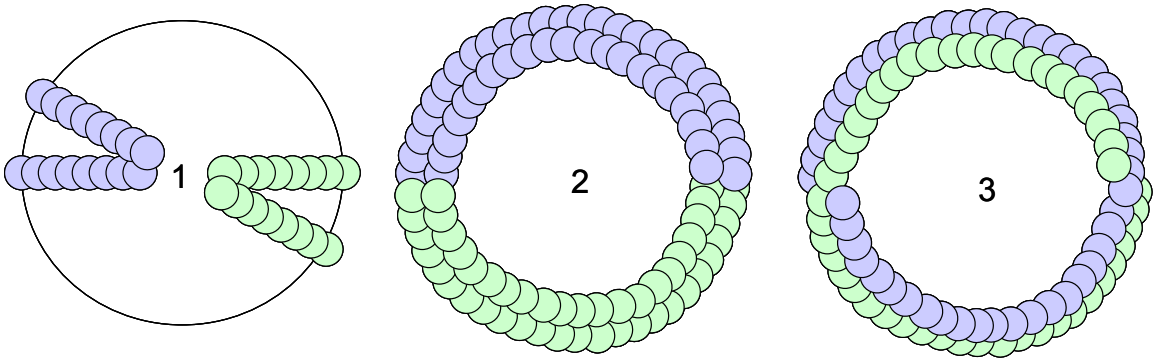

Figure 5-10: Illustration of the three uv-plane scanning strategies considered (number 2 baselined)

5.4.3 Retargeting Manoeuvres

Figure 5-11 shows how the observation targets listed in the Objectives Chapter with an elevation of ~±50° are distributed compared to the Sun, Earth and the Vernal Equinox. The targets should be chosen in such a way that the Sun angle is minimal during observation, and that the retargeting manoeuvres are optimised. For the ΔV-calculations a retargeting angle of 22.5° has been used.

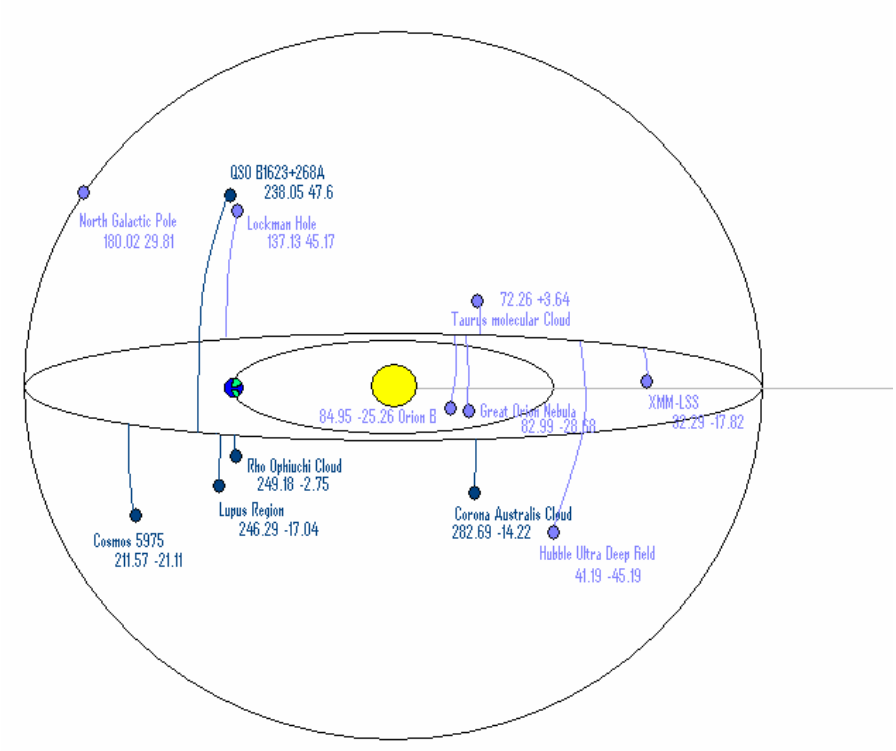

Figure 5-11: FIRI Target Sphere

5.4.4 Communications

The amount of data to be downloaded is dependent on the calibration strategy. Since two calibration targets are used, the amount of data will be tripled if the calibration needs to be done at every ODL point. If the calibration only needs to be done once per uv-plane scan the impact on the total data amount is minor.

For stability reasons the data downlink will not be done at the same time as the observation. This has an impact on the overall time per target.

For details and budgets of the Communications and Data handling subsystems, see relevant chapters.

5.4.5 Observation "Menu à la Carte"

Based on the observation strategy chosen the impact in terms of time, propellant and amount of data has been calculated per uv-plane, and per uv-line. The results of these calculations can be seen in Table 5-21 and Table 5-22. The spacecraft needs to be spun up initially (for the concentric semicircle strategy) and the cost for this is given in Table 5-20. The spin-up is performed with the telescopes next to the hub to minimise the moment of inertia.

Initial spin-up	
Propellant cost:	**208.70 g**
Required time:	**41.97 s**

Table 5-20: Cost of the Initial Spacecraft Spin-Up (Telescopes next to hub)

One UV-plane scan		
Propellant cost:	**47.75**	**g**
Pointing to target (22.5º change)	*41*	*g*
Increase/decrease of angular speed (with RW)	*0*	*g*
Counteraction of SRP (off-load RW per 24h)	*6.39*	*g*
Required time:	**21.5**	**h**
Pointing to target (22.5º change)	*8.3*	*s*
Stabilisation after repointing	*30*	*min*
Changing the ITD total time (23 times)	*11.6*	*h*
(Changing the ITD 1m, AOCS	*2*	*min)*
(Changing the ITD 1m, Mechanisms	*5*	*min)*
(Changing the ITD 1m, Structures	*23*	*min)*
Observation	*8.9*	*h*
Data Rate:		
Calibration every UV-point	***392***	***Gbit***
Calibration every UV-plane	***131***	***Gbit***

Table 5-21: Impact of One uv-Plane Scan

One UV-line scan		
Propellant cost:	**456.7**	**g**
Pointing to target (22.5º change)	*36.0*	*g*
Stopping the rotation	*208.7*	*g*
Spin-up after observation	*208.7*	*g*
Counteraction of SRP (off-load RW per 24h)	*3.3*	*g*
Required time:	**12.77**	**h**
Pointing to target (22.5º change)	*28.7*	*s*
Stabilisation after repointing	*30*	*min*
Stopping the rotation	*48.3*	*s*
Stabilisation after stopping the rotation	*30*	*min*
Changing the ITD total time (23 times)	*11.6*	*h*
Observation	*9*	*min*
Spin-up after observation	*48.3*	*s*
Data Rate:		
Calibration every UV-point	***7.13***	***Gbit***
Calibration every UV-plane	***2.64***	***Gbit***

Table 5-22: Impact of One uv-Line Scan

The cost of adding a uv-line scan with a given angle, 15°, 45° and 90°, to the first line is given in Table 5-23, Table 5-24 and Table 5-25 respectively.

15°		
Delta Propellant (1N thrusters)	**75.90**	**g**
Delta Propellant (10N thrusters)	**240.03**	**g**
Delta Time (1N thrusters)	**12.80**	**h**
Retracting the telescopes to the hub	*30.0*	*min*
Changing the UV-plane position	*4.0*	*min*
Stabilisation after position change	*30*	*min*
Changing the ITD total time (23 times)	*11.6*	*h*
Observation	*8.9*	*min*
Delta Time (10N thrusters)	**12.76**	**h**
Retracting the telescopes to the hub	*30.0*	*min*
Changing the UV-plane position	*1.3*	*min*
Stabilisation after position change	*30*	*min*
Changing the ITD total time (23 times)	*11.6*	*h*
Observation	*8.9*	*min*
Data Rate:		
Calibration every UV-point	***7.13***	***Gbit***
Calibration every UV-plane	***2.64***	***Gbit***

Table 5-23: Impact of adding one uv-Line Scan with a 15° Angle Change

45°		
Delta Propellant (1N thrusters)	**131.47**	**g**
Delta Propellant (10N thrusters)	**415.75**	**g**
Delta Time (1N thrusters)	**12.85**	**h**
Retracting the telescopes to the hub	*30.0*	*min*
Changing the UV-plane position	*6.9*	*min*
Stabilisation after position change	*30*	*min*
Changing the ITD total time (23 times)	*11.6*	*h*
Observation	*8.9*	*min*
Delta Time (10N thrusters)	**12.77**	**h**
Retracting the telescopes to the hub	*30.0*	*min*
Changing the UV-plane position	*2.2*	*min*
Stabilisation after position change	*30*	*min*
Changing the ITD total time (23 times)	*11.6*	*h*
Observation	*8.9*	*min*
Data Rate:		
Calibration every UV-point	***7.13***	***Gbit***
Calibration every UV-plane	***2.64***	***Gbit***

Table 5-24: Cost of adding one uv-Line Scan with a 45° Angle Change

90°		
Delta Propellant (1N thrusters)	**185.93**	**g**
Delta Propellant (10N thrusters)	**587.95**	**g**
Delta Time (1N thrusters)	**12.90**	**h**
Retracting the telescopes to the hub	*30.0*	*min*
Changing the UV-plane position	*9.8*	*min*
Stabilisation after position change	*30*	*min*
Changing the ITD total time (23 times)	*11.6*	*h*
Observation	*8.9*	*min*
Delta Time (10N thrusters)	**12.79**	**h**
Retracting the telescopes to the hub	*30.0*	*min*
Changing the UV-plane position	*3.1*	*min*
Stabilisation after position change	*30*	*min*
Changing the ITD total time (23 times)	*11.6*	*h*
Observation	*8.9*	*min*
Data Rate:		
Calibration every UV-point	***7.13***	***Gbit***
Calibration every UV-plane	***2.64***	***Gbit***

Table 5-25: Cost of adding one uv-Line Scan with a 90° Angle Change

Around 320 targets per year can be observed (full uv-plane scans), when including time for observation, communication, retargeting and orbit maintenance and excluding calibration. It was decided to include also 35 uv-line scans per year in the propellant budget, see Table 5-26. The design has ample margin to realise the final observation scheme, or for an extension of the lifetime.

In Propellant budget:	
Total nr of UV-plane scans:	**1600.00**
Nr of UV-plane scans (per year)	*320.00*
Nr of years	*5.00*
Total nr of UV-line scans:	**175.00**
Nr of UV-line scans (per year)	*35.00*
Nr of years	*5.00*

Table 5-26: Total Number of uv-plane and uv-line scans in the propellant budget

5.5 Requirements Compliance

In the following tables (Table 5-27 to Table 5-33) the compliance of the design with the requirements are stated. Where possible they have been quantified. It shall be noted that all requirements have been met except and that the spacecraft was not compatible with a Soyuz launch and therefore launch with Ariane 5 has been taken as baseline and except for the total cost of the mission. To meet several of the requirements, technology development will be required. Refer to the Technology Development Plan CDF-49(C) for details.

Requirement ID (Prefix-#)	Requirement Level	Title	Required		Achieved	Compliance (Y/N)	Rationale and/or Comments
PM - Programmatic Requirements							
PM.SCH Schedule and Budget							
PM.SCH-1	1-Drivers	Schedule		2020-2025	End 2024	Y	
PM.SCH-2	1-Drivers	Design life		5 years	5 years	Y	
PM.SCH-3		Technology Readiness				Y	
PM.SCH-4	1-Drivers	Launch Vehicle Selection		Soyuz, Ariane 5	Ariane 5	Y	

Table 5-27: Programmatic Requirements Compliance Table

Requirement ID (Prefix-#)	Requirement Level	Title	Required		Achieved	Compliance (Y/N)	Rationale and/or Comments
MS - Mission Systems Requirements							
MS.OBS Observation Strategy							
MS.OBS-1	2-Space Segment	Observation angles		±45deg	±45deg	Y	
MS.OBS-2	2-Space Segment	uv-coverage				Y	
MS.OBS-3	2-Space Segment	Geometric resolution		0.5	0.5	Y	
MS.OBS-4	2-Space Segment	uv-coverage strategy			concentric circles	Y	
MS.LOP Launch and Orbit Parameters							
MS.LOP-1	2-Space Segment/Ground Segment	Orbit			L2-orbit	Y	
MS.LOP-2	2-Space Segment/Ground Segment	Orbit-Visibility				Y	
MS.GSO Ground Station and Operations							
MS.GSO-1	2-Ground Segment	Data collection, S/C monitoring and control				Y	
MS.GSO-2	2-Ground Segment	Data delivery				Y	
MS.GSO-3	2-Ground Segment	Data reliability and delivery timeliness				Y	

Table 5-28: Mission System Requirements Compliance Table

Requirement ID (Prefix-#)	Requirement Level	Title	Parent ID (Prefix-#)	Required		Achieved	Compliance (Y/N)	Rationale and/or Comments
SS - Spacecraft System Requirements								
SS.GEN - Spacecraft General Requirements								
SS.GEN-1	2-Space segment	Height	PM.SCH-5				Y	
SS.GEN-2	2-Space segment	Diameter	PM.SCH-5				Y	
SS.GEN-3	2-Space segment	Launch Frequencies	PM.SCH-5				Y	
SS.MAR - Spacecraft Margin Philosophy								
SS.MAR-1	2-Space segment	Link Budget					Y	
SS.MAR-2	2-Space segment	System margin					Y	
SS.MAR-3	2-Space segment	Maturity margin					Y	
SS.MAR-4	2-Space segment	Power margin					Y	
SS.MAR-5	2-Space segment	Propellant margin					Y	
SS.MAR-6	2-Space segment	AOCS impulse					Y	

Table 5-29: Spacecraft System Requirements Compliance Table

Requirement ID (Prefix-#)	Requirement Level	Title	Required		Achieved	Compliance (Y/N)	Rationale and/or Comments
IR - Interferometer Requirements							
IR.GEN - General Interferometer Requirements							
IR.GEN-1	3-Subsystem	Type				Y	
IR.GEN-2	3-Subsystem	Wavelength range	wavelength range	25-300μm, 25-500μm (goal)	25-300μm	Y	
IR.GEN-3	3-Subsystem	Angular Resolution		0.25" @ 30μm, 2.5" @ 300μm	0.25" @ 30μm, 2.5" @ 300μm	Y	
IR.GEN-4	3-Subsystem	Field of view (FOV)		1' (Disc)	1' (Disc)	Y	
IR.GEN-5	3-Subsystem	Line sensitivity		1E-21W/m2			
IR.GEN-6	3-Subsystem	Spectral resolution	spectro-meter	~3000 at 150μm	~3000 at 150μm	Y	
			photometer	~ 3	~ 3	Y	
IR.OPT - Optics Requirements							
IR.OPT-1	3-Subsystem	Size		1m	1.02m	Y	
IR.OPT-2	3-Subsystem	Temperature		<5K	<5K	Y	
IR.DFR - Detector and Filter Requirements							
IR.DFR-1	3-Subsystem	Detector temperature		<100mK	Bath at 50mK	Y	
IR.DFR-2	3-Subsystem	Sensitivity		~10 mJy			
IR.DFR-3	3-Subsystem	NEP photometry		1E-18W/√Hz	1E-18W/√Hz	Y	Requires technolgy development
IR.DFR-4	3-Subsystem	NEP spectroscopy		1E-20W/√Hz	1E-20W/√Hz	Y	Requires technolgy development

Table 5-30: Interferometer Requirements Compliance Table

Requirement ID (Prefix-#)	Requirement Level	Title	Required		Achieved	Compliance (Y/N)	Rationale and/or Comments
BR - Boom Requirements							
BR.GEN - Boom Structural Requirements							
BR.STR-1	3-Subsystem	Boom length		2x14m booms	2x14m booms	Y	
BR.STR-2	3-Subsystem	Stiffness		±0.5deg	±0.5deg	Y	

Table 5-31: Boom Requirements Compliance Table

Requirement ID (Prefix-#)	Requirement Level	Title	Required		Achieved	Compliance (Y/N)	Rationale and/or Comments
SC - Service Module Requirements							
SC.ACS - Spacecraft AOCS Requirements							
SC.ACS-1	3-Subsystem	APE		13"	8.6"	Y	
SC.ACS-2	3-Subsystem	AME		0.017"	0.017"	Y	Covered by the Optics Subsystem
SC.DHS - Spacecraft DHS Requirements							
SC.DHS-1	3-Subsystem	Data Storage	calibration per uv-plane	292Gbits	1280Gbits	Y	
			calibration per uv-point	828Gbits	1280Gbits	Y	
SC.COM - Spacecraft Communications Requirements							
SC.COM-1	3-Subsystem	Frequency band		Ka 26GHz	Ka 26GHz	Y	
SC.COM-2	3-Subsystem	Freq band option		Shall be considered	Option incl in report	Y	
SC.POW - Spacecraft Power Requirements							
SC.POW-1	3-Subsystem					Y	
SC.THE - Spacecraft Thermal Requirements							
SC.THE-1	3-Subsystem					Y	
SC.STR - Spacecraft Structure Requirements							
SC.STR-1	3-Subsystem					Y	
SC.MEC - Mechanism Requirements							
SC.MEC-1	3-Subsystem	Telescope carrier mechanism		1cm		Y	

Table 5-32: Service Module Requirements Compliance Table

Requirement ID (Prefix-#)	Requirement Level	Title	Required		Achieved	Compliance (Y/N)	Rationale and/or Comments
PL - Payload Module Requirements							
PL.THE - Spacecraft Thermal Requirements							
PL.THE-1	3-Subsystem	Mirror Temperature		5K	4K	Y	
PL.THE-2	3-Subsystem	Detector temperature		100mK	100mK	Y	

Table 5-33: Payload Module Requirements Compliance Table

6 CONFIGURATION

6.1 Requirements and Design Drivers

6.1.1 Requirements

The configuration shall comply with the following requirements:

- Shall fit in an existing fairing of the Ariane 5 Launcher (Small, Medium or Large Fairing)
- Shall interface with the launcher through an adapter
- Shall accommodate 2 telescopes that can move along an axis such that a maximum distance of 30 m could be attained
- Shall accommodate optical benches in a central hub between the two telescopes
- Shall accommodate all the required thermal shields, solar panels and radiators
- Shall accommodate electronic boxes and other equipment of all subsystems.

6.1.2 Design Drivers

The following aspects have driven the design:

- Maximum mutual distance between the two telescopes of 30m
- Load path of the design in launch configuration.

6.2 Baseline Design

In Figure 6-1 the whole composite with a height of 6.4m and a maximum diameter of 3.8m, is shown inside the Ariane 5 medium fairing which has a usable volume diameter of 4.57m. The fully deployed configuration is shown in Figure 6-2.

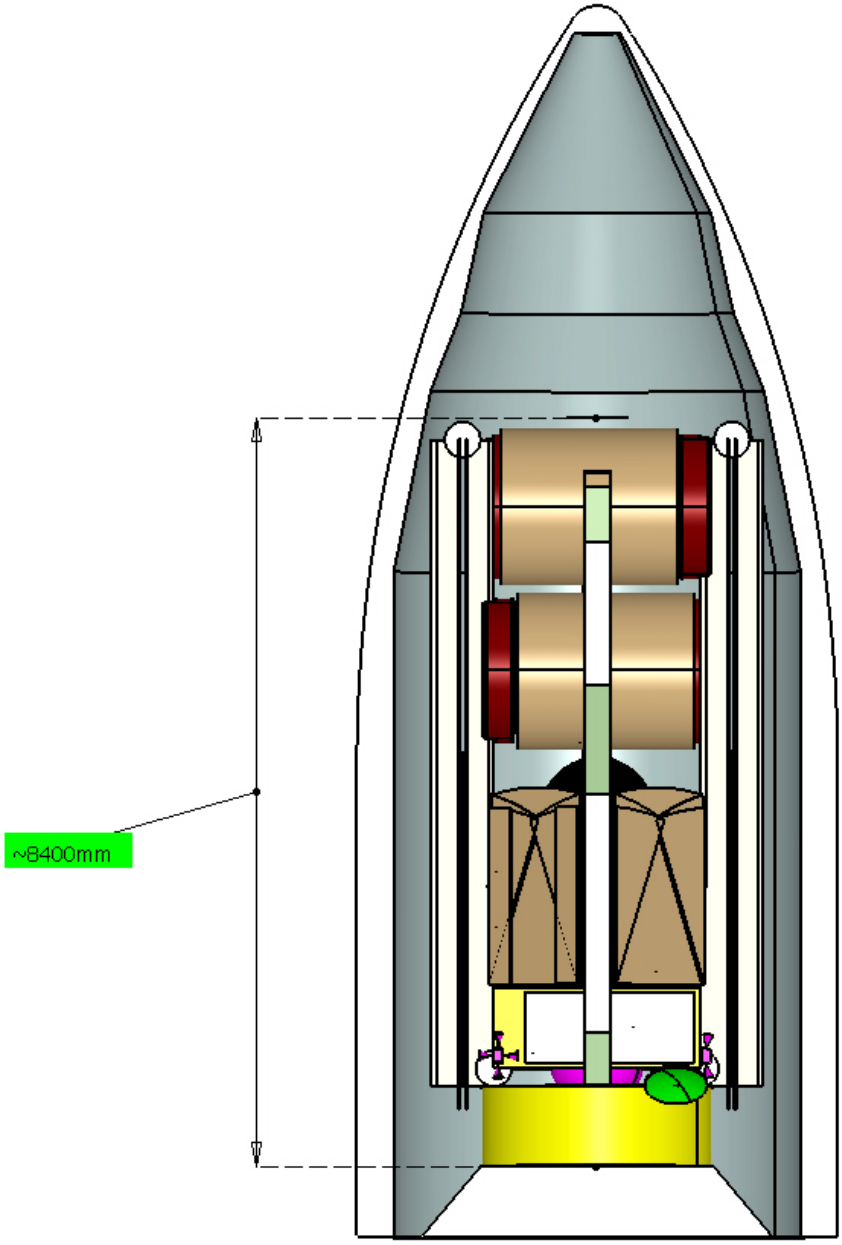

Figure 6-1: Stowed configuration inside Medium Fairing Ariane 5

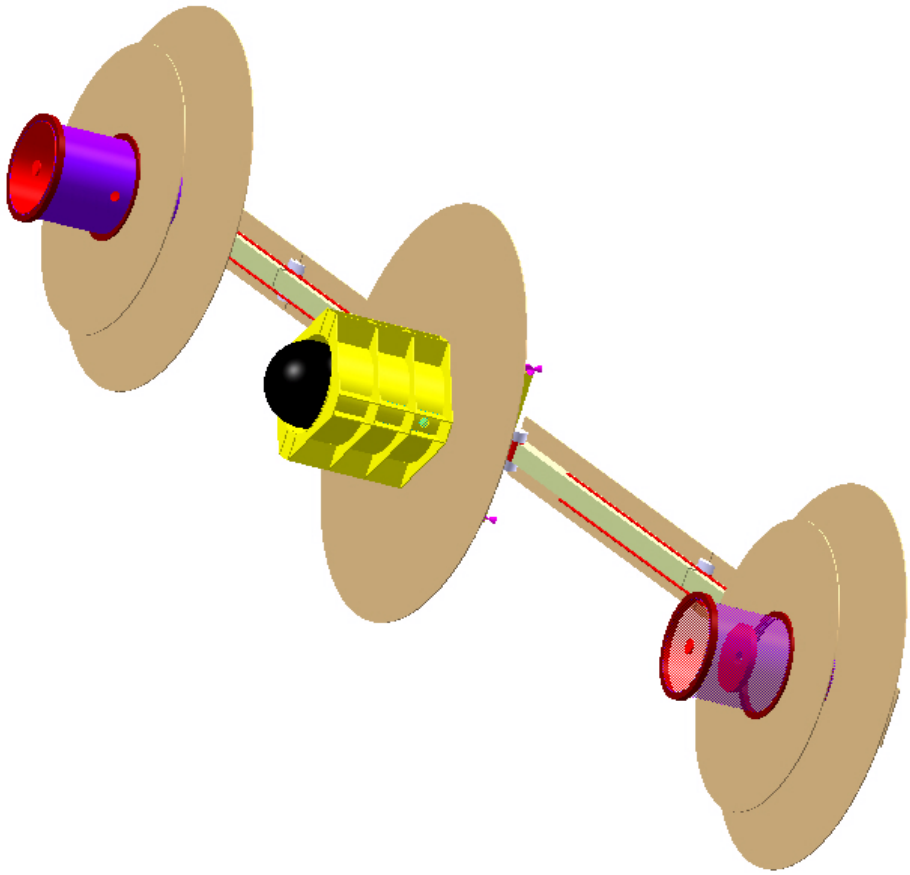

Figure 6-2: Fully deployed configuration

In Figure 6-3 the main parts are shown:

- Dedicated Launch Vehicle Adapter (LVA);
- Central Hub consisting of:
  - Service Module (SVM)
  - Payload Module (PLM)
- Telescope 1
- Telescope 2
- Structural support beams.

Each telescope has its own dedicated service module underneath the optical compartment. The temperature in the SVM of the telescopes is similar to the SVM of the Hub at room temperature whereas the temperature inside each optical compartment is kept very low. The temperature inside the Payload Module of the Hub is kept very low as well.

In total there are four structural beams that support the telescopes and the hub. These beams transfer the inertia loads of the main parts to the LVA I/F during launch.

A dedicated cylindrical adapter is proposed for FIRI with a diameter of 2624 and a height of 900 mm. This height is required to distribute over the circumference the 4 concentrated loads of the

four structural support beams, such that the over flux load at the interface with the launcher is within acceptable limits.

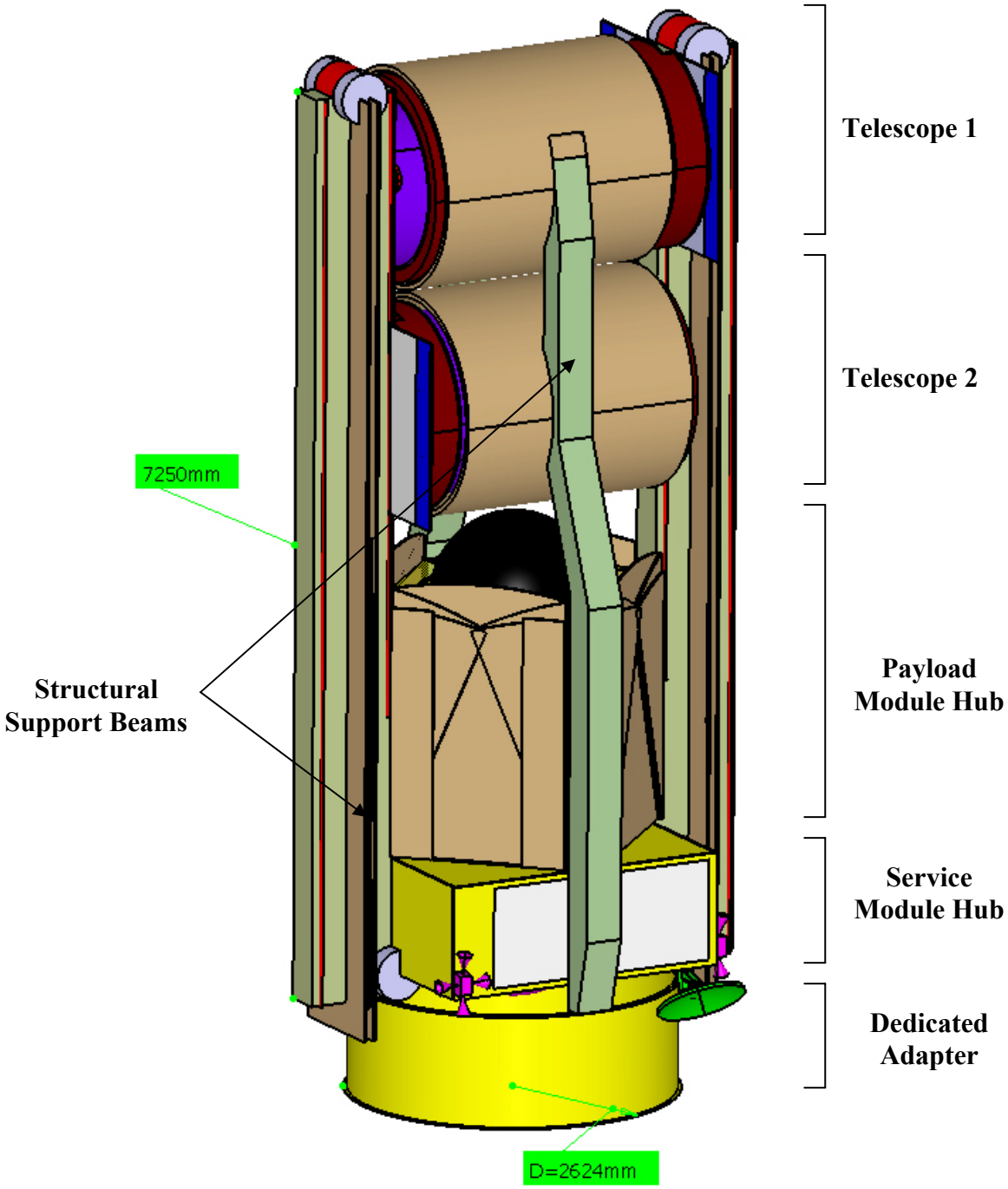

Figure 6-3: Stowed configuration

In Figure 6-4 the ejection from the LVA is shown. Two structural support beams are disposed. The other two structural support beams remained and are connected to the SVM of the hub by

hinges. Each of those remaining support beams actually consists of two parts. After deployment, they served as support for the movable telescopes, making it possible that the two telescopes could get the required mutual distance of 30m. This is illustrated in Figure 6-5 to Figure 6-7.

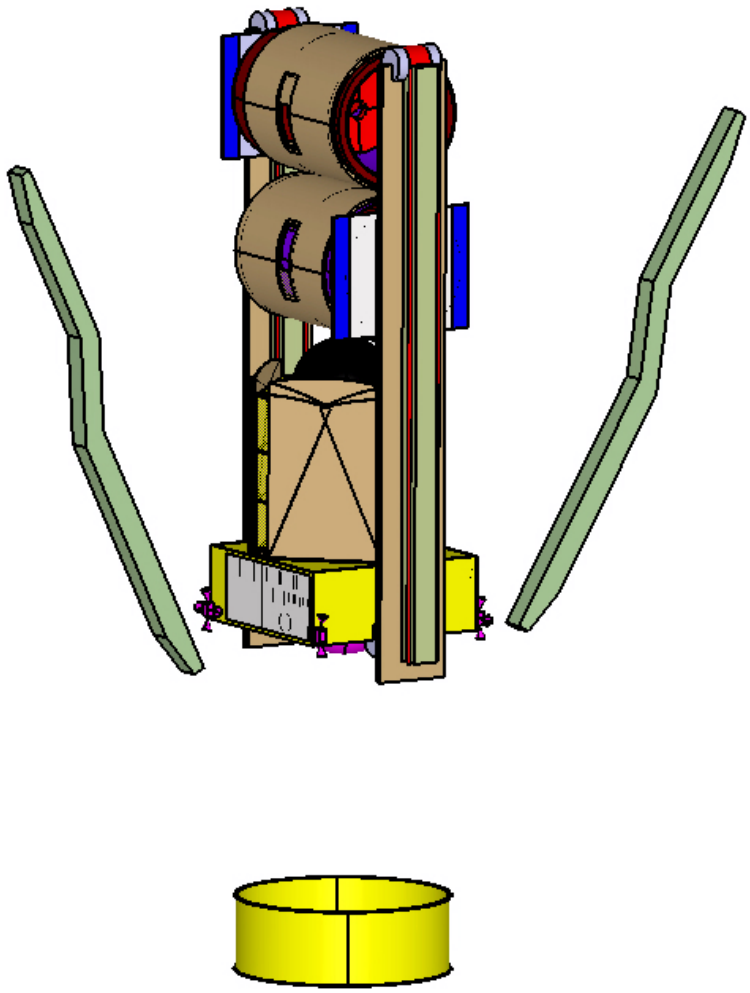

Figure 6-4: Ejection from the launcher

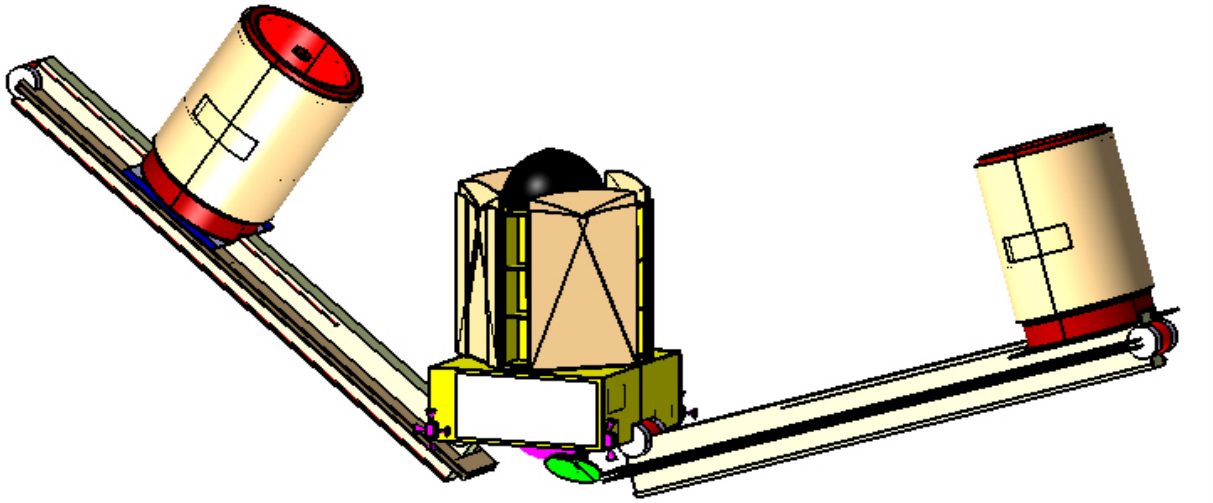

Figure 6-5: First phase deployment of the remaining structural support beams

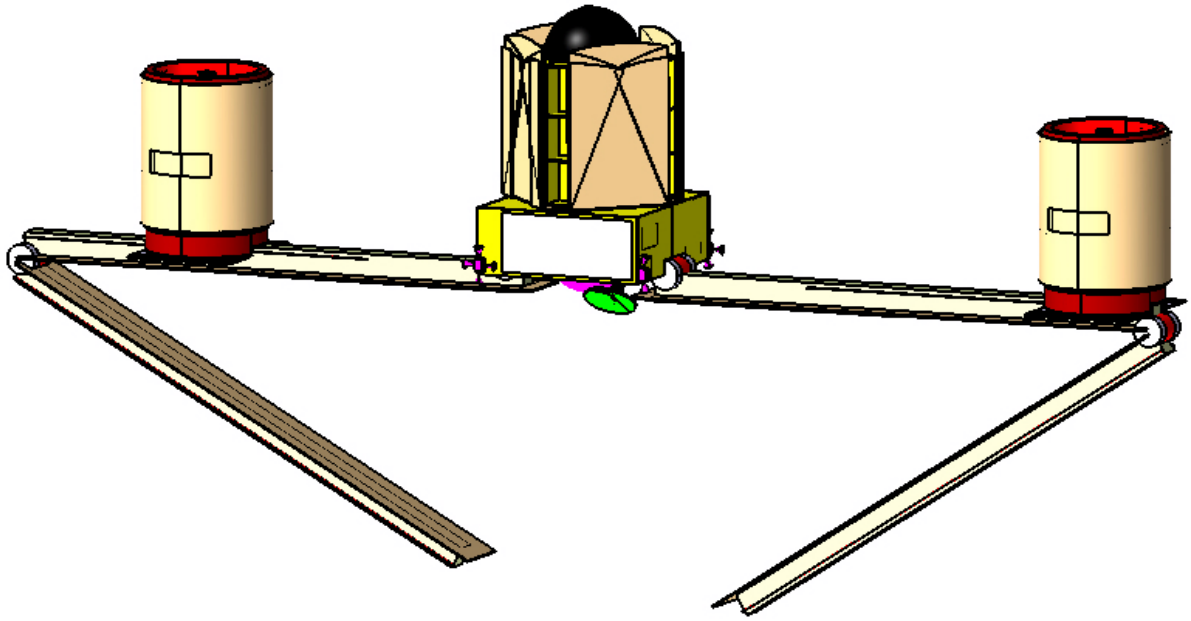

Figure 6-6: Second phase deployment of the remaining structural support beams

The maximum distance between the telescopes is 30 m. This is shown in Figure 6-7. The minimum distance between the telescopes is 8.2m. This is shown in Figure 6-8. The thermal shields prevent any closer distance.

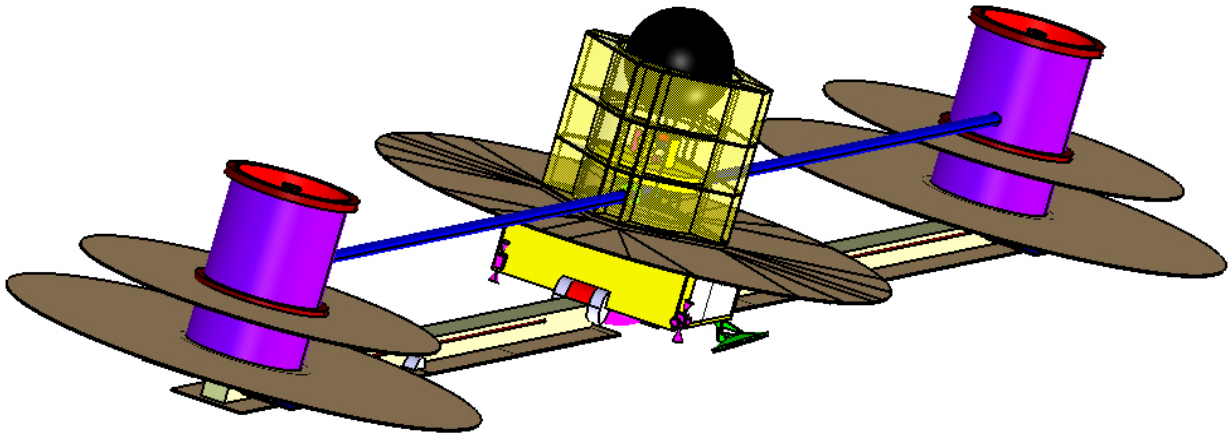

Figure 6-7: Telescope 1 and 2 at its maximum distance of 30m

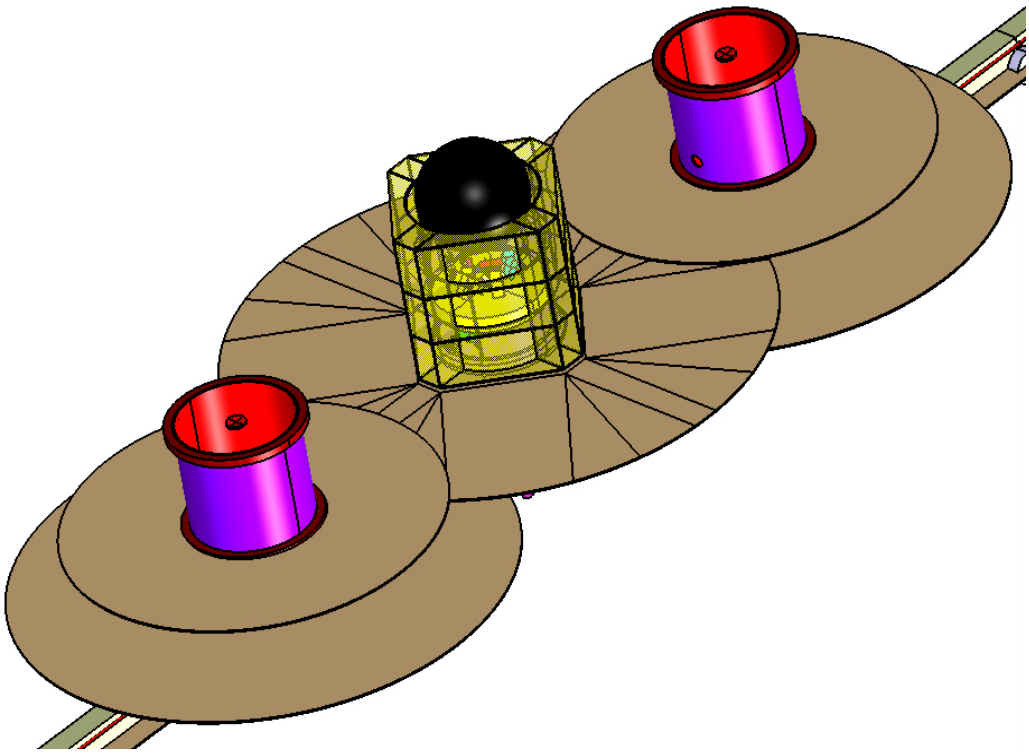

Figure 6-8: Minimum distance between Telescope 1 and 2

In Figure 6-9 the deployment of the thermal shield of the PLM of the hub is shown. It opens like an umbrella and should protect the PLM, including the Cryostat (black sphere), from the sun, keeping them always in the shadow (sun angle is 45 degrees).The diameter of the thermal shield is 6.3m.

Also the telescopes have to be protected from the sun. Each telescope has two thermal shields with a diameter of 4.4m and 5.8m respectively. The distance between those shields is 0.74m.They will be deployed in a similar way as the thermal shield of the Hub.

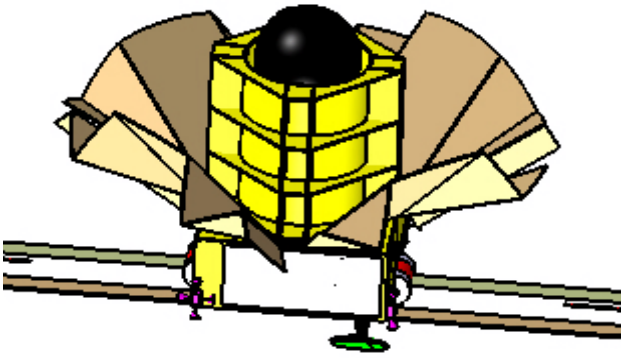

Figure 6-9: Deployment of the thermal shield of the PLM of the Hub

In Figure 6-10 the optics of the Hub are shown. All the parts fit inside a cryogenic vessel. The diameter of this vessel is 1300mm and has a height of 1000mm (see Figure 6-11). This vessel is contained in two other vessels. The dimensions of those two other vessels are shown in Figure 6-12 and Figure 6-13.

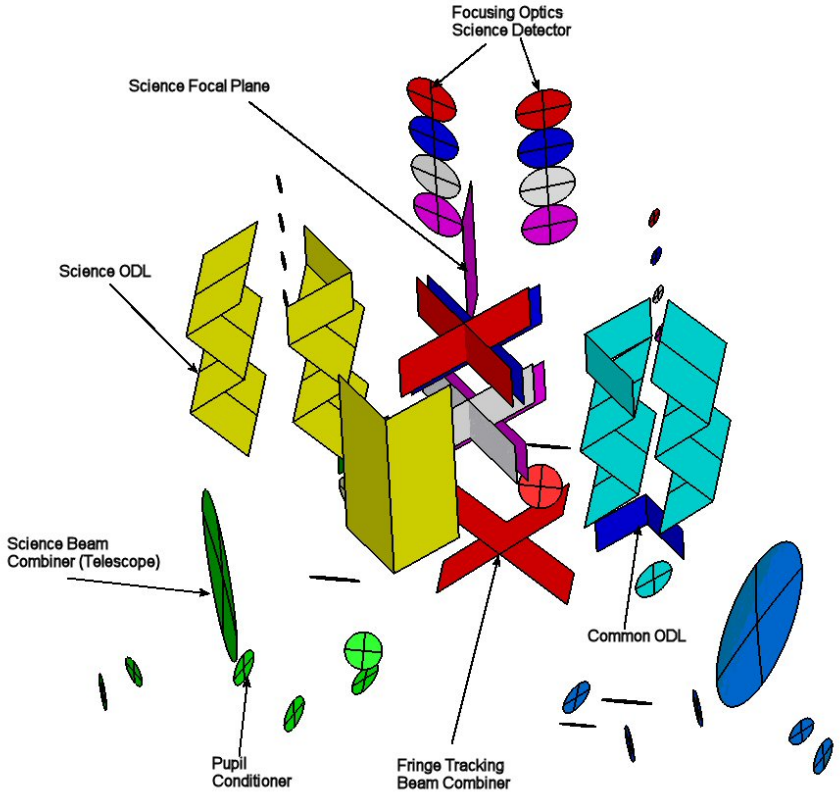

Figure 6-10: Optics Hub

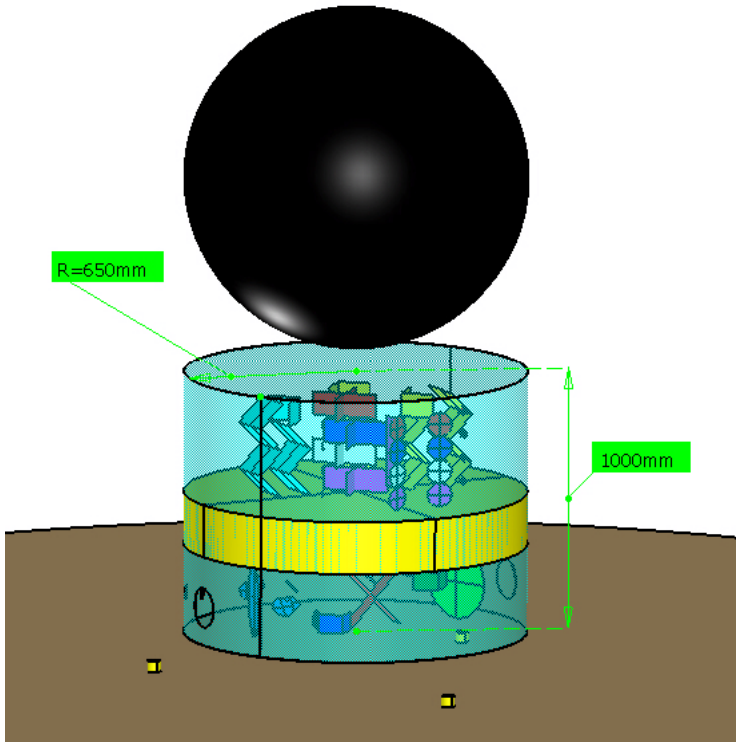

Figure 6-11: Optics inside Cryogenic Vessel 1 beneath Cryostat

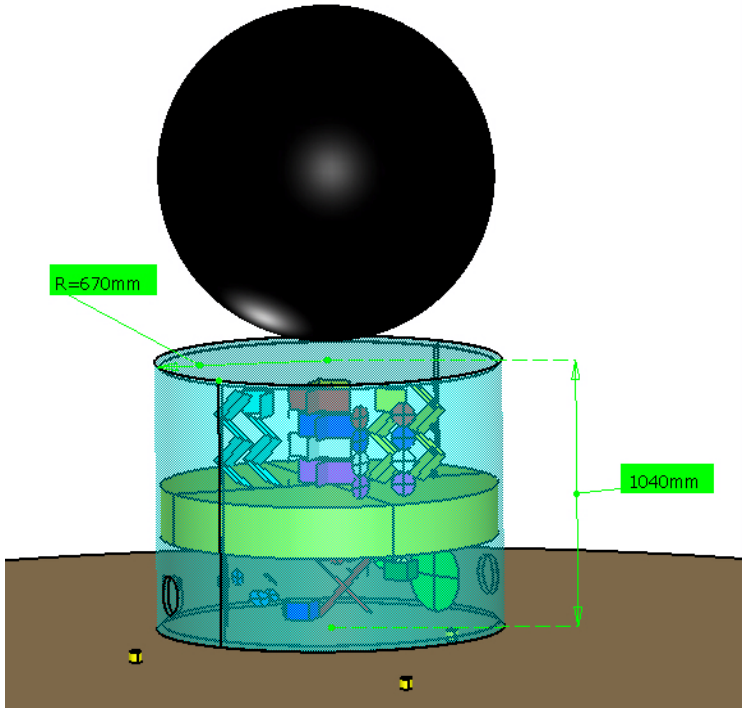

Figure 6-12: Cryogenic Vessel 2 and Cryostat

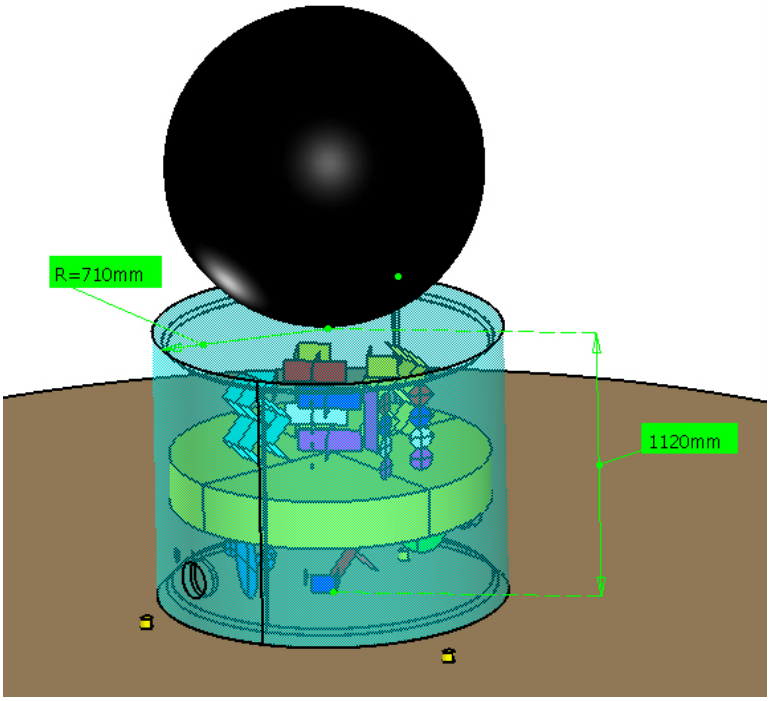

Figure 6-13: Cryogenic Vessel 3 and Cryostat

The vessels and the Cryostat are supported by a structure (yellow coloured) which can be seen in Figure 6-14. Note the apertures in the cryogenic vessels and in the structure as well on both sides for vision between the optics in the hub and the mirrors in both telescopes. The diameter of the central cylinder is 1500mm and its height is 1890mm. Shear panels are required to attach the structure to the four structural support beams. The bottom and the top panel together with the horizontal panels stiffen the structure. The 'box' is let open to increase the required radiating area. The diameter of the Cryostat is shown as well and is 1.3m.

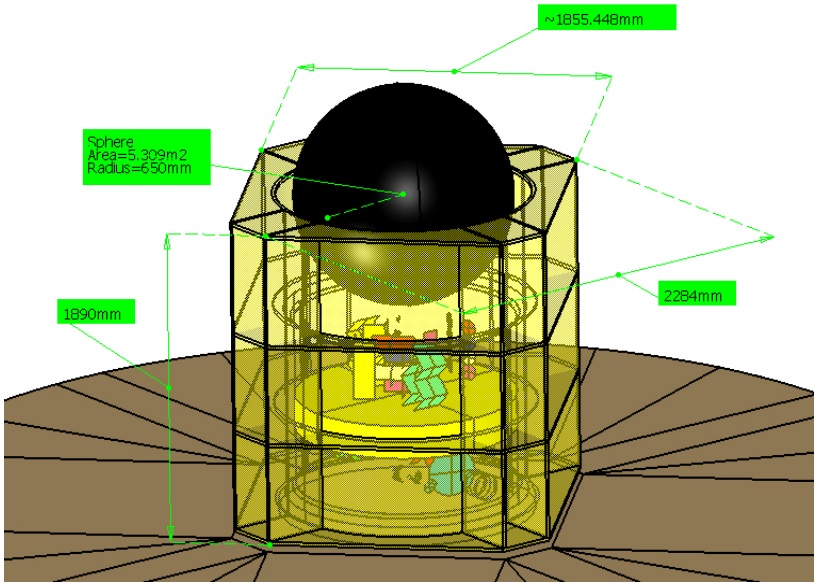

Figure 6-14: Structure of the Payload Module of the Hub

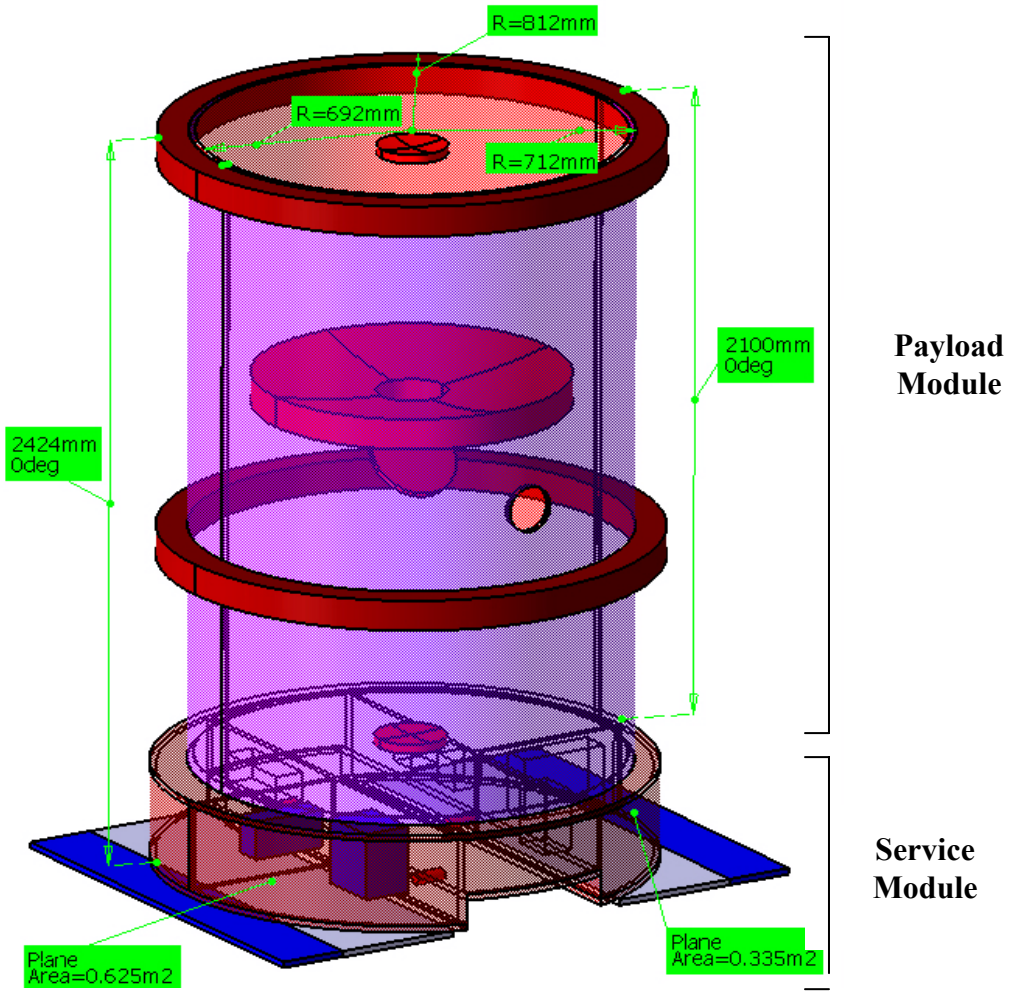

Figure 6-15: Telescope

In Figure 6-15 one of the two telescopes is shown. The total height is 2424mm. The lower part is the Service Module which is kept at room temperature. Above it is the Payload Module. It contains the four mirrors which are kept at a very low temperature inside a dedicated optical compartment (outer radius is 692mm). During launch the two parts are attached stiff to each other. In operation mode the Payload Module is mounted iso-statically on top of the Service Module.

The structure consists of three ring frames (outer radius is 812mm) and a cylinder structure (outer radius = 712mm). The frames are attached to the four support beams during launch and are released in orbit. Finally the telescope, through the Service Module, will be attached to one of the two remaining structural support beams with three bearings that could glide on two rails on the support beam.

Inside the Service Module the following equipment are accommodated: 6 electronic boxes of the Communication Subsystem and the battery and PCDU of the Power Subsystem. Furthermore

each telescope is equipped with its own solar panels (area 2 x 0.335m^2) and radiators (area is 2 x 0.625m^2).

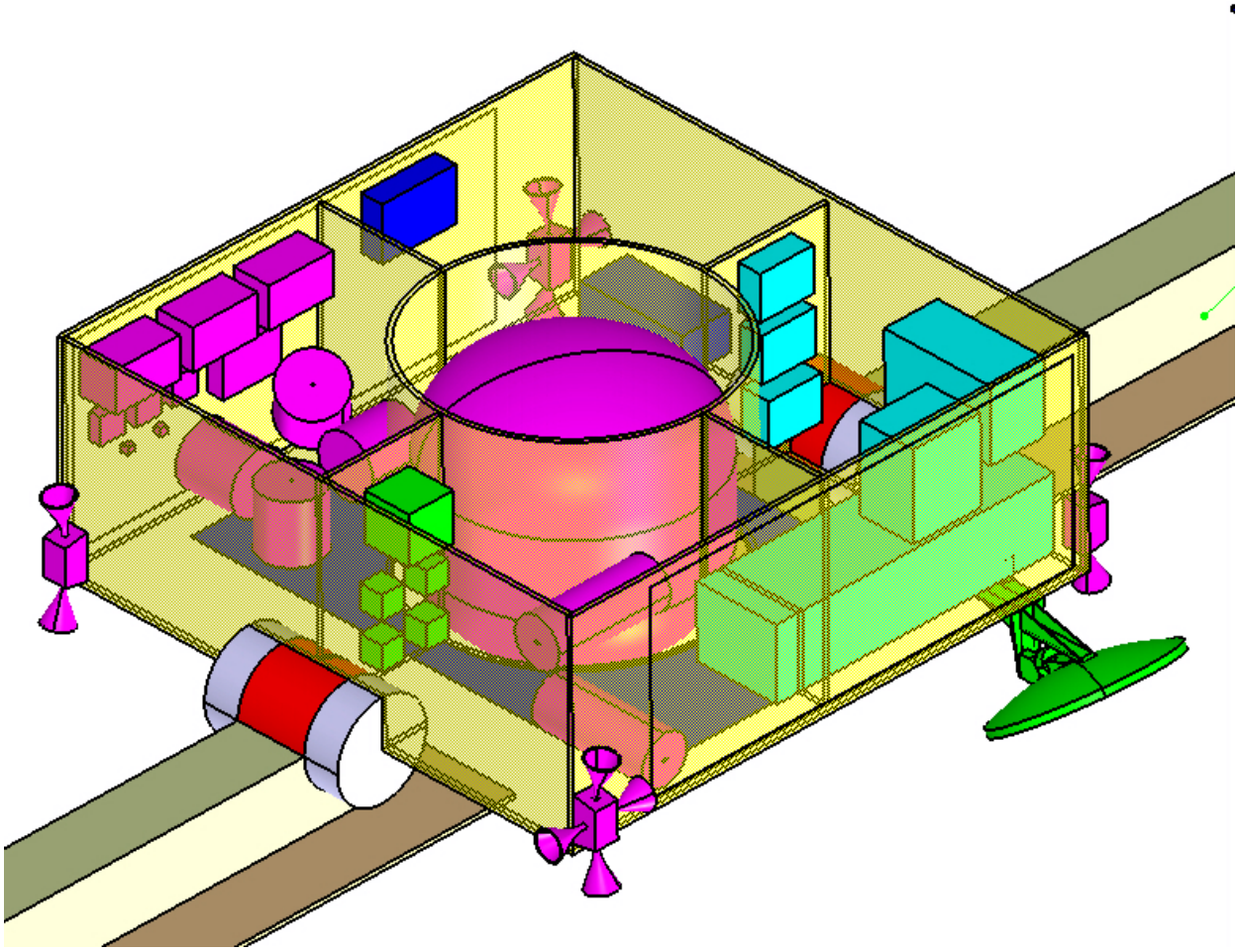

Figure 6-16: Service Module of Hub (top view, without top panel and PLM)

In Figure 6-16 the Service Module of the Hub is shown. It consists of a central cylinder (outer diameter 1190mm) that carries the propellant tank (volume approximately 700 litre), four shear panels, four lateral panels and a top and bottom panel. The outer dimensions of the box are 2324mm by 2324mm. The height of the box is 900mm. During launch 4 brackets connect the SVM to the four support beams. Two of those support beams remain attached to the Hub through hinges. The dimension of the cross section of a beam is 300mm by 300mm. Each beam has a thermal shield of 900mm width.

Also the equipment is shown: purple are AOCS units, dark blue are Power units, light blue are DHS units and green are Communication units. The SVM is also equipped with a solar panel on the bottom panel with an area of 1.827m^2. This area is complemented with extra area on the bottom of the beams (2 times 3m^2), see Figure 6-17. Two opposite sides of the SVM have radiators. Each radiator has an area of 1.52m^2.

In orbit the Payload Module of the Hub is attached iso-statically to the Service Module; similar to the Payload Module of a telescope.

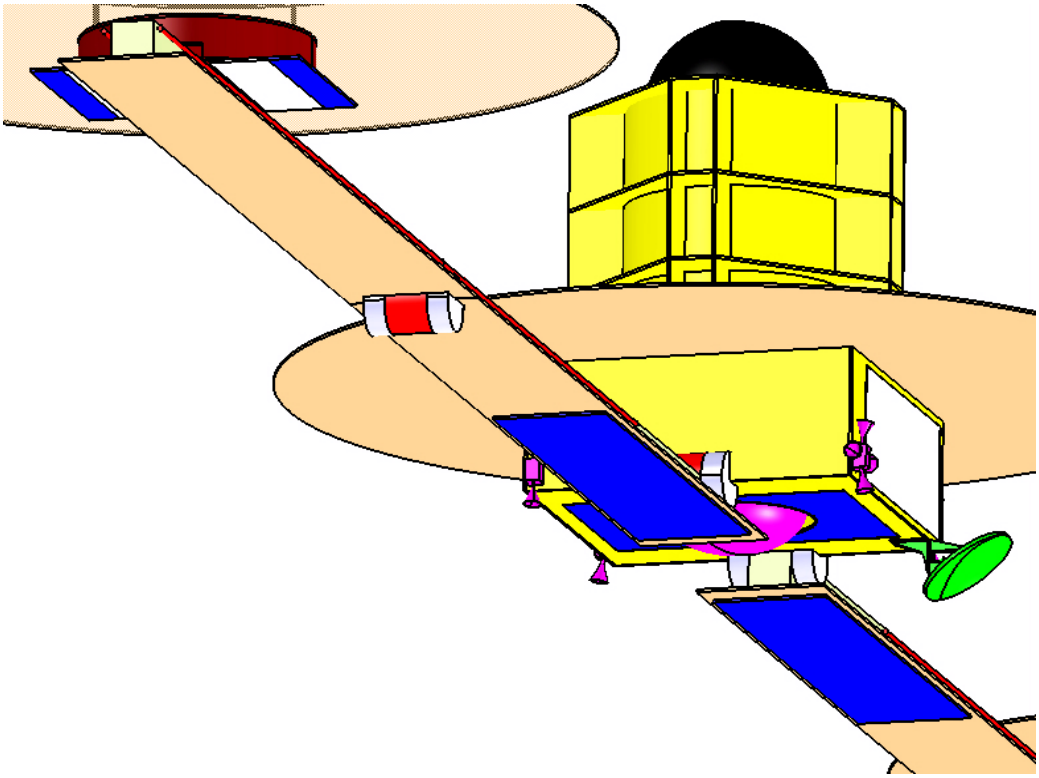

Figure 6-17: Service Module of Hub (bottom view with PLM)

6.3 Structural Analysis

6.3.1 Eigen-Frequency Analysis of Stowed Configuration

A Finite Element Method (FEM) model of the stowed configuration was created to check that the structure is stiff enough to meet the eigen-frequency requirements for the Ariane 5.

6.3.1.1 Model Assumptions

Clamped boundary conditions were assumed at the LV payload adaptor.

It was assumed that both the inboard and outboard segments of each boom carry loads during launch.

The SVM was assumed to have two connections on each side (at its top and bottom panels) to the respective boom or structural support beam. A similar assumption was made for the PLM.

The load paths between the booms, structural support beams, PLM and SVM remain open points for further study. Determination of the optimal load paths (via the corresponding HDRM) into the SVM and PLM would need to take into account the dynamic and thermoelastic behaviour of the intergrated stack, which was beyond the scope of this study.

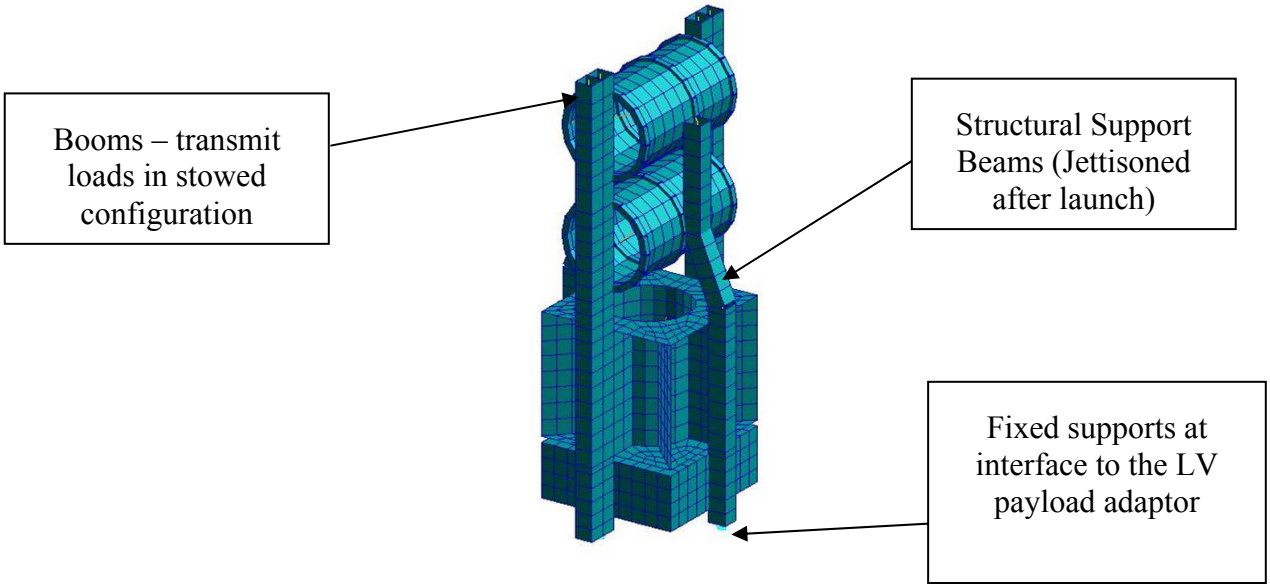

Figure 6-18: FEM Model of Stowed Configuration

The first three vibration modes of the stowed configuration are shown in Figure 6-19.

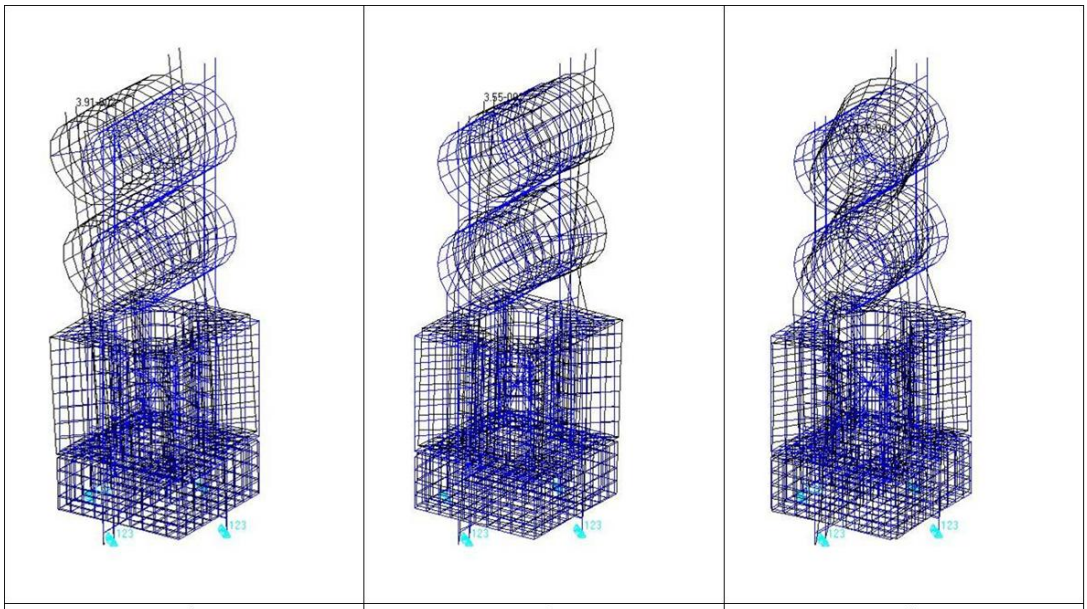

Mode 1	Mode 2	Mode 3
Lateral X-direct	Lateral Y-direction	Torsion Z-axis
13.5Hz	15.9Hz	28.6Hz

Figure 6-19: Results of Eigen-Frequency Analysis

The results are summarised in Table 6-1, which also includes the frequency requirements for the Ariane 5 launcher (with additional 15% margin for analysis). The FIRI structure satisfies all the relevant frequencies.

Mode	Frequency Requirement (Ariane 5)	Requirement with 15% margin	FIRI
Lateral X	9Hz	10.4Hz	13.5Hz
Lateral Y	9Hz	10.4Hz	15.9Hz
Torsion	-	-	28.6Hz
Longitudinal	31Hz	35.7Hz	>44Hz

Table 6-1: Summary of Eigen-Frequency Analysis

6.3.2 Dynamic Response Analysis of Deployed Configuration

Each retargeting or translation of the telescopes along the booms will excite vibration modes of the structure. The FIRI configuration has long booms and relatively heavy point masses (telescopes), which will have vibration modes with low damping and thus, long decay times. The vibration decay time will directly impact available science time, although notches can be applied to the controllers to reduce excitations of any significant modes.

To assess the dynamic response, a FEM model (see Figure 6-20) was constructed for the satellite in the deployed configuration. It was assumed that the worst case dynamic response occurs when the telescopes are located at (or near) the tip of the booms.

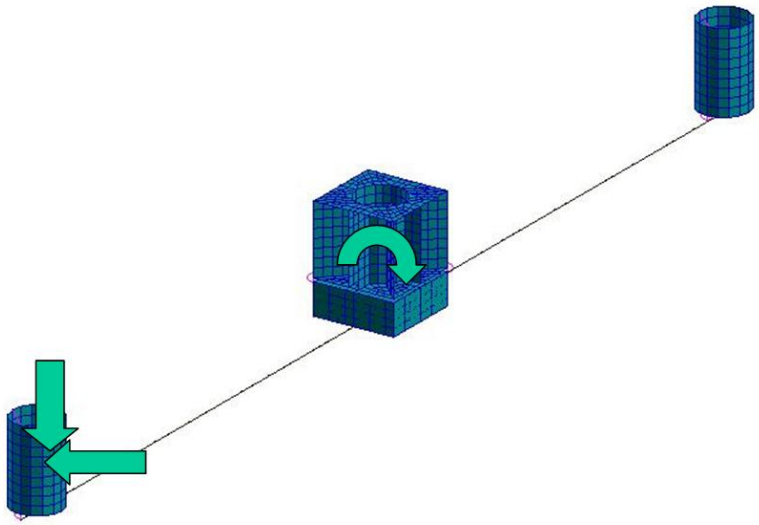

Figure 6-20: FEM Model of the Deployed Configuration

Damping is difficult to predict but experience on other slender spacecraft bodies has shown that the following typical damping factors (percent of critical damping) that can be expected:

- Typical un-damped slender body modes: 0.1%-1%
- Passive damping (e.g. visco-elastic layers): 2-10 times more then un-damped
- Active damping (e.g. piezo-layer, tuned mass): 5-40 times more than un-damped

A modal analysis of the stowed configuration produced the first 6 modes shown in Figure 6-21. The lowest mode is 0.25Hz.

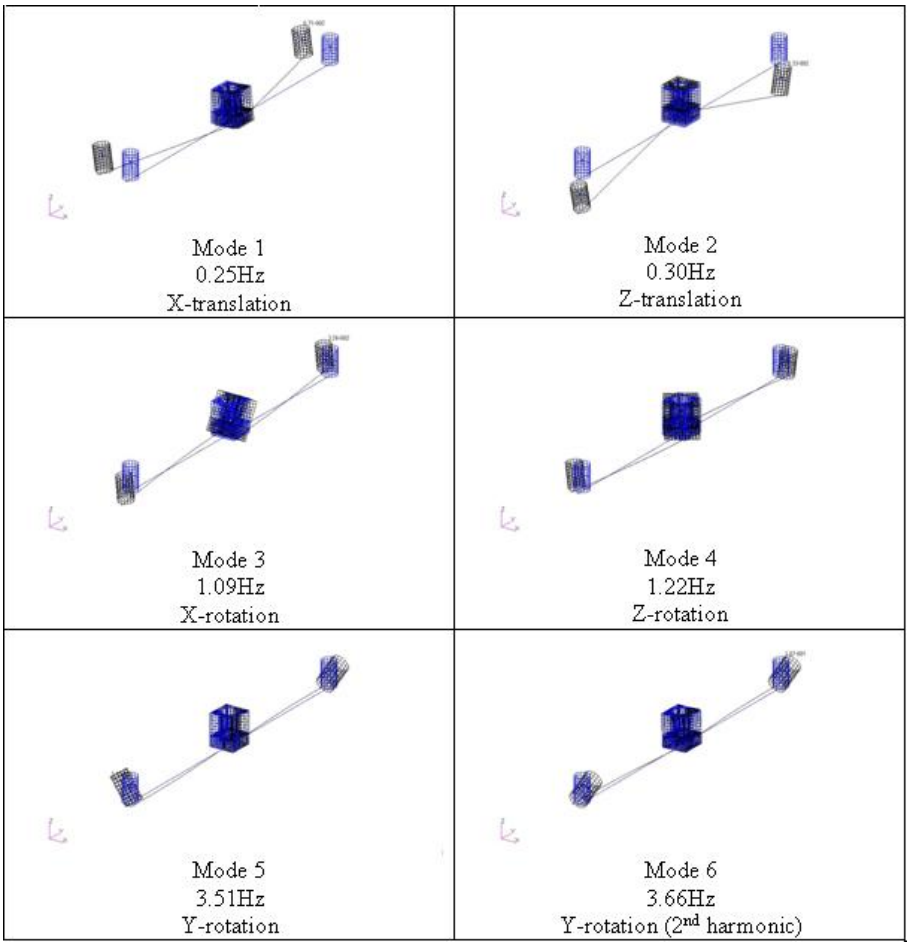

Figure 6-21: First 6 Vibration Modes of Deployed Configuration

The load transfer between the mechanism of the telescope and the beam is critical and contains large uncertainties.

6.3.2.1 Harmonic Response to AOCS Inputs

Harmonic response analysis was conducted for AOCS inputs such as those used to re-target the spacecraft. The AOCS inputs were represented as torques applied at the hub.

The displacement response was calculated as a gain with respect to the input torque. A range of damping ratios was considered. The results are shown in Figure 6-22. Similar graphs can be constructed for other control inputs and responses. This information is used to design filters for the AOCS.

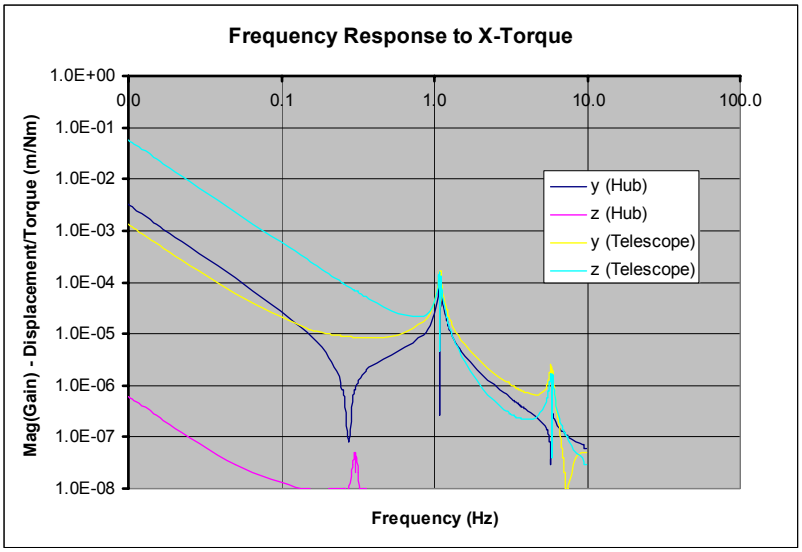

Figure 6-22: Harmonic Response to Torque about X-axis at Hub (Damping 1% of Critical)

6.3.2.2 Transient response to Telescope repositioning

The following assumed acceleration time history was for the telescopes are:

- 0 - 20 s: $0.1 mm/s^2$
- 20 - 230: $0 mm/s^2$
- 230 - 250: $-0.1 mm/s^2$

It is noted that there is a delay of 210s between the initial acceleration and the deceleration. Significant damping occurs during this time period so as a simplification, only the response to one acceleration/deceleration event was considered.

The mass of the telescopes was assumed to be 500kg. Thus the acceleration profile was represented as a 20s pulse of outwards force acting on the centre of mass of the each telescope (in opposing directions). The magnitude of this force was $0.1 \times 10^{-3} m/s^2 \times 500kg = 0.5N$. The transient response of the system due to this input was calculated and the displacements of the hub and telescopes are shown in Figure 6-23.

The left graph of Figure 6-23 shows a rapid decay in displacement response, in which the amplitude is below 1 micron after 50s. This response would be expected for a system that has some form of enhanced damping (either passive or active).

The right graph of Figure 6-23 shows a more gradual decay. After 80s the amplitude is below 10microns. This response is considered more realistic for a simple un-damped system. Therefore, all displacement responses are well below the required maximum tip displacement of 5 cm. However, the effects of boom dynamics on the optics has not been assessed during this CDF study.

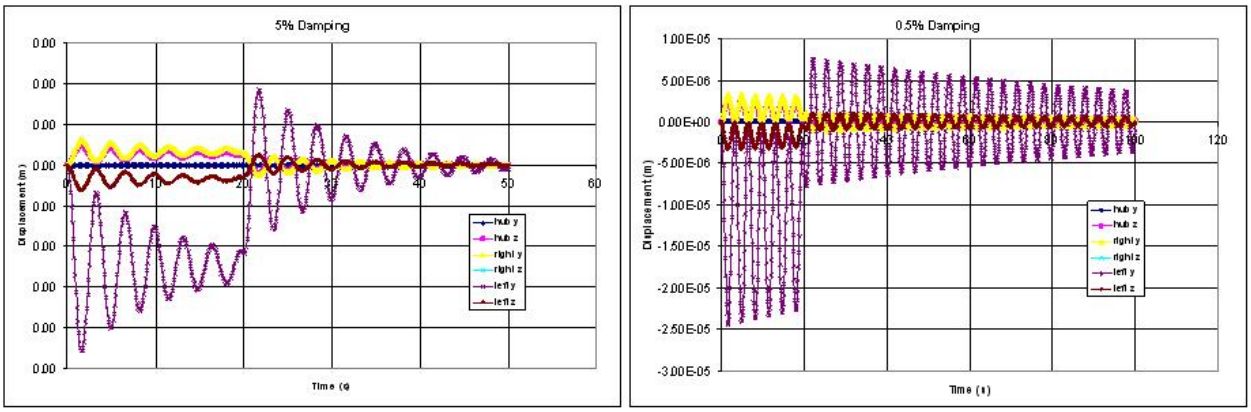

Figure 6-23: Transient response to Telescope Deceleration for 5% and 0.5% of Critical Damping

7 PAYLOAD MODULE

7.1 Optics

7.1.1 Introduction

Because of the degrading effects of the Earth's turbulent atmosphere, the spatial resolution achieved by ground based optical astronomy is limited to the extent of the seeing disk - the image of a point source (e.g. a single star), taken through the atmosphere. The size of the seeing disk is independent of telescope diameter, but changes only with wavelength and climatic conditions. In the absence of atmosphere turbulences (for instance in space or with adaptive optics on ground), the resolution of a telescope with a single aperture is limited by the diffraction which scales inversely with telescope pupil diameter.

The achievable resolution with single space-based telescopes is not enough for many areas of astronomical research. Indeed, imaging extrasolar planets would require telescope diameters of at least 100 metres. This is currently out of reach of the state-of-the-art technology in telescope launching and manufacturing.

Such resolutions are achievable by interferometry and a technique called synthesis imaging or aperture synthesis which was developed and implemented on ground. This technique is based on the interference of the electromagnetic waves coming from different telescopes or antennas observing the same object. The principles are discussed in detail in 7.1.2.1.

Originally developed for observations in the millimetre and above spectral range, aperture synthesis was adapted for ground based observations in visible and near-infrared (NIR) spectral range. Various ground based telescopes and observatories like the Very Large Telescope (VLT), the Keck observatory, the Large Binocular Telescope (LBT) have successfully performed observations of astronomical objects using this technique.

Such techniques applied for space-based observation will overcome the resolution limitation discussed above while keeping the other advantages linked to space environment:

- Access to the entire electromagnetic spectrum (ultraviolet, mid-infrared)
- Turbulence free environment
- The frame time is not limited by Earth rotation.

There are also some drawbacks. For FIRI, the mechanical vibrations of the structure linking the telescopes must be minimised and even low-noise structures, residual motions must be actively corrected. This issue makes the operation of a space interferometer to the required extreme precision very challenging.

7.1.2 Description

7.1.2.1 Principles (RD[5]) of aperture synthesis technique

The aperture synthesis technique is based on the theory of wave diffraction. The basic result is summarised in the Van Cittert-Zernike theorem which states that the complex degree of coherence μ is equal to the normalized Fourier transform of the source intensity distribution.

The parameter μ is a complex quantity. In practice its phase and amplitude are measured. They can be derived from the interference pattern of the light from the source obtained when combining two light beams coming from two apertures separated by a distance B, commonly named Baseline or Inter-Telescope Distance (usually it is named Baseline, but has been changed to avoid confusion with the "baseline design") and by adding an Optical Path Difference (OPD) to one beam. Figure 7-1 illustrates the principle. The baseline introduces an OPD between the two wavefront coming from the two telescopes thus creating interference fringes when coherently combined. The scanning of the OPD is done with the delay line, the fringe pattern will change in time domain accordingly to the OPD applied.

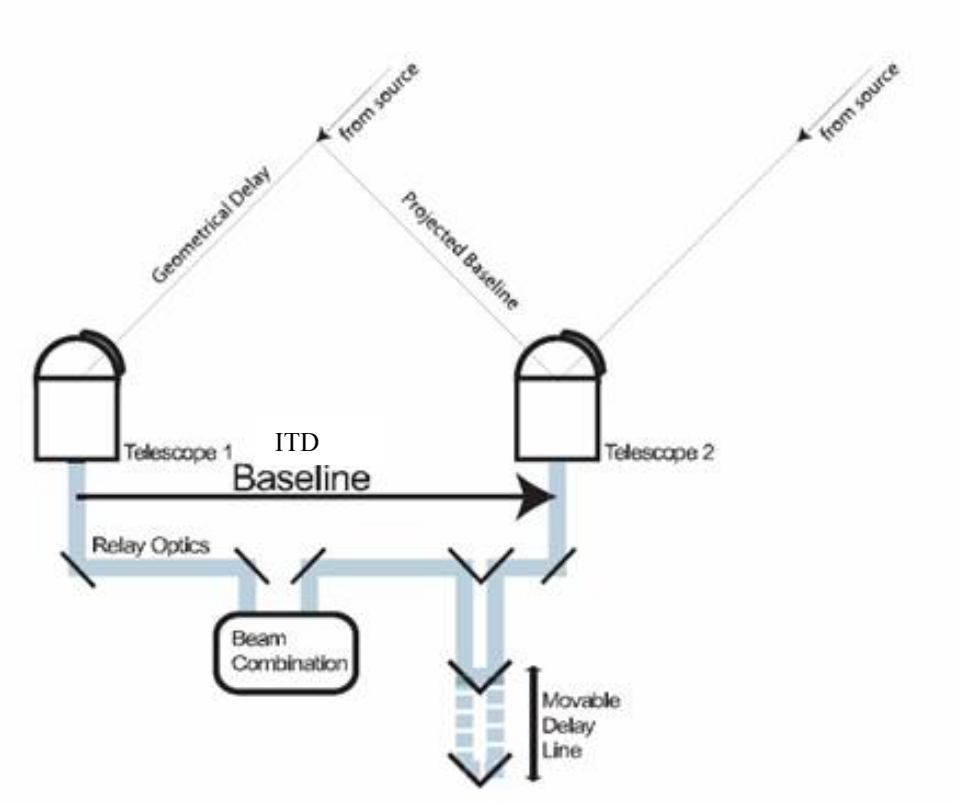

Figure 7-1: Principles of Aperture Synthesis Technique

Because the coherence quantity is the Fourier transform of the spatial distribution of the source intensity, μ is measured in the plane (uv) which is the Fourier conjugated plane of the plane (ITD_X, ITDy), with $u = \frac{ITD_x}{\lambda}$ and $v = \frac{ITD_y}{\lambda}$, U and V are the spatial frequencies, ITD_x and ITD_y are the inter telescope distance projection on the sky frame. The sampling of the uv-plane is achieved by changing the distance between the two telescopes and by rotating the line (base) linking the centre of the telescopes pupils.

In theory the source structure can be fully reconstructed via an inverse Fourier transform provided that the uv-plane coverage is complete. However, in practice, such coverage will have gaps leading to ambiguity in the source reconstruction. The ring-like residuals in Figure 7-2.d are one example of such ambiguities. The regularly spaced sampling points in the uv-plane introduce in the final image periodic artefacts which can be removed to a certain extent by numerical image post-processing algorithms (RD[5]).

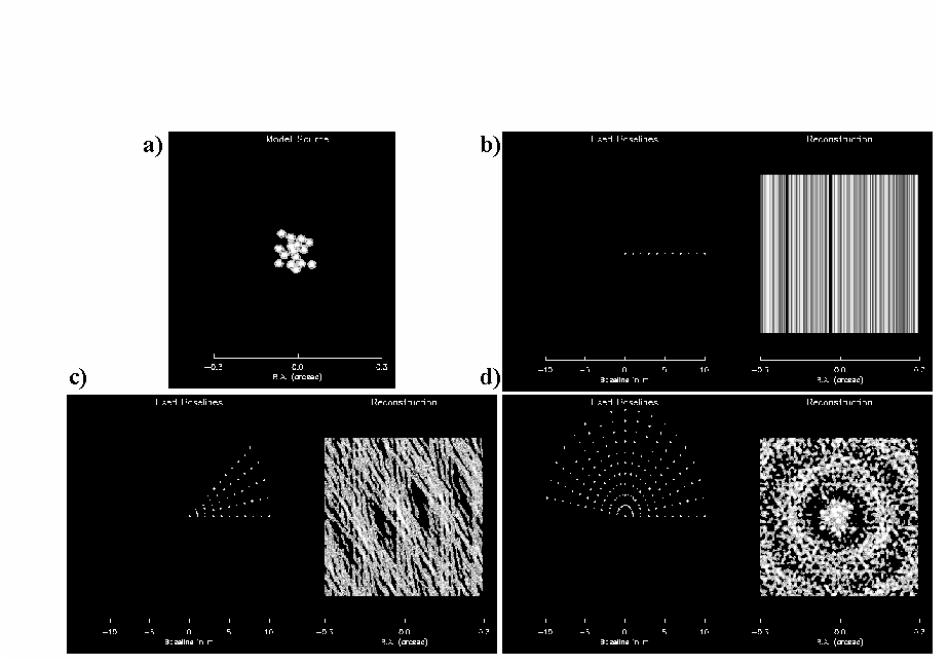

Figure 7-2: Principle of synthesis imaging (a) model source to be imaged, (b) – (d) image reconstruction (right) for various interferometer inter telescope distance distribution (left)

7.1.2.2 Resolution

As a first approximation, the maximum resolution is given by the longest inter telescope distance, i.e λ/ITD_{max}.

Nevertheless, since each point in the uv-plane corresponds to a certain frequency, emphasis can be put on specific resolution by applying weighting coefficients to the data obtained at different positions in the uv-plane or even by removing some points.

7.1.2.3 Interferometric Field of view (IFOV)

The IFOV (θ) is defined as being the area of the detector where data can be extracted without ambiguity (RD[8]).
The light coming from the source is emitted in a large bandwidth, thus the IFOV of an imaging interferometer is limited by the coherence length of the light, $L_c = \lambda^2/\Delta\lambda$, where λ and Δλ are the wavelength and the spectral bandwidth of observation. While the path lengths from the two interferometer elements ideally are equal in the centre of the field, an angular separation θ from the centre necessarily produces a path difference θITD. As long as this difference is small compared with L_c, the fringe contrast will not be affected, thus $\theta \leq \left(\frac{\lambda^2}{ITD \times \Delta\lambda} \right)$. The spectral bandwidth can be adjusted so the IFOV covers the Airy disk diameter of a single telescope.

7.1.2.4 Beam combination techniques

This paragraph deals with the beam recombination scheme which is not detailed in Figure 7-1. Two methods for beams recombination were envisaged in this study. The main specifics of each are presented below.

7.1.2.4.1 Image plane recombination (Fizeau Configuration)

In this configuration, the images of the object are overlapped onto the detector surface RD[11]. The fringes then appear in the image plane. The fringe pattern is modulated by the diffraction pattern on each point of the field of view. The image plane is thus filled with Young's fringes.

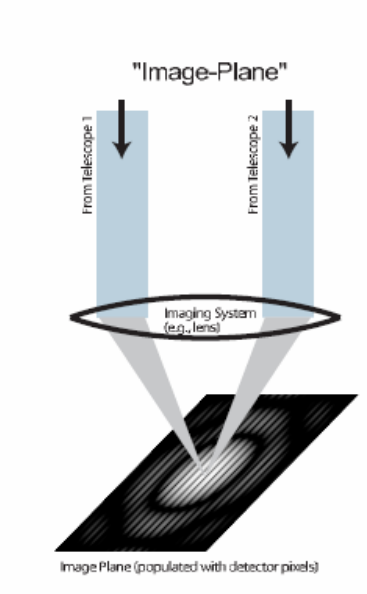

Figure 7-3: Image plane recombination

In this mode, the fringes sampling by the detector must respect the Nyquist's criteria consequently detectors with a large number of pixels might be required depending on the maximum number of fringes in the diffraction pattern.

The field of view in Fizeau recombination is larger than the diffraction limited primary beam.

7.1.2.4.2 Pupil plane recombination (Michelson Configuration)

The wavefront coming from the two telescopes are overlapped on an amplitude beamsplitter. The fringes are then formed at infinity and are imaged on the detector surface. If the Optical Path Difference (OPD) is zero, one does obtain the well-known Haidinger's fringes pattern. In order to measure the amplitude of the coherence, an OPD is applied to one of the two beams before recombination and the resulting intensity change is recorded in time (Figure 7-4 and RD[11]).

The light from off-axis sources which delay are larger than the coherence length are incoherently overlapped thus no fringe appear but during the OPD scanning, the delay corresponding to those sources will at a certain time be compensated by the added OPD. Consequently fringes will appear at a position in space shifted (due to off-axis angles) on the detector with respect to on-axis and shifted in time depending on the off-axis angle and on the OPD scanning velocity. The limited IFOV can be overcome by the use of a detector array and an optical delay line (ODL) with sufficient stroke (RD[14]).

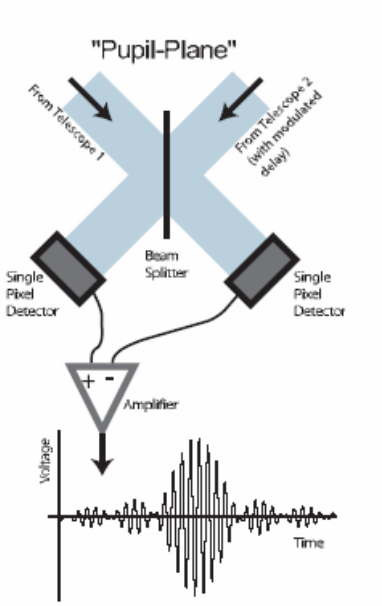

Figure 7-4: Pupil plane combination

7.1.3 Requirements and Design Drivers

Table 7-1 lists the requirements:

Parameter	Value
Science field of view (arcmin)	1 (full cone angle in the sky)
Spectral range (μm)	25 – 300
Maximum spectral Resolving Power	3000
Minimum Resolving Power	3
Pupil diameter	Collecting area equivalent to a 1 meter diameter unobscured pupil
Volume	As small as possible
Maximum inter-telescopes distance	30 meters
Temperature range	Cryogenic (5 K)
Visibility loss	TBD, for the study 10 % has been assumed, resulting in an AME of 17 mas (For information, the SPIRIT specification for uncalibrated visibility degradation is 6%) (RD[29]).

Table 7-1: List of parameters

7.1.3.1 Design drivers and requirements analysis

The design drivers and the analysis discussion are reported in Table 7-2.

Design driver	Analysis
Science field of view	1. The optical requirements of the different optical elements of the instrument apply all over the science field of view, considering the magnification factor at the different stages in the optical chain. In addition to the science FOV, the optical path to the fringe sensor unit (FSU) has to be compatible with the FOV needed for phase-reference and spacecraft attitude control purposes. 2. The science FOV will drive the choice of the beam recombination technique and the design of the beam combiner.
Spectral range	The use of refractive powered optics is excluded at those wavelengths. The design shall use only reflective optical elements. The spectral range might be divided into Several sub-bands in order to relax constraints on the design and on the detectors.
Maximum spectral Resolving power	This parameter will drive the design of the spectrometer. There are two possibilities: 1. A standalone instrument for spectroscopy uniquely 2. A Fourier Transform spectrometer also used for imaging
Pupil diameter	The actual diameter of the pupil shall be oversized in order to fit the requirement.
Volume	The volume of the light collecting telescopes shall be lower than 2 meters in height and 1.5 meters in diameter. The volume of the central hub beam combiner shall be lower than 1.2 meters in height and 1.3 meters in diameter.
Science objectives	1. As an alternative to a single space-based telescope, a stellar optical interferometer is proposed to meet the science objectives. 2. The optical interferometer, in order to operate correctly, needs several highly accurate metrology sub-systems for: • Fringe tracking and zero-OPD locking (i.e. for external OPD monitoring and phase referencing) • Relative tilt/lateral displacement monitoring of the beams • Absolute distance measurement of the inter-telescope distance. • Internal OPD monitoring within the central hub beam combiner 3. Output WFE of optics must be negligible over the science FOV, to avoid fringes visibility degradation. 4. Fringe tracking can not be done using the science target since it may be a faint object. Brighter objects are required and might fall outside the science FOV. Therefore the field of view for the fringe sensor unit (FSU) will be larger than the science field of view. 5. The uv-plane scanning requires that the image of the target on the detector rotates thus the detector shall include entirely the 1 arcmin circular FOV. 6. Polarisation issues must be limited by the use of a optically symmetric configuration (same number and order of S-P reflections, same coatings …)

Design driver	Analysis
Maximum inter-telescopes distances	1. The magnification of light collecting telescopes is limited by light free propagation diffraction along the maximum distance between the light collecting telescopes and the beam combiner (i.e. 15 meters). In order to reduce the size of the optics in the beam combiner, a second beam reduction stage is needed. 2. The distance will drive the choice of the beam mixing technique (RD[18])
Temperature range	To minimize thermal gradient effects (e.g. misalignments, stresses, etc.) the design of the optical units should be athermal and/or should make use of materials with very low CTE.
Visibility loss	All the contributors to visibility loss shall be identified. Their tolerances and/or calibration accuracy will be driven by their contribution to the visibility loss.

Table 7-2: Design driver analysis

7.1.4 Interferometer Instrument Description

7.1.4.1 Layout

Figure 7-5 shows the main sub-systems of the overall interferometer instrument.

Essentially, the interferometer consists of 2 main elements: the light collecting telescopes, located on the boom, and the central hub beam combiner, where the light coming from the collecting telescopes is coherently combined in order to extract the spatial and the spectral information of the science target. The rest of the optical sub-systems in between, e.g. hub relay telescopes, pupil conditioner, ODLs, several metrology systems, etc., are used to condition the two arms of the interferometer in order to attain proper fringes.

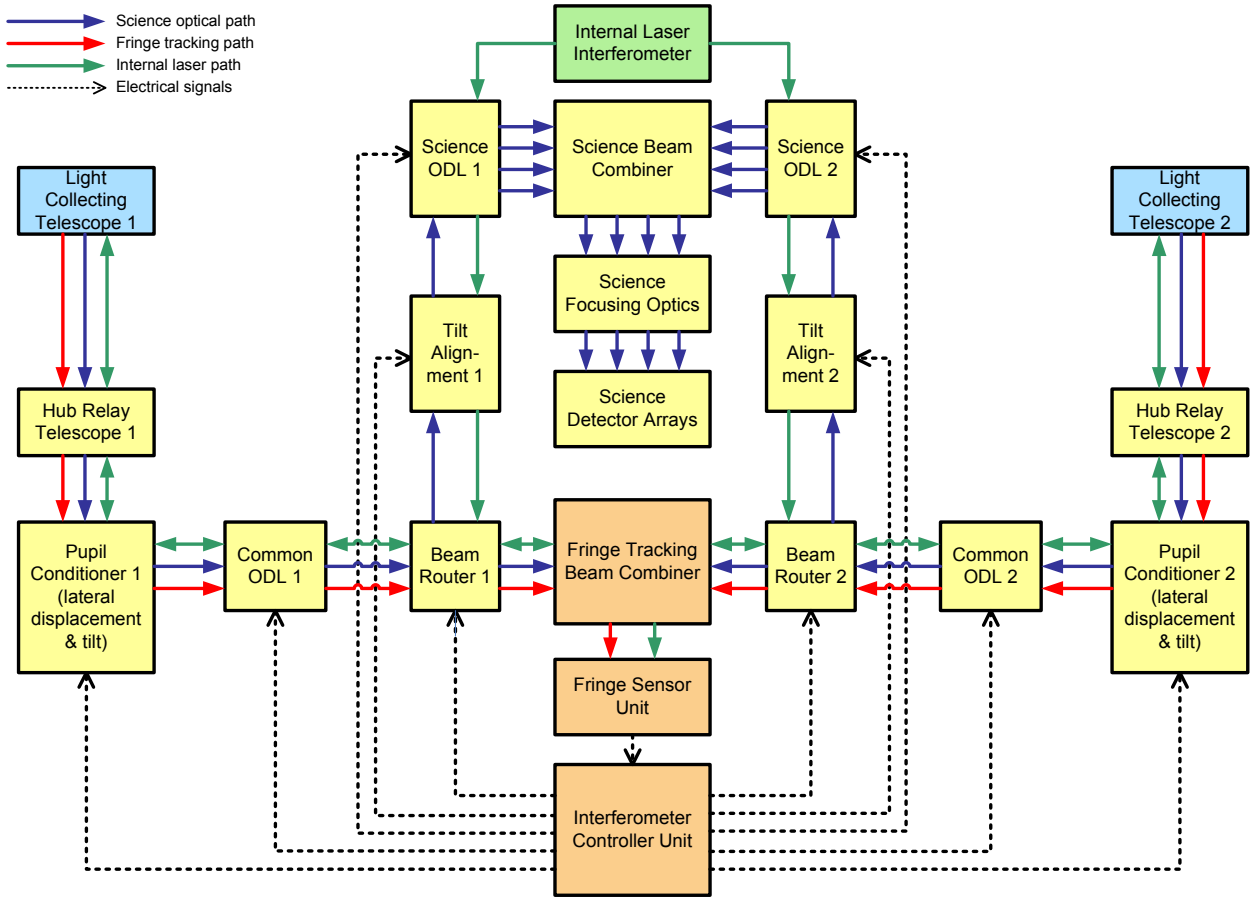

Figure 7-5: Block diagram of the optical interferometer

From the detected signal and the phase reference measured by the Fringe Sensor Unit (FSU) it is possible to extract the information of the complex visibility (i.e. complex degree of coherence μ) at different inter telescope distances (i.e. at different spatial frequencies or uv-points). This information is then used to reconstruct the spatial distribution of the science object under investigation.

The different optical paths (science, fringe tracking and internal metrology signals) are also represented in the interferometer block diagram, and will be described in the following sections.

7.1.5 Instrument Sub-Systems Breakdown (Science)

7.1.5.1 Light collecting telescopes

Those telescopes are afocal and provide a first stage for beam reduction. Their main purpose is to collect light and to provide plane wavefronts. Those two telescopes are identical (same optical characteristics, same optical configuration, same coatings etc…). Their optical axis must point to the same position in the sky in order to have coherent overlapping of the two collimated beams. Their position wrt to the hub and also wrt to each other must be stable during the measurements. Compensation of optical axis relative drift can be implemented via tip/tilt mirrors on both telescopes. In order to perform measurements at different inter telescope distances, the light collecting telescopes are mounted on carriages that move along the boom.

7.1.5.2 Hub relay telescopes

Those telescopes provide a second stage for beam reduction. They are afocal telescopes and are identical. The output wavefront must be, ideally, plane. They are located at the entrance of the hub beam combiner, fixed on the same optical bench as the beam combiner, in order to have a stable position during the measurements.

7.1.5.3 Pupil conditioner

A pair of tip-tilt mirrors provides adjustment of the tilt and the lateral deviation of one arm pupil inside the central hub beam combiner. Any differential tilt and/or lateral displacement offset between the two beams at the science beam combiner contribute to visibility loss, and therefore, have to be carefully controlled by the interferometer controller unit (ICU). For symmetry and redundancy purposes both arms of the interferometer are equipped with a pupil conditioner unit.

7.1.5.4 Optical delay-line (ODL)

An ODL is an opto-mechanical system that is able to introduce well-defined optical path variations without introducing significant wavefront errors, beam tilt and beam lateral deviation, in the full actuation range. There are two type of ODLs, the common ODLs and the science ODLs, both commanded by the interferometer controller unit (ICU).

The common ODL is the actuator used to acquire the fringes of a reference object in the FSU. By locking to the zero-OPD, the closed loop operation of the FSU and the common ODL provides a phase reference (i.e. a phase tracking centre) for the science measurements. The common ODL will compensate for external/internal OPD disturbances, for example, induced by differential deformation of the booms connecting the light collecting telescopes and the central hub beam combiner, or by potential microvibrations generated by the cryocoolers. The common ODL has a short stroke and a fast response, compared to the science ODL. The operating bandwidth will be dictated by the spectrum of the OPD disturbance.

The science ODL is accurately controlled by the internal laser interferometer. It is used to scan the fringes of the science object all over the science FOV. Linearity during the scanning is then a critical parameter. The stroke of the science ODL depends on the chosen beam recombination technique.

Two common ODLs and two science ODLs are needed in order to maintain complete symmetry of the optical trains and redundancy. However, only one of each needs to be actuated (one common ODL and one science ODL) at a time. In order to minimize the torques induced by the moving parts, especially during the fringe acquisition phase, if it is possible, the ODLs should preferably be located close to the centre of mass of the spacecraft and their design should minimize exported micro-vibrations.

7.1.5.5 Beam router

The beam router is responsible for routing the different optical signals (science, fringe tracking and internal laser signals) according to the operational modes of the interferometer. For example, it splits the science and the fringe tracking signals and directs them towards the science beam combiners and the fringe tracking beam combiner respectively. Depending on the operational mode, the beam router will transmit the internal laser signals towards either the light collecting telescopes (fringe acquisition mode) or the FSU (zero-OPD locking, tracking modes, science observation mode).

7.1.5.6 Tilt alignment

The tilt alignment consists of a tip-tilt mirror similar to the ones used in the pupil conditioner unit. It aligns the internal laser metrology to the optical axis of the FSU. The internal laser metrology is aligned with the centre of the science detector arrays.

7.1.5.7 Science beam combiner

The beams from both arms of the interferometer (i.e. science signals) are spatially overlapped in the science beam combiner. The main drivers are the compactness and the symmetry. Although symmetry requirements are not as strict as for nulling inteferometers, it is highly recommendable to have an inherent perfectly symmetric beam combiner, in order to relax the component specifications.

7.1.5.8 Science focusing optics

The overlapped beams are focused to the detector by means of the focusing science optics. Given the spectral range only reflective optics are feasible. For the 4 selected sub-bands, it is highly desirable to have similar focusing optics for each sub-band, in order to reduce complexity.

7.1.6 Metrology Subsystem

7.1.6.1 Fringe tracking metrology sub-system

Many unwanted OPD perturbations may occur during the measurement causing the fringes to move unexpectedly on the detector. One option could be to use the science signal itself to compensate for the OPD perturbations. However, in most of the cases, the signal is too faint, and therefore, insufficient to compensate for the expected spectrum of internal and external OPD disturbances. In that case, a dedicated fringe tracking metrology sub-system using a different spectral range of the science target is required. Likewise the science interferometer, it contains the fringe tracker beam combiner, the fringe tracker focusing optics and the fringe sensor unit.

For FIRI, the fringe tracking metrology has the following functions:

- Fringe tracking and zero-OPD locking (i.e. for external/internal OPD monitoring and phase referencing) of a reference object.
- Spacecraft position & attitude monitoring, in special during science operation mode (e.g. accurate rotation of the interferometer about the science object during the uv-plane scanning)
- Relative tilt/lateral displacement monitoring of the beams (i.e. for the alignment of the FOV of both light collecting telescopes)
- Alignment sensor of the light collecting telescopes optical axis wrt the science focal plane (i.e. FOV of the science detector arrays)

7.1.6.2 Internal laser metrology sub-system

The internal laser metrology has several functionalities depending on the operational mode. On the one hand, during fringe acquisition it can be used in conjunction with the absolute laser metrology to stabilize the OPD and to enable the acquisition of the fringes of the reference object. On the other hand, during the science measurement mode, the displacement of the science

ODL must be monitored in order to retrieve the applied OPD for each sampling point of the interferogram. An error on the OPD sampling may induce errors in the visibility measurement.

7.1.6.3 Absolute laser metrology sub-system

For the uv-plane scanning, the knowledge of the absolute distance measurement between the light collecting telescopes and central hub beam combiner is of great importance. This metrology sub-system measures this absolute distance and monitors it during the uv-plane scanning in order to ensure its stability.

7.1.6.4 Interferometer controller unit

The metrology information gathered by the FSU is used by the ICU to command the different actuators in the optical chain (e.g. common ODLs, pupil conditioner units, science ODLs, etc), as represented in Figure 7-5.

7.1.7 Assumptions and Trade-Offs

7.1.7.1 Beam reduction factor

7.1.7.1.1 Light collecting telescopes

The beam reduction factor is defined as the ratio of the entrance pupil diameter over the exit pupil diameter; it is also the angular magnification of an afocal system. The magnification of the LCT is limited by the free propagation diffraction of the beam at the shortest wavelength. The maximum magnification is given by the Fresnel number: $M << D/\sqrt{(\lambda L)}$ thus $M << 15$ @300µm for L=15 meters and D= 1 meter. The minimum magnification is limited by the allowed volume to the telescope. Therefore a trade-off considering diffraction effects and optics size is needed to optimize the intermediate beam diameter (i.e. diameter of the beam relayed from the LCT to the hub telescope).

Figure 7-6 illustrates the diffraction losses calculated in ZEMAX (software tool) as the magnification increases. The energy contained in the diffraction side lobes increases wrt to the energy contained in the main central lobe.

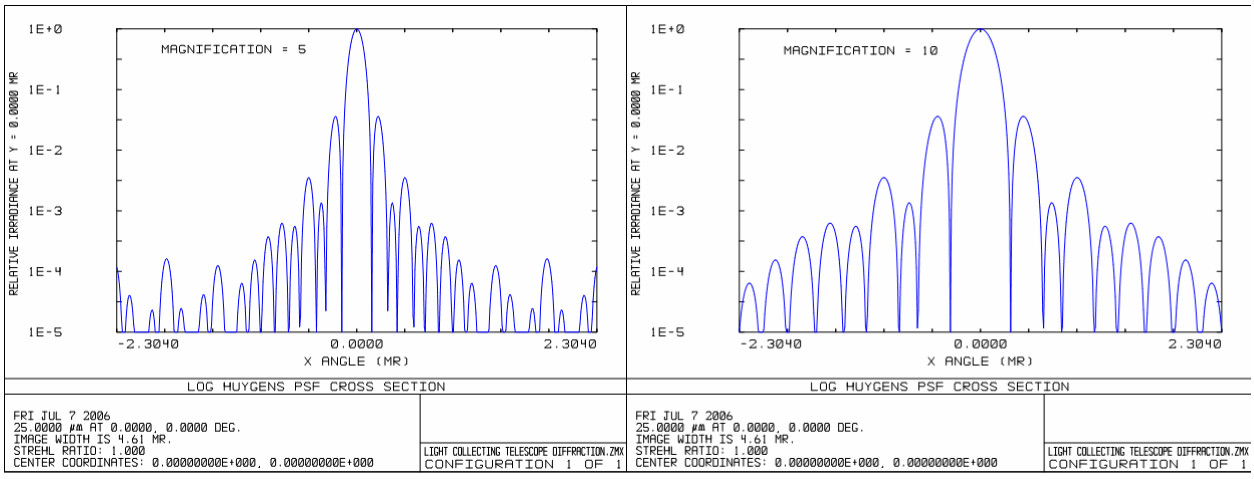

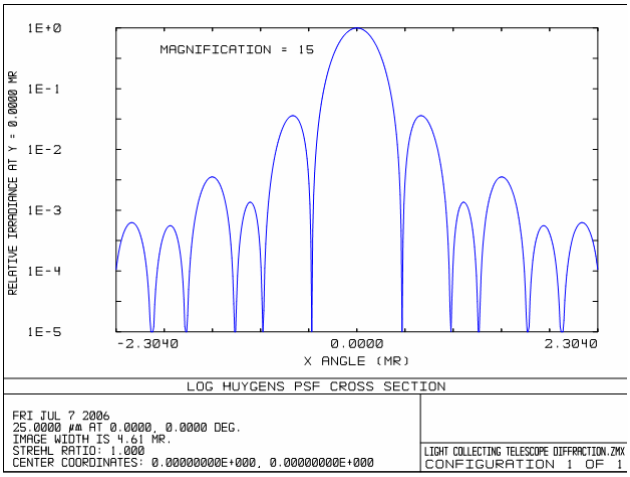

Figure 7-6: On -axis diffraction angular spectrum in logarithmic scale after 15 meters propagation at wavelength λ=25µm

The spatial distribution of the field energy (on-axis) after 15 meters free space propagation at a wavelength λ=300µm, for several intermediate beam diameters (15 cm, 20 cm and 25 cm) and with different central obscuration conditions (no obscuration and 20% central obscuration[1]) has been estimated using ASAP (software tool), and summarized results are shown in Figure 7-8 - Figure 7-10.

These simulations conclude that the influence of the central obscuration concerning the spatial shape and size after 15 meter propagation is not of much importance. It is interesting to note that spatial shape is highly dependent on the intermediate beam diameter. The reason for this is that at 15 m distance we are still in the near-field zone for the considered intermediate beam diameters. In order to collect >90% of the photons, the diameter of the hub telescope has to be >18 cm, >22 cm, >26 cm for the different simulated intermediate beam diameter cases (15 cm, 20 cm and 25 cm). Note that these minimum diameters for the hub telescope only consider the on-axis field. Taking into account the off-axis fields (i.e. science and fringe tracking FOV requirements) the minimum diameter of the hub telescope is shown in Figure 7-7, for different maximum wavelengths. From these results one would take intermediate beam diameters ~15 cm.

[1] Central obscuration is defined as the ratio between the primary mirror and secondary mirror diameters.

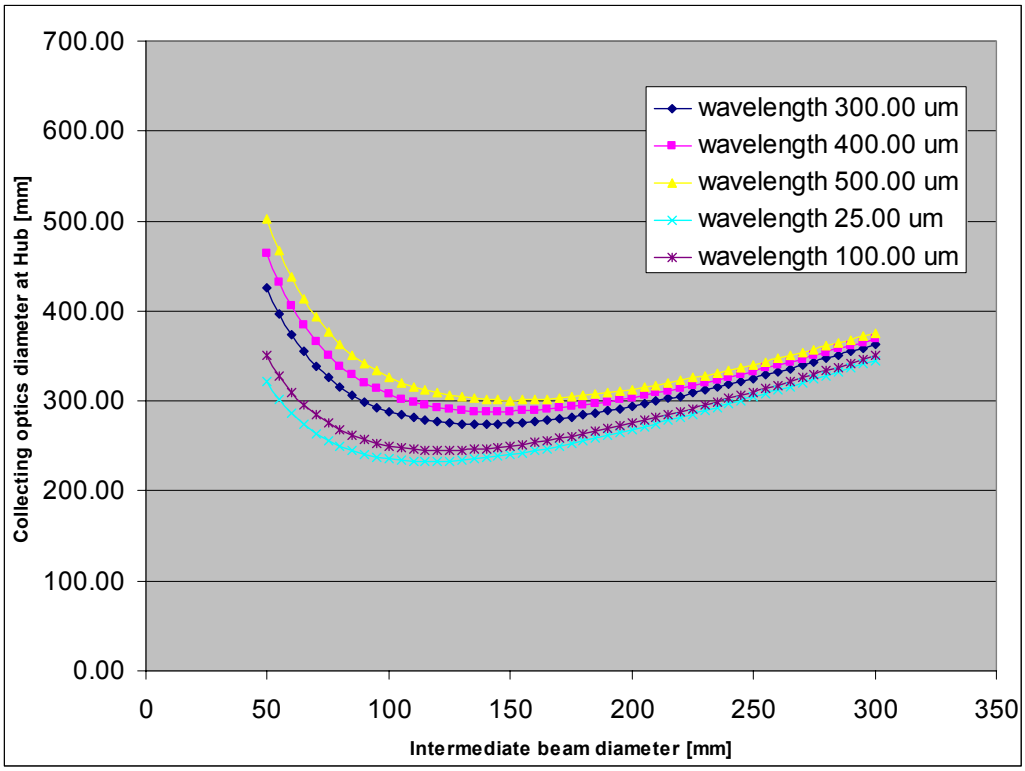

Figure 7-7: Minimum diameter of the hub telescope to collect >90% of energy as a function of the intermediate beam diameter propagated along 15m for several wavelengths (half FOV on the sky=1.5arcmin)

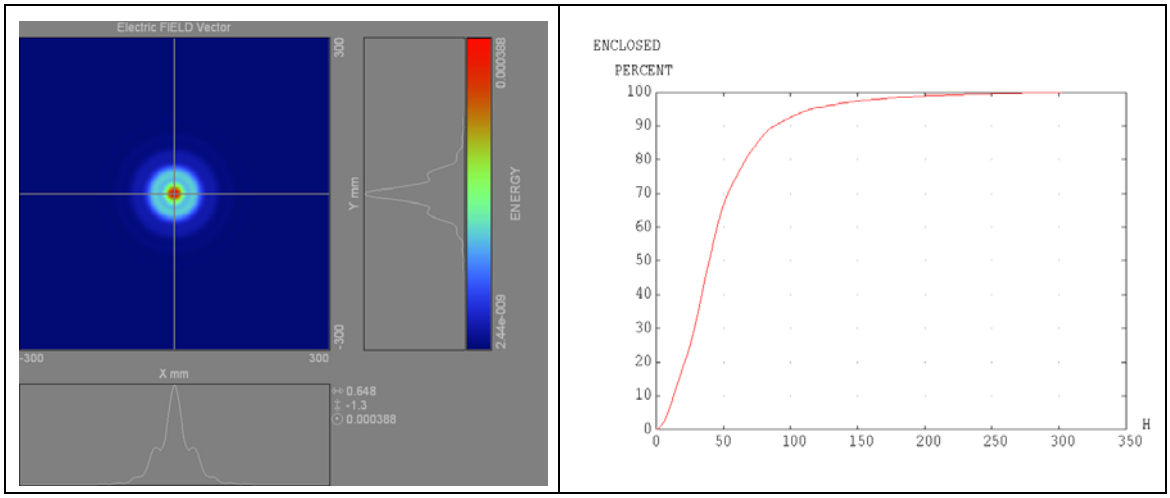

λ=300μm intermediate beam diameter=15 cm, obscuration (diameter ratio)=0%, propagation length=15 m

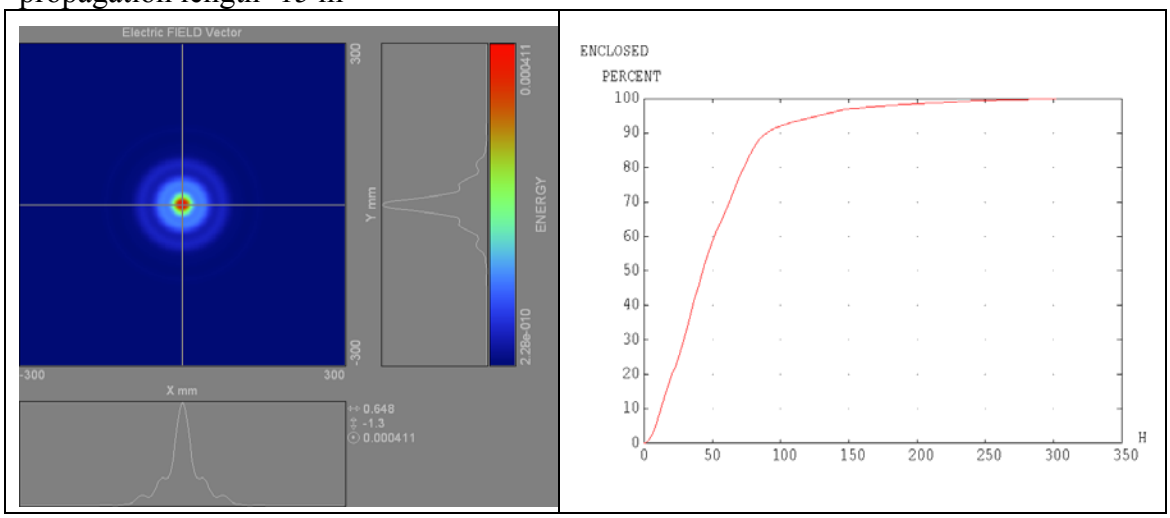

λ=300μm, intermediate beam diameter=15 cm, obscuration (diameter ratio)=20%, propagation length=15 m

Figure 7-8: Spatial distribution of the (on-axis) field energy after 15 meters propagation for an intermediate beam diameter of 15 cm (magnification=6.7)

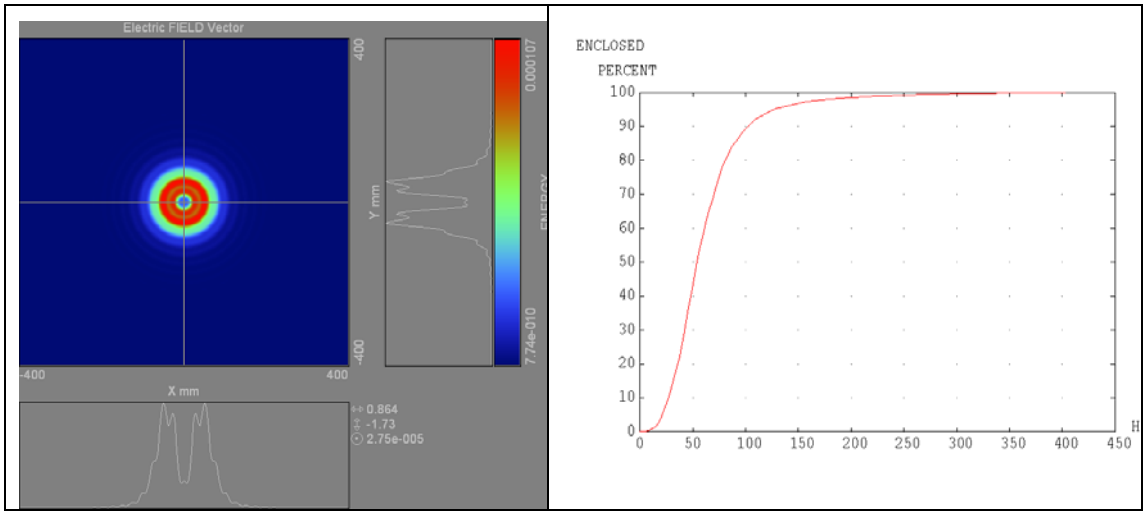

λ=300μm, intermediate beam diameter=20 cm, obscuration (diameter ratio)=0%, propagation length=15 m

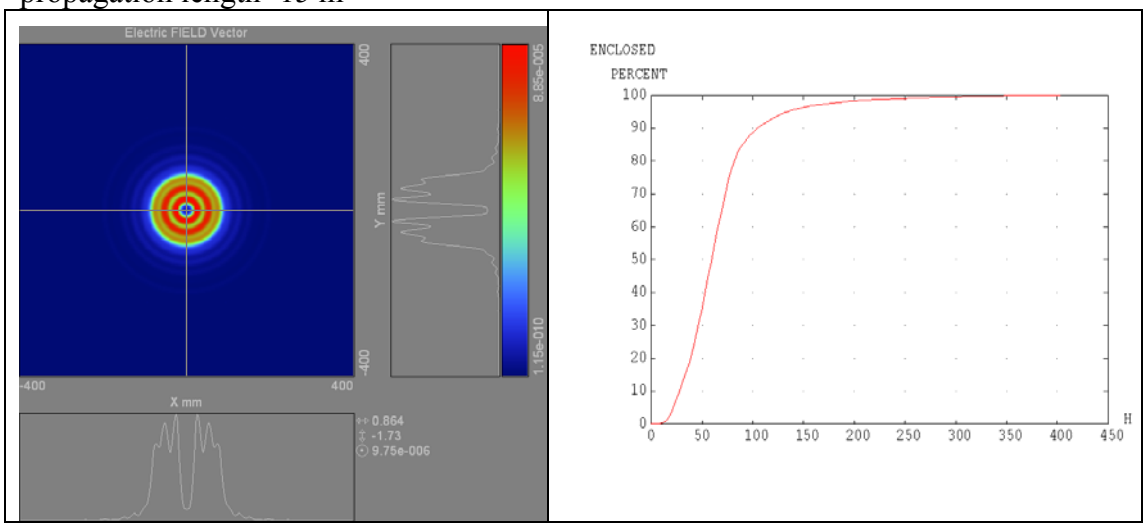

λ=300μm, intermediate beam diameter=20 cm, obscuration (diameter ratio)=20%, propagation length=15 m

Figure 7-9: Spatial distribution of the (on-axis) field energy after 15 meters propagation for an intermediate beam diameter of 20 cm (magnification=5)

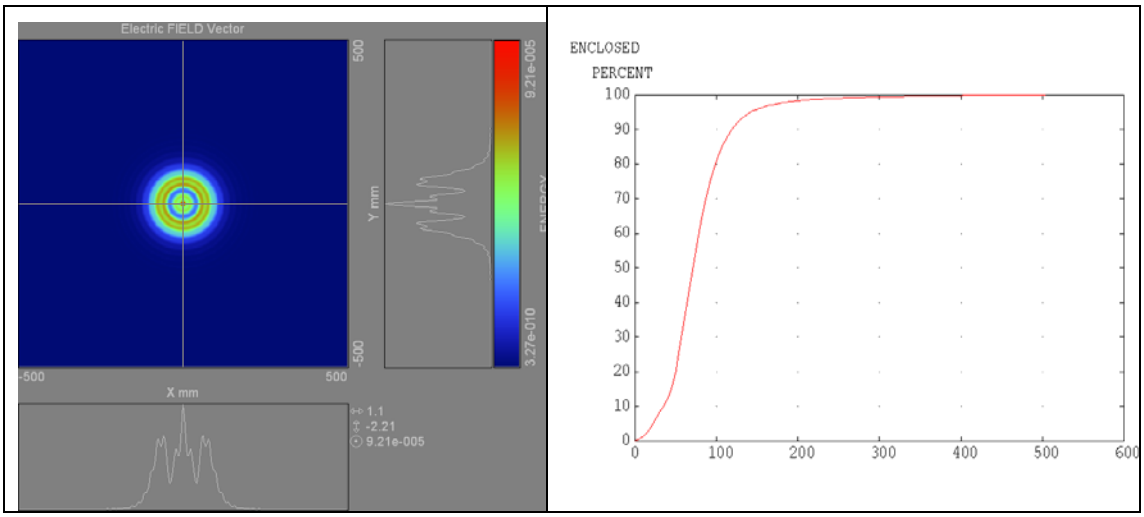

λ=300μm, intermediate beam diameter=25 cm, obscuration (diameter ratio)=0%, propagation length=15 m

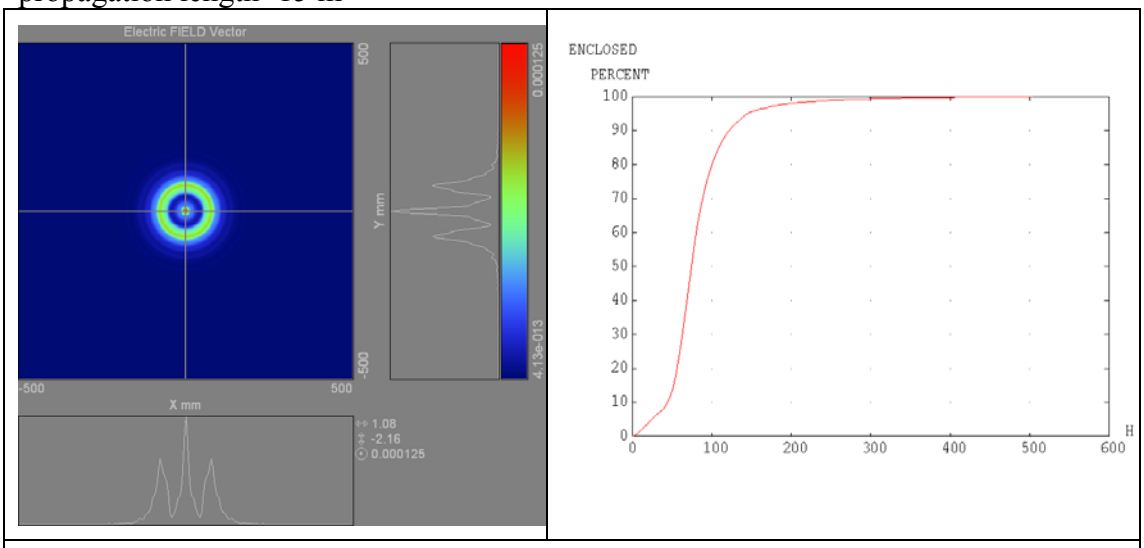

λ=300μm, intermediate beam diameter=25 cm, obscuration (diameter ratio)=20%, propagation length=15 m

Figure 7-10: Spatial distribution of the (on-axis) field energy after 15 meters propagation for an intermediate beam diameter of 25 cm (magnification=4)

However, it is interesting also to evaluate the influence of the minimum diameter of the hub telescope vs the science/fringe tracking FOV. In this case the wavelength used is 400µm. The results are shown in Figure 7-11. The minimum diameter is highly dependent on the FOV to be relayed from the LCT to the central hub beam combiner. As shown in the figure, in order to accommodate a larger FOV (if needed in the future) it is desirable to increase the intermediate beam diameter (reduction of the intermediate magnification).

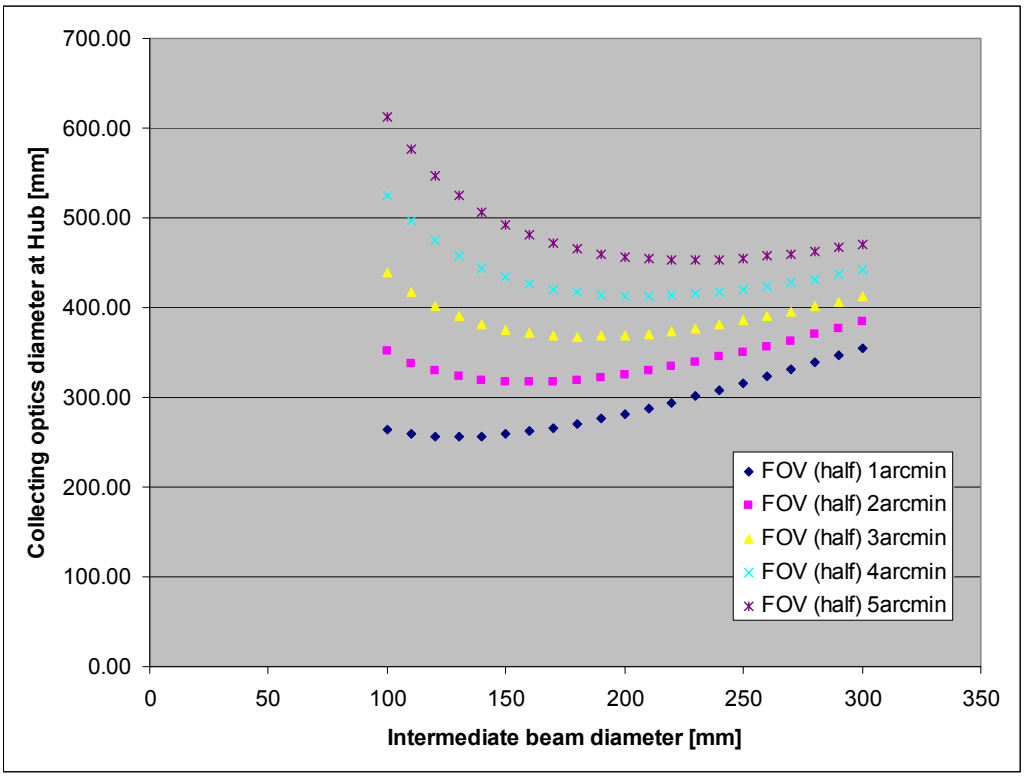

Figure 7-11: Minimum diameter of the hub telescope to collect >90% of energy as a function of the intermediate beam diameter propagated along 15m, for several half FOV on the sky (wavelength=400um)

In view of the need of a FOV for fringe tracking larger than the science FOV it has been selected an intermediate beam diameter of 200mm. In order to limit the diameter of the hub telescope (<300mm) the maximum wavelength corresponds to <300um.

In conclusion, the minimum diameter of the hub telescope to collect >90% of the photons is ~280mm, considering a 1.5arcmin (half) FOV on the sky at a wavelength of 300µm. The intermediate magnification is M=5. This magnification is compatible with the volume specified in Table 7-2. In order to minimize the diffraction losses, this magnification for the light collecting telescopes is chosen as baseline.

7.1.7.1.2 Hub telescopes

The Fresnel criterion drives the maximum magnification. For the hub telescopes the magnification must be M << 6.7 assuming a maximum light path length of 3 meters.

Likewise for the intermediate beam diameter, an optimum internal beam diameter exists, considering diffraction effects within the central hub beam combiner, internal magnification and

optics size. Figure 7-12 shows this trade-off. In order to limit the size of the optics in the central hub beam combiner the maximum wavelength should be <300µm, as also found in the previous section. Taking an internal beam diameter (i.e. pupil diameter) in the central hub of 40 mm, the diameter of the science focusing optics after 3 meters propagation is ~90 mm at 300µm wavelength. This corresponds to an internal magnification of M=5. The overall magnification of the optical chain (intermediate plus internal) is M=25.

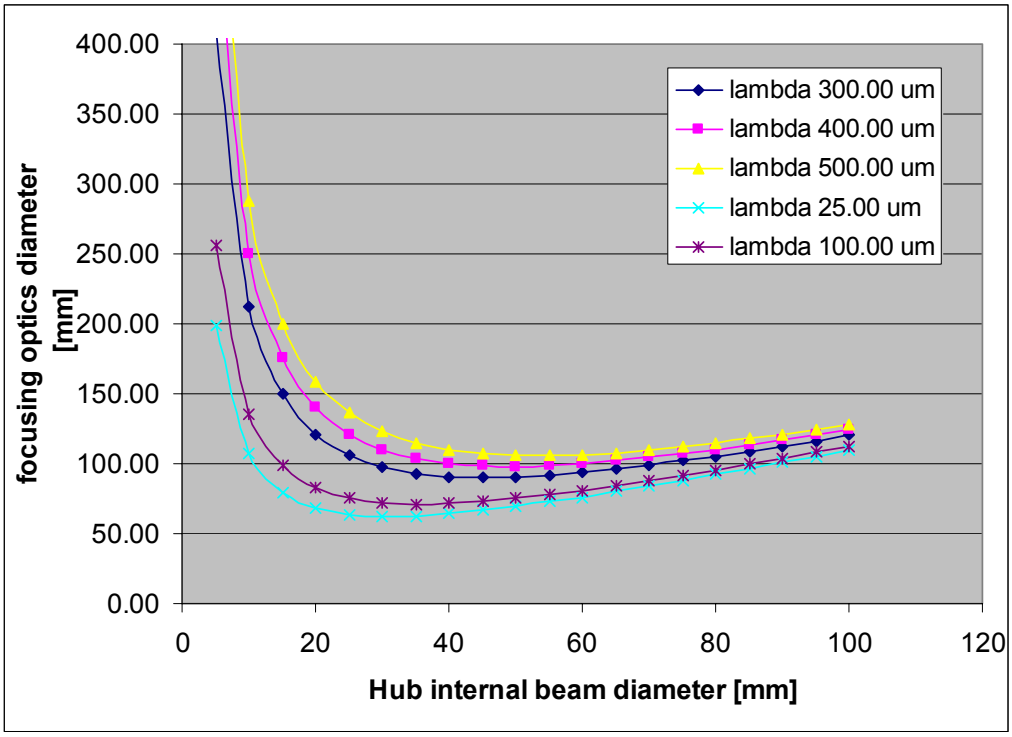

Figure 7-12: Minimum diameter of the science focusing optics as a function of the internal beam diameter in the central hub, at several wavelengths. The science (half) FOV is 0.5 arcmin and the propagation length 3 meters

7.1.7.2 Light collecting telescopes concept trade-off

Two designs are studied and compared: one without intermediary image (option 1) and one with intermediary image (option 2). Both are compliant with the magnification reported in 7.1.7.1.1.

Both designs are afocal and have a magnification equal to 5. Both are compliant with the requirements of Table 7-1 and Table 7-2.

7.1.7.2.1 Option 1

- **Description**

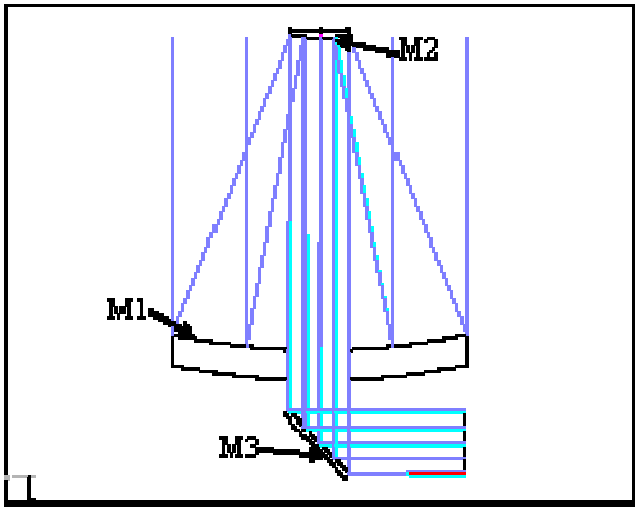

Figure 7-13: Option 1 optical layout

The telescope has two parabolic mirrors (M1 and M2) and one folding mirror (M3).

Such design is simple and the reflectors are easy to manufacture since the optically active surface is a pure parabola.

The detailed definition of the reflectors is reported in Table 7-3.

	M1	**M2**	**M3**
Radius (mm)	2500 CC	500 CX	Flat
Conic constant	-1	-1	X
Clear aperture diameter (mm)	1024 (without margins)	206 (without margins)	Ellipse : • major axis 297 with margins • minor axis 212 with margins
Obscuration diameter (mm)	220 (with margins)	X	X

Table 7-3: Reflectors optical definition

The useful area of M2 is annular as shown in Figure 7-14 due to the central obscuration of M1. The obscuration has an inner diameter of 44mm.

For M3, the projection of the M1 obscuration is a centred ellipse (Figure 7-14) whose dimensions are:

- ½ major axis : 27 mm
- ½ minor axis : 19 mm

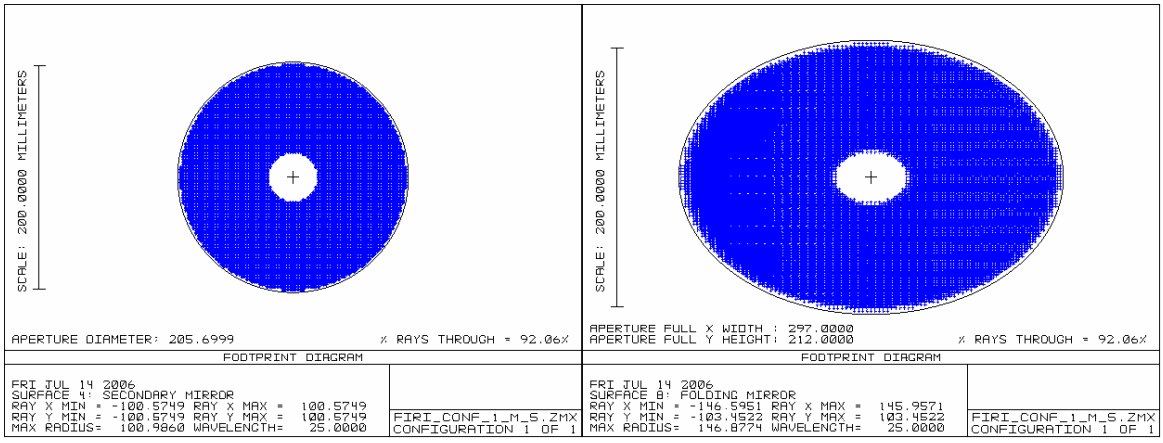

Figure 7-14: Beam footprint on M2 (right) and on M3 (left)

- **Volume**

The optical elements fit in a cylinder of diameter 1030 mm and length 1500 mm.

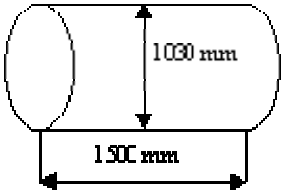

Figure 7-15: Option 1 volume

- **Mass**

The estimated total mass of the reflectors is 42 kg assuming that the reflectors are made of SiC and the mass density is 50 kg/m^2.

- **Performances**
  - Output Wavefront

Figure 7-16 shows the wavefront delivered by the telescope after a propagation of 15 meters.

The residual tilts are removed.

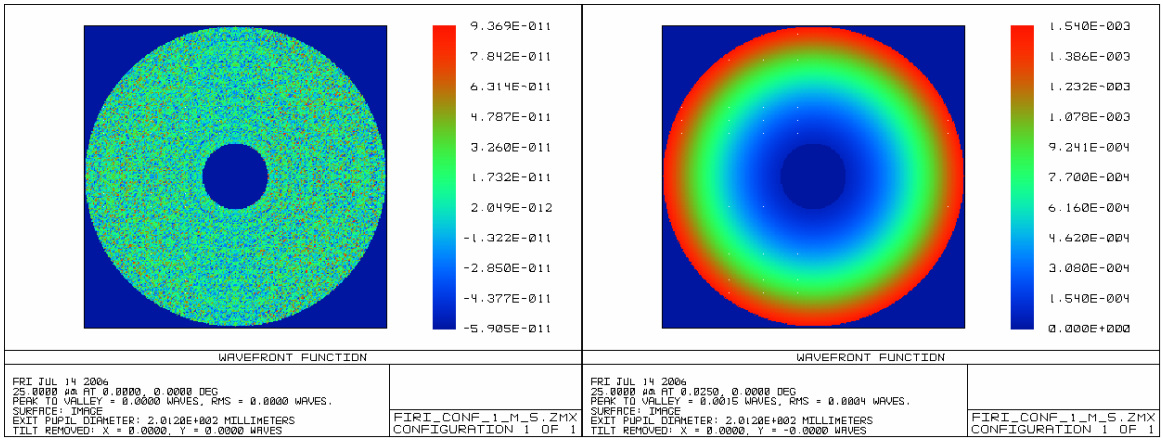

Figure 7-16: Wavefront map at telescope output on-axis (right) and off-axis (left)

The nominal WFE on off-axis beams is in worst case 10 nm RMS or λ/2500 @25µm which is negligible.

- Vignetting

The vignetting here is due only to the obscuration on M1. Any excessive tilt of the folding mirror will introduce vignetting of the detector FOV.

- **Coatings**

The reflectors will be coated with Aluminium single layer coating. The efficiency at large wavelength is 87% to 98% (RD[19]).

7.1.7.2.2 Option 2

- **Description**

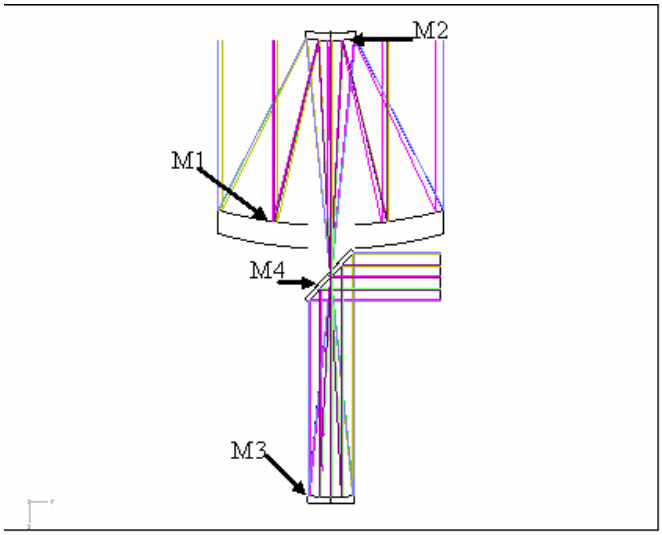

Figure 7-17: Option 2 optical layout

Option 2 includes two aspheric reflectors (M1 and M2), one parabolic reflector (M3) and one folding mirror (M4).

This design, more complex than option 1, has the advantage of an intermediary image which may be useful if one wants to implement a supplementary instrument.

The detailed definition of the reflectors is reported in Table 7-4.

	M1	**M2**	**M3**	**M4**
Radius (mm)	2000 CC	550 CX	-1860 CC	Flat
Conic constant	-1.026	-2.643	-1	X
Clear aperture diameter (mm)	1024 (without margins)	226 (without margins)	212 (without margins)	Ellipse : • Major axis : 298 with margins • Minor axis : 210 with margins

	M1	M2	M3	M4
Obscuration diameter (mm)	226 (without margins)	0	0	Ellipse : • Major axis : 8 with margins • Minor axis : 6 with margins

Table 7-4: Reflectors optical definition

The useful area on M2 and M3 is annular as shown in Figure 7-18. For M2 the inner diameter is 49mm and for M3 the inner diameter is 40 mm.

The actual central obscuration is larger on M4 but since the reflector is at the intermediary image, the central obscuration is used as field stop. Thus the central obscuration is fitted to the size of the intermediary image.

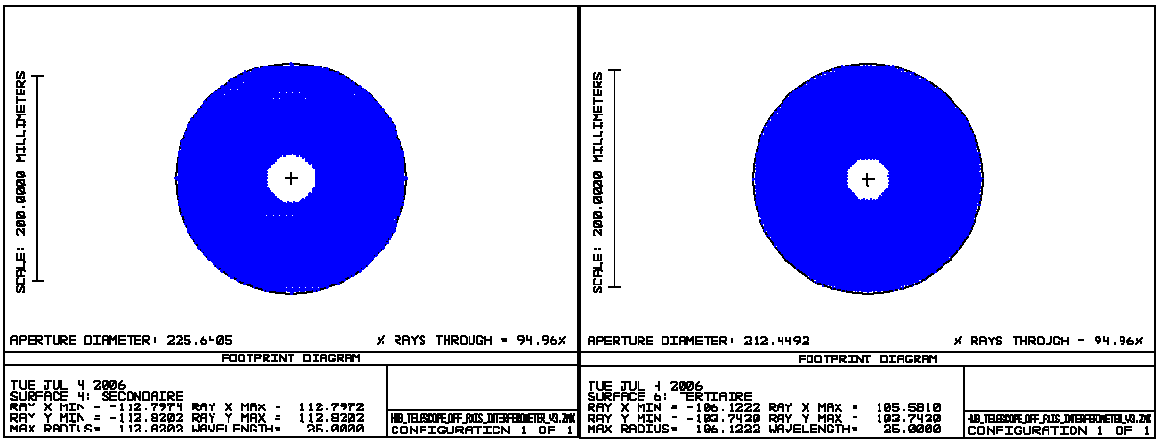

Figure 7-18: Beam footprint on M2 (right) and on M3 the right (left)

- **Volume**

The optical elements fit in a cylinder of diameter 1030 mm and length 2000 mm.

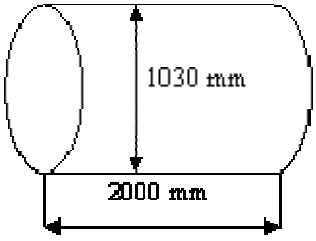

Figure 7-19: Option 2 volume

- **Mass**

The estimated total mass of the reflectors is 46 kg assuming that the reflectors are made of SiC and the mass density is 50 kg/m^2.

- **Performances**
  - Output wavefront

Figure 7-20 shows the wavefront at the telescope output after a propagation of 15 meters.

The residual tilts are removed.

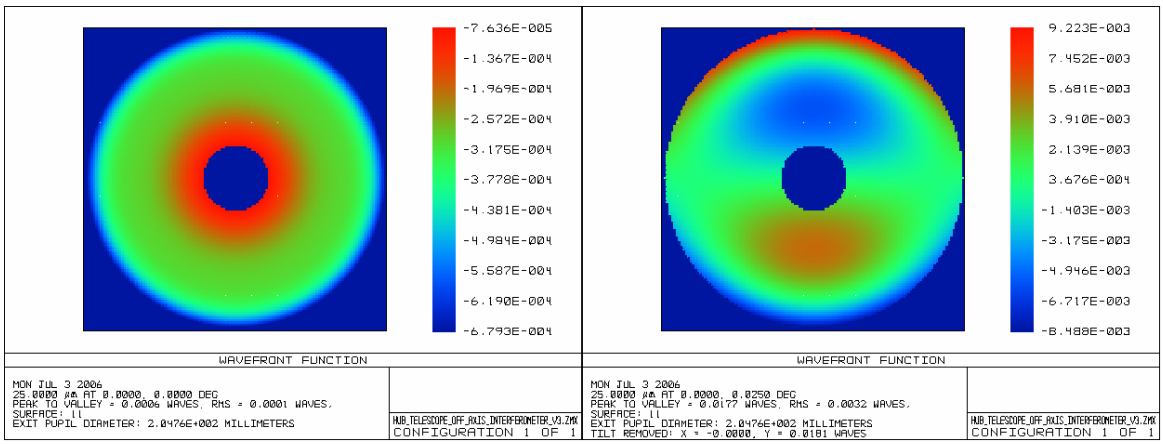

Figure 7-20: Wavefront map at telescope output on-axis (right) and off-axis (left)

The nominal WFE on off-axis beams is in worst case 80 nm RMS or λ/313 @25µm.

- Vignetting

A strong vignetting may appear if an excessive tilt is applied to the flat mirror M4. Furthermore in that case, since the central aperture of M4 acts as a field stop, the FOV might be reduced.

- **Coatings**

The reflectors will be coated with Aluminium single layer coating. The efficiency at large wavelength is 87% to 98% (RD[19]).

7.1.7.2.3 Conclusion

Although option 2 is 4 kg heavier than option 1, it allows the accommodation of supplementary means of metrology for spacecraft attitude control (star tracker for instance) and/or telescope pointing control.

The design of option 2 thus is more flexible and versatile than the design of option 1. For this reasons, option 2 is chosen as the baseline for the design.

7.1.7.3 Beam mixing technique trade-off

As stated in RD[28], the pupil plane recombination presents the best performances for narrow FOV while in the image plane recombination the FOV is larger and thus the imaging time is lower. Nevertheless, the tolerances required by wide field operation are easily achieved in pupil plane recombination (RD[16]) and image plane technique is not so robust (see RD[28]).

In RD[9] a technique for spectrometry taking advantage of the pupil plane recombination is presented. A Fourier Transform Spectrometer can be implemented by adjusting the ODL stroke to the desired spectral resolving power. In the Fizeau configuration a supplementary instrument is needed to do the spectroscopy of observed objects. Furthermore the limited IFOV in pupil plane configuration is overcome by using a detector array with fewer pixels than the image plane configuration since the fringes are obtained in the time domain and not in the spatial domain.

For those reasons the pupil plane combination is chosen.

7.1.7.4 Spectrometer

As a consequence of the trade-off done in 7.1.7.3, the spectroscopy will be performed using the double-Fourier spatio-spectral interferometry method reported in RD[9].

In order to measure the phase and amplitude of the complex visibility and to scan completely the required FOV, the ODL displacement will be symmetric wrt the zero position corresponding to the bright fringe at the centre of the FOV.

For a FTS, the FOV is limited by the condition $\Omega \times R = 2\pi$, with Ω the solid angle subtended by the FOV and R the spectral resolving power. For R=3000, the maximum FOV at the FTS entrance is 1.5 degrees which is compliant with the chosen total magnification (M_{total}= 5x5 = 25).

7.1.7.5 Sub-band splitting trade-off

The observation of the entire spectral bandwidth with a single focal plane array raises several issues:

- The needed OPD stroke to achieve the maximum resolving power is about +/- 300 mm. Such stroke is challenging to reach at cryogenic temperatures
- The resolving power, calculated at the average wavelength λ_0 of the bandwidth, is not constant over the bandwidth and changes proportionally to the ratio λ / λ_0
- For large bandwidth, the coherence length represents only a small percentage of the primary beam. Thus the IFOV is much smaller than the diffraction limit for large bandwidth
- The detector technology limitations may not allow to cover the entire bandwidth.

Based on the above assessment, the chosen configuration includes four sub-bands. The main features are summarized in Figure 7-21.

Case: 4 sub-bands

	wavelenght_ min [um]	wavelength_ central [um]	wavelenght_ max [um]	inherent spectral resolution	number of fringes	ODL mechanical troke [mm]	Number of reflections	required mechanical ODL speed [mm/sec]	min spectral resolution	central spectral resolution	max spectral resolution	min Time per UV plane [days]
sub-band 1	25.0	35.8	46.5	1.661	2.322	53.648	2.000	0.447	2142.857	3000.000	3428.571	3.577
sub-band 2	46.5	66.6	86.6	1.661	2.322	49.925	4.000	0.416	2076.923	3000.000	3692.308	3.577
sub-band 3	86.6	123.9	161.2	1.661	2.322	46.460	8.000	0.387	2040.000	3000.000	3720.000	3.577
sub-band 4	161.2	230.6	300.0	1.661	2.322	43.236	16.000	0.360	2086.957	3000.000	3913.043	3.577
						50.000						

Figure 7-21: Main characteristics of the 4 sub-band splitting option

7.1.7.6 Fringe tracker sub-system

7.1.7.6.1 FOV

The fringe tracking is done by observing interference of light coming from one reference object in the field of view of the fringe tracking sensor. The science targets are, in most cases too faint

to be used for fringe tracking purpose. Brighter objects in the visible to near IR spectral range shall be used.

The FSU could also be used as a kind of highly accurate star tracker, providing spacecraft position & attitude information to the AOCS system. For that purpose a second object is needed within the FOV of the FSU. Another option that was investigated was the accommodation of so-called wide field cameras at the LCT's location. That possibility is being considered for interferometers based on free flying formation (i.e. DARWIN). However, it seems more convenient to have a centralized fine attitude sensor in the central hub beam combiner. Yet, given the selected LCT design, it should be feasible to implement wide field cameras on each moving LCT, if deemed necessary in the future.

7.1.7.6.2 Method

The methods for fringe tracking can be classified into two categories: coherencing and cophasing. Coherencing is aimed to keep the OPD drift within the coherence length while cophasing purpose is to keep it smaller than the wavelength. According to the accuracy required for the control of the spacecraft attitude, cophasing is best suited.

The basics of one method to achieve cophasing is described in RD[23].

Several cophasing strategies have been analysed. As FIRI has two LCTs those cophasing options that use at least three apertures have been immediately discarded (e.g. phase closure, large optical gyroscope). Concerning cophasing strategies based on dual field operation two implementation options were traded-off: multiplexed beams and separated beams. Based on the outcomes of Table 7-5, the option of separated beams has been selected for the cophasing strategy.

	Benefits	**Drawbacks**
Dual field based on multiplexed beams	Minimum FOV transferred from the collecting apertures to the central hub beam combiner (reference object and science object are co-aligned)	• Implementation of a field separator in the LCTs is compatible with LCTs design, but technically very challenging • Proposed for some ground-based and space-based interferometers
Dual field based on separated beams	• It is operational in several ground-based interferometers (heritage, experience) • Technically less complex	Large FOV (including science and reference objects) conveyed from the collecting telescopes to the central hub beam combiner

Table 7-5: Trade-off of dual field cophasing strategies

7.1.8 Optical Delay Lines

7.1.8.1 Optical component options

The different options for implementing the optical elements located in the moving part of the ODL are described in Figure 7-22 and compared in Table 7-6.

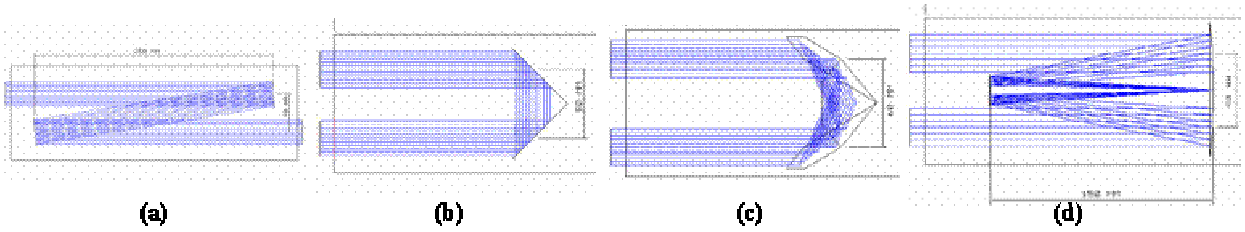

Figure 7-22: Optical components of the ODL, (a) flat mirrors, (b) roof top mirrors, (c) hollow retroreflector, (d) cat's eye

	Benefits	Drawbacks
Flat mirrors	• Excellent WFE • 2 internal reflections • Negligible polarization effects (small incidence angle)	• Very sensitive to all type of misalignments (tilt and lateral displacement) • Large internal path (diffraction effects) • Large footprint
Roof-top mirrors	• Insensitive to one in-plane rotation axis • Very short internal path • 2 internal reflections • Flat mirrors (excellent WFE) • Medium volume / footprint	• Sensitive to one in-plane rotation axis • Sensitive to lateral displacements • Polarization effects (45deg incidence angle)
Hollow retroreflectors	• Insensitive to tilt misalignment • Medium internal path (diffraction effects) • Flat mirrors (excellent WFE), provided parallelism error is small	• 3 internal reflections • Large volume / footprint • Sensitive to lateral displacements • Polarization effects (~55deg incidence angle)
Cat's eye	• Negligible polarization effects (small incidence angle) • Re-imaging capability	• Very large internal path (diffraction effects) • Very large volume / footprint • Sensitive to lateral displacements • 3 internal reflections • Limited FOV • Sensitive to particle contamination (impact onWFE)

Table 7-6: Optical components trade-off for the ODL

Roof-top mirrors allow the most compact configuration (i.e. very short internal path), which is crucial to keep the overall optical chain in the beam combiner <3m (i.e. minimize diffraction effects). With respect to a hollow retroreflector it has one reflection less and smaller cross-section. The main drawback is the sensitivity to one rotation axis in the plane orthogonal to the propagation direction. Nevertheless, given the fact that the interferometer is operating at large wavelengths, it is considered that the guidance mechanism will be capable of meeting the alignment requirements. With a similar reasoning, it is considered that (differential) polarization effects induced by the large incidence angle will be sufficiently small. Therefore, the roof-top mirror is the baseline for the optical configuration of the ODL.

7.1.8.2 Optical layout trade-off

In general, the OPD introduced by an ODL is of the form *~(2^K)*mechanical stroke* (with *k*=number of internal trips). Due to the splitting into several sub-bands, one ODL would, in principle, be needed for each science sub-band. However, it is possible to merge all ODLs into a single compact one, such that only one mechanical stroke is used, provided the following equation is fulfilled:

$$\frac{\lambda_{MAX}}{\lambda_{\min}} = 2^N$$

For our case, the maximum wavelength is 300μm, the minimum wavelength is 25μm and the number of sub-bands *N* is 4. With these values and the constraint that k is equal to 1 for sub-band 1, 2 the sub-band 2 etc…, the mechanical stroke needed for each sub-band is quite similar (see Figure 7-21), and therefore it allows to combine all ODLs into a single large one (i.e. only one actuator). The optical path difference (OPD) for each sub-band depends on the number of internal reflections within the ODL (power of 2).

Two different optical layouts (with a single mechanical stroke) have been investigated, both based on roof-top mirrors. The most straightforward implementation is the one shown in Figure 7-23. It basically combines the rooftop mirrors for each spectral sub-band into one moving multiple roof-top units. The non-moving optical part contains the dichroic filters that split the total science wavelength range into 4 spectral sub-bands (see the 4 beams reaching the rear reference plane). A more interesting optical configuration for the science ODL is represented in Figure 7-24, where the multiple rooftop unit is folded into a more compact device. This compact ODL design is preferred, as it halves the number of rooftop mirrors, it also halves the number of critical alignments on moving optics, and most important it reduces by a factor 2 the footprint required on the optical bench, at the expense of increasing the height, which is not so critical. The compactness will allow some mass reduction on the moving part, and in turn, a reduction of the power consumption/dissipation, which is a critical system level constraint. In addition, it is expected some reduction on the footprint required for the science beam combiners (see the 4 beams on a smaller area of the rear plane). The two options are described in Figure 7-23 and Figure 7-24, the trade-off is summarised in Table 7-7.

Single large ODL

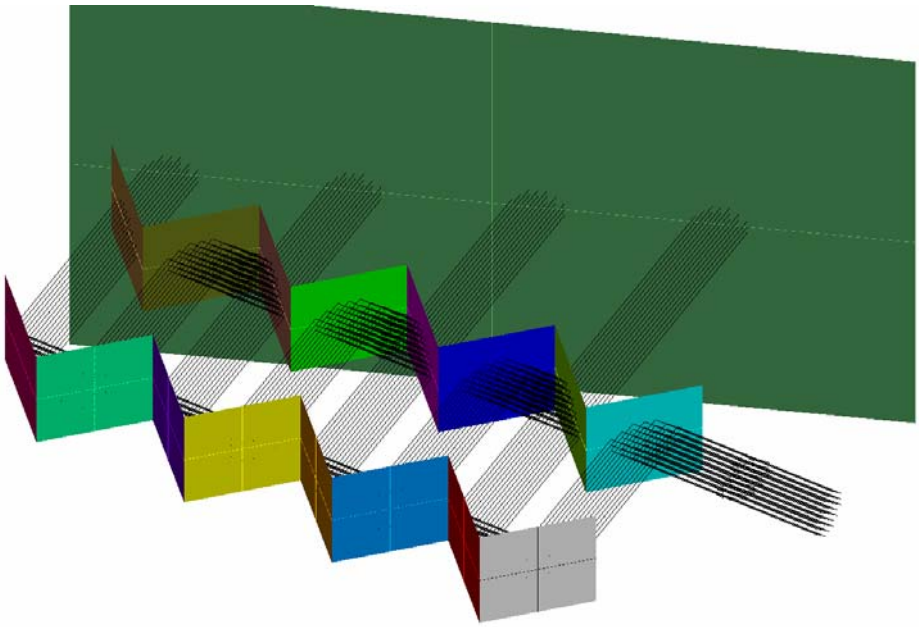

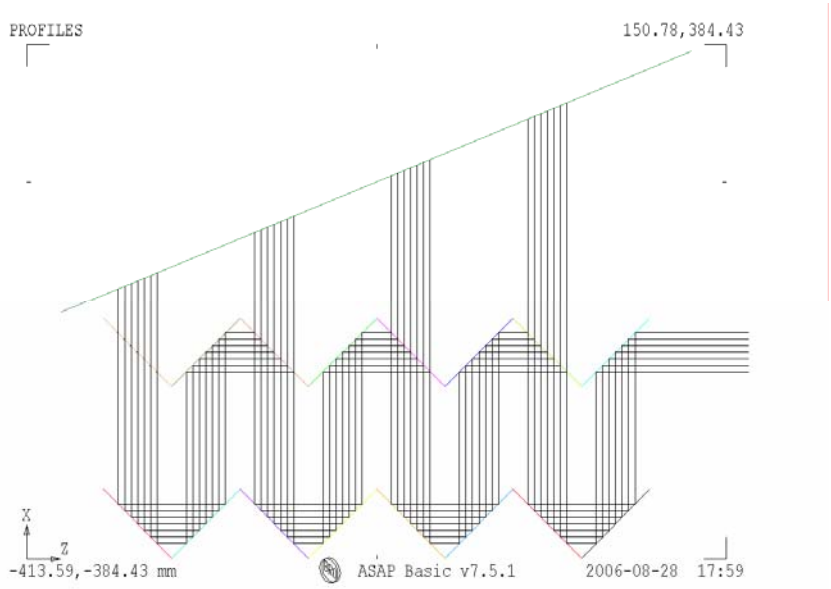

Figure 7-23: Large ODL: 3-D model, top view drawing, benefits and drawbacks

Single compact ODL

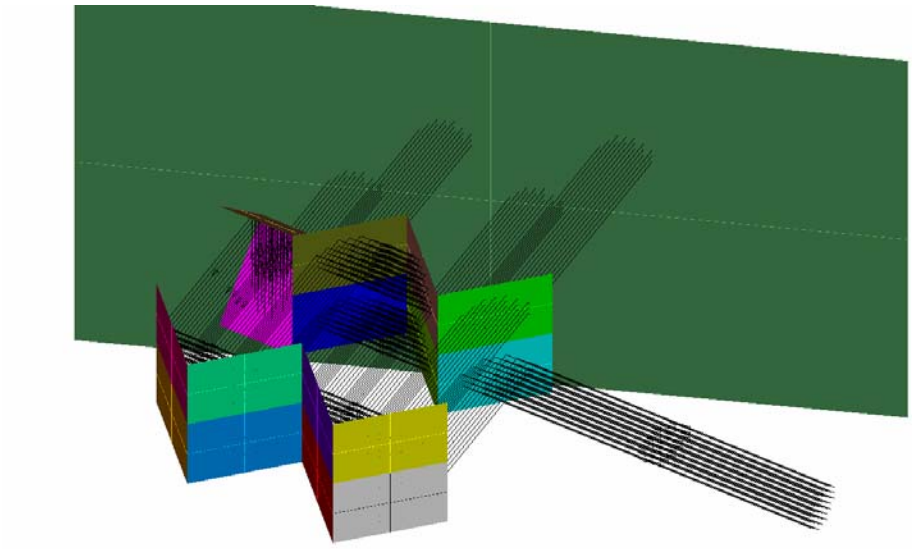

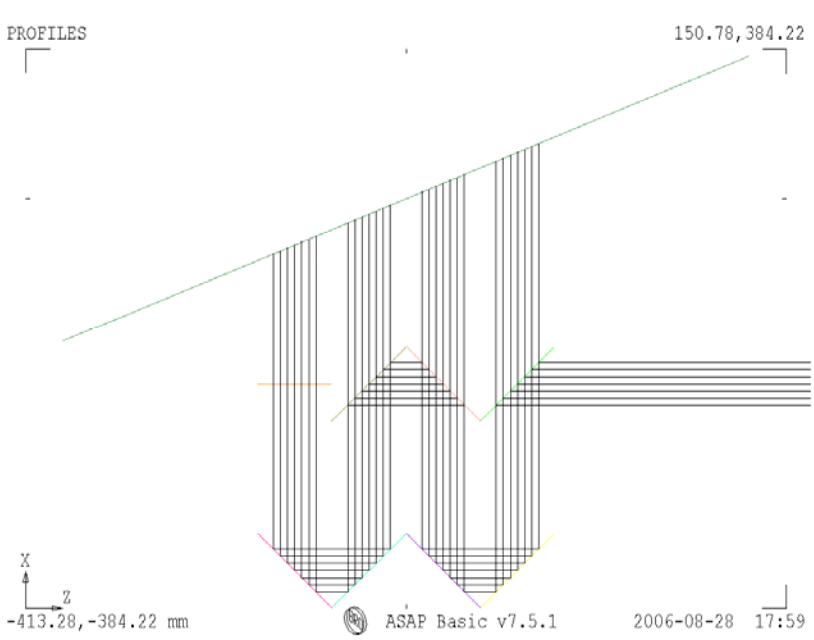

Figure 7-24: Compact ODL: 3-D model, top view drawing, benefits and drawbacks

	Benefits	Drawbacks
Single large ODL	All beams are propagating in the same plane	• Very large footprint, occupying almost completely one optical bench (see 7.1.11 for further details) • Large aspect ratio (length/height), which makes the moving structure of the ODL more complex, and in turn the dynamics more difficult to control • 4 moving rooftop mirrors
Single compact ODL	• Compact footprint (factor ~2 reduction efficient utilization of the optical bench (see 7.1.11 for), allowing a more further details) • Aspect ratio (length/height) close to unity, which makes the structure more symmetric and the dynamics easier to control • Only 2 moving rooftop mirrors	• Beams at different heights inducing a more complex beam recombination optical layout • Larger roof-top mirrors

Table 7-7: ODL optical layout trade-off

It is concluded that the compact ODL is selected as the baseline.

7.1.9 Beam Combiner Options For Pupil Plane Recombination

The compactness is one of the most important criteria used to determine the best beam combiner configuration (BC). Several options have been investigated in detail: single beam splitter, Michelson beam combiner, Sagnac beam combiner, Mach Zehnder interferometer, modified Mach Zehnder interferometer and windmill beam combiner. Table 7-8 summarizes benefits and drawbacks of the different alternatives. The different configurations are described in Figure 7-25.The configuration that offers perfect symmetry, no differential polarization effects and the smallest footprint is found to be the windmill beam combiner. This type of beam combiner has been selected for both the fringe tracking and the science paths. As a matter of example the windmill configuration allows a factor 4 reduction on the footprint compared to another perfectly symmetric configuration based on a modified Mach Zehnder interferometer. The option of using a single beam splitter is the simplest and the most compact one. However it is clearly non-symmetric and dispersion effects make this option very challenging considering the large sub-band wavelength range.

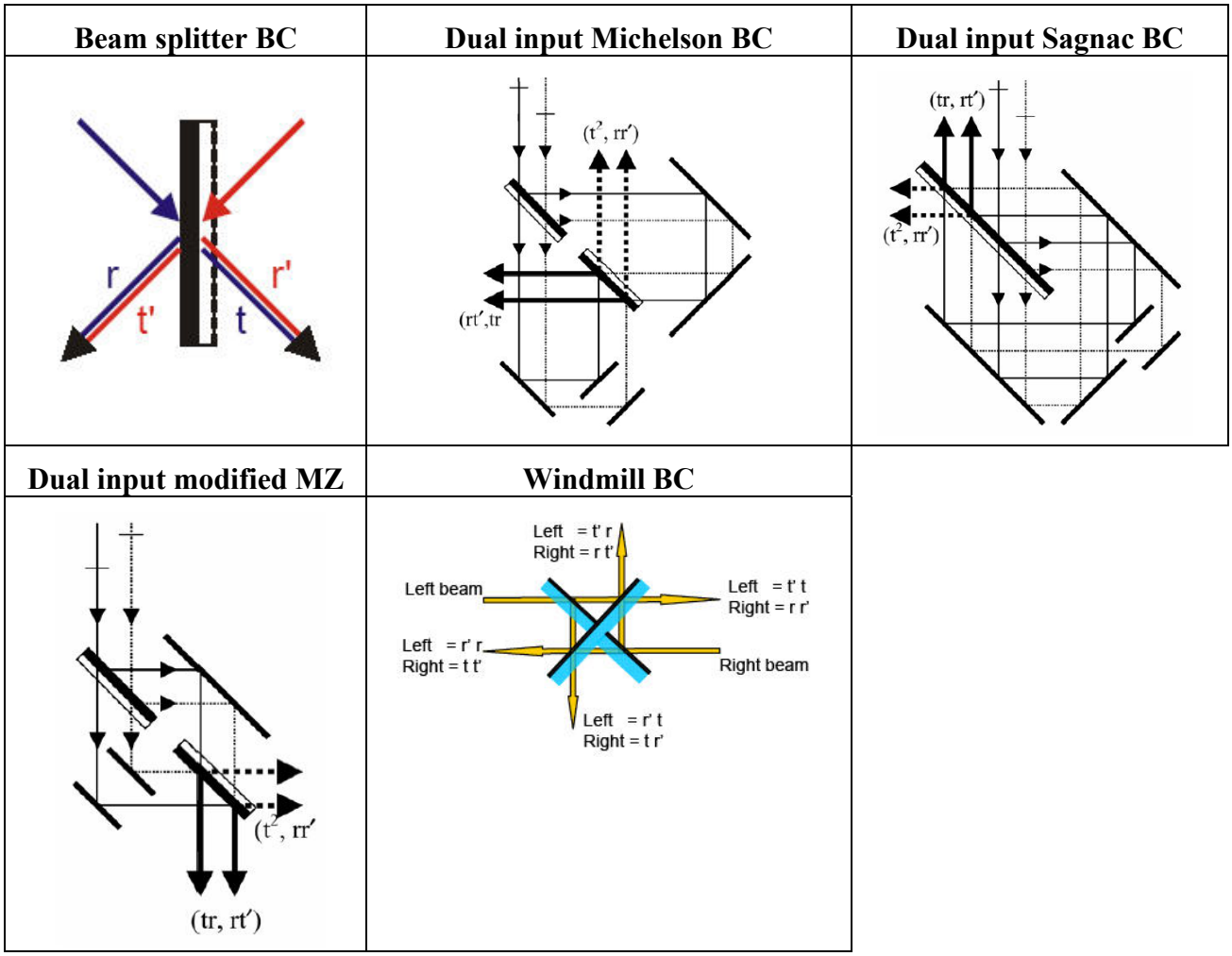

Figure 7-25: Beam combiner implementation options

	Benefits	Drawbacks
Beamsplitter SC	Simplest Lowest cost Most compact	Inherently asymmetric Broadband operation difficult
Dual input Michelson BC	Highly symmetric Broadband operation	Large footprint Large losses Complex alignment
Dual input Sagnac BC	Highly symmetric Broadband operation	Very large footprint Large losses Very complex alignment
Dual input modified Mach-	Highly symmetric	Moderate compactness

	Benefits	Drawbacks
Zender	Broadband operation	Moderate alignment complexity Moderate losses
Windmill BC	Highly symmetric Broadband operation Low losses Smaller beamsplitters	Large footprint Complex alignment

Table 7-8: Beam combiner trade-offs for pupil plane recombination

7.1.10 Science Focusing Optics

There are two different options for the science focusing optics, depending on whether the pixel size of the science detector array is the same for all sub-bands (Table 7-9) or can be specifically tailored for each sub-band (Table 7-10). The first option is technically feasible but needs different focusing optics for each sub-band. The second option is highly recommendable as it simplifies the design and the mounting of the focusing optics, it saves some footprint in the optical bench and, according to detector's state of the art, it is also technically more convenient (absorber dimensions are proportional to the wavelength, suspension legs with similar lengths and, therefore, similar thermal conductance (read sensitivity)). All in all, the option of detector array size tailored to each sub-band is more attractive, as the focusing optics can be designed to have the same optical parameters (i.e. same focal length).

FOV 1arcmin (full, round)

sub-band	detector pixel diameter [um]	lambda_central [um]	focusing optics focal length [m]	Rounded Num pixels per line detector	Detector array length [mm]
1.00	1000.00	35.765	2.237	18.000	18.00
2.00	1000.00	66.566	1.202	10.000	10.00
3.00	1000.00	123.894	0.646	6.000	6.00
4.00	1000.00	230.593	0.347	4.000	4.00

Table 7-9: Focal length values of the science focusing optics in case of fixed pixel diameter (1mm)

FOV 1arcmin (full, round)

sub-band	detector pixel diameter [um]	lambda_central [um]	focusing optics focal length [m]	Rounded Num pixels per line detector	Detector array length [mm]
1.00	500.00	35.765	1.118	18.000	9.00
2.00	930.60	66.566	1.118	10.000	9.31
3.00	1732.05	123.894	1.118	6.000	10.39
4.00	3223.71	230.593	1.118	4.000	12.89

Table 7-10: Focal length value of the science focusing optics in case of tailored pixel diameter for each sub-band

7.1.11 Optical Design Of The Central Hub Beam Combiner

Several configurations have been investigated in order to accommodate the hub relay telescopes and the optics of the central hub beam combiner within a cylinder of <1.3meters diameter and <1.2meters height (goal <1meter height). All these parts are surrounded by the 5 K vessel. Within the 5 K vessel there is a small vessel containing the detector arrays at 50 mK.

The list of designs is as follows:

1. Design with on-axis hub relay telescopes (similar to light collecting telescope design)
    a. Option with large science ODLs (Figure 7-26)
    b. Option with compact science ODLs (Figure 7-27)
2. Design with off-axis hub relay telescopes
    a. Option with tailored science focusing optics (fixed pixel diameter) (Figure 7-28)
    b. Option with fixed science focusing optics (tailored pixel diameter) (Figure 7-29)

Table 7-11 reviews the main benefits and drawbacks for each of the analysed designs. Note that during this analysis some specifications were updated (e.g. detector pixel size, location of the FSU, etc). The off-axis hub telescope design is sensitive to mis-alignment which induces WFE and asymmetry as far as polarization is concerned. Nevertheless it is expected that the induced visibility loss due to polarization effects will be acceptable, given the operating wavelength range. Therefore option 2.b is selected as a baseline for the optical layout.

		Benefits	**Drawbacks**
Design with on-axis hub relay telescopes[2] (fixed pixel diameter of 300µm assumed)	**Option with large science ODLs**	• on-axis hub relay telescopes less sensitive to mis-alignment	• 3 optical benches needed due to large science ODL footprint • Size of the 50mK too large (it could be reduced with some modifications in the science focusing optics) • Maximum number of reflections • Additional obscuration losses • Dimensions: 1.3meters diameter, 1.5meters height
	Option with compact science ODLs	• on-axis hub relay telescopes less sensitive to mis-alignment • 2 optical benches needed thanks to compact science ODL • Dimensions: 1.3meters diameter, 1.1meters height	• Size of the 50mK too large (it could be reduced with some modifications in the science focusing optics) • Maximum number of reflections • Additional obscuration losses

[2] At the time of the on-axis hub telescopes it had been assumed a fixed pixel diameter of only 300µm. This value was reviewed afterwards and designs using off-axis telescopes had considered the new detector pixel size value(s).

Design with off-axis hub relay telescopes	**Option with tailored science focusing optics**	• Less number of reflections • No additional obscuration losses • Less internal optical path (less diffraction effects) • Size of the 50mK is 10x10x30cm^3 • Dimensions: 1.3meters diameter, 1.1meters height	• Some polarization performances degradation using off-axis hub relay telescopes • Science focusing optics complexity
	Option with fixed science focusing optics[3]	Less number of reflections No additional obscuration losses • Less internal optical path (less diffraction effects) • Size of the 50mK is 10x10x30cm^3 • Dimensions: 1.3meters diameter, 1.1meters height • Same science focusing optics for all sub-bands	• Some polarization performances degradation using off-axis hub relay telescopes

Table 7-11: Trade-off of optical designs for the central hub beam combiner

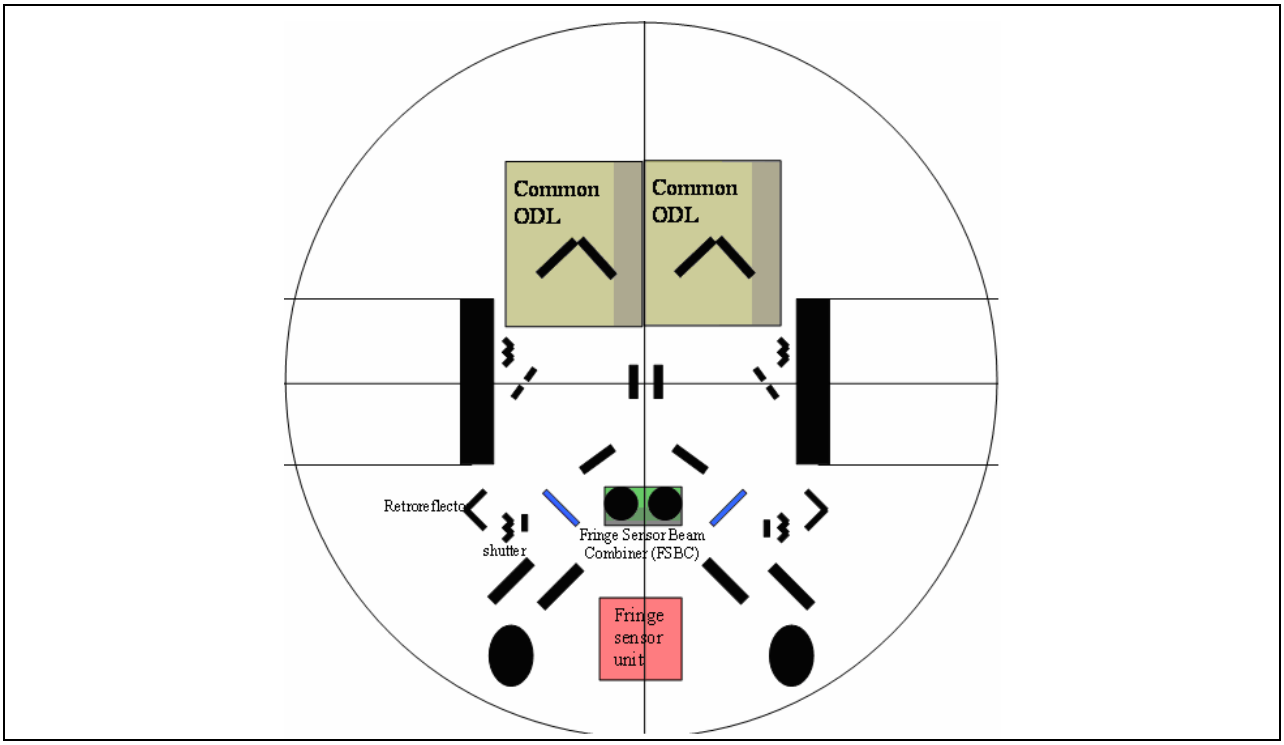

[3] In this design the FSU has already been removed of the 5K vessel (in a *warm* optical bench)

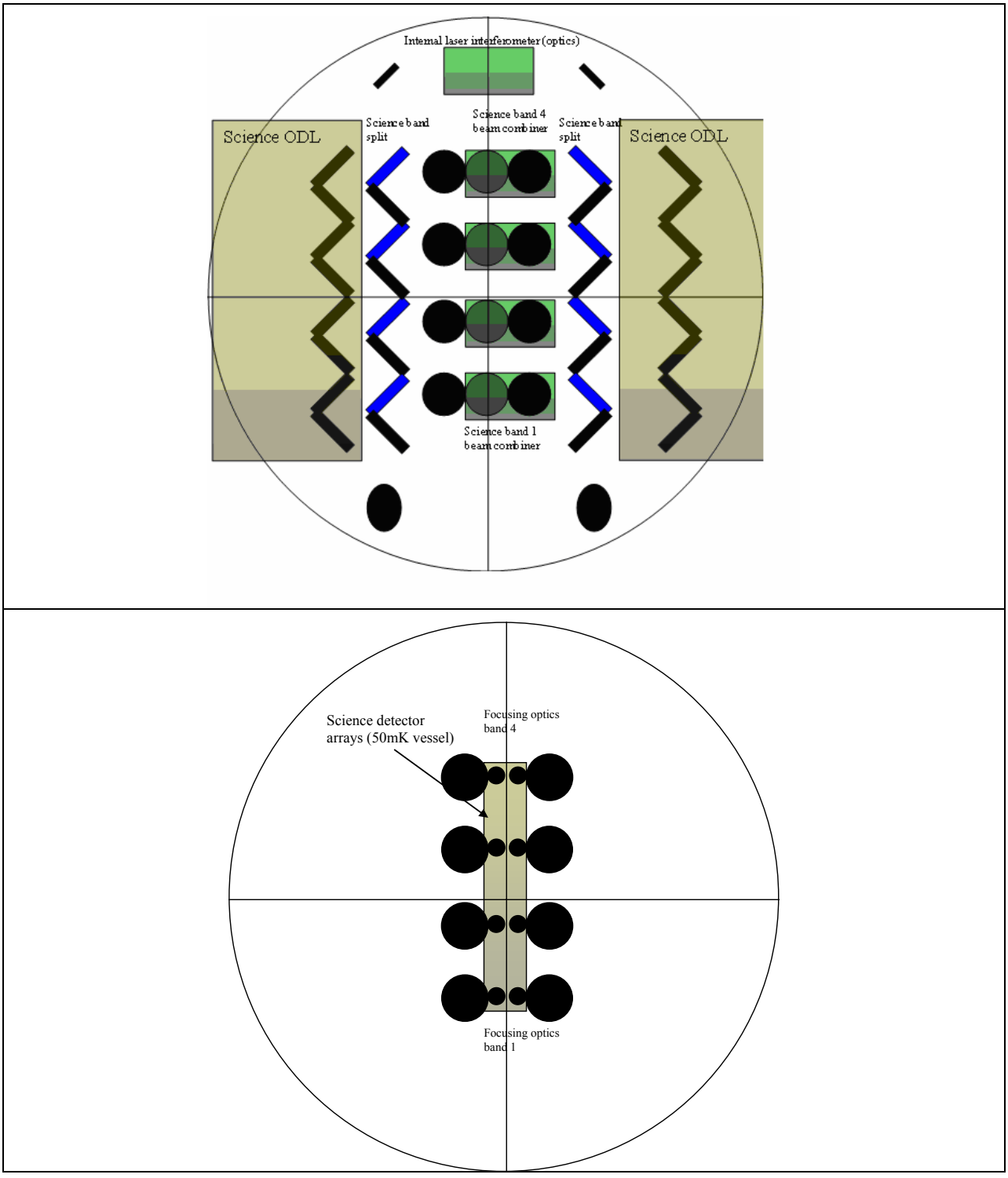

Figure 7-26: Design 1.a: on-axis hub relay telescopes with large science ODLs. 1st stage (on-axis relay hub telescopes, pupil conditioner, common ODL, beam router and fringe sensor unit). 2nd stage (science large ODLs, science beam combiner, internal laser interferometer). 3rd stage (focusing optics and science focal plane)

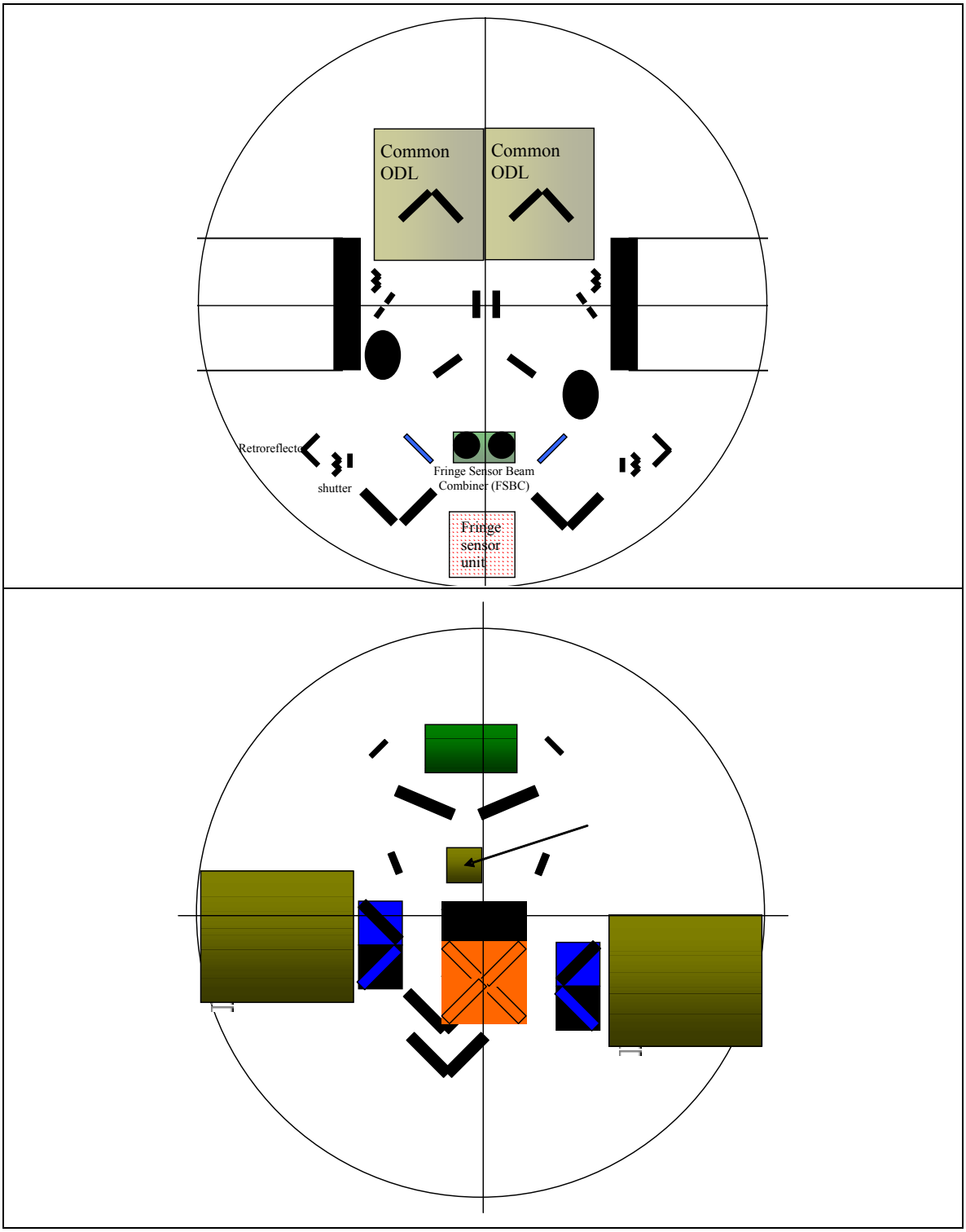

Figure 7-27: Design 1.b: on-axis hub relay telescopes with compact science ODLs. 1st stage (on-axis relay hub telescopes, pupil conditioner, common ODL, beam router and fringe sensor unit). 2nd stage (science compact ODLs, science beam combiner, internal laser interferometer, focusing optics and science focal plane)

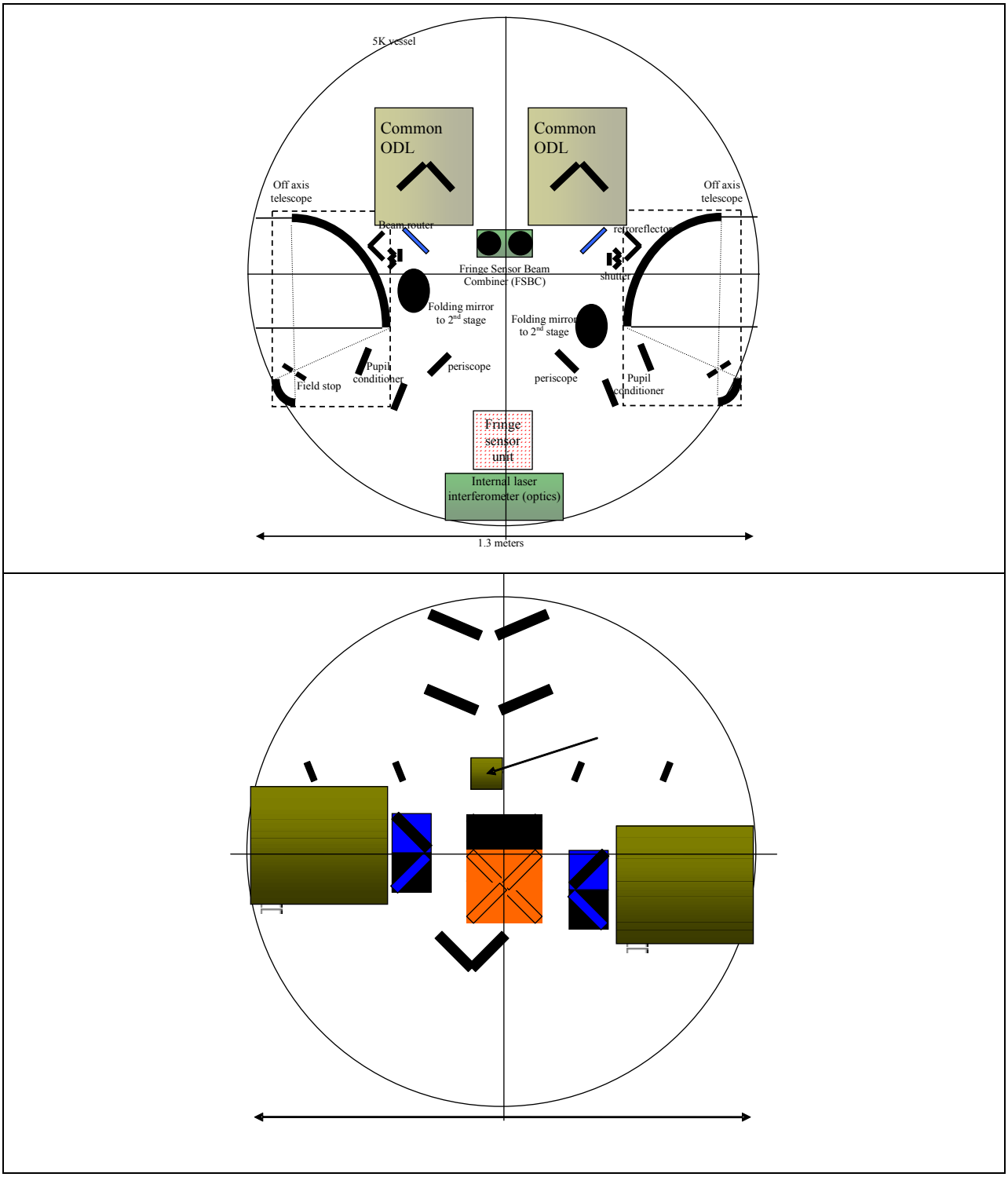

Figure 7-28: Design 2.a: off-axis hub relay telescopes with tailored science focusing optics. 1st stage (off-axis relay hub telescopes, pupil conditioner, common ODL, beam router, internal laser interferometer and fringe sensor unit). 2nd stage (science compact ODLs, science beam combiner, tailored science focusing optics and science focal plane)

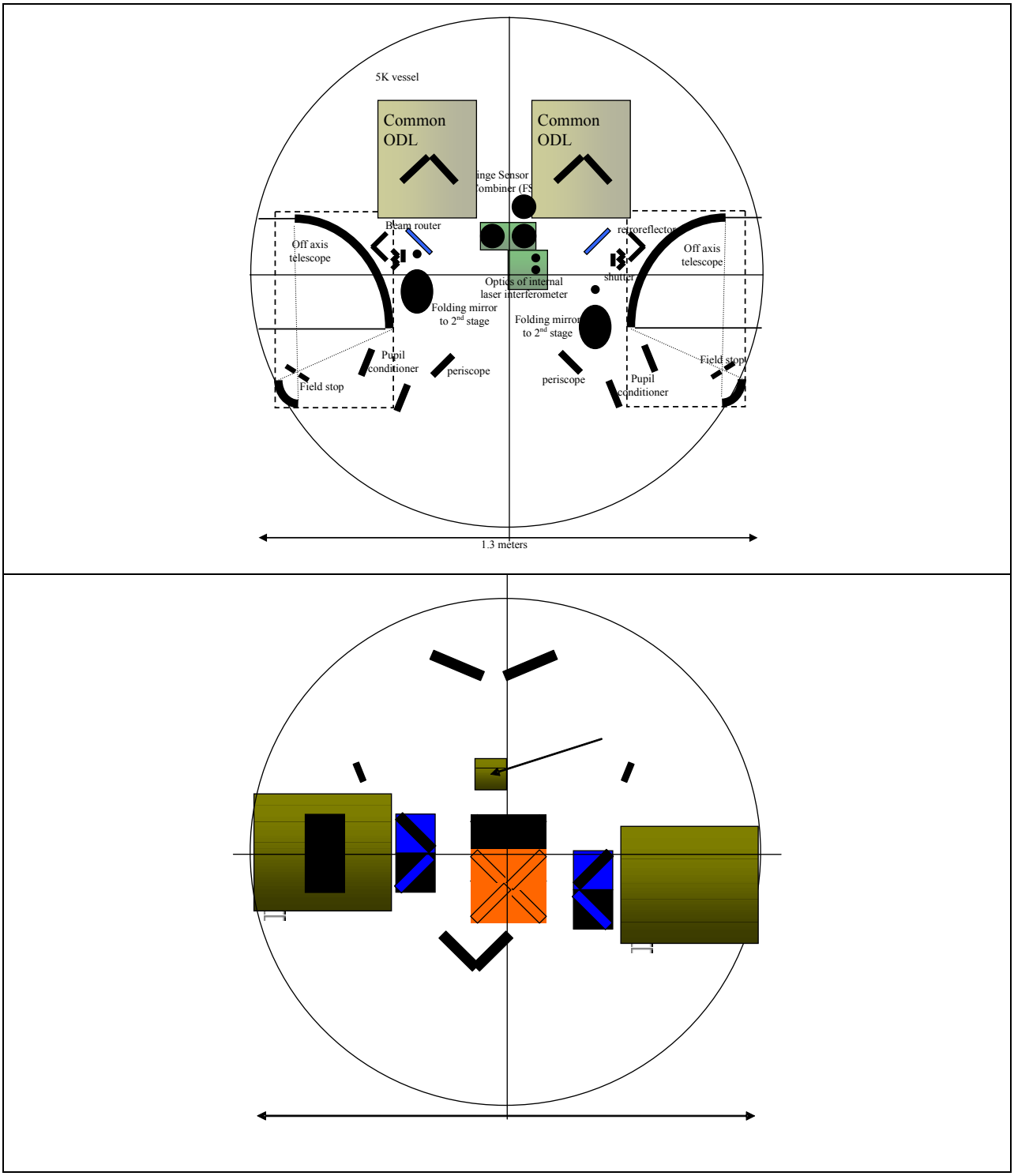

Figure 7-29: Design 2.b: off-axis hub relay telescopes with fixed science focusing optics. 1st stage (off-axis relay hub telescopes, pupil conditioner, common ODL, beam router, internal laser interferometer and fringe sensor beam combiner). 2nd stage (science compact ODLs, science beam combiner, fixed science focusing optics and science focal plane). Note that FSU has been removed from the 5K vessel and size of the laser interferometer optics has been optimized

7.1.12 Baseline Design

7.1.12.1 Light collecting telescopes

The main characteristics of the baseline design are reported in 7.1.7.2.2.

A refocusing capability on M2 is to be foreseen in order to compensate for changes in the telescopes structure and reflectors shape at cryogenic temperature. Since their temperature will be monitored and controlled, the refocusing shall be done only once, just before the beginning of scientific operations.

An example of cryogenic temperature effects on SiC telescopes WFE is reported in RD[27]. The measured WFE variation with refocusing is 337nm RMS. The equivalent visibility transfer function is 0.997@35.75µm. In 7.1.15.1.3 it is shown that this contribution to visibility error is too large and must be calibrated. Meanwhile, the WFE must be reduced to a minimum in order to improve the calibration accuracy.

7.1.12.2 Hub telescopes

7.1.12.2.1 Optical layout

The off-axis configuration shown in Figure 7-30 allows saving of volume and mass wrt on axis configuration while achieving the same optical wavefront quality without adding vignetting. By design, the hub telescope is free of cross-polarisation effect expressed in RD[30]. Nevertheless, such design is sensitive to mis-alignment thus WFE and polarisation effects might appear if the mis-alignment is too important.

The reflectors are two off-axis parabolas which share the same focus point. The distance and radius of curvature of each reflector is chosen in order to minimize the volume and the mass of the telescopes.

At the intermediary image position, one can implement a movable reflector on which will be imaged the FTS calibration source.

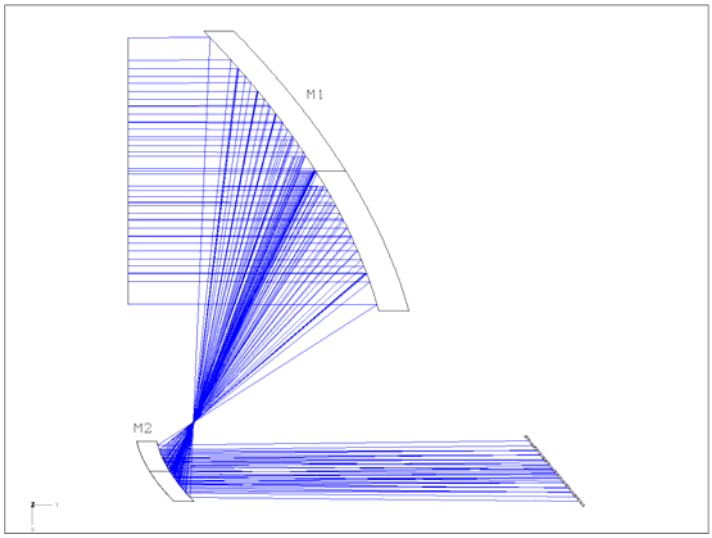

Figure 7-30: Off axis configuration

The volume can not be reduced further without increasing tremendously the sensitivity of the telescope to any change in the telescope geometry due to temperature gradient, vibrations etc…

A trade-off between the optimum volume and the sensitivity to perturbations shall be made in a further stage including a complete tolerancing of the system.

7.1.12.2.2 Reflectors description

As shown in Figure 7-31, the projection of parabolas clear aperture on a plane perpendicular to the optical axis have a diameter of 280 mm for M1 and 60 mm for M2. The distance perpendicularly to the optical axis between the centres of both parabolas is 300 mm.

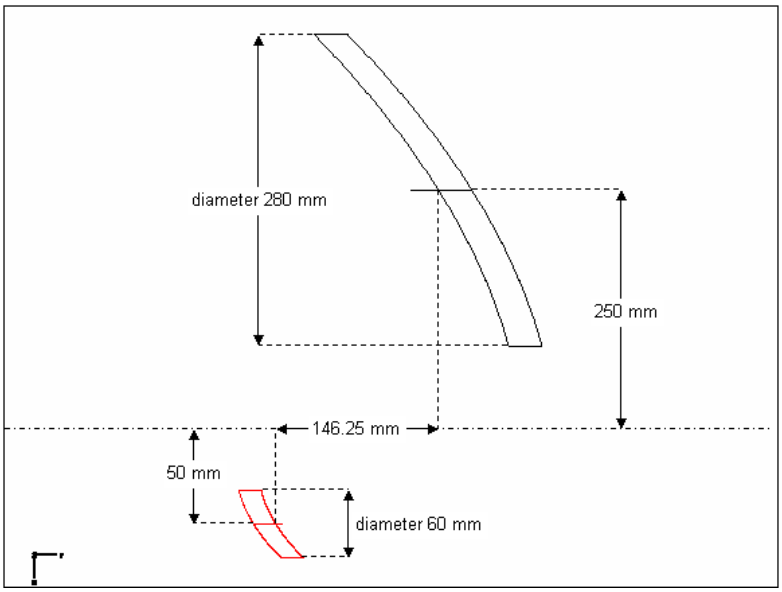

Figure 7-31: Projection of parabolas

The definitions of the reflectors surface are reported in Table 7-12.

			Off –axis distances (mm)	
	Radius of curvature (mm)	Conic constant	X axis	Y axis
M1	400 CC	-1	0	-250
M2	80 CC	-1	0	50

Table 7-12: Reflectors definition

7.1.12.2.3 Performances

The wavefront shown in Figure 7-32 include the contribution of the light collecting mirrors.

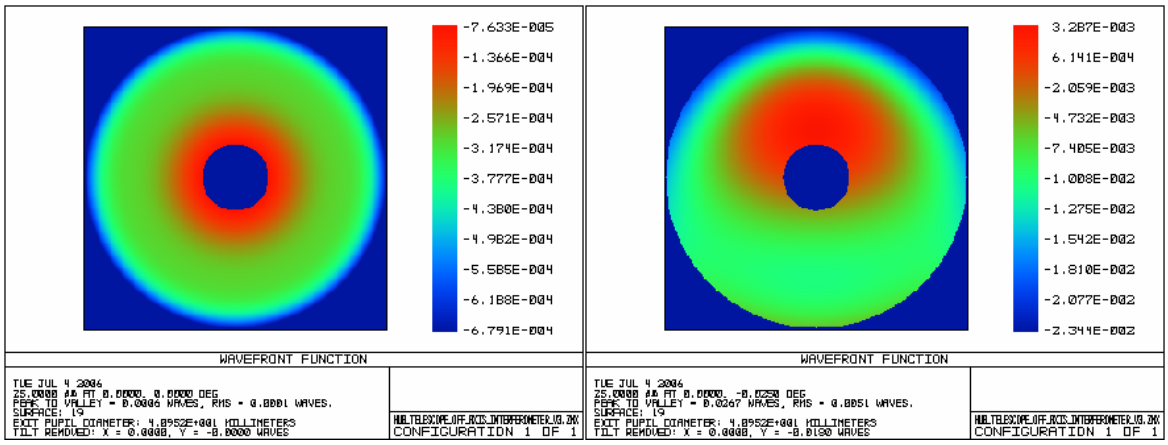

Figure 7-32: Wavefront on-axis(right) and off-axis(left)

The hub telescope has no impact on-axis since the wavefront is unchanged wrt the one shown in Figure 7-20. For angles off-axis, the WFE RMS contribution of the hub telescope is 0.004λ = 0.1 µm or λ/250 RMS @25 µm.

7.1.12.2.4 Estimated mass

The mass of the optical elements is estimated assuming a 50 kg/m^2 density.

The estimated mass is then 3 kg for the optical elements of the telescope.

7.1.12.2.5 Coatings

The reflectors will be coated with Aluminium single layer coating. The efficiency at large wavelength is 87% to 98% (RD[19]).

7.1.13 Central Hub Beam Combiner

7.1.13.1 Overall optical layout

The optical layout of the central hub beam combiner is shown in Figure 7-34. It is based on a Michelson-type interferometer with a detector array compatible with double (spatio-spectral) Fourier mode operation. By performing multiplexing in the spatial domain (detector arrays instead of a single pixel detector) and by properly scanning the science ODL it is theoretically possible to achieve with a pupil plane interferometer the required large field of view, and simultaneously, to attain the specified high spectral resolution. In order to decrease the total height, a single double-sided cryogenic optical bench is implemented. The final envelope of the central hub beam combiner is a cylinder of:

- 1.3meters diameter
- 1meter height.

The top view optical layout of the lower and upper sides is depicted in Figure 7-33(a) and (b) respectively, with the associated block diagram. The following functionalities are implemented:

- Lower side (Figure 7-33(a)): it includes for each arm of the interferometer the hub relay telescope, a field stop and a calibration body, the pupil conditioner (pair of tip/tilt mirrors to adjust the tilt and the lateral position of the relayed beam), a couple of mirrors in a periscope configuration (for beam height adjustment), the common ODL (to ensure zero-OPD locking between both arms of the interferometer), the beam router (that splits and

routes appropriately the science signal, the fringe tracking signal and the internal metrology channel), the fringe tracker beam combiner, the collimating and beam splitting optics of the internal laser metrology and the internal metrology alignment (tip/tilt mirror redirecting the beams towards the upper side).

- Lower side (Figure 7-33(b)): it contains the science ODLs, the science sub-band splitting optics, the science beam combiners, the science focusing optics and the 50 mK vessel with science focal plane, where the detector arrays are located.

Figure 7-33(c)-(g) show lateral views, 3-D view of the lower and upper side and an overall 3-D view of the single double-sided optical bench. The common ODLs are located closed to the centre of mass of the spacecraft in order to reduce induced forces and torques. It is very important to keep the total optical path at minimum, to reduce diffraction effects for the longest wavelength. The target is to keep the science path from the pupil location in the hub to the science focal plane <3m. The internal pupil diameter in the hub is 40mm, a reasonable trade-off between optics size and diffraction effects. This means that the internal angular magnification in the central hub beam combiner is 25. The optics is sized to be compatible with a 1arcmin (sky) full science FOV and 3arcmin (sky) full fringe tracking FOV. The fringe tracking beam combiner is of the same type as the science beam combiner (windmill beam combiner).

On the upper side, the science signal goes through the science ODLs, which introduce the necessary OPD for recovering the spectral information (i.e. Fourier Transform Spectrometer) and for achieving large FOV (i.e. large astrometric delays). The design of the science ODL is very compact and minimizes the footprint on the optical bench. The science ODLs are located very close to the centre of mass of the central hub beam combiner, with the movement along the inter-telescope direction, to minimize exported microvibrations. Note that a separate science beam combiner, focusing optics and detector array are used for each spectral sub-band. Because of the operating wavelength the optics are significantly bulky (compared to a visible or near-IR interferometer). The distribution of the science detector arrays in the 50mK vessel drives completely the layout of the science focusing optics. The overall dimensions of the 50mK vessel are 10x10x30 cm^3. Smaller volumes could be possible from the detector point of view. However the complexity of the focusing optics becomes an issue, and therefore the proposed design is a good compromise between optical complexity and volume of the 50mK vessel.

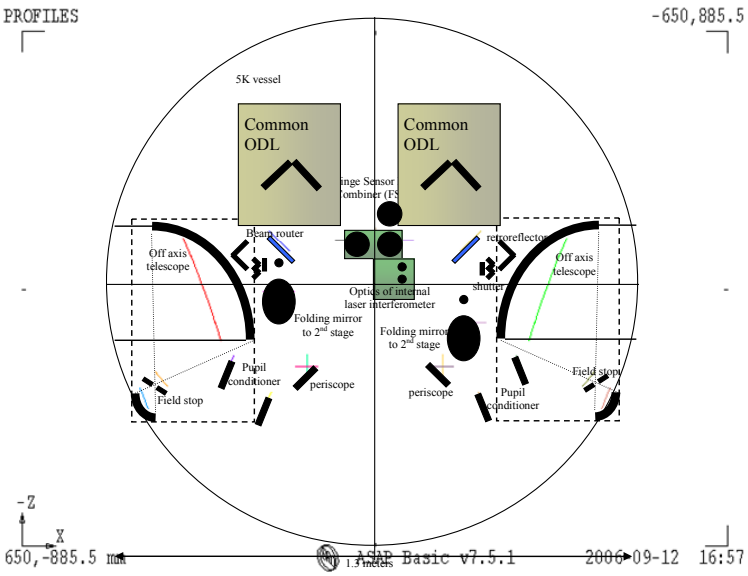
PROFILES
-650,885.5
5K vessel
Common ODL
Common ODL
Beam router
retroreflector
Off axis telescope
Off axis telescope
shutter
Optics of internal laser interferometer
Folding mirror to 2nd stage
Folding mirror to 2nd stage
Pupil conditioner
periscope
periscope
Field stop
Pupil conditioner
Field stop
-Z
X
650,-885.5 mm
1.3 meters
ASAP Basic v7.5.1
2006-09-12
16:57


PROFILES
1145,650
Y
Z
190.77,-650 mm
ASAP Basic v7.5.1
2006-09-22
19:43

A and B

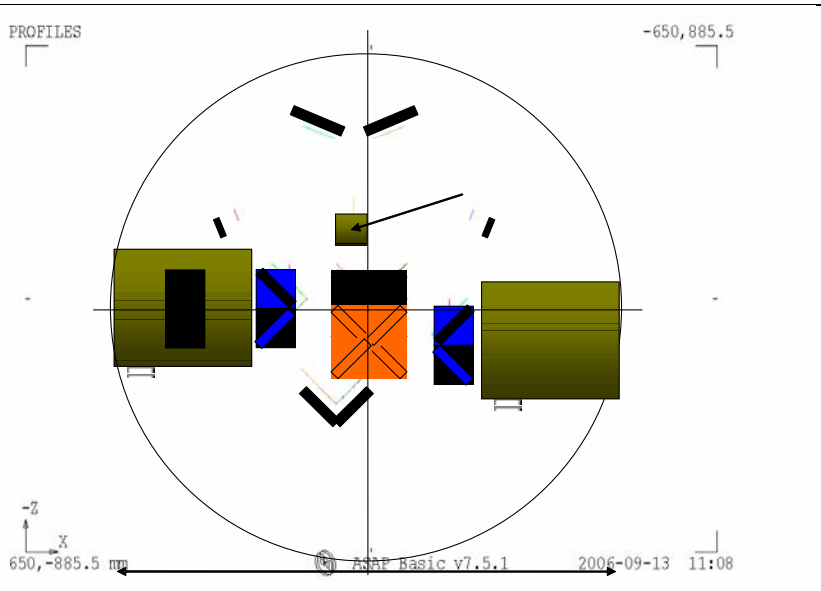

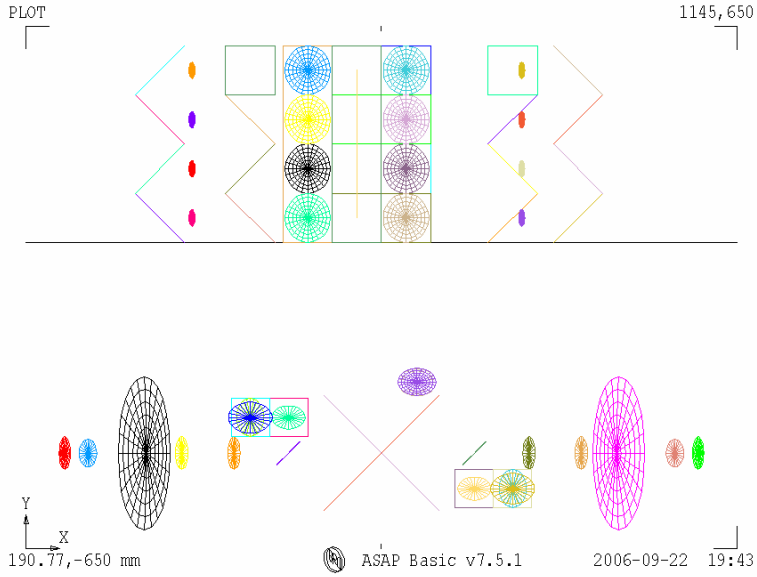

C and D

Figure 7-33: Optical layout of the central hub beam combiner using a single double-sided optical bench. (a) lower side with block diagram and optical layout, (b) upper side with block diagram and optical layout, (c) lateral view, (d) front view

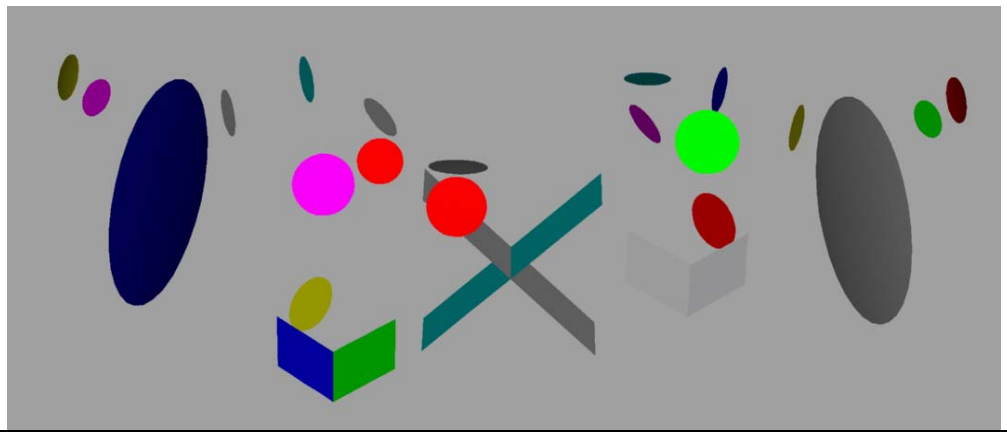

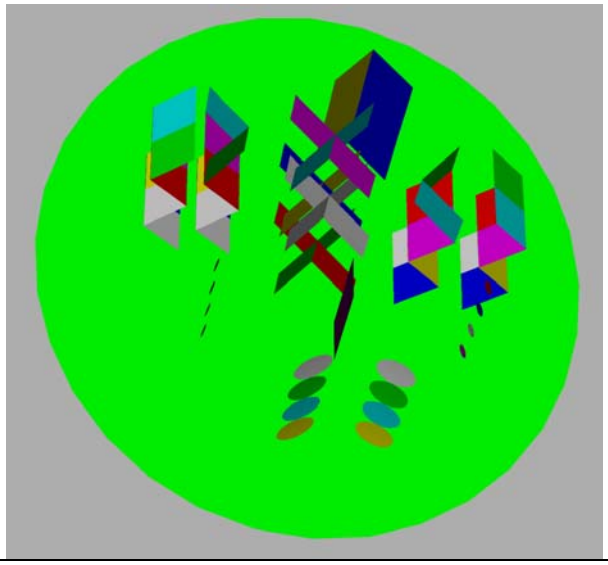

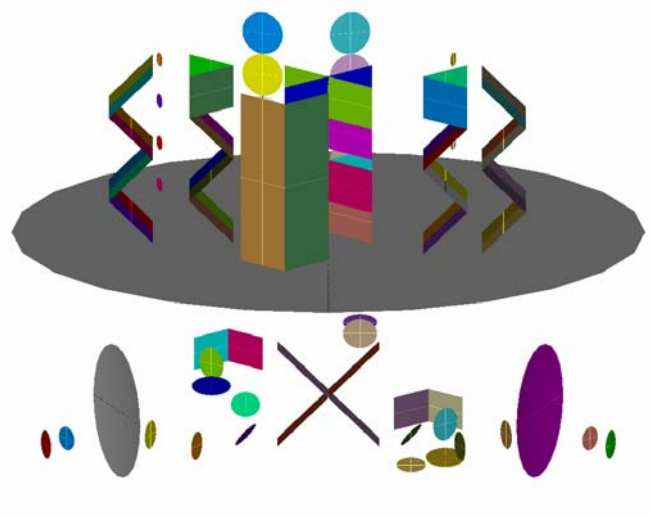

Figure 7-34: Optical layout of the central hub beam combiner using a single double-sided optical bench. (e) 3-D view lower side details, (f) 3-D view upper side details and (g) 3-D view single double-sided optical bench

7.1.13.2 Metrology sub-systems

7.1.13.2.1 Fringe tracker metrology sub-system

The fringe tracker metrology sub-system is an interferometer operating in parallel to the science interferometer. The cophasing strategy is based on dual field operation with separated beams, as discussed in 7.1.1. It basically tracks the fringes of a bright reference object (close to the dim science object under study) in order to establish a phase reference for the science image reconstruction.

The fringe tracking signal follows the same optical path as the science signal, from the LCTs up to the beam router inside the central hub beam combiner. At the beam router, the science and the fringe tracking signal are split. The fringe tracking signal goes towards the fringe tracking beam combiner (inside the 5K vessel), and finally, after recombination, it is transferred to the FSU (located outside the 5K vessel on a *warm* optical bench, see 7.1.13.2.4), which includes the fringe tracking focusing optics and the fringe tracker sensors. The fringe tracking signal operates at visible – near IR wavelength in order to reduce the size of the optics (given the large needed FOV) and to increase the resolution. This different operating wavelength band will not affect the mirror surface roughness requirements. It has been calculated that the minimum FOV for the FSU compatible with all the required functionalities (described in 7.1.6.1) is ±1.5 arcmin. This FOV ensures (with >95% probability) at least two objects adequate for fringe tracking and spacecraft attitude monitoring (i.e. fine star tracking). The different signals reaching the FSU are represented in Figure 7-35.

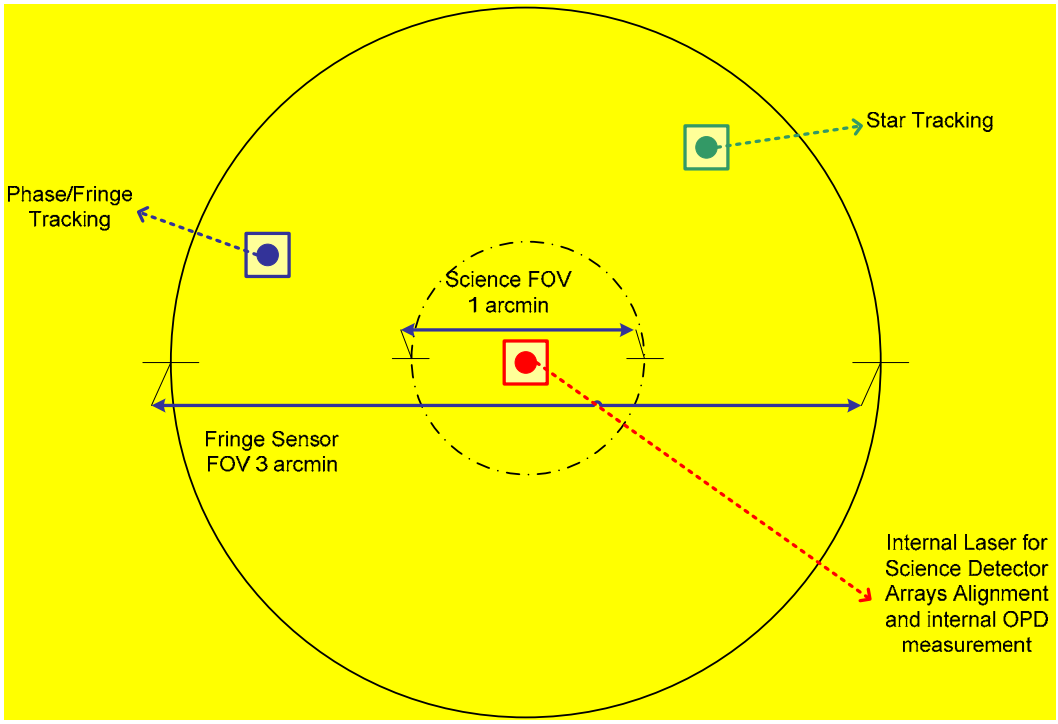

Figure 7-35: Metrology signals at the FSU

The positions of the 2 signals of the internal laser metrology are aligned to the centre of the FSU by means of the internal metrology tilt alignment mirrors. The overlap of the 2 beams produces

fringes (i.e. by correct commanding of the science ODLs in science observation mode). The pupil conditioner units adjust the position of the images generated by each LCT in the FSU such that fringes of the reference object are observed once the common ODLs are properly adjusted. The common ODLs will operate continuously in order to lock to the zero-OPD position. The FOV of the FSU is sufficiently large to ensure the detection of a second bright non-resolved point source that can be used for attitude control of the spacecraft.

The main specifications of the FSU are:

- Operating environment: outside the 5K on the *warm* optical bench
- OPD accuracy: 125nm
- OPD resolution: 50nm
- Tilt accuracy: 15marcsec
- Tilt resolution: 7.5marcsec
- 2160x2160 pixels (better 2500x2500): one operation and one redundant
- Wavelength range: 0.6um-2um (e.g. 1064nm or 1550nm).

These specifications assume that the accuracy of the AOCS sub-system is <4arcsec. Inside the FSU it is envisaged to include a lateral position sensor to monitor lateral beam displacements (~25um accuracy). The metrology data collected by the FSU is used by the ICU to command the different actuators in the optical chain (e.g. common ODLs, pupil conditioner units, internal metrology tilt alignments, science ODLs and beam router), as represented in Figure 7-5.

7.1.13.2.2 Internal laser metrology sub-system

A possible implementation of the internal laser metrology sub-system is by means of a heterodyne interferometer. A similar internal laser metrology is under development for DARWIN mission. It is conceived to have both narrowband and broadband sources being on active/idle state depending on the operational mode. For instance the broadband source could be used to calibrate the zero-OPD between the science focal plane and the FSU. It is assumed that the alignment between the internal laser metrology and the science focal plane is well preserved during the entire mission lifetime, relying only on passive alignment stability characteristics of the optical bench (~arcsec).

The sources will be located on the *warm* optical bench (see 7.1.13.2.4). The metrology signals will be transferred to the cold optical bench by means of fibres. The collimating and the beam splitting optics will be located on the lower side of the cryogenic optical bench. The signals will then be routed backwards through the science ODLs and redirected by the beam router towards the fringe tracker beam combiner. The recombined and the reference beams are transferred to the FSU located on the *warm* optical bench where detection takes place.

The main characteristics are summarized in Table 7-21.

7.1.13.2.3 Absolute laser metrology sub-system

The main function of the absolute laser metrology is explained in 7.1.6.3. Similar technology is under development for DARWIN mission (i.e. dual wavelength interferometer). It is located on the *warm* optical bench (see 7.1.13.2.4) inside the central hub beam combiner. Small hollow retroreflectors are accommodated in the LCTs as counterparts for the absolute laser metrology sub-system.

This sub-system is mandatory provided no RF metrology system is available. In case an RF metrology were available (i.e. with absolute longitudinal distance accuracy <0.5cm), the internal laser metrology sub-system, in cooperation with the common ODLs and the FSU (and with an appropriate configuration of the beam router), could replace the functionality of the absolute laser metrology sub-system.

The main performances are listed in Table 7-21. Full redundancy is considered for each arm of the interferometer. Given the significant amount of mass, size and power consumption it would be recommendable to have an RF metrology sub-system accurate enough such that the absolute metrology subsystem can be disembarked.

7.1.13.2.4 Warm optical bench

In addition to the single double-sided cryogenically cooled optical bench (inside the 5K vessel), it is foreseen to accommodate a *warm* optical bench outside the 5K vessel, just underneath the cold optical bench, in order to facilitate the beam transfer between the benches (i.e. fringe tracking signals and internal laser metrology signals). The free beam diameter of the fringe tracking signals (i.e. 2 beams) transferred from the cold bench to the warm bench is >85mm. For the internal metrology signals, fibres are used for the two outgoing signals and, for the incoming beams (i.e. 4 signals, 2 of them coaligned with the fringe tracking signals), free beam diameters ~25mm are needed. A schematic of the *warm* optical bench and its parts is shown in Figure 7-36.

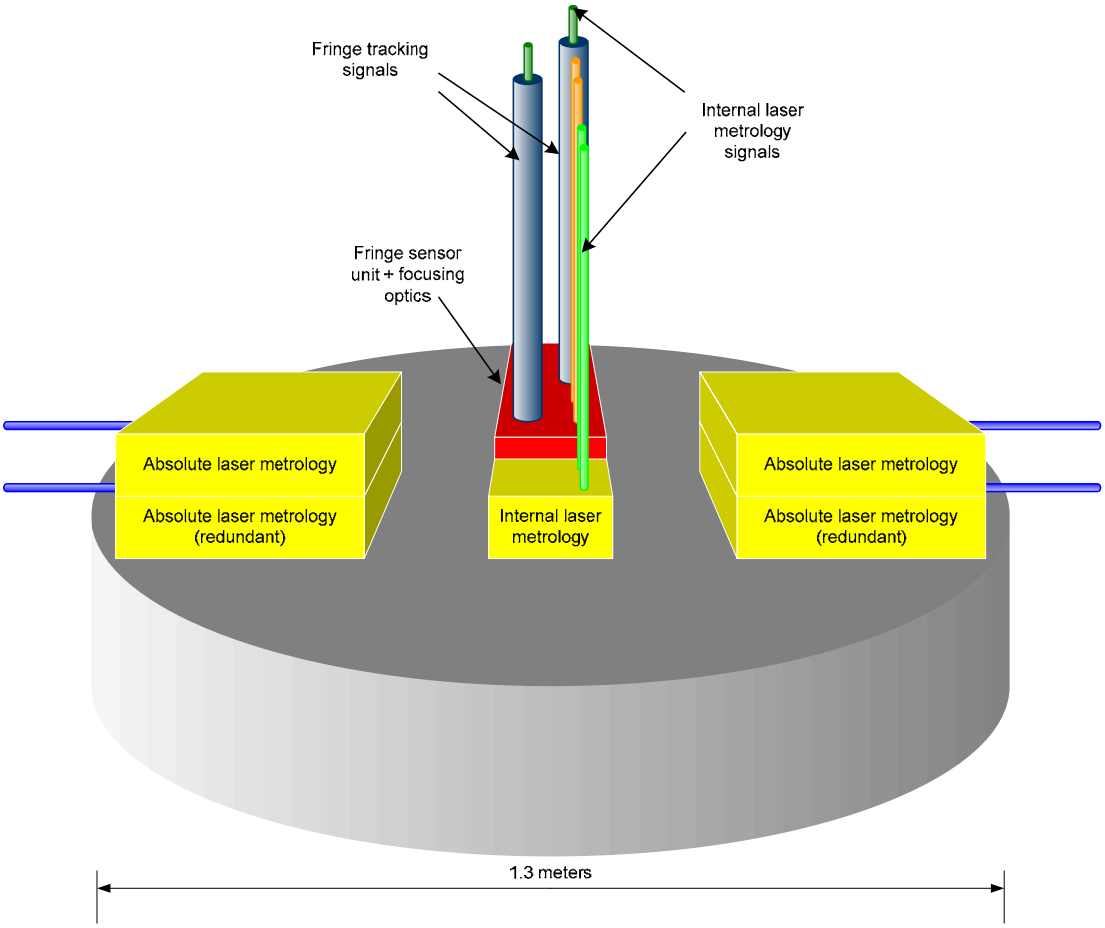

Figure 7-36: Warm optical bench and warm optical parts

It contains the following sub-systems:

- Absolute laser metrology (for each interferometer arm, operational and redundant unit)
- Optical head unit of the internal laser interferometer
- Fringe sensor unit (including beam splitters, focusing optics, operational & redundant fringe sensor detector arrays and operational & redundant lateral position sensors).

The main characteristics are summarized in Table 7-22. Given the targeted tilt accuracy/resolution of the FSU, it is mandatory to ensure sufficient alignment stability between the cold and the warm optical benches. Passive and/or active alignment techniques have to be investigated in a future study. In case the required alignment stability cannot be met, then the FSU will have to be transferred into the 5K vessel. However this would require important technology development.

7.1.13.3 Science sub-systems

7.1.13.3.1 Alignment mechanisms in the light collecting telescope

The requirements of the telescope pointing mechanism, the field separator pointing mechanism and the secondary mirror alignment mechanism are listed in Table 7-21. These specifications take into account +/-15 cm maximum vertical displacement of the LCTs at the edges of the boom (i.e. boom deformation).

7.1.13.3.2 Pupil conditioner and internal tilt alignment

The specifications are summarized in Table 7-22. Those requirements are in line with a maximum visibility loss ~15% of the fringe tracking signal at the shortest wavelength (worst case) considered for the fringe tracker metrology sub-system (i.e. 0.6μm). At longer wavelength visibility loss is reduced. The 15% maximum visibility loss allows to be compliant with the required 6% of maximum visibility total science loss of the optical system.

7.1.13.3.3 Common ODL

For redundancy purposes each arm of the interferometer is provided with one common ODL. The common ODLs are used in conjunction with the Fringe Sensor Unit (FSU) in order to acquire fringes from a reference object, to lock into the zero optical path difference (i.e. two arms of the interferometer perfectly cophased) and to keep tracking the zero OPD position on this sufficiently bright non-resolved point source. By keeping this zero OPD position on the off-axis reference source, a phase reference (i.e. phase tracking centre), necessary for correctly recovering the spatial information of the on-axis extended science object, can be established.

The main specifications of the common ODL are presented in Section 7.4:

From the technical complexity point of view, with the exception of the extremely low dissipation requirement, the common ODL is much simpler than the science ODL. The ODLs pre-developments for DARWIN mission have demonstrated on-ground dynamic performances (~nm OPD stability and resolution, mechanical stroke <1cm, operating temperature 40K) similar to or even better than what is needed for the common ODL for FIRI.

7.1.13.3.4 Beam router

The functional description is provided in 7.1.5.5. The main characteristics are summarized in Table 7-23.

7.1.13.3.5 Science Optical Delay-line

The science ODL is managing the complete science wavelength range. For redundancy purposes each arm of the interferometer is provided with one full science ODL. A single mechanical unit is handling simultaneously the optical path scanning for each spectral sub-band. The most important benefit of this approach is the reduction of the overall system complexity, as only one actuator and one guidance mechanism are needed. The moving part of the ODL holds the optics that adjusts the optical path difference for all the science sub-bands. Because of that, the mass and size of the optics is larger than the optics needed for only 1 sub-band. However, by means of a proper design, the optics can be quite compact, and estimations of the overall mass, size, and dissipated power favour the design of a compact science ODL handling all the spectral sub-bands (savings ~ 30%) rather than having smaller separate science ODLs for each spectral sub-band.

The main specifications of the science ODL are presented in Section 7.4:

As far as the actuator trade-off is concerned, either a voice coil or a linear motor is the preferred option. Inchworms are discarded due to the lack of sufficient cryogenic operation heritage with respect to voice coils. As a matter of example, for the DARWIN ODLs at 40K a voice coil actuator has been selected and successfully tested.

A critical part of the ODL is the guidance mechanism.

- **OPD and mechanical stroke**

The total mechanical stroke is driven by:

- The FTS
- The scanning of the science FOV.

For the spectrometer the maximum OPD stroke is given, at first order, by $OPD_{FTS} \approx \lambda R$. Since the four sub-bands use the same delay-line, the OPD is driven by the smallest average wavelength thus OPD_{FTS} = +/- 53.63 mm.
The science FOV corresponds, at the maximum distance ITD_{max} between the LCT, to an OPD of +/-4.36 mm.
The total OPD and mechanical stroke is given in Table 7-13.

		OPD stroke (mm)	Mechanical stroke (mm)
Spectrometer		+/- 53.63	+/-26.82
Field scanning		+/- 4.360	+/-2.18
Total	**Needed**	**+/- 58**	**+/- 29**
	Margins	**+/- 12**	**+/- 6**
	Required	**+/- 70**	**+/- 35**

Table 7-13: OPD and mechanical stroke

The margin will compensate for any drift of the zero position of the science delay-line.

With those requirements, resolving power lower than 3000 can be achieved by applying a smaller OPD stroke but on contrary larger resolution can not be achieved.

- **OPD step and sampling points**

  The OPD step is driven by the correct sampling of the reconstructed spectrum of the science target. The Nyquist criterion requires that $\Delta OPD \leq \frac{\lambda_{\min}}{2}$, with λ_{min} the lowest wavelength of observation at each sub-band. The minimum number of sampling points is the same for any sub-band, as the necessary OPD to achieve the required spectral resolution is also dependent on the sub-band. The minimum OPD step for each sub-band is reported in Table 7-14.

Sub-band	OPD step (μm)	Mechanical step (μm)
1	12.5	6.25
2	23.25	5.81
3	43.3	5.41
4	80.6	5.04

Table 7-14: OPD step and mechanical step

The number of sampling points is given by the smallest needed mechanical step over the needed mechanical stroke thus the useful number of sampling points is 2x29mm/5.04μm = 11508 points.

7.1.13.3.6 Science beam combiner

The science beam combiner is based on the windmill concept explained in 7.1.9. A separate beam combiner is used for each sub-band. Two identical outputs are available for operational and redundancy use. The main characteristics are listed in Table 7-22.

7.1.13.3.7 Science focusing optics

The focusing optics is based on a 2-mirror design. According to 7.1.10, the design has similar optical characteristics (i.e. effective focal length) for all sub-bands. The main specifications are summarized in Table 7-10 and Table 7-22.

7.1.13.3.8 Focal Plane Array

The specified spectral range is divided in four sub-bands which are summarised in Table 7-15.

Sub-band	**λ_{min} (μm)**	**λ_{max} (μm)**	**$\lambda_{average}$ (μm)**
1	25	46.5	35.75
2	46.5	86.6	66.55
3	86.6	161.2	123.90
4	161.2	300	230.60

Table 7-15: Sub-bands definition

7.1.13.3.9 FTS calibration sub-system

The FTS must be calibrated in-flight. The calibration deals with the wavenumber (shift of the measured wavenumber due to source size) and radiometric calibration of the detectors (flat-field calibration). The calibration source includes two blackbodies at two different temperatures. The temperatures are: 31K (TBC) and 13K (TBC), they correspond to the peak emission at λ = 93.5μm and λ = 223μm. More than two temperatures might be needed if the total flux emitted by the blackbodies in each sub-band is not sufficient to achieve the calibration accuracy which is TBD.

The blackbodies can be obtained with a simple plate which emissivity at both temperatures is calibrated and temperature monitored.

For such calibration it is necessary to measure the spectrum of the blackbodies, thus the light emitted by the calibration source must entered into the two arms of the interferometer.

The exact design of the FTS calibration sub-system is TBD. The temperatures of the blackbodies must be optimised accordingly to the required accuracy on spectral resolution and SNR.

7.1.13.4 Optical throughput

The total reflection efficiency (from the LCT entrance to the science detector array) is represented in Figure 7-37, as a function of the reflection coefficient per surface. For a typical value of 98%, the overall reflection loss is ~50% for sub-band 4 (longest wavelength) due to the larger number of internal reflections. For sub-band 1 (shortest wavelength) the overall efficiency is ~63%.

The breakdown budget of the optical throughput for the worst case science sub-band (i.e. sub-band 4) is presented in Table 7-16. It has been assumed a reflection coefficient per surface of 98%. The optical throughput is ~21%. For sub-band 1 it increases up to ~28%. Note that the science beam combiners provide two identical outputs. The values given above are per output.

For the fringe tracking optical path, worst optical throughput was expected as the reflection coefficient at visible/near-IR wavelengths degrades. For a typical value of 90%, the overall throughput is ~7% (per output). The breakdown budget is given in Table 7-17. Likewise the science beam combiners, two identical outputs are also available at the fringe tracker beam combiner.

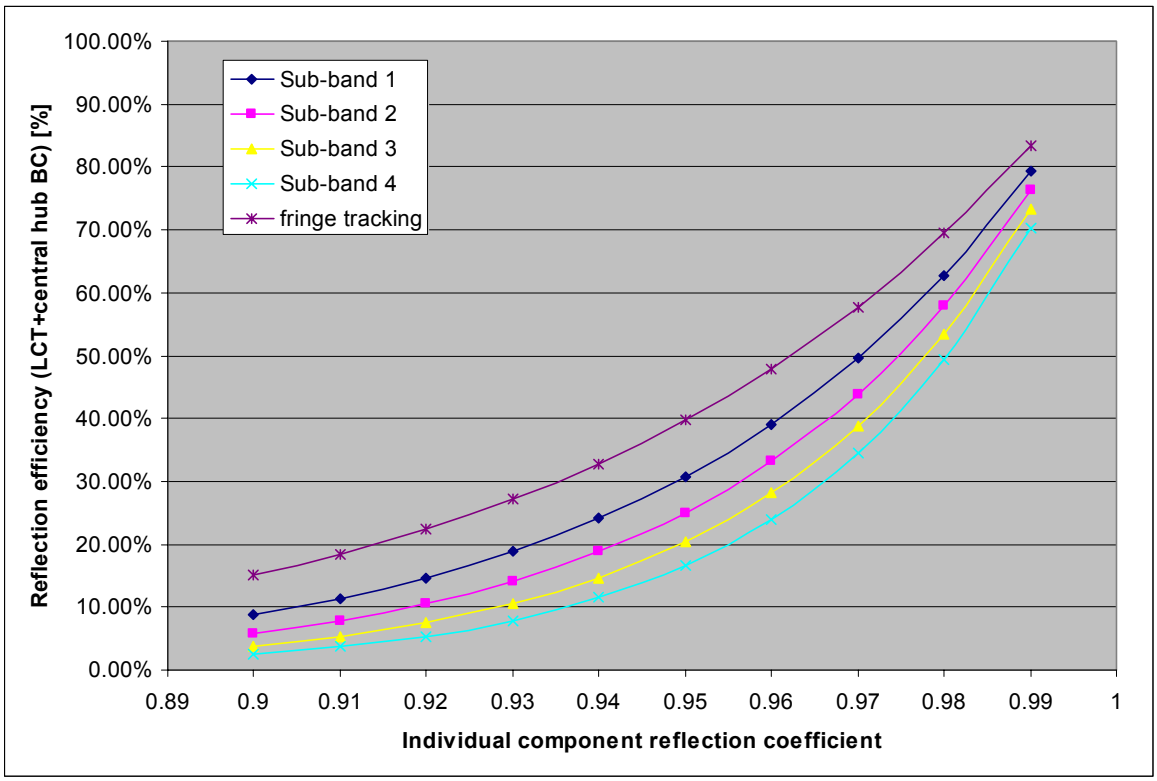

Figure 7-37: Overall reflection losses as a function of the individual reflection coefficient for the different sub-bands

LCT	blocking loss	0.22	dB	secondary mirror
	reflection loss	0.36	dB	with 98% reflection coefficient per component
Central hub	diffraction loss	0.46	dB	at hub telescope entrance
	reflection loss	2.72	dB	worst case sub-band 4 with 98% reflection coefficient per component
	beam combiner loss	3.01	dB	inherent efficiency wrt total collected power by inteferometer
Interferometer optical loss [dB]		6.77	dB	
Interferometer optical throughput [%]		21.03%		Optical power available at each of the 2 identical outputs of the science beam combiner with respect to the total collected optical power by the 2 LCTs.

Table 7-16: Optical throughput breakdown budget for science optical path (sub-band 4 worst case)

LCT	blocking loss	0.22	dB	secondary mirror
	reflection loss	1.83	dB	with 90% reflection coefficient per component
Central hub	diffraction loss	0.04	dB	at hub telescope entrance
	reflection loss	6.41	dB	fringe tracking with 90% reflection coefficient per component
	beam combiner loss	3.01	dB	inherent efficiency wrt total collected power by inteferometer
Interferometer optical loss [dB]		11.51	dB	
Interferometer optical throughput [%]		7.06%		Optical power available at each of the 2 identical outputs of the fringe tracker beam combiner with respect to the total collected optical power by the 2 LCTs.

Table 7-17: Optical throughput breakdown budget for fringe tracking optical path

7.1.13.5 Mass and power consumption budgets

The overall mass, power dissipation and power consumption of the (cold/warm) optical parts in the LCTs and the central hub beam combiner are summarized in Table 7-18. For more details refer to Table 7-21-Table 7-22. Note that the ODLs include both common and science ODLs (operational and redundant, mechanism & optics). Important mass and power consumption savings could result in case the absolute laser metrology is finally discarded (see 7.1.16.4 for discussion). Additional significant mass reductions are possible by not having fully implemented ODLs on one of the arms of the interferometer.

			Total Mass [kg]	Total Dissipated Power [W]	Total Power Consumption [W]
Light Collecting Telescopes (2)	Cold parts		93.1	0	4
	Warm parts		0.2	0	0
Central Hub Beam Combiner	Cold parts	Cold optics	49.01	0	14
		ODLs	180	0.022	133
		Cold optical bench	45	0	0
	Warm parts	Warm optics	71.55	55	55
		Warm optical bench	35	0	0
Total			473.86	55.022	206

Table 7-18: Overall mass, power dissipation and power consumption of the optical parts

7.1.13.6 Alignment procedures and operational modes

In order the interferometer to be able to operate in the science observation mode, the following list of alignment procedures and operational modes are envisaged:

- Interferometer pre-alignment: the LCTs are brought to opposite edges of the boom and the full interferometer is pointed coarsely towards the scientific object, using only standard attitude sensors (i.e. star trackers). The central hub beam combiner is internally prealigned using the internal laser metrology (e.g. alignment of the science focal plane array and the FSU).

- Light Collecting Telescope alignment: the LCTs are pointed towards the scientific object by means of the telescope pointing mechanism, in order to have the scientific object within their diffraction limited FOV of +/-3arcmin. Standard or specific (TBC) star trackers can be used as attitude sensors for this alignment. It is assumed that defocus has previously been compensated for. Otherwise the secondary mirror alignment mechanism adjusts the position and the tilt of the secondary mirror.
- Relay beam alignment: the field separator pointing mechanism is scanned until it illuminates the hub relay telescope. An image of the sky (i.e. containing the phase reference object and a second bright point source) is detected in the FSU by coarsely aligning the pupil conditioner tip/tilt mirrors. Same operation is carried out for both telescopes and the relative tilt and lateral displacement of the two beams is minimized. The FOV of the LCTs overlap in the FSU but they are still out of coherence.
- Coarse inter telescope distance adjustment: the objective is to reach an OPD smaller than the common ODL stroke. This is achieved by moving the carriages with the LCTs and monitoring the absolute longitudinal distance by means of the RF metrology. If it is not sufficiently accurate then the absolute longitudinal distance between the LCTs and the central hub can be measured more precisely using the absolute laser metrology sub-systems. Possible offsets have been calibrated during the commissioning phase.
- Fine inter telescope distance adjustment: the internal laser metrology takes over and stabilizes the OPD between the LCTs and the central hub beam combiner by operating the common ODLs. Fringes from the internal laser metrology are used to monitor the relative OPD.
- Fringe scanning mode: one of the common ODLs is scanned in order to get the fringes of the phase reference object in the FSU.
- Zero-OPD acquisition mode: once within the coherence length, one of the common ODLs is finely scanned in order to get the zero-OPD position in the FSU and lock into it.
- Zero-OPD tracking mode: the common ODL is continuously adjusted according to the FSU measurements, in order to compensate for any potential external/internal OPD disturbance. The measured OPD accuracy is then within the specified values.
- Science observation mode: one of the science ODLs is scanned in order to record the interferogram associated to 1 uv-point. The science ODL is monitored by the internal laser metrology. It is assumed that the whole interferometer is spinning at very low constant angular speed (i.e. not to blur fringes). After having recorded the interferograms for all the orientations the inter telescope distance is adjusted (i.e. step in using the LCT carriage). The fringes of the phase reference object could be lost while manoeuvring. In that case, the process starts again from the coarse inter telescope distance adjustment step or the fine inter telescope distance adjustment step, depending on the smoothness of the carriage movement. The science observation mode ends when the complete uv-plane is sampled.

7.1.14 Visibility Error Budget

The error budget given here is preliminary. It depends on assumptions which are TBC. The top-down approach of the visibility error budget is to be completed.

The purpose here is to list all the possible contributors to the visibility loss. An example of error budget breakdown is shown assuming a visibility loss of 6%.

7.1.14.1 Visibility transfer factor requirement

The visibility transfer factor T is defined as the ratio of the fringe pattern visibility measured and the actual visibility of the light source (RD[13]). The visibility transfer factor includes the effects which depress the amplitude of the observed fringes.

The total visibility factor is obtained by multiplying all the visibility transfer factors for each error contributors.

The visibility loss of 6% corresponds to a transfer factor of 0.94.

7.1.14.2 Visibility loss contributors

The contributors at system level to visibility loss are:

1. Amplitude of interfering beams mismatch (including polarisation mismatch)
2. Interfering wavefront relative tilt
3. Optical aberrations (wavefront error)
4. OPD change during scanning of the uv-plane and also during measurement for one point in the uv-plane.
5. Pupil shift

Each of those contributors can be split into contributors at components level. The complete top-down breakdown of visibility error budget must be done in a complete and future study.

The main identified error contributors are presented in Table 7-19.

7.1.14.2.1 Preliminary visibility error budget breakdown

The error budget shown in Table 7-19 is a basis for an accurate and complete error budget taking into account the actual impact of each contributor. For this feasibility study each main perturbation source is supposed to contribute equally in the visibility error budget.

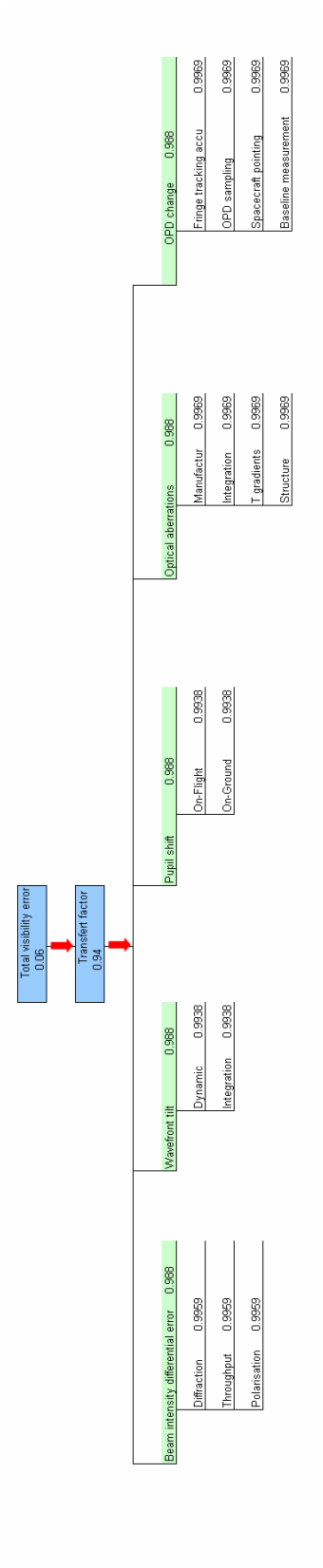

Table 7-19: An example of visibility error budget breakdown

7.1.14.2.2 Intensity beam mismatch

The visibility defined as follow $\mu = 2\sqrt{I_1 I_2}\,/\,(I_1 + I_2)$ leads to the calculation of the influence of beam intensity mismatch on visibility loss. According to Table 7-19, the intensity mismatch between the two must be lower than 27%. This value must be split between the differential diffraction pattern, the polarisation mismatch between the two interfering beams and the differential throughput between the two arms of the interferometer.

The contribution of differential phase-shift between polarisations, differential throughput and diffraction are supposed to be calibrated.

7.1.14.2.3 Wavefront tilt

A tilt of the beam induces a tilt of the interfering wavefronts inside the hub. Thus the visibility transfer factor is scaled by the diffraction angular spectrum illustrated in Figure 7-38 due to pupil diameter at hub entrance.

For the value of T defined in Table 7-19, the maximum tilt between the wavefronts in the hub is 62µrad or 13 arcsec@25µm.

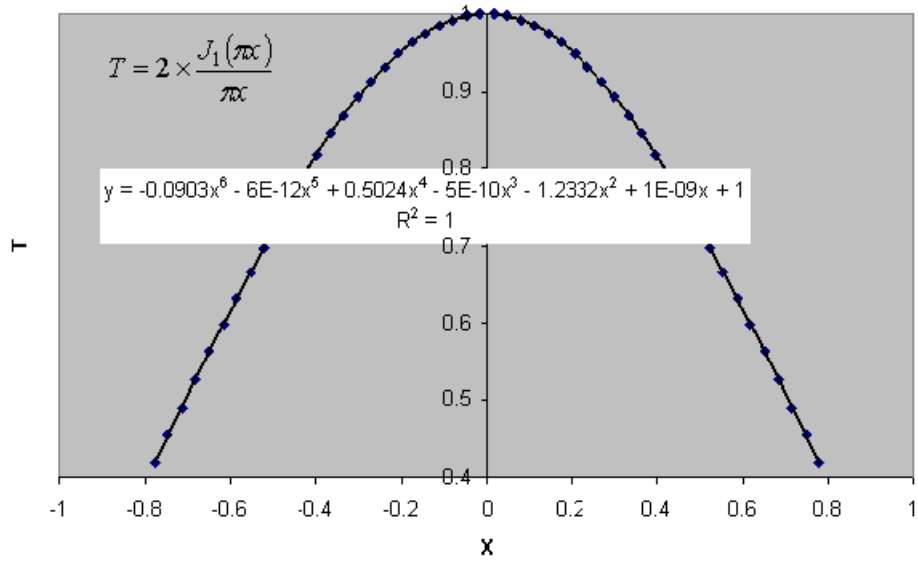

Figure 7-38: Diffraction angular spectrum

The wavefront tilt sources are:

- Integration and alignment on-ground of optical elements. This can be calibrated even at cryogenic temperatures. Thus the calibration residuals and accuracy appear in the error budget.
- Relative tilt of interferometer's arm optical axis due to structure vibrations. This contributor is corrected in real-time. The correction residuals are part of the visibility error budget.

7.1.14.2.4 Optical aberrations

According to RD[13], the visibility loss due to the optical aberrations is equivalent to the Strehl ratio due to those aberrations. Thus for T = 0.988, the WFE allowed in the hub is WFE_{RMS} = 0.009λ.

For the different sub-band at the central wavelength this leads to the numbers reported in Table 7-20 for each arms of the interferometer.

Sub-band	WFE_{RMS} (µm)
1	0.22
2	0.42
3	0.78
4	1.44

Table 7-20: WFE for each sub-band and for one arm of the interferometer

Those WFEs are applicable during operations. The contribution of WFEs due to integration and alignment of the optical sub-systems are supposed to be calibrated. The contribution of calibration residuals to the error budget are reported in Table 7-19. Contributions due to temperatures gradient and changes in the structure are also reported in Table 7-19.

7.1.14.2.5 OPD change

Any OPD change will be detected by the fringe tracking sub-system and compensated by the delay-line. Consequently, in the visibility budget appears the residuals of the OPD correction. In the worst case, where the fringe tracking is done over an integration time significant wrt to the frequency of the OPD perturbations, the factor T can be described by (RD[12]) $T = \mathrm{sinc}\left(\pi \times \frac{OPD}{\lambda}\right)$. Thus at the lowest central wavelength the OPD correction residuals must be lower than 1.55µm for T=0.9969 and λ=35.75µm. The assumptions leading to this conclusion are TBC.

In Table 7-19 are reported the residuals left after calibration of OPD sampling error, fringe tracking accuracy and spacecraft attitude calibration.

This OPD variation corresponds to a tilt of spacecraft of 0.0106 arcsec for B = 30 meters at λ=35.75µm.

The OPD sampling error is directly 1.55µm.

The inter telescope distance stability during one spectrum measurement must be better than 7.5 mm. This distance is accurately monitored thanks to the metrology sub-system. This OPD variation can thus be compensated by data post-processing in order to achieve a transfer factor greater than T=0.9969.

7.1.14.2.6 Pupil shift

According to RD[12], the pupil contribution is estimated by $T = 1 - \frac{8\delta}{\pi D}$, where δ is the pupil displacement and D the pupil diameter in the interferometer.

With a magnification of 25, the displacement is δ=16µm. Such displacement may occur during integration and then it can be calibrated on-ground and/or after launch. In that case calibration must be performed unless the structure design ensures that the pupil shift will be always below 16µm.

7.1.15 Interferometer Calibration

The purpose of the calibration is to assess and correct for biases introducing systematic errors in the measurements. Emphasis has to be put on the field-dependent errors which can have tremendous effect in the image reconstruction and thus their systematic effects must be assessed and corrected.

In this paragraph the main contributors to systematic errors are identified and their calibration discussed to a certain extent. It is not the purpose here to propose a complete calibration strategy since it would require more involvement and time than the one attributed in the context of the CDF study.

7.1.15.1 On ground

7.1.15.1.1 FTS

The spectral resolution depends on the instrument spectral response function also referred as Instrumental Line Shape (ILS). An accurate knowledge of the ILS is required in order to have the specified spectral resolution. Any systematic distortion (optical misalignment, drift of the ODL metrology's laser, ODL mechanism hysteresis etc…) of the ILS occurring in the instrument shall be calibrated on-ground. Diffraction also may have an impact on the ILS and its effect shall be calibrated (RD[21]). The ILS calibration has been addressed in several publications as RD[21] and RD[22].

7.1.15.1.2 OPD

Any systematic field-dependent OPD error can be removed from the visibility error budget with a proper calibration. This calibration is part of the FTS calibration.

The contributors can be optical misalignment, drift of the ODL metrology's laser, ODL mechanism hysteresis etc…

7.1.15.1.3 WFE

The contribution to the error budget of integration and alignment of optical elements shall be calibrated accurately by measuring the wavefront at LCT and Hub telescopes level. The visibility transfer factor can then be assessed as stated in 7.1.14.2.4.

This calibration can be done by evaluating by tests the visibility transfer factor for each optical sub-system and then multiplying them to figure the total contribution to the visibility error budget.

The document RD[27] reports measurements of WFE at 9K for the Japanese telescope ASTRO-F made of sandwich-type SiC. The measured WFE variation, with refocusing, between ambient and cryogenic environment is about 337 nm RMS. This WFE applied to FIRI without calibration corresponds to a visibility transfer factor of 0.997@35.75µm.

7.1.15.1.4 Fringe tracker

The fringe tracker is itself an interferometer. It shall undergo the same calibration for OPD systematic errors. WFE and ILS calibration might be required if the fringe tracking method is based on envelop detection.

7.1.15.1.5 Beams intensity mismatch

The throughput on each arm of the interferometer can be different since the properties of coatings and beamsplitters on each arm can be different. The differential throughput contribution to visibility loss shall then be calibrated on-ground with a calibrated light source.

In flight, aging of coatings, dust deposition will degrade the performances of the reflectors thus enhancing the beam intensity mismatch. Calibrations evenly spaced in time shall be performed in order to monitor the performances degradation. The frequency of in-flight calibration are TBD.

7.1.15.2 In flight

7.1.15.2.1 Straylight

At those wavelengths the straylight is mainly due to self emission of interferometer components warmer than 5K. The boom supporting the LCT is the main contributor.

The straylight adds on each pixel of the FPA a constant background flux during the measurement. In fact, since the straylight coming from each arms of the interferometer are not coherent, the fringes contrast is not degraded. If the straylight contribution is assumed to not change during one spectrum measurement, its contribution can be calibrated and removed from the measured signal by post-processing. Nevertheless, the detectors saturation threshold shall not be reached during the measurement for the maximum signal. A proper baffling design is required to achieve the reduction of straylight effects.

A preliminary analysis shows that straylight will change at different inter telescope distances (i.e. inter-telescope distance). The hub relay telescopes were baffled considering only geometric characteristics of the spacecraft (e.g. height of the sunshields on the LCT and on the central hub beam combiner, boom height, maximum anti-sun angle, etc.). For inter telescope distances >17meters the lower sunshield of the LCT at 150K temperature reaches the primary mirror of the hub relay telescope. For inter telescope distances >20meters, the boom is visible by the primary mirror. In order to reduce the potential impact of straylight, a field stop will be implemented in the intermediate image of the hub relay telescope. A more detailed analysis shall be performed with the final spacecraft configuration in future stages.

7.1.15.2.2 Spacecraft attitude

Basically, the interferometry measures the projection of the ITD between the LCT along the line of sight of the science target. The resulting OPD is expressed as follows (see Figure 7-39).

OPD = ITD x sin(θ). While ITD is measured and monitored during the measurement, a stable reference for θ has to be found. The fringe tracking reference objects can be used for this

purpose. Thus the stability of relative position of the science target with respect to the reference object must be assessed with the fringe tracker. Any shift of the OPD can be compensated with the delay-line while the accurate knowledge of the angular reference shift can be used in post-processing for data registration in the uv-plane.

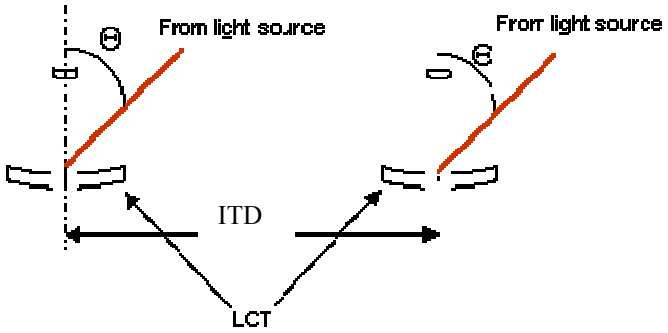

Figure 7-39: Interferometry measurement

The issue of spacecraft attitude calibration has been addressed in RD[25] and RD[26] for the SIM mission.

7.1.15.2.3 FTS

The calibration of the instrument is split in two parts:

- **Calibration before scientific operations**

  A conservative procedure requires checking of the FTS performances and calibration done on-ground, to be in a thermal environment, which is complicated. Such validation can be made by observation of a known source and comparing the measured spectrum with a reference spectrum of the same object. The source can be an internal source or a bright astronomical object which spectrum is known with an accuracy compatible with the required calibration accuracy.

  If a discrepancy larger that the one allowed is observed, the instrument shall undergo a complete calibration procedure either using an external light source or an internal light source.

  A careful design of the FTS can avoid this step if it ensures that no sources of ILS's distortions, OPD biases and WFEs are added during the launch phase.

- **Calibration during scientific operations**

  The most conservative approach consists of a spectrum measurement performed before each scientific measurement of the two blackbodies described in 7.1.13.3.3. The actual frequency of calibration and exact procedure are TBD. It depends on the detector temporal drift and also on the required NER and SNR.

7.1.15.2.4 Fringe tracker

As for the FTS, the fringe tracker performances shall be checked prior to any scientific measurements. The checking and/or calibration can be done by two different ways:

- Observation of a well known astronomical object
- Observation of a internal and calibrated light source

This calibration shall be done before the spacecraft attitude calibration.

The actual frequency of the calibration is TBD.

7.1.16 Open Issues

7.1.16.1 Straylight

As seen in 7.1.15.2.1, since the FTS is intrinsically immune to straylight, it does not have a direct impact on the measurement as long as the detector pixels are not saturated. The maximum allowable straylight level and the proper baffle design must be defined thoroughly. It needs to be analysed in detail the impact of the straylight variation at different inter telescope distances on the science measurements.

7.1.16.2 Visibility error budget

The top-down approach must be completed and validated by a further analysis of all contributors to visibility loss.

The specification on the visibility loss must be defined. For information, the uncalibrated visibility loss specified for SPIRIT is 6% (RD[29]).

7.1.16.3 Fringe tracking metrology sub-system

The details of the fringe tracking method are TBD.

7.1.16.4 Absolute laser metrology sub-system

The needs of the absolute laser metrology depend on the availability of an RF metrology sufficiently accurate (i.e with an accuracy lower than the common ODL mechanical stroke).

7.1.16.5 Calibration

The accuracy of the measurements is driven by the calibration strategy of the scientific instruments and also of the metrology sub-systems.

As a general remark, the required accuracy and frequency of calibration are TBD. The required calibration accuracy can be derived from the visibility error budget.

7.1.16.5.1 FTS

The FTS calibration covers:

- Radiometric and wavenumber calibration of the spectrometer
- WFE calibration
- Systematic OPD biases.

The required accuracy for calibration wrt to science requirements is still TBD.

The exact procedure and frequency for FTS calibration is TBD.

7.1.16.5.2 Fringe tracker

The accuracy and the calibration strategy is TBD. This calibration is of importance to obtain reliable and non-biased scientific measurements.

7.1.16.6 LCT refocusing capabilities

The stroke and accuracy for the M2 reflector refocusing of the LCTs are TBD.

7.1.16.7 Primary Reflector diameter

The reflector M1 is oversized in order to keep a collecting area equivalent to an unobscured 1 meter diameter entrance pupil. The diameter is then larger than 1 meter which is the manufacturing limit for monolithic reflectors in SiC. Limiting the diameter to 1 meter will imply a 5% obscuration of the collecting area. The compatibility of this obscuration with the science objectives is TBD.

7.1.16.8 Optical delay lines

An optimization exercise should be carried out in order to further reduce the mass, the dissipated power and the power consumption of the ODLs.

7.1.16.9 Interferometer operational modes

A preliminary list of the operational modes is discussed in 7.1.13.6. However, a more in-depth analysis should be performed in the future.

7.1.17 List of Equipment

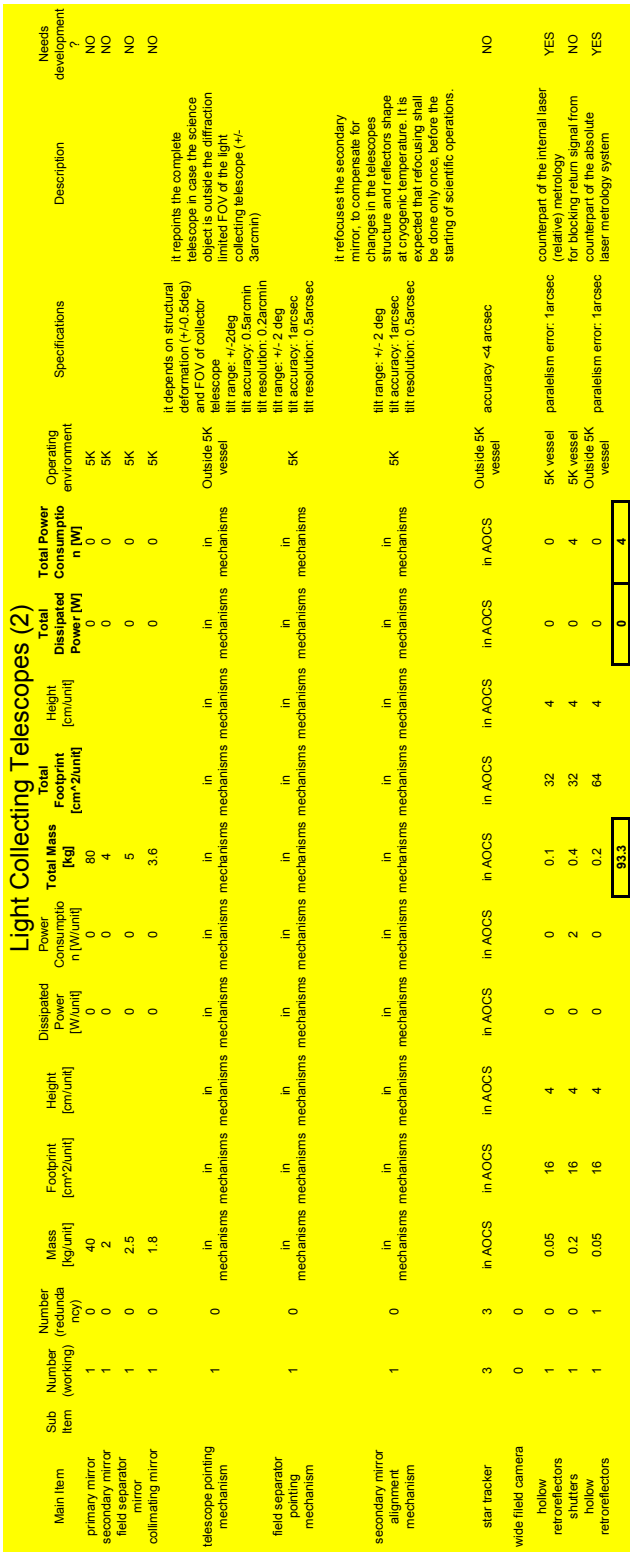

Light Collecting Telescopes (2)

Main Item	Sub Item	Number (working)	Number (redundancy)	Mass [kg/unit]	Footprint [cm^2/unit]	Height [cm/unit]	Dissipated Power [W/unit]	Power Consumption [W/unit]	Total Mass [kg]	Total Footprint [cm^2/unit]	Height [cm/unit]	Total Dissipated Power [W]	Total Power Consumption [W]	Operating environment	Specifications	Description	Needs development ?
primary mirror		1	0	40			0	0	80			0	0	5K			NO
secondary mirror		1	0	2			0	0	4			0	0	5K			NO
field separator mirror		1	0	2.5			0	0	5			0	0	5K			NO
collimating mirror		1	0	1.8			0	0	3.6			0	0	5K	it depends on structural deformation (+/-0.5deg)	it repoints the complete telescope in case the science object is outside the diffraction limited FOV of the light collecting telescope (+/- 3arcmin)	NO
telescope pointing mechanism		1	0	in mechanisms	in mechanisms	in mechanisms	in mechanisms	in mechanisms	in mechanisms	in mechanisms	in mechanisms	in mechanisms	in mechanisms	Outside 5K vessel	and FOV of collector telescope tilt range: +/-2deg tilt accuracy: 0.5arcmin tilt resolution: 0.2arcmin		
field separator pointing mechanism		1	0	in mechanisms	in mechanisms	in mechanisms	in mechanisms	in mechanisms	in mechanisms	in mechanisms	in mechanisms	in mechanisms	in mechanisms	5K	tilt range: +/- 2 deg tilt accuracy: 1arcsec tilt resolution: 0.5arcsec		
secondary mirror alignment mechanism		1	0	in mechanisms	in mechanisms	in mechanisms	in mechanisms	in mechanisms	in mechanisms	in mechanisms	in mechanisms	in mechanisms	in mechanisms	5K	tilt range: +/- 2 deg tilt accuracy: 1arcsec tilt resolution: 0.5arcsec	it refocuses the secondary mirror, to compensate for changes in the telescopes structure and reflectors shape at cryogenic temperature. It is expected that refocusing shall be done only once, before the starting of scientific operations.	
star tracker		3	3	in AOCS	in AOCS	in AOCS	in AOCS	in AOCS	in AOCS	in AOCS	in AOCS	in AOCS	in AOCS	Outside 5K vessel	accuracy <4 arcsec		NO
wide field camera		0	0														
hollow retroreflectors		1	0	0.05	16	4	0	0	0.1	32	4	0	0	5K vessel	paralelism error: 1arcsec	counterpart of the internal laser (relative) metrology	YES
shutters		1	0	0.2	16	4	0	2	0.4	32	4	0	4	5K vessel		for blocking return signal from	NO
hollow retroreflectors		1	1	0.05	16	4	0	0	0.2	64	4	0	0	Outside 5K vessel	paralelism error: 1arcsec	counterpart of the absolute laser metrology system	YES
									93.3			0	4				

Table 7-21: Main characteristics of the optical items in the light collecting telescopes.

Central Hub Beam Combiner

Main Item	Sub Item	Number (working)	Number (redundancy)	Mass [kg/unit]	Footprint [cm^2/unit]	Height [cm/unit]	Dissipated Power [W/unit]	Power Consumption [W/unit]	Total Mass [kg]	Total Footprint [cm^2/unit]	Height [cm/unit]	Total Dissipated Power [W]	Total Power Consumption [W]	Operating environment	Specifications	Description	
hub relay telescope		2	0	3	1625	32	0	0	6	3250	32	0	0	5K	diffraction limited FOV of the hub relay telescope (+/- 2deg)	it collects in the central hub beam combiner the beams transferred from the light collecting telescopes	YES
pupil conditioner	mechanism	2	0	in mechanisms	in mechanisms	in mechanisms	in mechanisms	in mechanisms	in mechanisms	in mechanisms	in mechanisms	in mechanisms	in mechanisms	5K	tilt range: +/- 3.25 deg tilt accuracy: 0.5arcsec tilt resolution: 0.2arcsec beam lateral dispacement accuracy: 100um WFE: lambda/20 RMS (lambda=633nm) free beam diameter:6cm	Each pupil conditioner contains a pair of tip tilt mirrors to compensate for relative lateral beam displacement and relative beam tilt on each arm of the interferometer	YES
	optics	2	0	0.3	100	7	0	0	0.6	200	7	0	0	5K	WFE: lambda/20 RMS (lambda=633nm) free beam diameter:6cm		NO
periscope		2	0	0.4	64	16	0	0	0.8	128	16	0	0	5K	WFE: lambda/20 RMS (lambda=633nm) free beam diameter:6cm		NO
internal metrology tilt alignment	mechanism	2	0	in mechanisms	in mechanisms	in mechanisms	in mechanisms	in mechanisms	in mechanisms	in mechanisms	in mechanisms	in mechanisms	in mechanisms	5K	tilt range: +/- 1 deg tilt accuracy: 0.5arcsec tilt resolution: 0.2arcsec	tip tilt mirror to align the internal laser metrology to the optical axis of the main fringe tracker. The internal laser metrology is aligned to the optical axis of the science detector arrays	YES
	optics	2	0	0.3	81	9	0	0	0.6	162	9	0	0	5K	WFE: lambda/20 RMS (lambda=633nm) free beam diameter: 7.5cm stroke: 2cm mechanical stroke (4cm optical stroke)		NO
common optical delay line	mechanism	1	1	15	750	15	0.002	8	30	1500	15	0.002	8	5K	OPD resolution: 100nm OPD stability: 300nm RMS WFE: lambda/20 RMS (lambda=633nm) FOV (full): 75arcmin	for tracking the zero-OPD position given by the reference source	YES
	optics	included in mechanism	included in mechanism	included in mechanism	included in mechanism	included in mechanism	included in mechanism	included in mechanism	included in mechanism	included in mechanism	included in mechanism	included in mechanism	included in mechanism	included in mechanism			
Field rotator	mechanism	0	0														
	optics	0	0														
Beam router		2	0	0.8	240	8	0	0	1.6	480	8	0	0	5K	internal alignement stability: 1arcsec WFE: lambda/20 RMS (lambda=633nm) stroke: 7cm mechanical stroke (14cm optical stroke)	it demultiplex / multiplex the different signals for metrology and science	YES
science optical delay line	mechanism	1	1	75	1050	45	0.02	125	150	2100	45	0.02	125	5K	OPD resolution: 100nm OPD stability: 300nm RMS WFE: lambda/20 RMS (lambda=633nm) FOV (full): 25arcmin	It scans the OPD generating the interferogram for recovering the energy spectral information of the source at each particular baseline	YES
	optics	included in mechanism	included in mechanism	included in mechanism	included in mechanism	included in mechanism	included in mechanism	included in mechanism	included in mechanism	included in mechanism	included in mechanism	included in mechanism	included in mechanism	included in mechanism			
science sub band splitter		2	0	6	200	40	0	0	12	400	40	0	0	5K	4 sub-bands with identical spectral resolution at each sub-band central wavelength: 35.8um, 66.6um, 124um and 231um	It splits science beam into 4 sub-bands	YES
science beam combiner		4	0	4.9	1225	10	0	0	19.6	4900	10	0	0	5K	compact highly symmetric beam combiner		YES
science focusing optics		4	4	0.37	200	12	0	0	2.96	1600	12	0	0	5K	2 mirrors off-axis focusing optics	Not possible to be accommodated within the 100mK vessel	YES
main fringe tracker beam combiner metrology		1	0	3.2	200	25	0	0	3.2	200	25	0	0	5K	OPD accuracy: 125nm OPD resolution: 50nm tilt accuracy: 15nasec tilt resolution: 7.5nasec 2160x2160 pixels (better 2500x2500) wavelength range: 0.6um-2um	it has several functions: - high precision OPD sensor to control the common ODLs (reject external and internal OPD disturbances) to provide the phase reference and OPD stabilization - high precision star tracker to provide accurate rotations about the science object - alignment sensor for the science FOV of each light collecting telescope - alignment sensor of the science FOV and the science focal plane	YES

Table 7-22: Main characteristics of the optical items in the central hub beam combiner (1)

Central Hub Beam Combiner

Main Item	Sub Item	Number (working)	Number (redundancy)	Mass [kg/unit]	Footprint [cm^2/unit]	Height [cm/unit]	Dissipated Power [W/unit]	Power Consumption [W/unit]	Total Mass [kg]	Total Footprint [cm^2/unit]	Height [cm/unit]	Total Dissipated Power [W]	Total Power Consumption [W]	Operating environment	Specifications	Description	
secondary fringe tracker metrology	main fringe tracker focusing optics	1	1	0.75	100	10	0	0	1.5	200	10	0	0	Outside 5K vessel		on the warm optical bench	NO
	main fringe tracker sensor	1	1	in detectors	in detectors	in detectors	in detectors	in detectors	in detectors	in detectors	in detectors	in detectors	in detectors	Outside 5K vessel		only 1 operating, on the warm optical bench	NO
	lateral displacement sensor	1	1	in detectors	in detectors	in detectors	in detectors	in detectors	in detectors	in detectors	in detectors	in detectors	in detectors	Outside 5K vessel		only 1 operating, on the warm optical bench	NO
	secondary fringe tracker beam combiner	0	0														
	secondary fringe tracker focusing optics	0	0														
	secondary fringe tracker sensor	0	0														
internal relative laser metrology	laser optical unit	1	0	10	400	10	15	15	10	400	10	15	15	Outside 5K vessel	wavelength range: 0.6um-2um	Each unit includes cold redundancy (3 for narrow band and 3 for broadband). Only 1 source operates at a time. On the warm optical bench	NO
	fibre harness	1	0	0.05	1	50	0	0	0.05	1	50	0	0	Outside 5K vessel		optical harness interfacing the warm and cold parts of the internal laser	YES
	laser collimating and beam splitting optics	1	0	0.25	100	10	0	0	0.25	100	10	0	0	5K		cold optics of the internal laser metrology	YES
absolute laser metrology		2	2	15	800	10	20	20	60	3200	10	40	40	Outside 5K vessel	10um/Hz^0.5, 10Hz	based on HPOM developments and Proba-3	NO
cryo optical bench		1	0	45	16900	20	0	0	45	16900	20	0	0	5K	passive alignment stability ~arcsec for entire mission lifetime	single double-sided optical bench (i.e. cryo optics will be mounted on both sides of the bench)	YES
warm optical bench		1	0	35	16900	15	0	0	35	16900	15	0	0	Outside 5K vessel			NO
shutters		2	0	0.2	25	5	0	2	0.4	50	5	0	4	5K			NO
calibration body		2	0	0.5	100	10	0	5	1	200	10	0	10	5K			NO

Table 7-23: Main characteristics of the optical items in the central hub beam combiner (2)

7.1.18 Options

7.1.18.1 Beam recombination

A technique use to extend the FOV in pupil plane recombination uses a staircase reflector (RD[15] which compensates automatically the OPD=ITDxsin(θ) (see 7.1.15.2.2). In that case, since the observation time is driven by the OPD stroke needed for spectrometry, a separated spectrometer had to be implemented in order to gain time. Nevertheless, the width and depth of staircases need to be adapted wrt the inter telescope distance (RD[28]). This method has been tested on-ground but needs validation and qualification for space applications.

7.2 Detector

7.2.1 Requirements and Design Drivers

The requirements for the FIRI detectors are essentially driven by the required broadband and the demanding sensitivity:

- Nominal wavelength band: 25 – 300 μm
- Detector performance in NEP: 10^{-18} W/√Hz for photometry and 10^{-20} W/√Hz for spectroscopy RD[31]

The performance specifications for photometry and spectroscopy are to be considered as required and goal performance, respectively, for the purpose of this study. Meeting these performance requirements represents a technological challenge. While an NEP of 10^{-18} W/√Hz has been achieved for select wavelength bands, these do not fully overlap with the FIRI waveband, especially at the long wavelengths, and hopes of improving on these results in terms of performance using proven technology is low. Therefore, the development of novel or emerging technologies is imperative.

Wave Band	Pixel size		Number of pixels (array matrix)	NEP
	Option 1	Option 2		
25 – 46.5 μm	1000 μm	500 μm	324 (18×18)	10^{-18} - 10^{-20} W/√Hz
46.5 – 86.6 μm	1000 μm	930.6 μm	100 (10×10)	10^{-18} - 10^{-20} W/√Hz
86.6 – 161.2 μm	1000 μm	1732.05 μm	36 (6×6)	10^{-18} - 10^{-20} W/√Hz
161.2 – 300 μm	1000 μm	3223.71 μm	16 (4×4)	10^{-18} - 10^{-20} W/√Hz

Table 7-24: Wavebands, corresponding number of pixels and performance

Additional drivers are the required pixel dimensions, the optical fill factor, the detector array size and the response time of the detectors resulting from the optical design and the mission observation strategy. The optical design dictates that the total waveband needs to be split into four sub-bands covered by four detector matrices having different array matrix sizes. The wavebands and corresponding array sizes are summarised in Table 7-24 together with the two options for the pixel size provided by the optical design.

The optical fill factor needs to be maximised in order to adequately image the planar fringe patterns impinging on the detector matrices. Another important consideration is the mission requirement to have fast uv-plane coverage of the astronomical target resulting in an upper limit constraint to the detectors response time. Hence, we have the following additional requirements:

- Pixel size/pitch: 500 μm to 3223.71 μm
- Optical fill factor: to be maximised
- Response time: ≥ 0.1 ms.

Furthermore, the detectors need to be operated at very low temperature - an ancillary requirement to obtain ultimate sensitivity - and to be integrated into large format arrays and

integrated to suitable readout electronics. During the course of the study it was shown that an operating temperature down to 50 mK could be provided to the FPA. This possibility will be assumed to estimate ultimate sensitivity.

Finally, a major driver for the mission is cost reduction. Since one cannot rely on existing technology, considerable research and development efforts are expected. These can be mitigated if resources are focused on a single novel or emerging technology development.

7.2.2 Assumptions and Trade-Offs

7.2.2.1 Assumptions

In view of the specification commonalities required for the four detector matrices and the need to minimize development costs, the trade-off exercise will be preferably geared towards the selection of a single detector technology. This assumption alone eliminates a number of existing technologies as a preferred option for FIRI. In particular, the whole class of heterodyne detection is currently unable to cover the whole band with a single technology. More important in excluding heterodyne detection, however, is the fact that coherent detectors are fundamentally quantum-limited, which sets their intrinsic noise a few orders of magnitude above the FIR background noise. Direct detectors do not suffer from this limitation and can in principle be background-limited making them the preferred option for FIRI RD[32].

Hence, coherent detectors will not be considered for the baseline detector design. However, it should be stressed that in future design iterations a heterodyne detector may very well be considered as a complementary instrument. A complementary heterodyne instrument would allow additional high resolution ($R \geq 10^4$) spectroscopy studies of select sources not attainable otherwise (see for instance RD[33]). The current optical design allows for two sets of four detector arrays to be accommodated in the FPA. Hence, if the option of having a complementary heterodyne instrument were to be opted for, this instrument could be accommodated as a replacement of one of the baseline two direct detector array sets.

To summarise, the following assumptions have been made regarding the baseline detectors:

- Single detector technology covering the whole band
- Only direct detectors shall be considered for the baseline design

7.2.2.2 Detector Technology Trade-offs

In the following sections two different types of detectors RD[34] currently used for FIR detection will be briefly described and discussed. These are grouped according to their operating principle, i.e. photon detectors versus bolometers.

Novel FIR detector concepts are also being studied and developed. These include KID, CEB, STJ SQPC and others RD[34], RD[35], RD[36]. Although novel concepts should definitely play an important part in the FIRI detector technology development plan — and some of them are showing much promise — it is still too early to include them in the present technology trade-off analysis.

7.2.2.2.1 Photon detectors

Photon detectors are characterised by the wavelength dependent nature of their interaction with light. Their principle of operation can be modelled by a quantised two-level electron energy

system. Light can induce electron transitions between the two levels if the photon energy is equal or larger than the energy gap. Clearly, the longer the wavelength one wishes to detect, the smaller the energy gap has to be, leading to a low temperature operation requirement in the FIR regime to reduce thermal noise.

The two-energy-level model is a simplification of the actual physical processes taking place in the detector. These processes interact and often average out leading to an effective two-energy-level system. A variety of photon detectors are therefore possible, ranging from bulk photoconductors to photodiodes and BIB detectors. The materials used may be intrinsic semiconductors, exhibiting a natural energy gap, or extrinsic ones where impurities are added by doping to create additional energy gap configurations. The energy gap can also be engineered through fabrication of quantum energy wells or composite semiconductor superlattices to tune the effective energy gap to the required wavelength range. Finally, one can vary the energy gap of a bulk semiconductor detector by physically altering the crystal lattice constant. These so-called stressed photoconductors can achieve sensitivity to longer wavelengths than their unstressed counterparts.

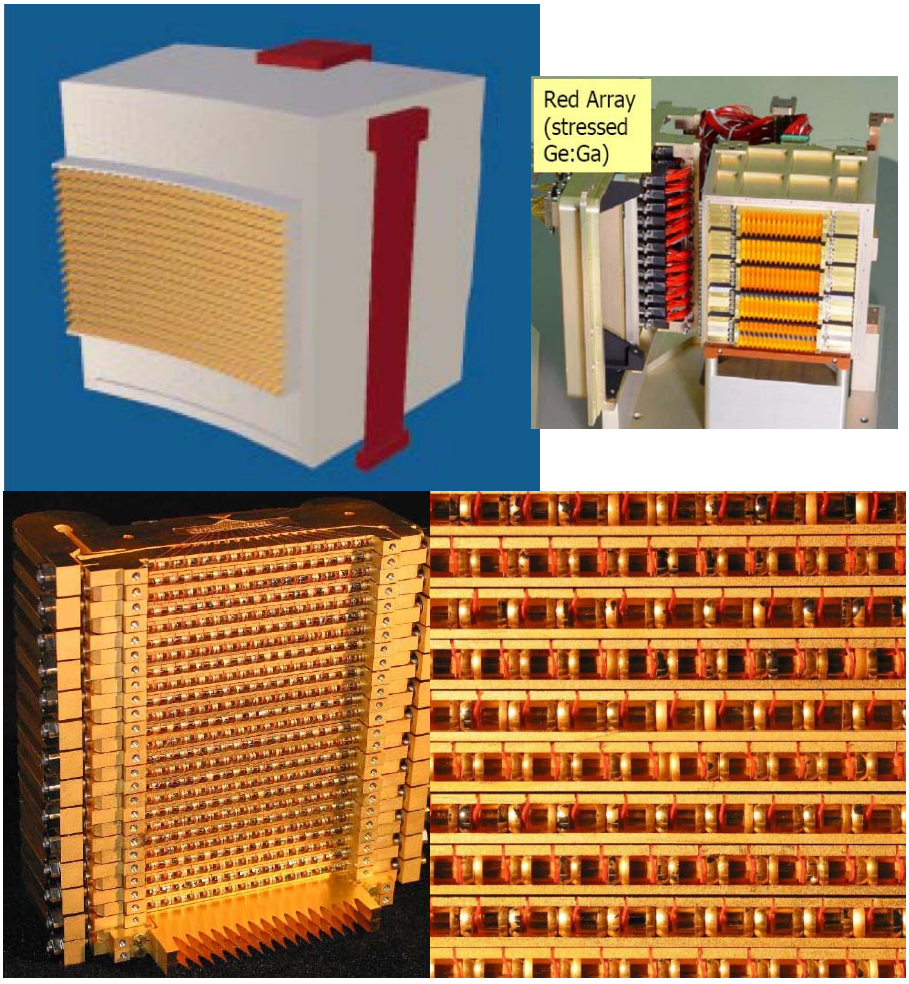

Figure 7-40: Solid model of the 16 × 25 stressed Ge:Ga photoconductor array for PACS (top left) RD[37]; actual hardware, including stressing frame, in remaining pictures RD[34], RD[38]

To date the best proven technology with both record sensitivity and longest wavelength in the FIR regime has been achieved by stressed GeGa bulk photoconductors—10^{-18} W/√Hz between

100 – 210 μm at an operating temperature of 2.2 K. They will be used in the PACS instrument, shown in Figure 7-40, onboard the Herschel Space Observatory. On the down side, the fabrication of stacks of stressed bulk photoconductors is rather challenging and research into extending the sensitivity to longer wavelengths and improve on the performance is in its last throes RD[34].

7.2.2.2.2 Bolometric detectors

Bolometric detectors measure the total absorbed energy impinging on them and are therefore intrinsically broadband. They are essentially sensitive thermometers that are periodically read out to measure a power flux. Their principle of operation is illustrated in Figure 7-41. The power flux P impinges on an absorber that has a heat capacity C and is operating at temperature $T_0+\Delta T$. The absorber is linked to the heat bath, which is at temperature T_0, by a thermal link with thermal conductivity G. The thermal balance equation is simply

Equation 7-1: Bolometer thermal balance equation

$$P = G\Delta T ,$$

which gives the absorbed power as a function of the absorber temperature increase. The temperature variation of the absorber is measured by monitoring its temperature-dependent electrical resistance $R(T)$. The noise mechanisms associated with the bolometer, in addition to the background noise originating from the sky and the readout noise, are the phonon noise and the Johnson noise given in Equation 7-2 and Equation 7-3, respectively, where k is the Boltzmann constant and S is the detector responsivity.

Equation 7-2: Bolometer phonon noise

$$NEP = \sqrt{4kT^2G}$$

Equation 7-3: Bolometer Johnson noise

$$NEP = \frac{\sqrt{4kTR}}{S}$$

The response time of the bolometer is given by

Equation 7-4: Bolometer intrinsic response time

$$\tau = \frac{C}{G}.$$

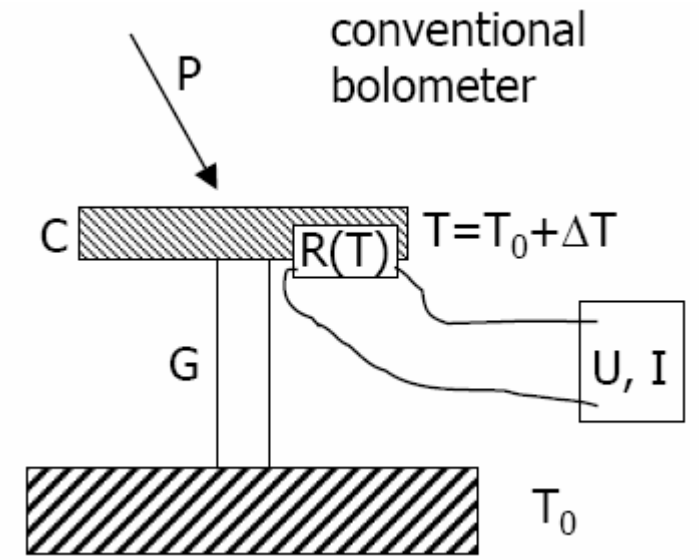

Figure 7-41: Bolometer principle of operation RD[34]

7.2.2.2.3 Transition Edge Sensors

Transition Edge Sensor are superconducting bolometers temperature biased at the critical temperature, T_c, as shown in Figure 7-42. Since the transition is very sharp the responsivity is very high.

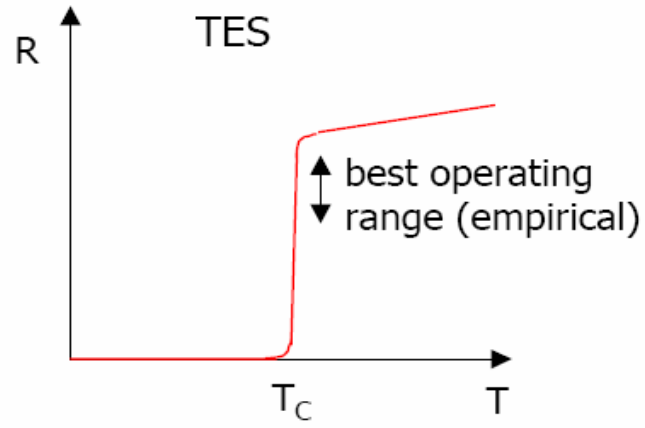

Figure 7-42: TES principle of operation: electrical resistance as a function of temperature RD[34]

Traditionally, superconducting bolometers were biased with a constant current and R was measured by reading out the voltage RD[35]. The responsivity is then given by Equation 7-5.

Equation 7-5: Responsivity of current-biased bolometer

$$S = \frac{\Delta U}{\Delta P}$$

The drawback of this biasing scheme is the positive electro-thermal feedback brought about by the increase of bias power, $P_{bias} = I^2 R$, when incoming radiation heats up the absorber. This leads to thermal runaway as the temperature approaches T_c.

The last decade saw the introduction of voltage-biased TES where the voltage is kept constant and the current is read out by a SQUID as shown in Figure 7-43. This scheme leads to a negative electro-thermal feedback that stabilizes T at the transition point, T_c, since the total thermal power on the TES is given by Equation 7-6.

Equation 7-6: Total power on voltage-biased bolometer

$$P_{optical} + \frac{V^2}{R(T)} = \frac{V^2}{R(T_0)} = \text{constant}$$

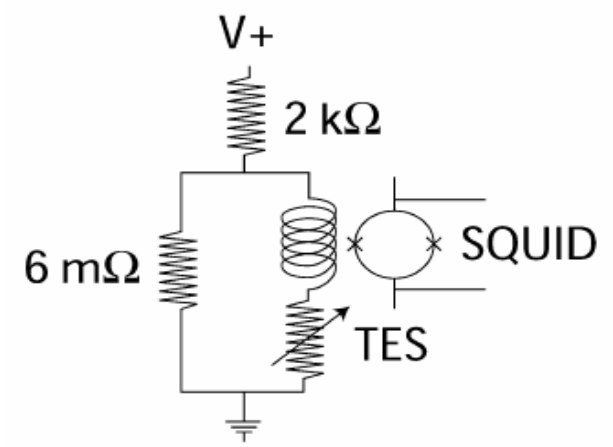

Figure 7-43: TES readout principle of operation RD[35]

In voltage-biased bolometers G chosen such that the total optical power is just enough to drive the TES normal and the bias voltage is chosen such that TES is at T_c at transition when no optical power is impinging on it.

Use of superconducting and low temperatures electronic components ensures a negligible Johnson noise term (Equation 7-3) for the bolometer. Similarly, the SQUID readout allows for low noise, low power dissipation and scalability to large format arrays. Hence, the sensitivity of the bolometer detector is solely determined by the phonon noise given in Equation 7-2. In the following subsections two approaches to reduce this noise will be presented.

7.2.2.2.4 Bulk Superconductor TES

For a bulk superconductor Equation 7-2 may be rewritten as Equation 7-7, where the thermal conductivity is simply the electron-phonon heat conductance, $G_{e\to ph}$; C_e is the electron heat capacity of the piece of bulk superconductor being considered, which depends on temperature, T, the volume, v, and the Sommerfeld constant, γ; $\tau_{e\to ph}$ is the electron-phonon relaxation time and is proportional to T^{-3}.

Equation 7-7: Bulk superconductor bolometer noise

$$NEP = \sqrt{4kT^2 G_{e\to ph}} = \sqrt{4kT^2 \frac{C_e}{\tau_{e\to ph}}} = \sqrt{\frac{4kT^3 \gamma v}{\tau_{e\to ph}}} \propto T^3 \cdot \sqrt{v}$$

The bulk superconductor bolometer noise can thus be decreased by reducing both volume and bias temperature. It is estimated RD[39], RD[40] that a superconducting Mo/Cu bilayer with volume $v = 8\times0.8\times0.1$ μm^3 operating at 80 mK could achieve NEP ≈ $4\cdot10^{-21}$ W/√Hz without the

need to provide any additional thermal weak link. This method of obtaining background limited TES bolometers is being investigated in Russia for applications in the 1000 – 200 μm waveband region RD[40].

7.2.2.2.5 Weak Thermal Link TES

Most currently available TES bolometer arrays do not rely on the bulk superconductor properties but rather are based on the geometrical design of weak thermal links. The bolometer active volume is thus put in contact with the bath by means of thin legs or grids, which can be optimised independently to achieve the desired thermal conductivity.

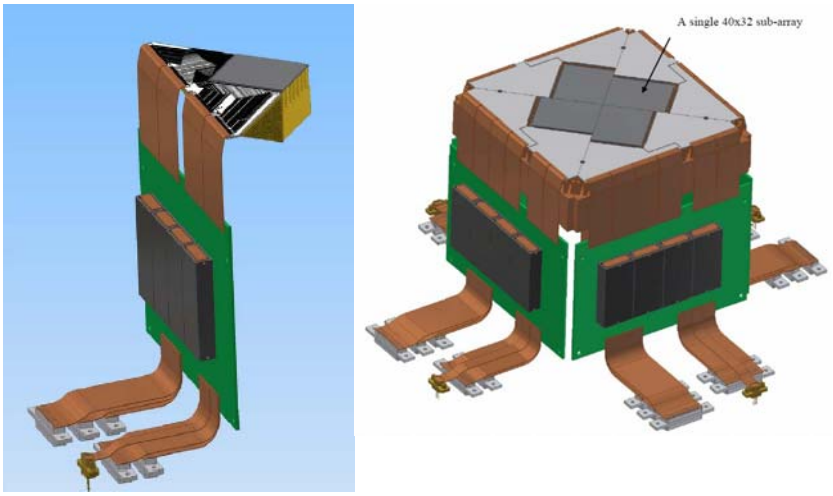

Figure 7-44: SCUBA-2 Camera RD[41], RD[42]

Examples of existing or planned arrays are SCUBA-2 and the South Pole Telescope spiderweb array shown in Figure 7-44 and Figure 7-46, respectively. The SCUBA-2 pixel geometry is shown in Figure 7-45. This is a filled array where the TES, thermal link and absorber functions are optimised independently using different materials. In addition, the array is hybridized onto a SQUID readout multiplexing backplane.

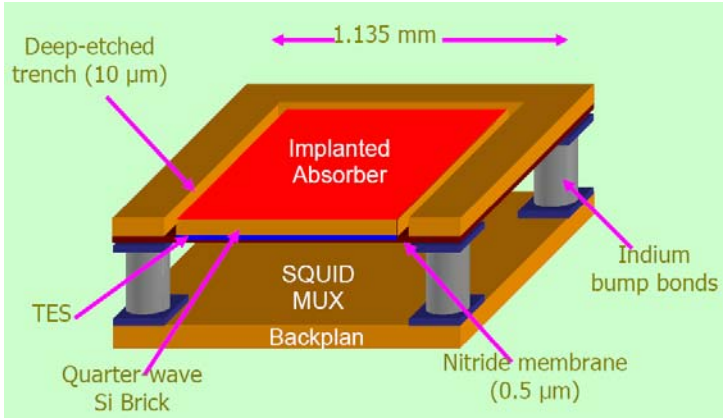

Figure 7-45: SCUBA-2 pixel geometry RD[43]

The SPT spiderweb pixel utilises an absorber that is very large compared to the TES active volume. The absorbed heat is collected by the radial grid that hosts the TES on one of its outermost nodes.

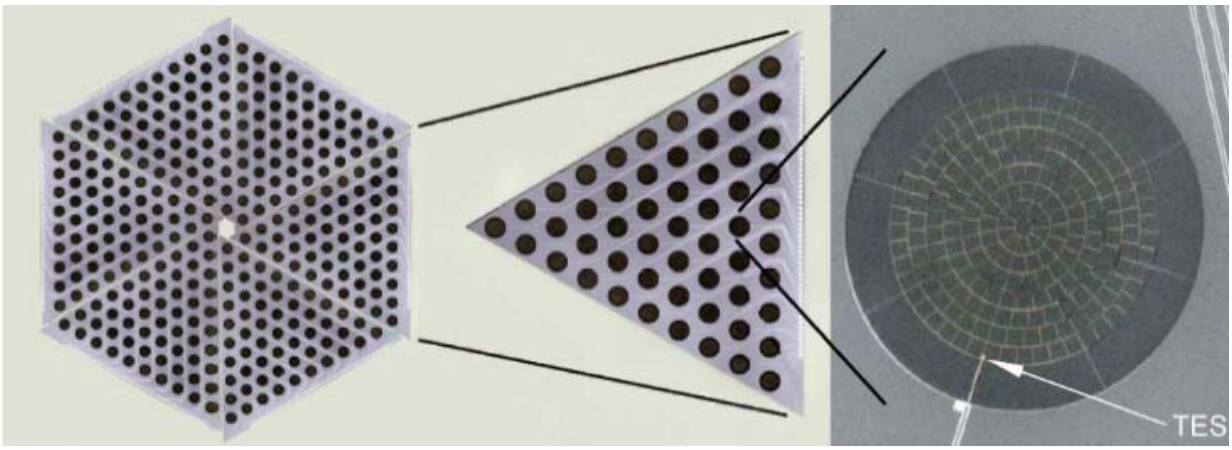

Figure 7-46: SPT TES spiderweb array (left) and pixel close-up (right) RD[43]

The circular absorber shape is most suited to the coupling scheme adopted, which is an array of close-packed conical feed horns and waveguides, as shown in Figure 7-47. The horn coupling scheme is among the most successful millimetre and submillimetre wave bolometer systems and is therefore still widely used.

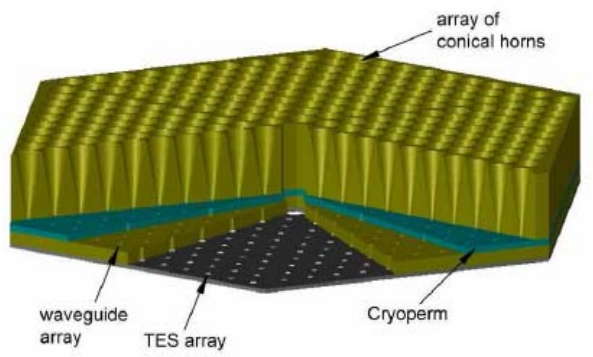

Figure 7-47: SPT TES horn array coupling scheme RD[43]

Presently available TES bolometer arrays have not yet been optimised for space applications and, contrary to the case of photon detectors, there is scope for improvement. Current research is addressing ways of achieving ultra-low thermal conductivity weak links. According to Equation 7-2 thermal conductivities as low as $2 \cdot 10^{-16}$ W/K are needed to achieve NEP = 10^{-20} W/√Hz at an operating temperature of 100 mK.

7.2.2.2.6 SRON Low-G legs TES Bolometer Development

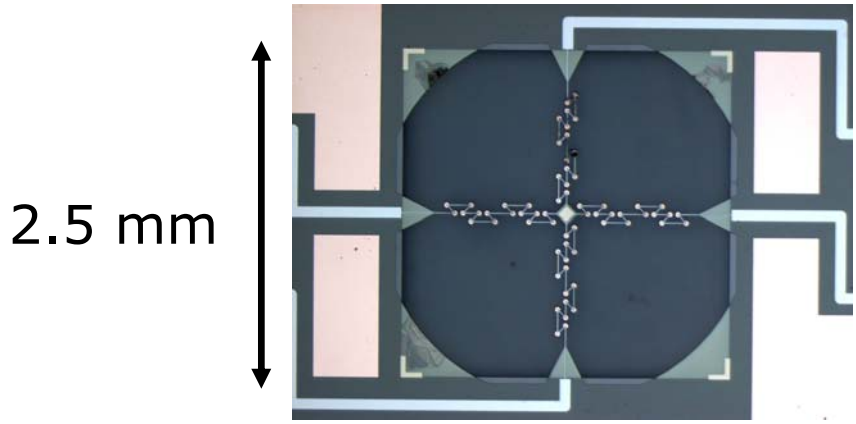

Figure 7-48: SRON TES bolometer with SiN legs RD[44]

Recent results RD[44] obtained at SRON show much promise for the future. In order to achieve ultra-low thermal conductivities the SRON team designed and fabricated several geometrical options to obtain SiN legs that are long and strong enough to hold the TES suspended in void. The structure was fabricated using MEMS techniques and is shown in Figure 7-48. The first batch produced high yield demonstrating reproducibility of the very thin structures. Close-ups of the structure and relevant dimensions are given in the Figure 7-49 and Figure 7-50.

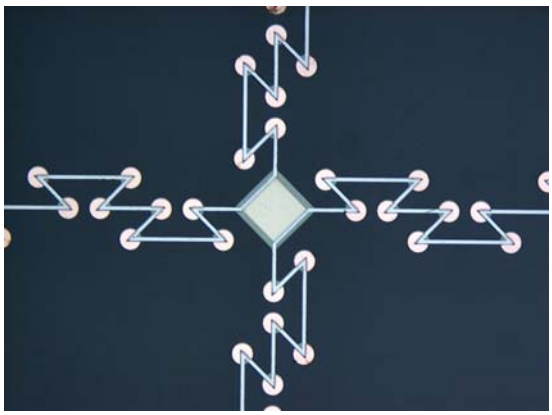

Figure 7-49: Detail of SRON SiN leg structure RD[44]

Tests performed at Cardiff University on the first batch were also very promising. The measured electronic NEP is 2×10^{-17} W/√Hz at 567 mK. This value extrapolates to NEP 6×10^{-19} W/√Hz at 100 mK. Optical measurement should be performed to confirm these results, but these are difficult to perform in view of the extremely low power levels involved. Dedicated testing facilities will be needed in order to pursue research in this field.

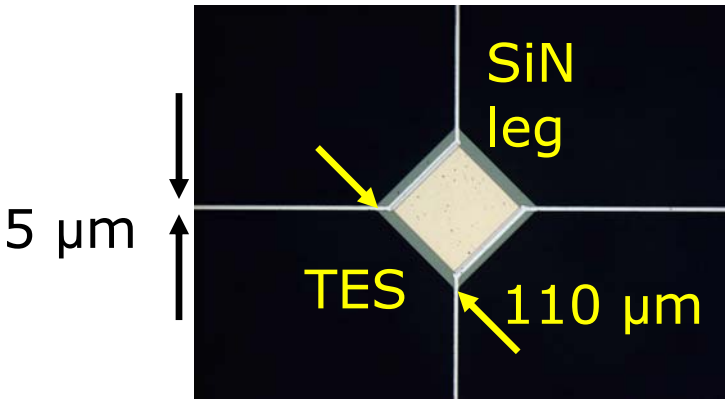

Figure 7-50: Detail of SRON central TES active area RD[44]

These results, as well as others obtained in the US, confirm that it is possible, indeed feasible, to obtain the required background-limited performance.

7.2.2.3 Comparison of select available detector array technologies

Table 7-25 lists and compares currently available FIR arrays and provides a summary of the detector trade-off analysis.

State-of-the-art sensitivity has been achieved with the stressed photon detectors but further improvements in both performance and wavelength extension (from 200 to 300 µm) are unlikely.

TES bolometers are promising but have not achieved the required performance yet. They are intrinsically broadband and can be fabricated in large-format arrays as required. Improving the sensitivity will require important technology development efforts but seems feasible and no showstoppers have yet been identified.

The real importance of Table 7-25 is that it introduces another important element to the design of the required FIR detectors that will need to be addressed by the technology development effort: the radiation coupling scheme.

	Technology	**NEP [W/√Hz]**	**Wavelength band**	**Array size**	**Optical coupling**	**Efficiency**	**Operating temperature**
PACS	Stressed and unstressed Ge:Ga	~ 10^{-18}	60 – 90µm 90 – 130µm 130 – 210µm	25 × 16 pixels	Filled arrays	30-40%	2 K
SCUBA-2	TES	$1.1 \cdot 10^{-16}$	450 µm	40 × 32 pixels	λ/4 Silicon Brick Absorber Suspended on 500 nm Nitride Membrane	93%	120 mK
SPT	TES	~ 10^{-17}	2000 – 600 µm	55 pixel sections	Horn-coupled (4K) spider web	40%	500 mK

Table 7-25: Comparison table of select available detector technologies

As can be seen in the table, the three cameras use very differing coupling scheme making use of different technologies. In the next section, suitable coupling schemes for FIRI will be reviewed and commented upon.

7.2.2.4 Coupling Schemes

Choosing a suitable coupling scheme is an important part of TES bolometer design. Several coupling schemes exist for FIR detectors. Efficiencies typically range from 40% to 80% depending on wavelength and bandwidth, amongst other parameters. The choice of coupling scheme is dictated by wavelength range, application (imaging or radiometry) and often the heritage of the designer. Sometimes the bolometer design is subordinated to the chosen coupling scheme. For instance, the spiderweb bolometer design shown in Figure 7-46 is optimised for horn-coupled arrays (Figure 7-47), which were chosen both because of the longer FIR wavelength regime and on heritage grounds.

The reason coupling schemes are so important in the FIR regime is because the wavelength of the radiation becomes comparable to the size of the detectors. In such a regime the absorption of radiation will be affected not only by the material properties and the aperture optics but also by the electrical configuration of the detector and the optics at pixel level. For maximum efficiency the bolometer must be impedance matched to the incoming radiation, i.e. free space, and optically matched to the relevant optics.

Two such schemes have already been encountered:

- Horns and waveguides: these trace back to microwave technology; they have a long heritage and are extremely successful to this day; they are more suited to longer wavelengths and not ideal for imaging. See Figure 7-47. The horn antennas are used to focus the radiation onto the spiderweb bolometer.
- Filled arrays: closer to an optical camera have high fill factor; high absorption efficiency is obtained by means of a $\lambda/4$ cavity behind the absorber, resulting in a reduced bandwidth See Figure 7-45. Electrical matching is obtained by implantation of a resistive layer to produce a sheet resistance of 377 Ω per square.

Other schemes, proven for heterodyne detection, are under investigation:

- Planar antenna coupling to free space: antenna is much larger that TES and defines the pixel size; several types exist to suit different needs; they are used together with on-pixel optics to match telescope optics.

The following sections will discuss planar antennas and on-pixel optics that could prove useful small volume TES bolometers both with bulk superconductors and the SRON TES bolometers discussed earlier. The horns and waveguides option will not be discussed further.

7.2.2.4.1 Planar Antennas

Planar antennas are obtained by planar lithography and can be integrated into the TES micro fabrication process. They have been successfully used for heterodyne detectors (SIS and HEB) and are being currently researched for direct detectors as well. Although no optical results have yet been obtained, they hold much promise for the near future.

Types of known planar antenna design options:

- Narrow-band single polarization (double slot, bowtie): double slot, shown in the right hand corner of the left picture in Figure 7-52, and bowtie, shown in Figure 7-56, ideal for narrow-band, single polarization and high efficiency coupling have a strong heritage from HEB mixer development.
- Narrow-band dual polarization (crossed slot pair): shown in the left hand corner of the left picture in Figure 7-52, same as the double slot but can be used to extract both polarizations.
- Broadband (10:1) single polarization (distributed single slot): shown in Figure 7-51 is a broadband single polarization distributed antenna. The single slot is distributed along a column of TES bolometers.
- Broadband (10:1) circular/no polarization (spiral, log-periodic): shown in Figure 7-53 are very broadband antennas with circular or no polarization dependence.

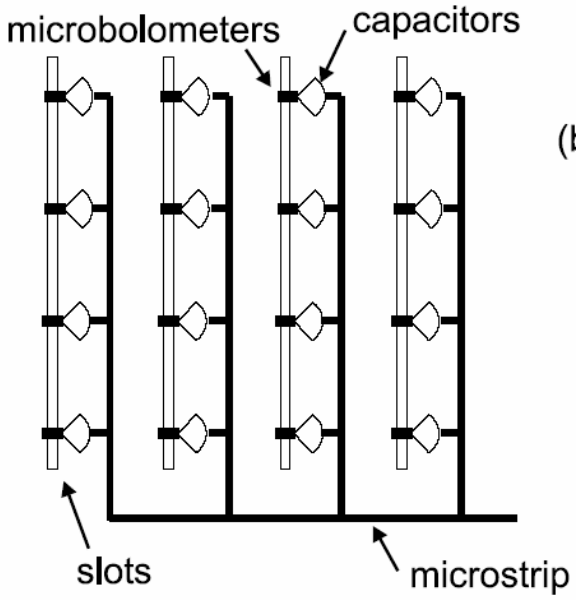

Figure 7-51: Broadband (10:1) single polarization (distributed single slot) planar antenna array RD[45]

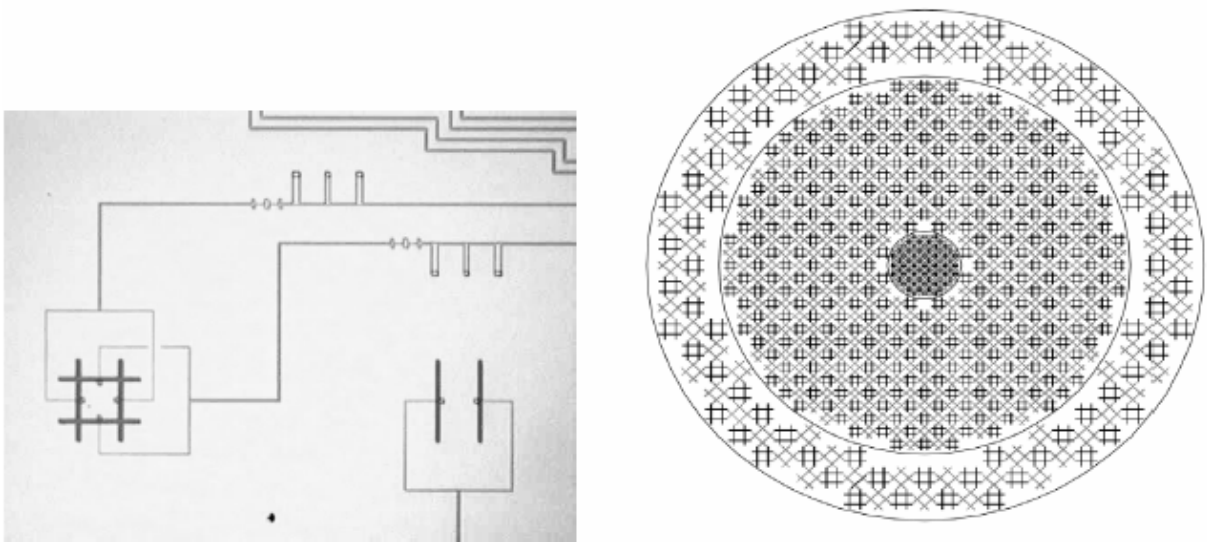

Figure 7-52: Narrow-band dual polarization (crossed slot pair) planar antenna array RD[46]

What is needed for FIRI is a coupling scheme that is both broadband and polarization independent. Spiral and log-periodic antennas are intrinsically broadband and are often used to characterize detectors over large wavelength ranges. An example of spiral antenna coupled to an HEB is given in the left picture of Figure 7-53. Its size is given by: $\lambda_{min} \leq$ arm radius $\leq \lambda_{max}$. A log-periodic antenna is shown to the right of the same figure. Both antennas are circularly polarized. This means that they are sensitive to radiation with any polarization direction. However, it also means that, unless the polarization is circular, half of the signal is lost. A big advantage of both antennas is that their impedance is real throughout the wavelength range they are designed for. However, this impedance may prove to be too large to be matched to superconducting TES bolometers.

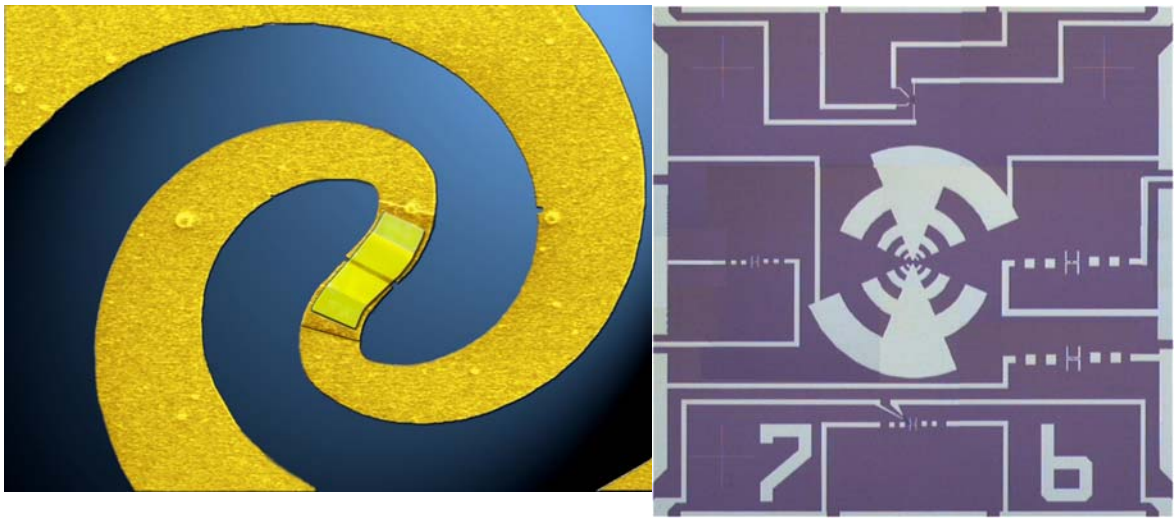

Figure 7-53: Micro fabricated spiral RD[47] (left) and log-periodic antennas RD[48] (right)

Table 7-26 gives a summary of coupling schemes that may be considered for the FIRI detector array design.

	Bandwidth	Polarization	Efficiency
Filled array (λ/4 back-short cavity)	20-40% (3dB)	Independent	> 80%
Horn-coupled absorber	> 30% (3dB)	Independent	~40%
Planar dual polarization	10% (3dB)	Dual quadrature	> 80%
Planar wide-band	> 170%	Circular/elliptical (3dB)	< 50%
FIRI	60%	Independent	To be maximised

Table 7-26: Optical coupling schemes summary

7.2.2.4.2 On-Pixel Optics

As is evident from Figure 7-51, Figure 7-52 and Figure 7-56 planar antennas can be fabricated into arrays and are therefore suitable for the realization of large format detectors. It is also noteworthy that they are often used in combination with secondary coupling schemes that are directly coupled to each pixel. These on-pixel optics elements may come in the form micro lens arrays, as shown in Figure 7-55, which were designed for the dual polarization planar antenna array shown in Figure 7-52. The rationale of adding micro lenses is to match the antenna arrays to the telescope optics. Other arrays use a λ/4 resonant cavity to obtain high efficiencies as shown in Figure 7-45 and is the case in the array shown in Figure 7-56. Finally, rear mirror geometries, shown in Figure 7-54, are being used with membrane HEB mixer arrays and could be extended to TES bolometers as well. The advantage would be to combine both focusing and resonant cavity functions in one.

In summary, on-pixel optics schemes include:

- Lenses
- λ/4 cavities
- Rear mirrors

These are used to:

- Increase efficiency
- Match telescope optics
- Reduce substrate losses.

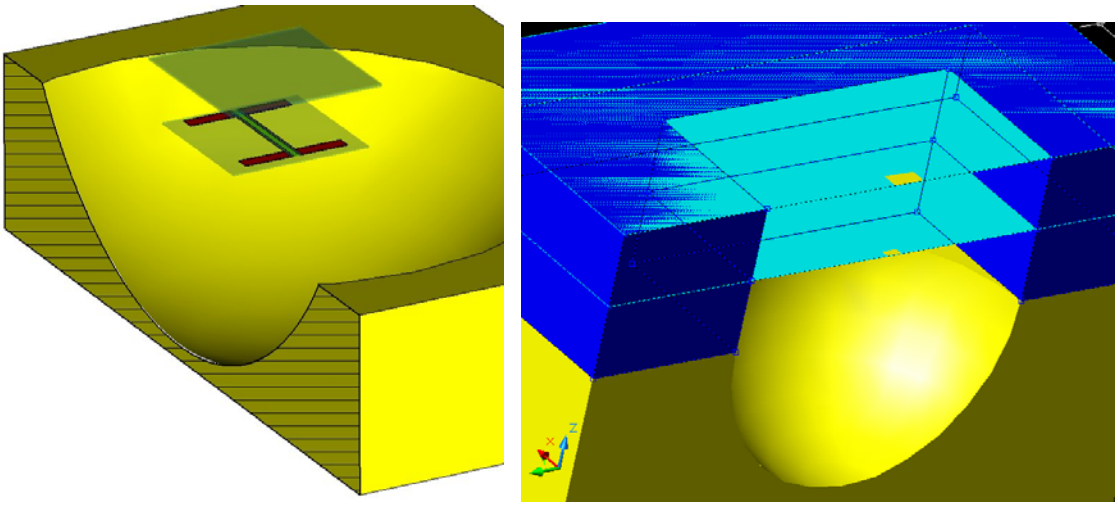

Figure 7-54: Rear focussing mirror RD[49]

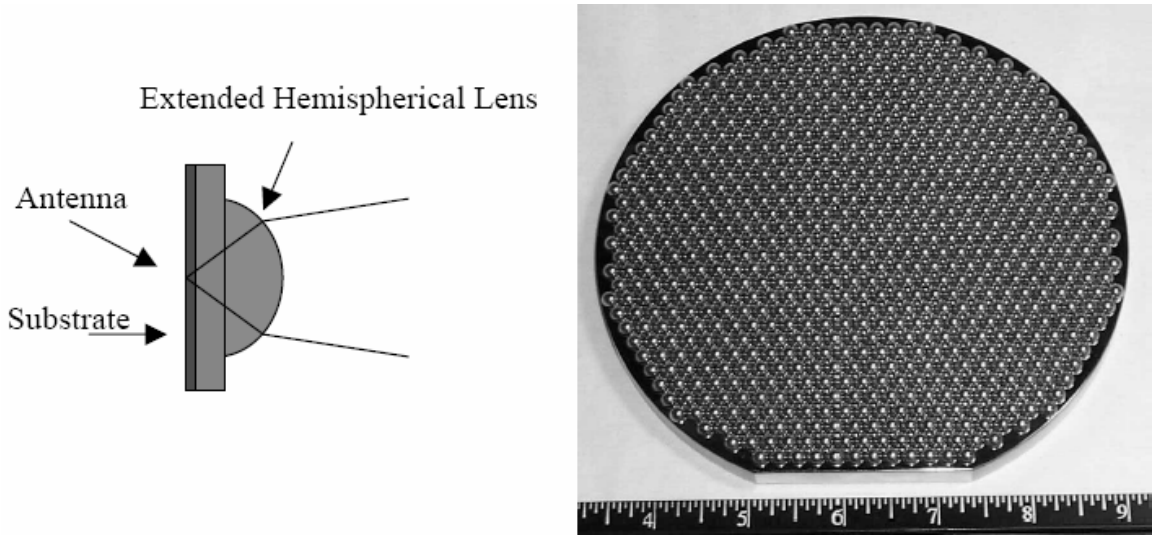

Figure 7-55: On-pixel focussing lens array.RD[46]

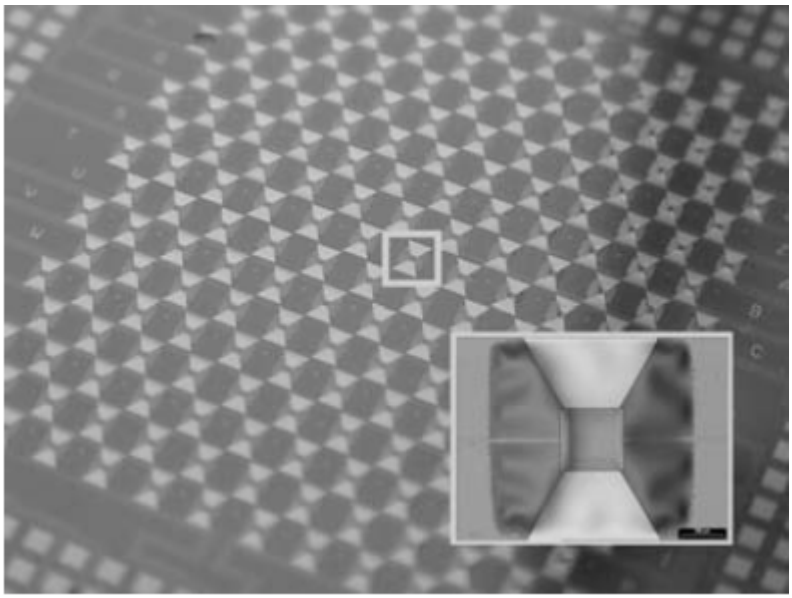

Figure 7-56: TES with bowtie antennas and λ/4 cavity coupling array RD[50]

7.2.3 Baseline Design

7.2.3.1 Detector Baseline

In the preceding sections it was shown that the required detector technology does not yet exist. However, two TES bolometer options have been described, one of which shows good promise of delivering the required sensitivity; the TES bolometer suspended by low-G SiN legs discussed in Section 7.2.2.2.6. The baseline detector technology is based on these and on the optical design option 2, summarised in Table 7-24, for the pixel sizes.

The detector baseline is given in Table 7-27. The choice of option 2 for the pixel size is preferred when using the low-G legs because this allows for a constant ratio of about 0.145 between the size of the TES active area and the legs length. Therefore, the scalability of an optimised structure — for both thermal conductivity and mechanical strength of the legs — from a given sub-band to another is ensured.

The coupling scheme of choice is the micro fabricated rear mirror behind each pixel. This solution has never been used in direct detectors and needs thorough investigation. It is hoped that this solution will offer both focusing and resonant cavity capabilities. Careful engineering may also allow for sufficient bandwidth. In case the dual function of beam forming and efficiency enhancing may not be achieved this way a hybrid rear mirror/cavity and lens array may be the appropriate solution.

Wave Band	Techno	Pixel Size	Optical coupling	Backup Table 7-25	TRL
25 – 47 μm	TES Low-G SiN legs	Bolometer size: 500 μm (SiN legs) Absorber size: 2 × λ ~ 70 μm	Resonant cavity/rear mirror, lens array	25 – 40μm SiSb BIB	2 – 3
46 – 87 μm	TES Low-G SiN legs	Bolometer size: 930.6 μm (SiN legs) Absorber size: 2 × λ ~ 135 μm	Resonant cavity/rear mirror, lens array	40 – 110μm single band unstressed Ge:Ga or two bands 40 – 50 Ge:Be and 50 – 110μm unstressed Ge:Ga	2 – 3
86 – 162 μm	TES Low-G SiN legs	Bolometer size: 1732.05 μm (SiN legs) Absorber size: 2 × λ ~ 250 μm	Resonant cavity/rear mirror, lens array	110 – 210μm stressed Ge:Ga	2 – 3
161 – 300 μm	TES Low-G SiN legs	Bolometer size: 3223.71 μm (SiN legs) Absorber size: 2 × λ ~ 460 μm	Resonant cavity/rear mirror, lens array	Up to 210μm stressed Ge:Ga	2 – 3

Table 7-27: Detector baseline

7.2.3.2 SQUID Readout

The choice readout for the baseline detector arrays consist of SQUID multiplexing unit, close or even integrated onto the detector arrays, and SQUID amplifiers. These are being developed in Europe together with the TES calorimeter arrays for XEUS mission and will be available for FIRI, possibly requiring only a few modifications. Advantages of SQUID readouts are listed below:

- Large noise margin
- Low power dissipation ~ μW
- Near TES temperature operability
- Lower limit on TES time constant: τ ~ 0.1 – 1 ms
- Dynamic range: ~ 10^7

Currently, two approaches to multiplexing exist:

- Time domain (TDM): mature but √N loss in S/N
- Frequency domain (FDM)

Although FDM is not as mature as TDM, it is catching up fast particularly in the context of the XEUS technology development activities. This multiplexing scheme was first developed in Europe and it allows the simultaneous readout of 30 pixels per row. This number is deemed to increase in coming years.

Figure 7-57 shows an example of SQUID multiplexing cell and the principle of operation of FDM.

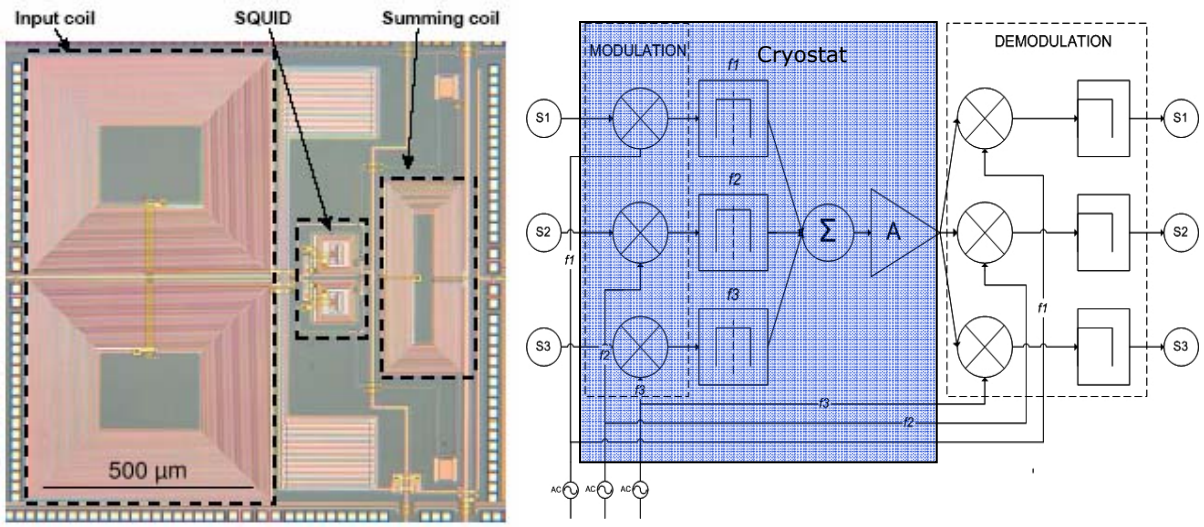

Figure 7-57: Optical micrograph of a unit cell of a SQUID TDM multiplexer wafer RD[51] (left); FDM operating principle for a detector column RD[52] (right)

7.2.3.3 Data Rate

An important parameter for the mission feasibility study is the expected data rate of the detector arrays. Study requirements and published results have been used to estimate worst case values, i.e. highest dynamic range and fasted response time. The results for the data rate are given below.

- Lowest response time: $\tau = 0.1$ ms
- Dynamic range of TES: P_{max} / noise floor
- Published results for $G = 10$ pW/K @ NEP = 10^{-18} W/√Hz
- Order of magnitude for ΔT @ 100 mK ~ 10 mK
- $P_{max} = G\,\Delta T \approx 10$ pW/K × 10 mK ≈ 10^{-13} W
- Noise floor = NEP @ 10 kHz MB = 10^{-18} W
- Dynamic range ~ 10^5 ~ 16 bit
- Data rate: 476 × 16 bit × 10 kHz ≈ 76 Mbps

7.2.3.4 Mass, Size and Power

The mass, size and power consumption estimate for the FIRI detectors is based on the SCUBA-2 camera (Figure 7-44) and is obtained by simple scaling of the array size. SCUBA-2 was not designed for space applications and was not optimised for mass, size and power. Therefore, the estimate is likely to represent a worst case scenario for the FIRI FPA. Comparison of the two arrays is given below:

SCUBA-2

- More than 5000 pixels
- Mass: 7 kg for focal plane, mostly thermal link (see Figure 7-58)

- Volume: ~4 litres
- Power dissipation: 2 – 3.5 μW

Integrated SQUID

Shield: 300-500 g

- Superconducting shield @ 500 mK
- Cryoperm shield @ 4 K

FIRI array size:

- Pixel sizes: see Table 7-24
- Arrays: 9×9 mm^2, 9.3×9.3 mm^2, 10.4×10.4 mm^2, 12.9×12.9 mm^2
- FP size ~ 4.16 × 1.29 cm2

Figure 7-58: BeCu hair brush – 40 by 40mm sq. Tines are 21mm long RD[40]

This leads us to the following baseline requirements:

Readout:

- FDM SQUIDs (cold)
- Frequency Domain MUX and deMUX (warm)
- Signal processing FPGA (warm)
- Detection chain total power: 25 mW/pixel ~ 10 W
- Shields: superconducting shield at 500 mK; cryoperm shield at 4 K; 500 g

Mass: ~10 kg

Volume: ~1-2 litre

Power dissipation:

- Cold electronics: 1nW/SQUID ~ 40 nW (TRL 4)
- Warm electronics: 25 mW/pixel ~10 W (TRL5)

Detector/SQUID dissipation: few µW

Detector Dynamic range: ~√(G/k) ~ 10^4 to 10^5 ~ 14 to 16 bit

Response time for SiN legs ~ few ms → 0.1 ms

Data rate 476 pixels × 16 bit × 10 kHz ~ 76 Mbps

7.2.4 List of Equipment

Table 7-28 gives a list of the detector equipment.

	Payload Module		MASS [kg]		
	Unit Name	Quantity	Mass per quantity excl. margin	Margin	Total Mass incl. margin
Part of:	Click on button above to **insert new unit**				
Instrument	18×18 TES array (25-47µm) + 29 SQUIDs	2	0.00	20	0.0
Instrument	10×10 TES array (46-87µm) + 10 SQUIDs	2	0.00	20	0.0
Instrument	6×6 TES array (86-162µm) + 3 SQUIDs	2	0.00	20	0.0
Instrument	4×4 TES array (161-300µm) + 1 SQUID	2	0.00	20	0.0
Instrument	Magnetic shield	1	0.50	10	0.6
Instrument	Warm electronics	1	10.00	5	10.5
Instrument	APS/MCT CMOS imaging array	1	0.05	10	0.1
			0.0	5	0.0
SUBSYSTEM TOTAL		**7**	**10.6**	**5.3**	**11.1**

Table 7-28: List of equipment

The last item in the list is an APS/MCT CMOS VIS/IR camera needed for fringe tracking. Currently available arrays with the following specifications would fit the requirements:

- Cypress/FillFactory HAS (High Accuracy Star tracker)
- ESA funded development at IMEC
- 1024 × 1024 pixel array (18 µm pitch)
- Radiation hard (100 krad)
- Cryogenic operation should not be a problem but should be tested
- Power: <350 mW with integrated ADC (<100 mW without)
- Backup: MCT array
  1. 2048 × 2048 pixel array (18 µm pitch)
  2. Max power consumption ~ 100 mW

Development activities for this camera are not envisaged.

7.2.5 Options

7.2.5.1 TES Detector

Some TES detector options were discussed in Section 7.2.2.2.4. The TES technology proposed in this chapter is based on low-G SiN legs because this solution offers the greatest flexibility: thermal conductance and TS superconductor properties can be optimised separately. In addition, the concept has recently been proven.

The bulk superconductor properties of the TES can also be used to achieve extreme sensitivity. This option is presently being investigated in Russia.

Other FIR detector concepts are being developed and should be closely monitored during the technology development phase.

7.2.5.2 Coupling Scheme

Coupling schemes options were discussed in Section 7.2.2.4. Although a solution was preferred in the baseline, it is difficult to predict what the ultimate coupling scheme may be since this is intricately tied to the bolometer design itself. It may well be that a completely different coupling scheme will be used as this question is often ultimately resolved by engineering trial and error.

7.3 Structures

7.3.1 Requirements and Design Drivers

The following requirements apply to the payload module structures:

- Provide support structure for optical elements in the hub
- Provide support for the telescopes
- Transmit shear forces between opposing booms and support beams while in launch configuration
- All parts of the payload module are at cryogenic temperatures during science operations

7.3.2 Baseline Design

The structural elements of the payload module are divided between two parts of the satellite; the hub and the telescopes.

During launch, the hub and telescopes are supported by launch locks attached to the booms (see 8.2.3.1) and structural support beams (see 8.2.3.3).

7.3.2.1 Payload Module Hub

The hub has a central load carrying cylinder attached to radial shear panels that are also load carrying (see Figure 7-59), isostatic structural supports for the optics payload canister and cryostat interface to the interior of the central cylinder. The radial shear panels transmit the shear load to the booms and structural support beams. Horizontal panels are included at the top and bottom and at two intermediate locations to give additional support. No close-out panels are used, which is also beneficial for thermal reasons since extra radiative surface exists. The baseline choice of material of the hub structure is sandwich panels with CFRP facesheets and aluminium honeycomb core, however the thermo-elastic compatibility between the optics and the PLM needs further study, and might drive the design to a fully Aluminium sturcture.

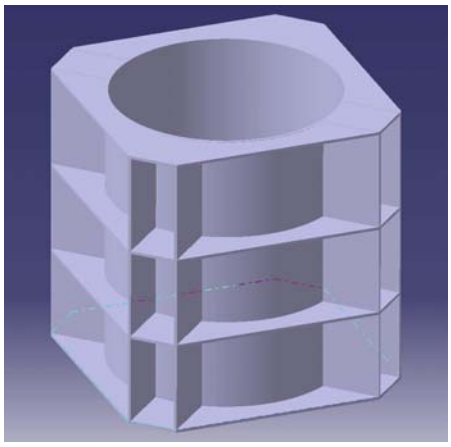

Figure 7-59: Payload Module Hub Configuration

During science operation the paylod module hub structure is at cryogenic temperature and a low-conductivity interface consisting of small fibre-glass struts (not shown) attaches it to the service module. This interface must only transmit very low forces occuring after launch. During launch, the payload module is supported by HDRM on the booms and structural support beams

7.3.2.2 Telescopes

The telescope structure is shown in Figure 7-60. It has a cylindrical external casing that is locally reinforced with 3 hard rings. The top and bottom hard rings form the external interface points for the booms and structural support beams, and the internal interface points for the telescope optical bench within. The cylindrical casing is aluminium (2mm thick) and the hard rings are also aluminium.

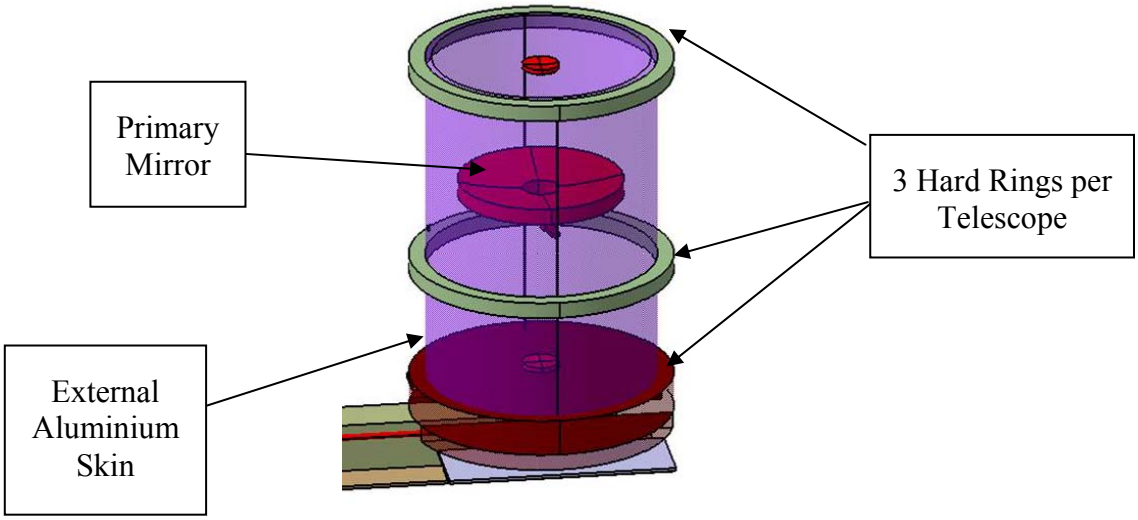

Figure 7-60: Telescope structure

The telescope optical bench is isostatically connected to the hard rings. The details of the telescope optical bench were not designed but the 5 mirror configuration is equivalent to the telescope of WFI [CDF Study Report No. CDF-46(A)(see Figure 7-60).

The main optical bench has isostatic interfaces to the middle hard ring of the telescope casing. Some details may differ from the WFI configuration (such as the lower optics bay) but the overall mass estimate is considered accurate as a first approximation.

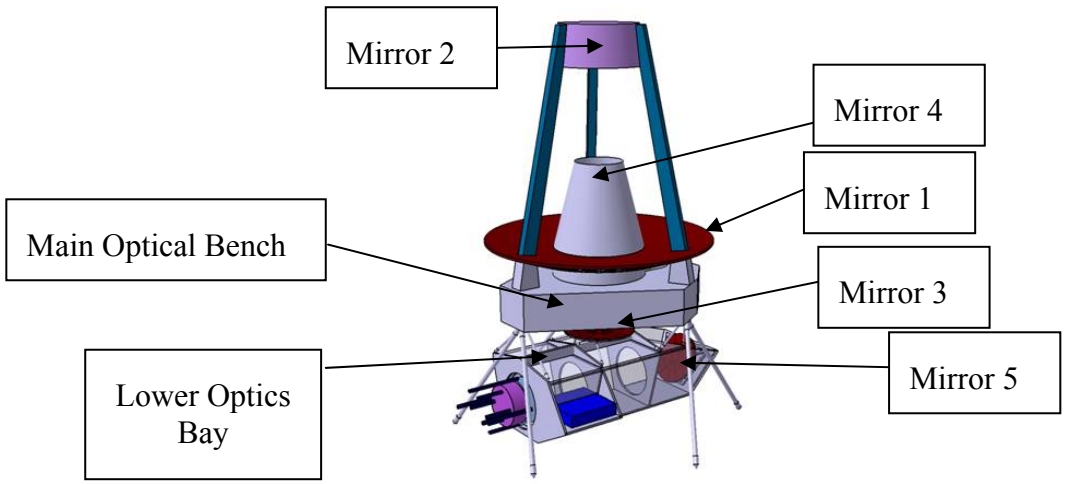

Figure 7-61: WFI Optical Bench

During science operation the telescope structure is at cryogenic temperature and a low-conductivity interface (e.g. small fibre-glass struts) is provided to attach to the telescope carrier. This is possible since this interface transmits only very low forces after deployment. However, an extra lock should be used during launch.

7.3.3 Mass Budget

The mass breakdown for the payload module is shown in Table 7-29. The structural mass of the instrument structural mounting was estimated as 84kg (with margin), which was 20% of the internally supported optics mass.

The mass of the FIRI telescope optical bench and its support structure was estimated as 22.68kg, which is 50% of the supported optics mass (the same mass ratio seen in the WFI design). This support structure mass was divided equally between the payload module and service module components of the telescopes. Thus, the Telescope Structural Mounting mass item in Table 7-29 is 11.34kg (50% of 22.68kg), and an identical mass appears in Table 8-2 for the telescope service module (SVM) structure.

The masses of the small fibre-glass struts connecting the cryogenic modules to the service modules are very small and are neglected from the mass budgets.

Item	Nr.	Material	Skin thick. [mm]	Core thick. [mm] or [mm2]	Unit density [kg/m2]/ [kg/m]	Item mass [kg]	Unit Margin [%]	Mass w marg. [kg]	All units [kg]
Top Floor	1	CFRP	2	26	7.799	30.12	20	36.14	36.14
Bottom Floor	1	CFRP	2	26	7.799	30.12	20	36.14	36.14
Central Cylinder	1	CFRP	2	26	7.799	69.29	20	83.15	83.15
Shear Panel	8	CFRP	2	26	7.799	13.72	20	16.46	131.68
Baffle (Instrument)	2	CFRP	0.75	9	3.119	1.22	20	1.47	2.94
Instrument Structural Mounting	1			3		70.00	20	84.00	84.00
Telescope Structural Mounting	2			10		11.34	20	13.61	27.22
Telescope Skin	2	Aluminium	2		5.540	57.60	20	69.12	138.23
Telescope Hard Ring	6	Aluminium	2		0.222	0.99	20	1.19	7.14
Baffle (Telescope)	2	CFRP	0.75	9	3.119	1.22	20	1.47	2.94
								TOTAL	**549.58**

Table 7-29: Payload Module mass breakdown

7.3.4 Options

Flight optics cover panels were considered to be unnecessary at this phase of the mission. Further analysis shall be performed to confirm this assessment.

Further study of thermo-elastic effects on the optics payload is needed to determine if CFRP facesheets are suitable for use on the payload module primary structure. Another option would be a fully aluminium payload module structure.

7.4 Mechanisms

The Payload Module mechanisms concern:

- Telescope mechanisms
- Instrument mechanisms.

7.4.1 Requirements and Design Drivers

The main design drivers for the definition of the Payload Module mechanisms are:

- Particulate and molecular contamination (TBD)
- Hard vacuum operation (<5K) with very low thermal dissipation allowed.

Functional requirements are driven and specified by the optics needs and will be presented for each mechanism in the following sections.

7.4.2 Assumptions and Trade-Offs

For the Payload Module mechanisms, no trade-off has been performed as all mechanisms need to be developed for FIRI. Therefore, the objective here assess the current state of the art, compare it to the FIRI needs and define the Technology Development Plan accordingly.

7.4.3 List of Equipment

For the FIRI mission, following the trade-off activities at mechanisms level but also in other disciplines, the following mechanisms have been identified for the Payload Module:

Location	Item identification
• Telescopes :	Field separator - FPA 2 DoF mechanism
• Instrument :	Internal metrology alignment - FPA 2 DoF mechanism
• Instrument :	Pupil conditioner - FPA 2 DoF mechanism
• Instrument :	Common ODL
• Instrument :	Science ODL
• Telescopes :	Refocusing mechanism

Table 7-30: List of equipment for Payload Module Mechanisms

7.4.3.1 Fine Pointing Assembly (FPA) 2 DoF tip/tilt mechanisms

7.4.3.1.1 Requirements

Three applications of Fine Pointing Assembly (FPA) 2 DoF tip/tilt mechanisms have been identified. They differ from each other by the pointing range, the pointing accuracy and resolution and, the mirror size.

Pupil conditioner:

- Function: Fine Pointing Assembly (FPA); 2 DoF tip/tilt mechanism
- Location: Beam combiner

- Pointing range: 4 degrees half cone
- Pointing accuracy: 0.5 arcsec
- Pointing resolution: 0.2 arcsec
- Lateral disp. accuracy: covered by pointing accuracy
- Frequency bandwidth: < 1 Hz TBC
- Mirror size: 70mm Ø x √2 TBC
- Operational temperature: < 5 K
- Power dissipation: Peak: < 5 mW No picture acquisition
  Stand-by: < 5 mW (0 W preferred)

Internal metrology alignment:

- Function: Fine Pointing Assembly (FPA); 2 DoF tip/tilt mechanism
- Location: Beam combiner
- Pointing range: 1 degree half cone
- Pointing accuracy: 0.5 arcsec
- Pointing resolution: 0.2 arcsec
- Frequency bandwidth: < 1 Hz TBC
- Mirror size: 90mm Ø x √2 TBC
- Operational temperature: < 5 K
- Power dissipation: Peak: < 2 mW No picture acquisition
  Stand-by: < 2 mW (0 W preferred)

Field separator:

- Function: Fine Pointing Assembly (FPA); 2 DoF tip/tilt mechanism
- Location: Telescope
- Pointing range: 3 degrees half cone
- Pointing accuracy: 1 arcsec.
- Pointing resolution: 0.5 arcsec.
- Frequency bandwidth: < 0.1 Hz TBC
- Mirror size: 200 mm Ø x √2 TBC
- Operational temperature: < 5 K
- Power dissipation: Peak: < 7 mW No picture acquisition
  Stand-by: < 7 mW (0 W preferred)

7.4.3.1.2 Design definition

The following rules may be applied for the design of the Fine Pointing Assembly (FPA) 2 DoF tip/tilt mechanisms for FIRI:

- Need for low thermal dissipation (superconductive winding materials)
- Minimisation of thermal conductive coupling due to wiring

- Low frequency bandwidth operation
- High thermal stability required
- High accuracy/resolution (control in open or close loop TBD)
- Flexible hinge based gimbal system preferred; no friction; no lubrication; no wear
- Actuator type TBD according to requirements (voice coil or linear actuator)
- Need for holding capabilities in position un-powered (TBC Vs power dissipation)
- Position sensing: capacitive, Linear Variable Displacement Transducer or Differential Impedance Transducer. TBD according to requirements.

7.4.3.2 Optical Delay Lines (ODLs)

7.4.3.2.1 Requirements

Common ODL:

- OPD: 40 mm
- OPD resolution: 100 nm
- OPD stability: 300 nm RMS
- FOV: 75 arcmin.
- Moving payload mass: 5 Kg (mirrors only)
- Mechanical stroke: 20 mm
- Scanning profile: TBD
- Lateral guidance accuracy: TBD
- Angular guidance accuracy: TBD
- Operational temperature < 5 K

Science ODL:

- OPD: 140 mm
- OPD resolution: 100 nm
- OPD stability: 300 nm RMS
- FOV: 36 arcmin.
- Moving payload mass: 12 Kg (mirrors only)
- Mechanical stroke: 70 mm
- Max. scanning speed: TBD
- Lateral guidance accuracy: TBD
- Angular guidance accuracy: TBD
- Operational temperature < 5 K

7.4.3.3 Refocusing mechanism

The main function of the mechanism is to compensate for longitudinal thermo-mechanical distortions inside the telescope and then relative motion between mirrors.

7.4.3.3.1 Requirements

- Mechanical stroke: ± 3 mm (TBC)
- Moving payload mass: 2 Kg (220 mm diameter mirror)
- Scanning profile: TBD
- Position accuracy and stability: TBD
- Lateral guidance accuracy: TBD
- Angular guidance accuracy: TBD
- Operational temperature < 5 K
- 1 shot mechanism TBC

7.4.3.3.2 Definition

The refocusing mechanism will be based on the Refocusing Mechanism Assembly (RMA) currently under development at Galileo Avionica and supported by ESA. Due to confidential restrictions, no more information can be given on this mechanism.

Un-powered holding in position capabilities will be required. The translation stage can be based on flexible blades and the actuator definition will depend on the requirements definition.

Only minor adaptations will be required for implementation on FIRI.

7.4.4 Power Dissipation for Mechanisms

Based on the current state of the art in Europe and the US, the following preliminary power dissipation for the Payload Module mechanisms can be anticipated:

Mechanisms	**Power dissipation at 5K***
• Field separator - FPA 2 DoF mechanism:	7 mW
• Internal metrology alignment - FPA 2 DoF mechanism:	2 mW
• Pupil conditioner - FPA 2 DoF mechanism:	5 mW
• Common ODL :	5 mW
• Science ODL :	15 mW
• Refocusing mechanism :	5 mW
Total	39 mW

* mechanism only without conductive contribution of cabling.

The extremely low level of power dissipation is of high importance for FIRI. A goal for future development is to further reduce the dissipation.

7.4.5 Summary

Table 7-31 presents the overall mass budget of mechanisms for the Payload Module:

Element 2		Payload Module		MASS [kg]			
Unit	Part of:	Unit Name Click on button above to **insert new unit**	Quantity	Mass per quantity excl. margin	Maturity Level	Margin	Total Mass incl. margin
1	Telescopes	Field separator - FPA 2 DoF mechanism	2	5.0	To be developed	20	12.0
2	Instrument	Internal metrology alignment FPA 2 DoF mechanism	2	5.0	To be developed	20	12.0
3	Instrument	Pupil conditioner FPA 2 DoF mechanism	4	5.0	To be developed	20	24.0
4	Instrument	Common ODL	2	25.0	To be developed	20	60.0
5	Instrument	Science ODL	2	80.0	To be developed	20	192.0
6	Telescopes	Refocusing mechanism	2	10.0	To be developed	20	24.0
-	Do not use	Click on button below to insert new unit		0.0	To be developed	20	0.0
SUBSYSTEM TOTAL			**6**	**270.0**		**20.0**	**324.0**

Table 7-31: Mass budget – Mechanisms – Payload Module

The total mass of mechanisms for FIRI is estimated to be: 1247 Kg

Volume, power consumption and risk assessment could be found in the mechanisms workbook.

Further analysis should be performed to select the drive approach of optics mechanism, the drive of the linear stages and the different types of drivers.

The development of such low dissipation mechanisms is very important for FIRI and very challenging.

7.5 Data Handling

7.5.1 Functional Requirements and Design Drivers

The main functional requirements of Payload Data Handling are the following:

- To acquire and store scientific data received from payload instruments via high-speed links
- To command and control the mirrors of the 2 telescopes for the interferometry
- To provide enough processing capability for the requested on-board data processing
- To playback the processed data to the Payload Mass memory
- To receive macro commands from SVM and to perform command - control and monitoring functions of the Payload Instruments

The selection of the technologies and the architecture is driven by three main factors:

- The Technology Readiness Level 5 should be achieved by 2015
- The Payload Data Handling shall be tolerant to any single point failure
- The risk shall be kept at minimum and whenever new technologies are developed, back up solutions shall be considered
- The cost shall be kept at a minimum.

7.5.2 Data Handling Requirements

FIRI observations consists of scanning 1373 uv-points per uv-plane. The science band (25-300um) is split into 4 sub-bands with a specific pixel number and ODL step number per sub-band. At each uv-point, each pixel will be read a certain number of time (the number of ODL steps) and the corresponding Optical Delay will be applied in between two readouts. The acquired data is 16 bits coded. Table 7-32 shows the respective pixel numbers, ODL step numbers and the corresponding Data Volumes to be acquired per sub-band.

		UV-point	UV-plane
Band 1		67.43 Mbits	92.58 Gbits
Nr of pixels	324.00		
Nr of ODL-points	13007.00		
Band 2		20.07 Mbits	27.55 Gbits
Nr of pixels	100.00		
Nr of ODL-points	12541.00		
Band 3		7.08 Mbits	9.72 Gbits
Nr of pixels	36.00		
Nr of ODL-points	12291.00		
Band 4		3.11 Mbits	4.27 Gbits
Nr of pixels	16.00		
Nr of ODL-points	12157.00		
Total Data:		97.69 Mbits	134.12 Gbits
Data rate:		4.20 Mbps	
Operations/FTS	83320784.48		

Table 7-32: Data volumes aquired per sub-band

The total amount of data per uv-point is about 98Mbps acquired in 23s, leading to an average data rate of 4.2 Mbps inside the payload with possible bursts according to the data transfer

scheme from detectors to memory. The total amount of data per uv-plane is 134.12 Gbits. On top of the science data, metrology and calibration have to be considered.

The metrology data (40 values including housekeeping and time tags) is acquired at each ODL step in parallel to the science data acquisition. It amounts to 11.43 Gbits data per uv plane.

The radiometric and spectral calibration requires to stop science data acquisition. It uses a black body emulator at 2 different temperatures. All pixels are used so that the data volume per calibration equals to 2 uv-points plus some 15% for the spectra storage.

This may be performed according to 2 possible schemes :

- Baseline : 1 calibration per uv-plane → 224.68 Mbits
- Option : 1 calibration per uv-point → 308.49 Gbits

TM downlinks happen every 2 complete uv-planes so that the required storage onboard is :

- For the baseline : 2*(134.12+11.43+0.225) = 291.55 Gbits
- For the option with calibration : 2*(134.12+11.43+308.49) = 908.08 Gbits

Science data does not need on-board processing, metrology data processing is marginal, calibration requires the computation of Fast Fourrier Transforms (for spectrometry) amounting to sum(Pi*Ni*log2(Ni)) operations where Pi is the number of pixel of sub-band i and Ni is the number of optical delay steps in band i. The FFT computation requires 83320785 operations per calibration uv-point. The FFT shall be ready within the time required for the acquisition of the second calibration uv point (23s) requiring 3.623 MIPS.

The command and control of the telescope mirrors for the interferometry requires a digital control loop frequency of about the detector integration frequency (13007/23) = 565 Hz by processing lower than 1000 operations per cycle so that the processing power required for the control loop is below 0.565 MIPS. The total required processing power is about 5 MIPS.

7.5.3 Assumptions and Trade-Offs

7.5.3.1 Memory modules

Mass memory design greatly depends on the technology of the memory devices used. The states of the art are 256 Gbits or 512 Gbits Single Data Rate SDRAM devices but the technology is progressing fast and more dense memory devices for space use are expected soon (Double Data Rate SDRAM or DDR2 SDRAM). Compared to SDR, DDR2 should provide for the same dimensions, double capacity, half standby power consumption, less than half peak power consumption and at least double speed. These memories are currently under radiation testing. The baseline is to use memory modules similar to the memory modules used in Cryosat mass memory. Details of the memory boards are given in Figure 7-62 and Table 7-33 below:

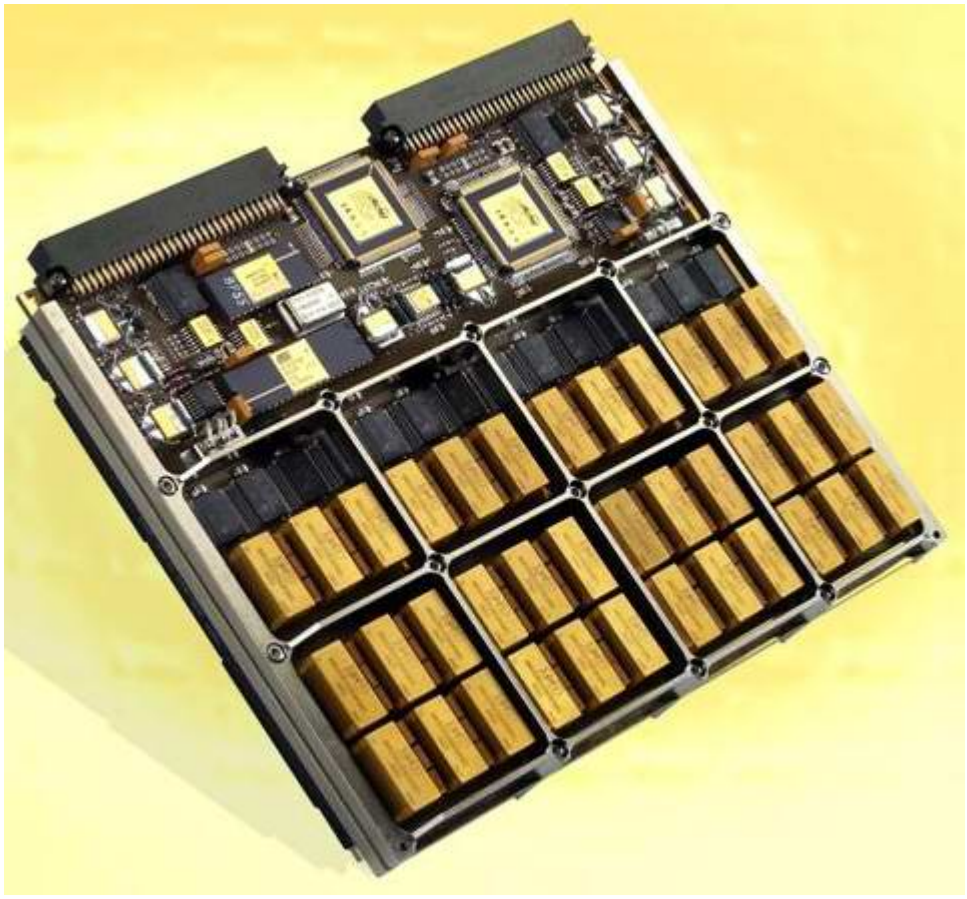

Figure 7-62: Mass memory module

Equipment	Gbit	Weight (Kg)	Standby Power (W)	Peak Power (W)	Incl. DC/DC	Length (mm)	Width (mm)	Height (mm)
SDRAM 256		**256**	**13**	**5**	**25 yes**	**360**	**302**	**240**
Number of boards (2 UV PLANES)	2.00	512.00	26.00	10.00	50.00	720.00	604.00	480.00
100% Hot redundancy (EoL = 50%*BoL)	2.00	512.00	26.00	10.00	50.00	720.00	604.00	480.00
Cold Redundancy	1.00	256.00	13.00	0.00	0.00	360.00	302.00	240.00
Total SDRAM Budget	**5**	**1280.00**	**65**	**20**	**100**	**360**	**302**	**1200**

Table 7-33: Mass memory module data

The baseline design considers a total of 5 modules, 65kg, a standby power of 20 W and a peak power 100W, occupied volume 360x 302x1200 mm.

The option with full calibration of 908.08 Gbits relates to 9 modules, 117kg, standby power 40W and peak power 200W, occupied volume 360x 302x2160 mm.

It is clear that for the full calibration option a lighter, more compact and less power-consuming technology should be used otherwise the mass memory could be a show stopper.

7.5.3.2 Processor modules

The state of the art in Europe is the AT697 processor based on LEON2 IP core (RD[74]). The performances are 86 MIPS (Dhryston 2.1) and 23 MFLOPS (whetstone). These performances are sufficient for FIRI. An Integrated Payload Processing Module (IPPM) hosting the AT697E is currently under development (Engineering Model) under contract 18780/04/NL/JA with Aurelia

Microelettronica. This module includes a 256 Mbyte SDRAM, 4 Mbyte Flash, 2 Mbyte SRAM, 8 SpaceWireLinks up to 100Mbps, 2 CAN links, 1 MIL-STD1553 and a DC/DC converter. Its weight will be around 1kg, average power consumption 5W and peak power consumption 15W. This equipment is selected as the baseline for both the hub (1 nominal + 1 redundant) and the remote parts of the payload (1 nominal + 1 redundant, per telescope). The amount of memory embedded into the IPPM is sufficient for the functioning of the remote parts of the payload. Figure 7-63 depicts the architecture of the IPPM:

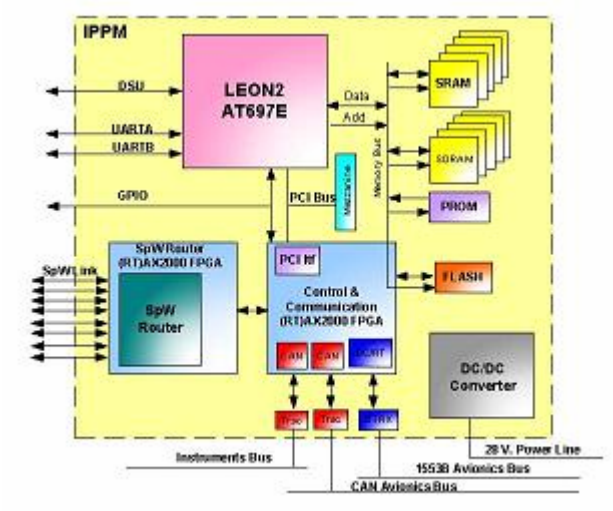

Figure 7-63: IPPM architecture

7.5.3.3 Communication with the telescopes

A wireless interface has been selected (1 nominal + 1 redundant) see 8.6.

7.5.3.4 Links and Routers

The hub payload hosts at least 4 nominal and 1 redundant memory module, 1 nominal and 1 redundant processor module as well as the detectors for the interferometry. To exchange data between modules, a distributed architecture involving routers has been selected in order to reduce the harness and simplify the redundancy scheme. The user rate of the links has to be above 4.2 Mbps. The solution to space applications requiring high speed links (up to 200Mbps) and dynamic switching is SpaceWire as described in the ECSS-E50-12A standard. Commmunication Controllers (SMCS 332 and SMCS 116 for example) are already available and an ASIC router prototype implementing 8 SpaceWire ports will be available in 2007. Numerous EGSEs are already available and they allow easy integration and testing. The required number of router depends on the requirement in terms of number of links to be provided. In the hub we have the following breakdown:

- Router ←→ sensor buffer : 1 nominal + 1 redundant
- Router ←→ memory modules : 5 nominal + 5 redundant
- Router ←→ Processor module : 2 nominal + 2 redundant.

The hub requires 8 SpaceWire ports for the routing capabilities which correspond to 1 router. Therefore the baseline design integrates 1 nominal and 1 cold redundant routing module. Table 7-34 gives the details about these routing modules.

Switching matrix module (Router)		**0.60**	**3.00**	**12.00**	**360.00**	**302.00**	**25.00**
Number of boards	1.00	0.60	3.00	12.00	360.00	302.00	25.00
100% Hot redundancy (EoL = 50%*BoL)	0.00	0.00	0.00	0.00	360.00	302.00	0.00
Cold Redundancy	1.00	0.60	0.00	0.00	360.00	302.00	25.00
Total Router Budget	**2.00**	**1.20**	**3.00**	**12.00**	**360.00**	**302.00**	**50.00**

Table 7-34: Routing modules

There are 16 cables connected to the routers plus 2 cables from the processor module to each of the two wireless interfaces. The total number of cables in the hub is 20. The average length of these cables is 1m and their density is about 85 g/m. The corresponding hub harness mass is 1.7 kg.

The payload data handling system at the telescopes hosts 2 cables 1 from each wireless interface to the Integrated Payload Processing Module, with a total of 4 cables and an additional mass of 340 g.

7.5.4 Baseline Design

A possible architecture of the payload data handling is given in Figure 7-64:

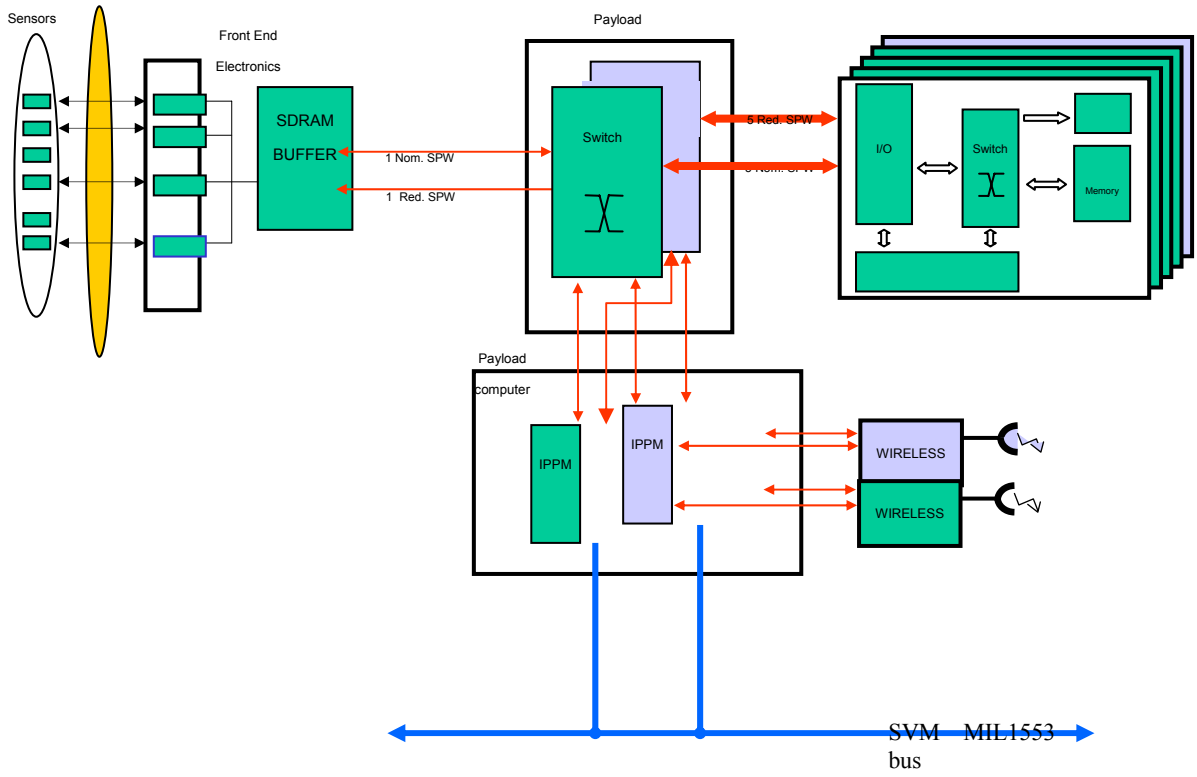

Figure 7-64: Payload architecture

7.5.5 Summary

Table 7-35 to Table 7-37 gives the budgets of the payload's Data Handling:

	Payload Module		MASS [kg]		
	Unit Name	Quantity	Mass per quantity excl. margin	Margin	Total Mass incl. margin
Part of:	Click on button above to **insert new unit**				
Instrument	Hub computer	1	3.2	10	3.5
Instrument	Hub Memory	1	66.2	5	69.5
Instrument	Hub Data Harness	1	1.7	5	1.8
Telescopes	Telescope Computer & Memory	2	2.0	10	4.4
Telescopes	Telescope Data Harness	2	0.3	5	0.7

Table 7-35: Payload module data handling unit mass

	Payload Module		DIMENSIONS [m]		
	Unit Name	Quantity	Dim1 Length	Dim2 Width or D	Dim3 Height
Part of:	Click on button above to **insert new unit**				
Instrument	Hub computer	1	240.0	185.0	125.0
Instrument	Hub Memory	1	360.0	302.0	1250.0
Instrument	Hub Data Harness	1			
Telescopes	Telescope Computer & Memory	2	240.0	185.0	100.0
Telescopes	Telescope Data Harness	2			

Table 7-36: Payload module data handling unit dimensions

	Dimensions (mm)	Mass (kg)	Power (W)
SVM computer	480x240x302	19.30	35.10
SVM Mass Memory	360x302x240	6.39	20.80
Payload (Hub) Computer	240x185x125	3.20	19.50
Payload (Hub) MM & harness	360x302x1250	67.90	112.00
Telescope Computer, MM & harness	240x185x100	4.68	30

Table 7-37: Data handling power table

Further analyses have to be performed during later phases concerning the wireless system and the harness in different temperature zones.

7.6 Thermal

7.6.1 Requirements and Design Drivers

7.6.1.1 Telescopes

The cryogenic design of the telescopes is mainly driven by the following requirements:

- Temperature of the optical elements below 5 K
- Protection from the Sun
- Cooling system mounted on a movable platform
- Minimise vibration.

7.6.1.2 Hub

The cryogenic design of the Hub is mainly driven by the following requirements:

- Temperature of the optical elements below 5 K
- Protection from the Sun
- Cooling down to 50-100 mK is required for the detectors
- Minimise vibration.

7.6.2 Assumptions and Trade-Offs

7.6.2.1 Active/passive cooling

Since FIRI is placed in an orbit far away from the Earth (L2), passive cooling can be considered. Looking to passive concepts applied on other Spacecrafts as e.g. Herschel, Planck and James Webb Space Telescope, the minimum achievable temperature is 35 K, whereas 50-60 K can be achieved with a simple design. It is therefore required to apply active cooling technologies to achieve temperatures below 5 K. Nevertheless, passive pre-cooling of the environment is required to minimise the heat load on the active cooling systems. The following figure shows the radiative heat load expected for FIRI vs. the temperature of the shields.

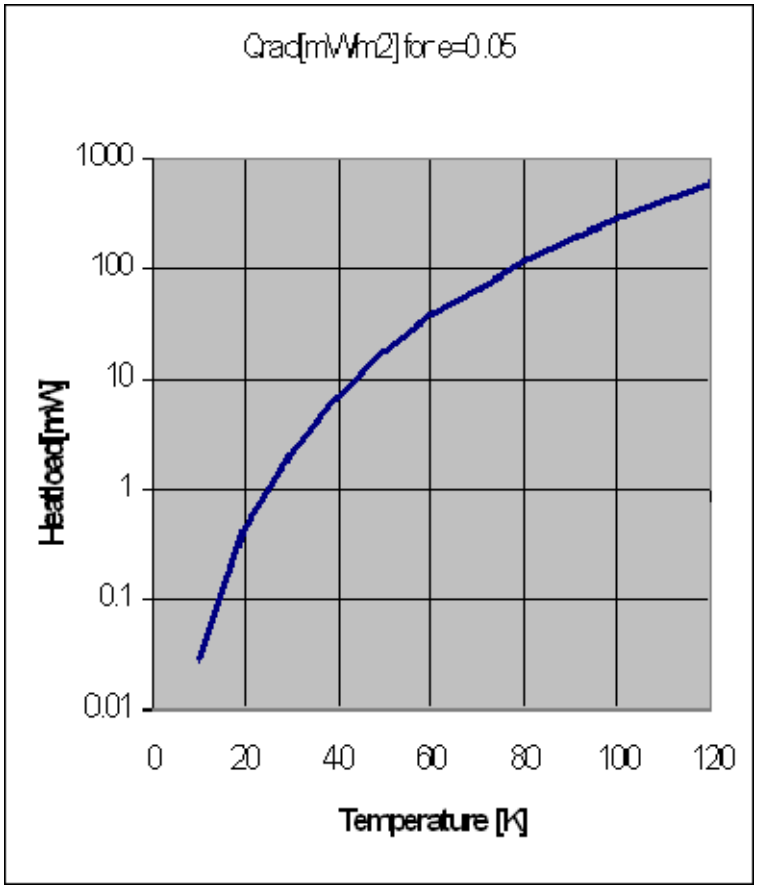

Figure 7-65: Heat load/m^2 surface vs. Temperature

Assuming, that the heat load at 5 K should be less than 10 mW and that several squaremeter's of shields will be required, an intermediate shield at around 30 K is required, which also requires active cooling. At this temperature, the heat load should be less than 100 mW, which leads to a 3rd Shield at 60 K. This can be achieved by passive means.

The basic architecture for FIRI cryogenic system will therefore be:

- One active cooled optical compartment at 5 K.
- At least one active cooled thermal shield below 30 K.
- A passive cooling system providing a temperature below 60 K.

To enable passive cooling, the cryogenic part of the Spacecraft needs to be protected from the sun by means of a sunshield.

7.6.2.2 Sunshield

The sunshield must be able to protect the telescopes and the Hub from the Sun, also considering that observations out of the solar plane are required. The size of the Sunshield is driven by the height of the modules and the maximum observation angle. Since the height of the telescopes are above 2m and a minimum observation angle of 45 deg is required a deployable Sunshield is the baseline.

Initial trade-off's performed showed, that individual Sunshield's for the telescopes and the Hub are the preferred solution, because:

- The size of a single shield would be 40x5m → deployment mechanism.
- A single sunshield would require dedicated room temperature compartments for the mechanisms and cooler electronics, individual sunshields allow the ambient temperature units to be mounted below.

Assuming that the Sunshield will be stowed around the telescope baffle during launch with an umbrella like deployment, a Sunshield size enabling observations up to 45 deg can be implemented, which is considered as the baseline for the rest of the study. Nevertheless, it has to be considered, that the size of the Sunshields will affect the minimum distances between the telescopes and the Hub, which might be a trade-off for future studies.

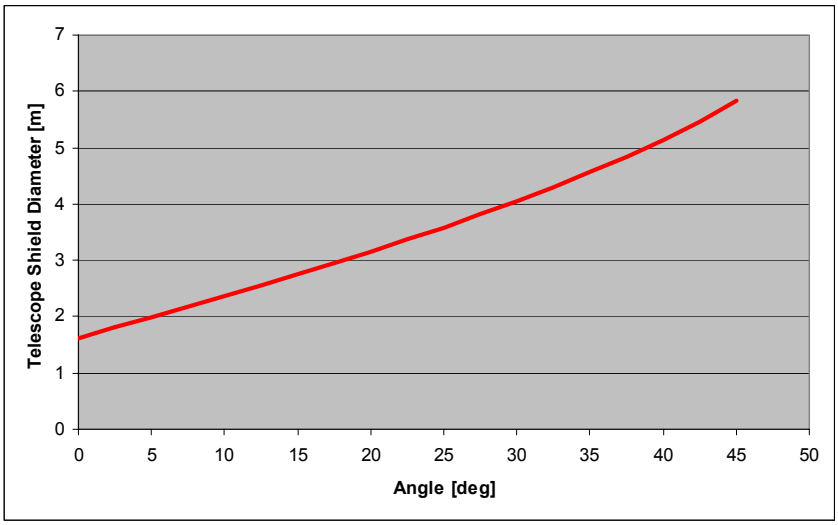

Figure 7-66: Size of the telescope primary sunshield vs. Observation angle

To prevent straylight from the Sun and to maintain a low temperature of the booms, additional Sunshields mounted on the booms are considered. This Sunshields can be used for mounting the solar arrays.

7.6.2.3 Active cooling system for 5 K

To achieve 5K in the optical compartments, several technologies are available, which are listed below:

- Helium cryostat: A first assessment showed that for 5 year lifetime a Herschel sized cryostat would be required for each of the telescopes and the Hub. Since this is outside the capabilities of an Ariane 5, this solution has been discarded.
- Solid hydrogen cryostat: The minimum temperature that can be achieved with a hydrogen cryostat is around 7 K, which is too high for FIRI. Nevertheless, the mass and volume required for a 5 year mission is comparable to an active cooling system (according to a trade-off for James Webb Space Telescope) and can be used for pre-cooling a Joule Thompson cooler. By pre-cooling a JT cooler to 8 K instead of 15-18 K achievable with active pre-cooling, the efficiency of the JT cooler increases significantly.

- He-Joule Thompson cooler with linear compressor. This technology is used on Planck to achieve 4,5 K and is easily scaleable. Drawback is the exported vibrations which needs an active control. The cooler requires pre-cooling below 20 K.
- He-Joule Thompson Cooler with sorption compressor (He-sorption JT). This technology is currently under development for Darwin. The compressors operate at 50 K and require therefore large radiator area, which complicates scaling. A big advantage is that the compressor is almost vibration-free. The cooler requires pre-cooling below 20 K.
- Hydrogen Joule Thompson cooler with sorption compressor (H2-sorption JT). The compressor of his cooler uses the same technology as the He-sorption JT, but operates around 100 K and provides cooling at 14-18 K. It can therefore act as a pre-cooler for the He-Joule Thompson coolers.
- Multi-stage Stirling and Pulse Tube coolers. These coolers can reach temperatures down to 4 K, with the disadvantage of exported vibrations. If only used, there is also the problem to attach the various elements to the cold-finger. For the highest efficiency and best distribution of the cold, using the Stirling or Pulse Tube coolers as a pre-cooler for a JT cooler seems the best solution.
- Reverse Turbo-Brayton cooler. The reverse Turbo-Brayton cooler consists of a high frequency centrifugal compressor and turbo-expander. Therefore almost no exported vibrations are expected, as shown on the Hubble Space Telescope for the NICMOS instrument. The main drawback of this solution is that not much expertise on this cooler is available in Europe and a long development programme would be required. This cooler has therefore not been considered.

Based on these elements, the design activities were focused to achieve a vibration free design using the Helium/Hydrogen sorption cooler with potential improvements by using a Hydrogen cryostat for further increasing the cooling power. An active cooling chain using a Stirling/Pulse Tube cooler together with a JT-cooler with a linear compressor are considered as a backup.

7.6.2.4 Detector cooling

After an initial trade-off on the detector technologies, an operating temperature range of 50-100 mK is required for at least part of the detectors. This temperature can in Space at the moment only be achieved by either an Adiabatic Demagnetisation Refrigerator (ADR) or a Dilution cooler.

A closed loop dilution cooler would require to separate the ^{3}He/^{4}He liquid in zero-gravity by simple means, a technology which is at the moment not available. For the current study the ADR is therefore considered as a baseline, since developments performed at NASA and ESA showed the feasibility of the concept. Depending on the final detector operating temperature, other sub-Kelvin coolers can be considered.

7.6.3 Baseline Design

7.6.3.1 Telescopes

Starting from the outside, the telescope upper and lower part act as low temperature radiators for the sorption compressors. The lower radiator operates at ~ 100 K and serves as a heat sink for the H2 sorption JT compressor, which pre-cools an intermediate shield and the He-JT line to below 20 K. The upper radiator acts as a heat sink for the He-sorption compressor at ~50K, which cools

the Optical compartment and the optical elements down to 5 K. Due to the large distance between the various elements, multiple cold-heads are foreseen to minimise the temperature gradients within the optics. The outline of the telescope cryogenic design is shown below and assumes a support via GFC and CFC chains to the 50K tube similar to Herschel.

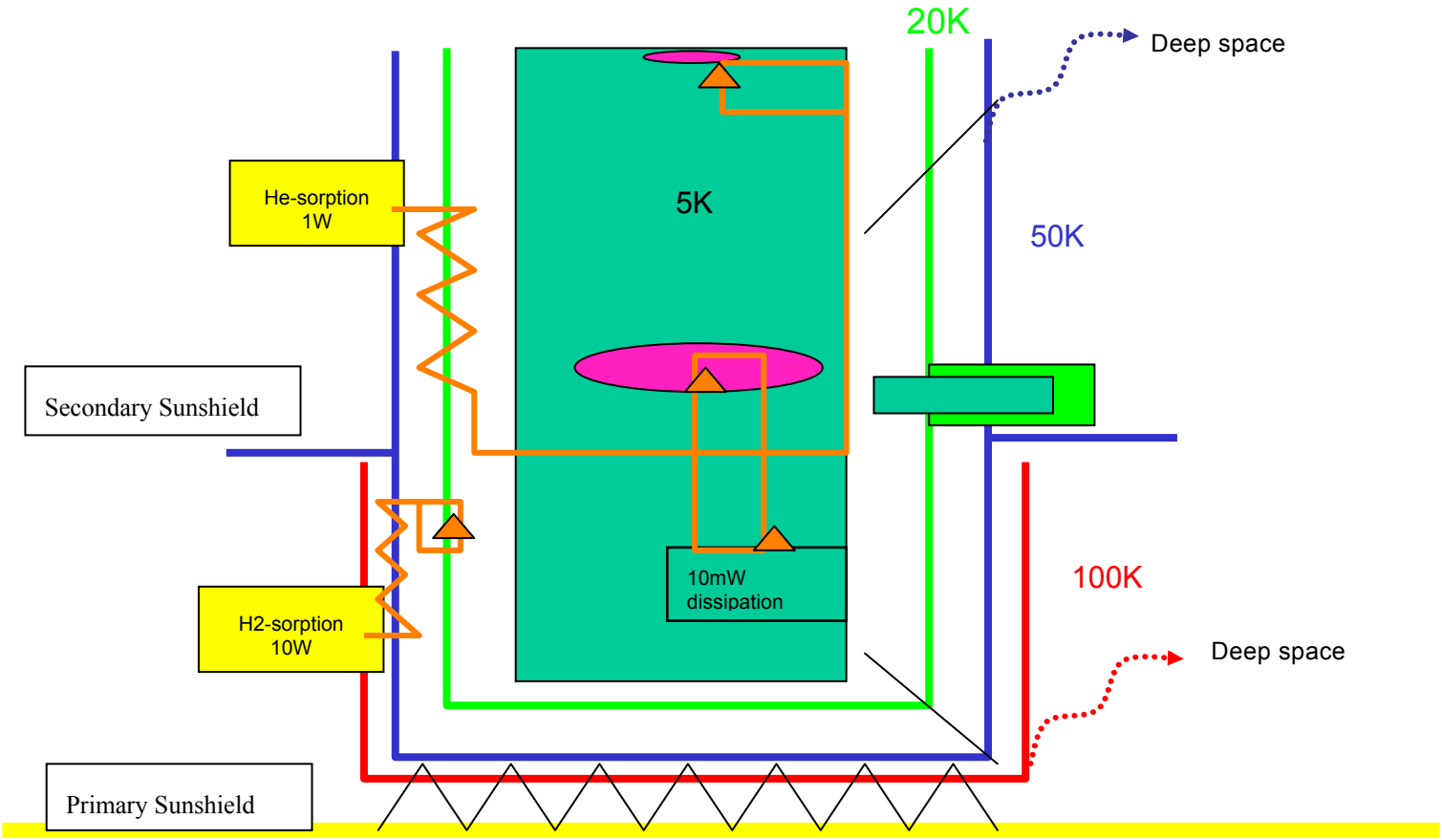

Figure 7-67: Telescope Cryogenic cooling concept

The 50 K radiator is mounted via isolating struts on the moving mechanisms mounted below the primary sunshield.

This design enables to cool the Telescope vibration free down to 5 K. For the tip tilt mechanism, an average dissipation of 10 mW is assumed. In case there are high peak power dissipations, a cryogenic Phase change material should be considered. The current design allows installation of additional elements on the 20 K shield, without disturbing the 5 K environment.

The primary Sunshield is assumed to be a double foil concept similar to GAIA, but a deployable Multi Layer Insulation (or V-groove) would greatly improve the heat sink temperature of the telescope radiators. The secondary Sunshield for the moment is only used to shield the 50 K radiator from the Sunshield, but can be used to increase the radiator area at 50 K if required.

7.6.3.2 Hub

Similar to the telescopes, the Hub takes advantage of passive pre-cooling, but the area available at 50 K is not sufficient, to support the use of Helium sorption cooler. The area at 100 K also needs to be limited to not disturb the telescopes when close to the Hub. In order to keep the

design as passive as possible, a solid Hydrogen cryostat has been implemented for cooling a shield at 8 K, and by using the vapour cooling of the exhaust gas, cooling another shield at around 30 K. Finally, the hydrogen gas will be vented to deep space via a low thrust vent head, in order to minimise the remaining Force on the S/C. A Helium JT cooler using either a linear compressor inside the service module or a sorption compressor on the 50 K radiator, in case the power dissipation would drop significantly, achieves cooling down to 5 K.

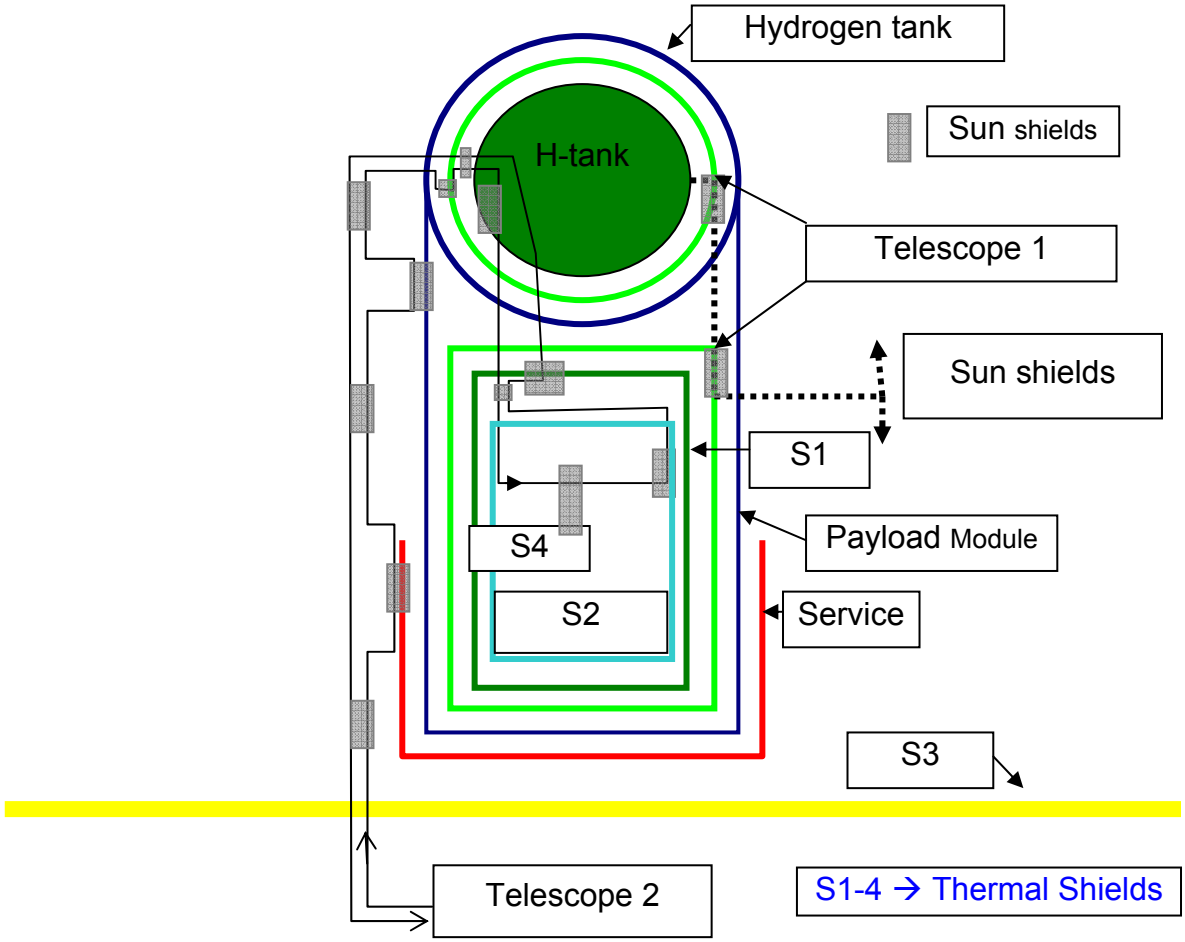

Figure 7-68: Hub cryogenic cooling concept

The Joule Thompson cooler line is not only used to cool down to 5 K, but also to transport heat between the 8 K shield around the optical compartment and the solid hydrogen.

The optical compartment and the thermal shields are supported on the structural cylinder by means of GFC and CFC chains similar to ISO and Herschel.

The cooling of the detectors is achieved by a continuous Adiabatic Demagnetisation Refrigerator. To minimise the heat load on the 5 K stage, it is assumed that the superconducting magnets can operate at temperatures above 8 K and are therefore thermally coupled to the thermal shields.

7.6.4 List of Equipment

7.6.4.1 Telescopes

The following cryogenic equipment is implemented on the Telescopes:

- Thermal shields (1mm thick Aluminium).
- Deployable Sunshields (double foil Mylar VDA).
- He-sorption JT cooler.
- H2 sorption JT cooler.
- Low conductive mechanical support structure similar to Herschel/Planck.
- 50 K radiator (black painted open honeycomb structure).
- 100 K radiator (black painted/ anodised 1mm thick Aluminium).
- Temperature/pressure sensors.

7.6.4.2 Hub

The following cryogenic equipment is implemented on the Hub:

- Thermal shields (1mm thick Aluminium).
- Deployable Sunshield (double foil Mylar VDA).
- He-JT cooler using a linear compressor.
- Solid Hydrogen cryostat.
- Low conductive mechanical support structure similar to Herschel/Planck.
- 50 K radiator (black painted open honeycomb structure).
- 100 K radiator (black painted/ anodised 1mm thick Aluminium).
- Temperature/pressure sensors.
- Adiabatic Demagnetisation Refrigerator.

7.6.5 Options

The following options for the cryogenic system of FIRI are identified:

- Sunshield: The baseline is a double foil Sunshield, but a deployable MLI or V-groove would increase the performance of the cryogenic radiators.
- 5 K cooling system: A system based on a Stirling or Pulse Tube pre-cooling to 15 K and a He JT cooler using a linear compressor is an alternative solution, which would require significantly more input power. In case the exported vibrations are not a concern, this option could become the baseline for the Hub cooling.
- Detector cooling system: Depending on the final operating temperature of the detectors, other coolers as e.g. ^{3}He sorption cooler for 300 mK or ^{3}He JT cooler for 1.5 K can be considered.

7.6.6 Summary

In the Payload Module there are all the units that are directly part of the cryogenic parts and instrumentation ; the rest are in the Service Module.

Element 2		Payload Module		MASS [kg]			
Unit	Part of:	Unit Name Click on button above to **insert new unit**	Quantity	Mass per quantity excl. margin	Maturity Level	Margin	Total Mass incl. margin
1	Telescopes	Telescope1-Thermal shields	1	75.0	To be modified	10	82.5
2	Telescopes	Telescope1+JT coolers	8	2.5	To be developed	20	24.0
3	Telescopes	Telescope1-BP	1	1.9	Fully developed	5	2.0
4	Telescopes	Telescope1-Miscellaneous (washers+fillers+MLI)	1	5.0	Fully developed	5	5.3
5	Telescopes	Telescope2-Thermal shields	1	75.0	To be modified	10	82.5
6	Telescopes	Telescope2+JT coolers	8	2.5	To be developed	20	24.0
7	Telescopes	Telescope2-BP	1	1.9	Fully developed	5	2.0
8	Telescopes	Telescope2-Miscellaneous (washers+fillers+MLI)	1	5.0	Fully developed	5	5.3
9	Instrument	PLM-Cryostat	1	360.0	To be developed	20	432.0
10	Instrument	PLM-Thermal shields	1	75.0	To be modified	10	82.5
11	Instrument	PLM-MLI & BP	1	11.9	Fully developed	5	12.4
12	Instrument	PLM-JT coolers	8	2.5	To be modified	10	22.0
13	Instrument	PLM-ADR cooler	1	80.0	To be modified	10	88.0
-	Do not use	Click on button below to insert new unit		0.0	To be developed	20	0.0
SUBSYSTEM TOTAL			**13**	**750.8**		**15.2**	**864.5**

Table 7-38: Payload Module mass budget

This Page Intentionally Blank

8 SERVICE MODULE

8.1 Propulsion

8.1.1 Requirements and Design Drivers

A propulsion system is required on FIRI

- to correct launcher dispersions
- to perform orbit maintenance
- to spin-up/spin-down the spacecraft
- to perform slew manoeuvres (repointing to a new science target) and
- to offload reaction wheels used to counteract the SRP.

The delta-V required for launcher dispersions is 30 m/s and for orbit maintenance 2 m/s per year, see Mission Analysis chapter. The manoeuvres required for observations and repointing are detailed in the Systems chapter and result in a total impulse of 642056Ns, with a 100 % margin included.

Six degrees of freedom and a thrust level of 10 N is required (see AOCS/GNC chapter).

8.1.2 Assumptions and Trade-Offs

Fine pointing and manoeuvring will be done using reaction wheels, and so a monopropellant system can be used as the only propulsion.

Hydrazine is compliant with the contamination requirements of the optics onboard.

The calculations for the propellant needed have been done assuming a dry mass of 4800 kg. A margin of 2 % has been added to the total propellant mass to account for residual propellant.

8.1.3 Baseline Design

A monopropellant system with Hydrazine has been chosen as baseline for FIRI. A scheme of a possible feed system is shown in Figure 8-1.

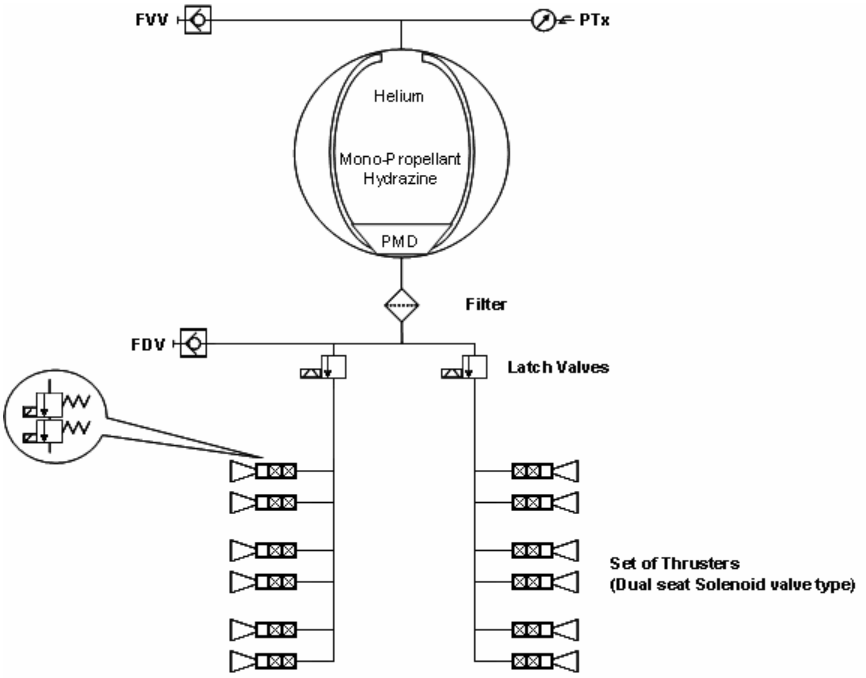

Figure 8-1: Scheme of an Example Monopropellant Feed System

Twelve 10 N Catalytic Hydrazine Thrusters (CHT), weighing 240 g each, will be accommodated on the spacecraft to comply with the six degrees of freedom and the 10 N thrust requirements. Data for the thruster is shown in Figure 8-2.

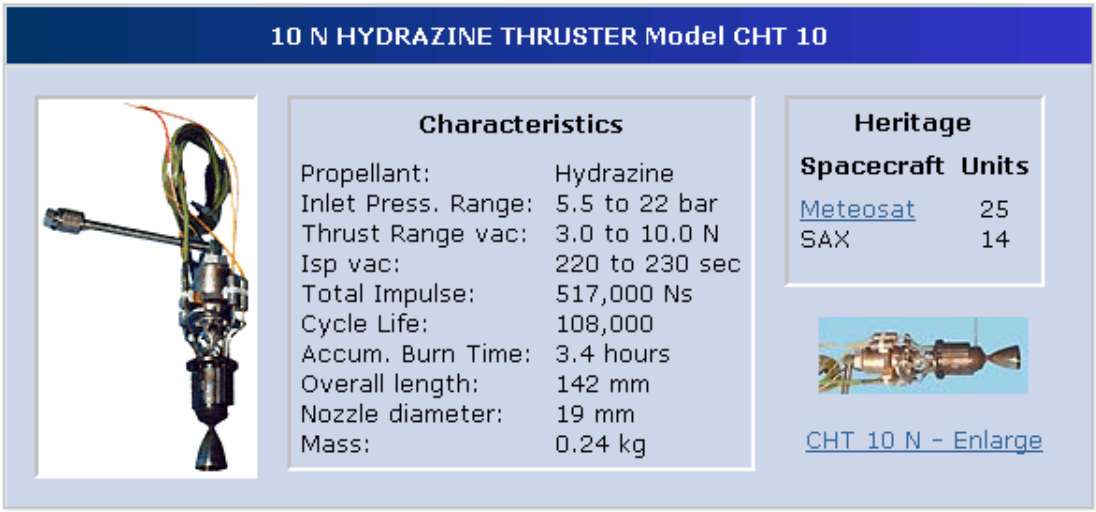

Figure 8-2: Characteristics of a 10 N CHT, RD[76]

The tank needs to accommodate 429 kg of propellant. In agreement with the customer a PSI tank, see RD[75], of 622.7 l was chosen as baseline. The tank weighs maximum 50 kg. It shall be noted that a European alternative should be investigated in later phases of the project, or that the tank should be ordered well in advance due to current import regulations.

An estimate of the other dry mass associated with the propulsion system, such as valves and pipes, is 10 kg.

The maximum power consumption for each Hydrazine valve is in the order of 14 W. The total power required will depend on how many thrusters are used simultaneously. The power is only consumed at the instance when the valve is opened or closed and will therefore not add to the sizing spacecraft power consumption.

8.1.4 List of Equipment

The equipment described above is summarised in Table 8-1.

Element 1		Service Module		MASS [kg]			
Unit	Part of:	Unit Name Click on button above to **insert new unit**	Quantity	Mass per quantity excl. margin	Maturity Level	Margin	Total Mass incl. margin
1	Hub	Monoprop Thrusters	12	0.24	Fully developed	5	3.0
2	Hub	Monoprop Other Dry Mass	1	9.4	Fully developed	5	9.9
3	Hub	Monoprop Tank PSI	1	49.9	Fully developed	5	52.4
SUBSYSTEM TOTAL			**3**	**62.2**		**5.0**	**65.3**

Table 8-1: Equipment List for the Propulsion Subsystem

8.2 Structures

8.2.1 Requirements and Design Drivers

The service module has the following requirements:

- Provide booms with a span of 14m that support the telescope rails with sufficient stiffness such that the telescope positioning error is less than 5cm
- Minimise thermal distortion
- Transmit loads from the payload adaptor to the various modules during launch

The service module consists of two parts; the booms and the hub. The primary function of the booms is to support the telescopes. Their secondary function is to transmit launch loads.

8.2.2 Assumptions and Trade-Offs

Due to the requirement to support the large independent mass of the telescopes, it was decided to use the booms as load carrying members during launch.

The service module does not reach cryogenic temperatures. However, some temperature variation is inevitable so thermal distortions must be minimised.

8.2.3 Baseline Design

8.2.3.1 Booms

The booms are CFRP square cross-section with 300mm side length and 2mm thick flanges. Each boom is 14m when deployed. This is divided into two sections each of which is 7m in length.

A closed section is needed to provide torsional stiffness, since the centre of mass of the telescopes is substantially offset with respect to the beam centreline.

8.2.3.2 Service Module Hub

The hub of the service module is a box structure with 2 internal shear panels in a cruciform pattern. Top and bottom panels assist in carrying the load. Closeout panels are included on the sides for equipment mounting.

The service module hub does not have a direct structural interface to the launch vehicle's adaptor. During launch, loads are transmitted into the box via launch locks on each of the four external side faces on the junction between the closeout panels and internal shear panels. The panels are designed for minimum mass as sandwich panels with carbon fibre facesheets and aluminium honeycomb core.

8.2.3.2.1 Thermal analysis of boom

A thermo-elastic analysis of a single boom was conducted using as input the worst case temperature profile taken from Figure 8-41.

The result of the thermo-elastic analysis is shown in Figure 8-3. The maximum thermo-elastic displacement was found to be 0.4mm. This presents no problem for meeting the deflection constraint of 5cm.

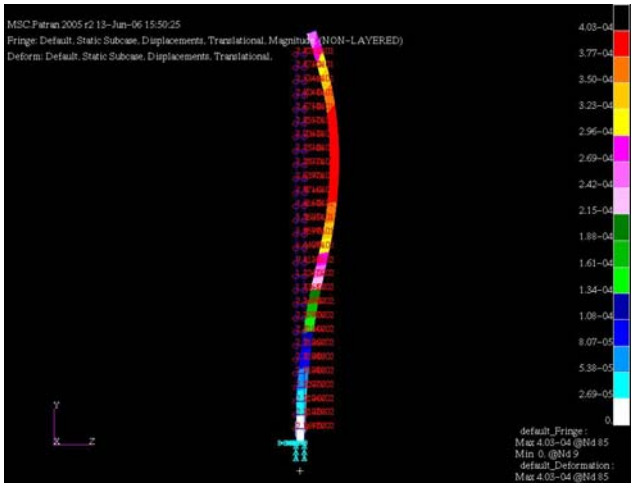

Figure 8-3: Thermo-Elastic Deflection of Boom

8.2.3.3 Structural support beams

Two structural support beams (shown in Figure 8-4) are used to secure the service module to the LV payload adaptor and to the remaining elements of the FIRI stack during launch. The support beams are jettisoned as part of the deployment sequence (prior to extension of the booms but after separation from the LV payload adaptor). These beams are assumed to be CFRP with cross-sections identical to the booms (see 8.2.3.1).

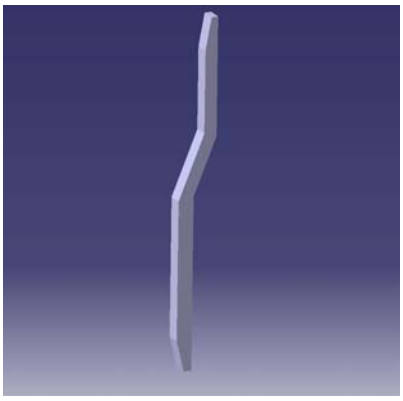

Figure 8-4: Support Beam

8.2.4 List of Equipment

The mass breakdown for the service module is shown in Table 8-2

The mass of the telescope service module (SVM) structure was found by scaling from the WFI design (see discussion in Paragraph 7.3.3).

Item	Nr.	Material	Skin thick. [mm]	Core thick. [mm] or [mm2]	Unit density [kg/m2]/[kg/m]	Item mass [kg]	Unit Margin [%]	Mass w marg. [kg]	All units [kg]
Top Floor	1	CFRP	2	16	7.479	40.39	20	48.47	48.47
Bottom Floor	1	CFRP	2	16	7.479	40.39	20	48.47	48.47
YZ Closeout	2	CFRP	0.5	9	2.292	4.79	20	5.75	11.51
XZ Closeout	2	CFRP	0.5	9	2.292	4.79	20	5.75	11.51
YZ Shear Panel	2	CFRP	2	16	7.479	15.64	20	18.77	37.54
XZ Shear Panel	2	CFRP	2	16	7.479	15.64	20	18.77	37.54
Boom	2	CFRP	2		3.931	55.04	20	66.04	132.09
Structural Support	2	CFRP	2		0.000	18.79	20	22.54	45.09
Telescope SVM Structure	2	CFRP				11.34	20	13.61	27.22
								TOTAL	**399.43**

Table 8-2: Service Module Mass breakdown

8.3 Mechanisms

The Service Module mechanisms concern:

- Telescope mechanisms
- Boom mechanisms
- Central hub mechanisms.

8.3.1 Requirements and Design Drivers

8.3.1.1 High level requirements

The main design drivers identified for the FIRI mission are as follows:

- Particulate and molecular contamination
- Need for stiff and backlash free support and motion of the telescopes
- Hard vacuum operating mechanisms (<5K) with very low thermal dissipation authorized
- Location of the telescope within a sphere of 5 mm diameter at boom tip
- Pointing of the telescope within a cone of 2 arcmin
- Linear accuracy of telescopes: < 1 cm
- Telescope stroke: 15 m
- Telescope duty cycle: in the order of 34500 forth and back cycles
- Type of motion: Translation
- Telescope mass: ≈ 500 Kg
- Telescope dimensions: ≈ 1 m diameter / 2 m high
- Number of cycles: in the order of forth and back motions
- Motion profile definition: “Stop and go”
- Synchronisation required: No if “Stop and go” motion type.

8.3.2 Assumptions and Trade-Offs

8.3.2.1 Objectives

The aim of the trade-off activities will be to achieve a design definition fulfilling with the following objectives:

- Reduce number of elements
- Reduce moving mass
- Reduce complexity
- Avoid development of new technologies; give priority to existing hardware, existing technologies and components off the shelf
- Failure tolerant and robust design
- Simplified deployment kinematics and dynamics
- Implement symmetrical configuration.

8.3.2.2 Scope of trade-offs

The trade-off will focus on the definition of the configuration of the telescope deployment and kinematics. In order to identify the most promising configuration, the following trade-off items have been identified, selected and conducted:

1. Telescope kinematics#1: Linear stage Vs Multiple DoF arm
2. Boom type #1: Tether Vs "Rigid" boom
3. Telescope kinematics #2: Moving telescope Vs Fixed telescope
4. Boom type #2: Telescopic tubes Vs Truss Vs Multiple segments
5. Boom deployment: One shot Vs Retractable/telescopic
6. Telescope carrier guiding unit: Magnetic bearing Vs Rolling elements bearing
7. Telescope carrier drive unit: Linear motor Vs Rotary actuator/rack Vs Cable
8. Telescope motion profile: Constant speed Vs "stop and go"

The following figures identify the chronology and the interdependencies between the identified trade-off items:

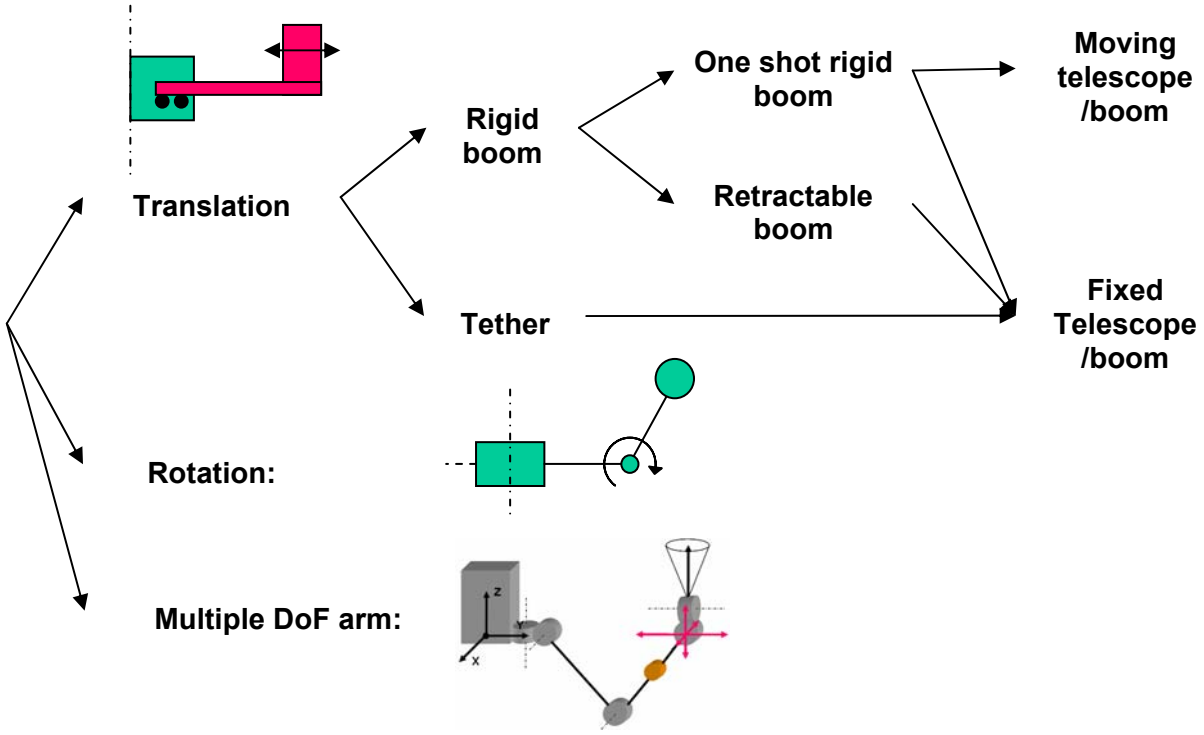

Figure 8-5: Trade-off overview 1/4

Note: The solution implementing a rotation type of motion for the telescopes has been rejected based on optical considerations.

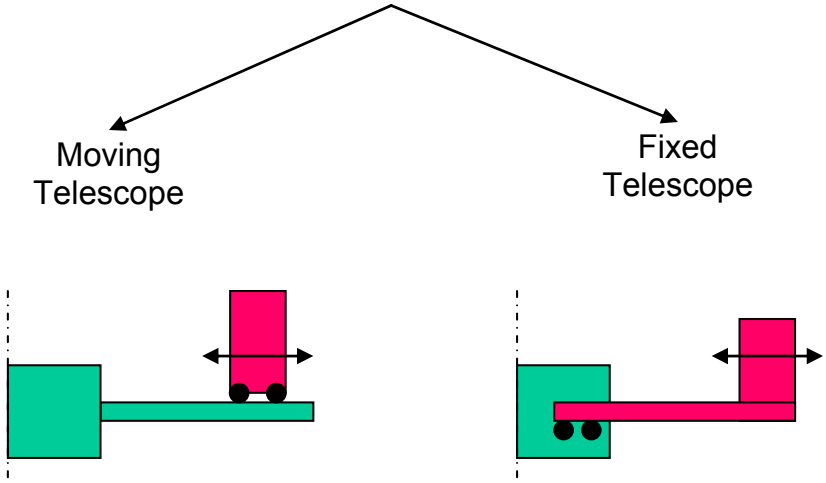

Figure 8-6: Trade-off overview 2/4

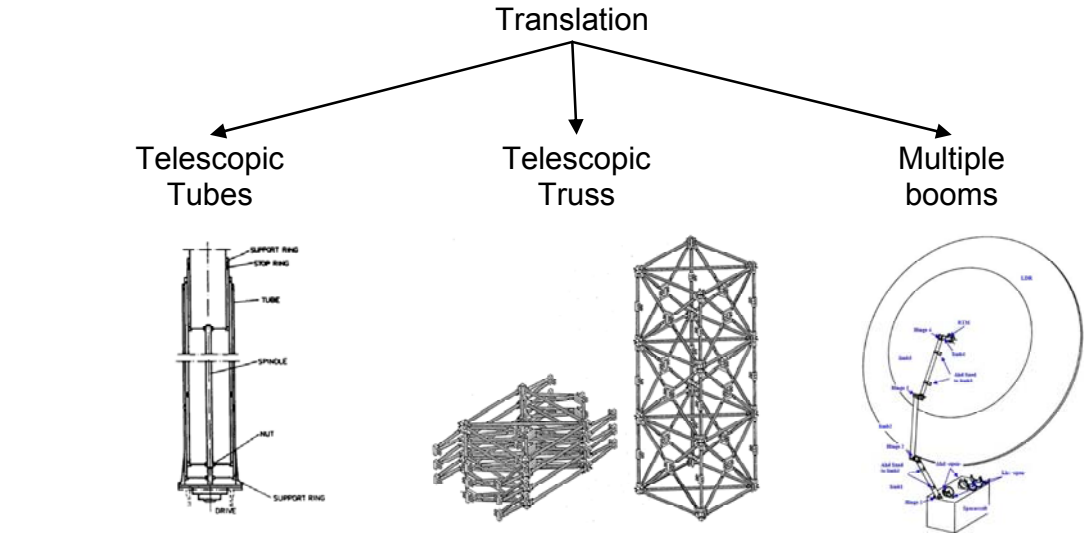

Figure 8-7: Trade-off overview 3/4

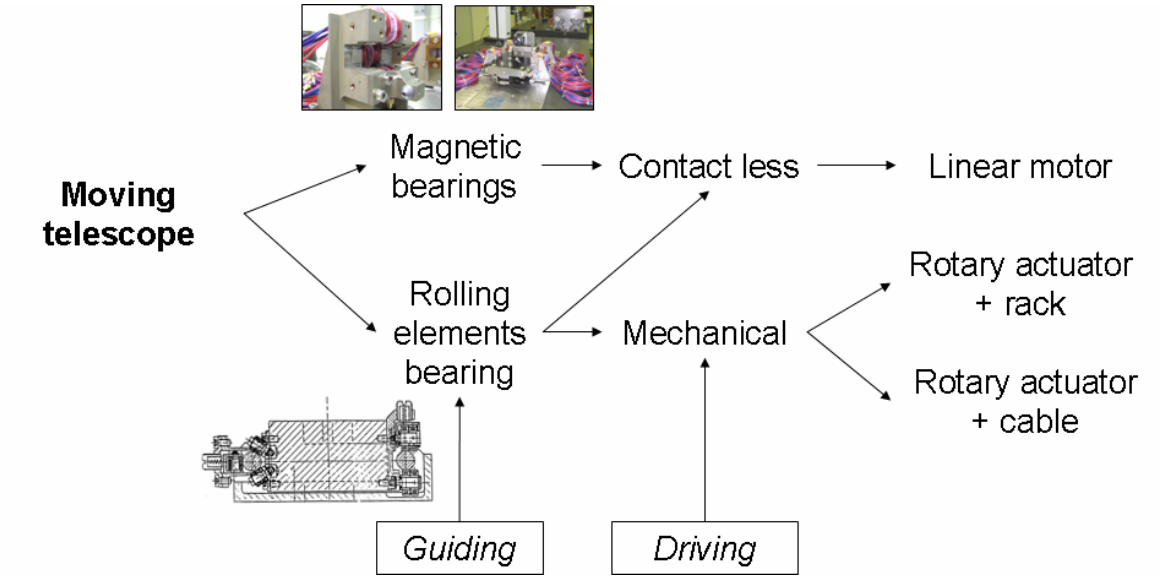

Figure 8-8: Telescope carrier - Trade-off overview 4/4

8.3.2.3 Telescope kinematics #1: Linear stage Vs Multiple DoF arm

Acknowledging the need for 5 DoF motion capabilities for the two telescopes, one could consider the use of a multiple DoF arm based on a simplified design of existing robotic arms already in use on board the ISS (see RD[58]; Canadarm2; see RD[57]) and the Space Shuttle (Canadarm; see RD[59]) or, to be flown on the ISS as the European Robotic Arm (ERA); see RD[56].

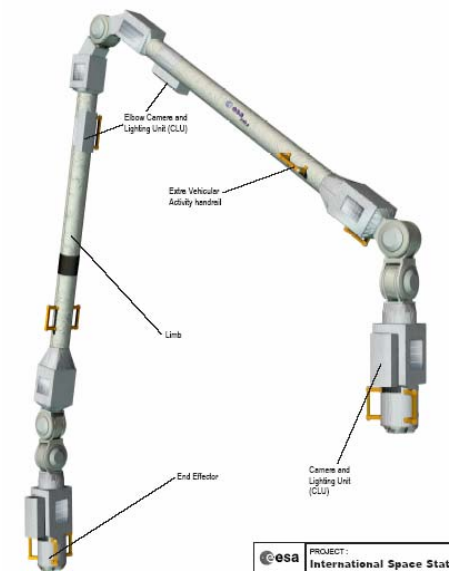

Figure8-9: ERA (Dutch Space)

The proposed Multiple DoF arm for FIRI would consist of two limbs and 5 motorised joints. The motorized joints are used to achieve the deployment of the telescope from the stowed configuration to the operational position. Then, they are used to provide the specified kinematics

to the telescopes (translation) and the required corrections in translation and rotation of the telescope motion over the full linear stroke. Kinematics during the observation mode are shown on Figure 8-10:

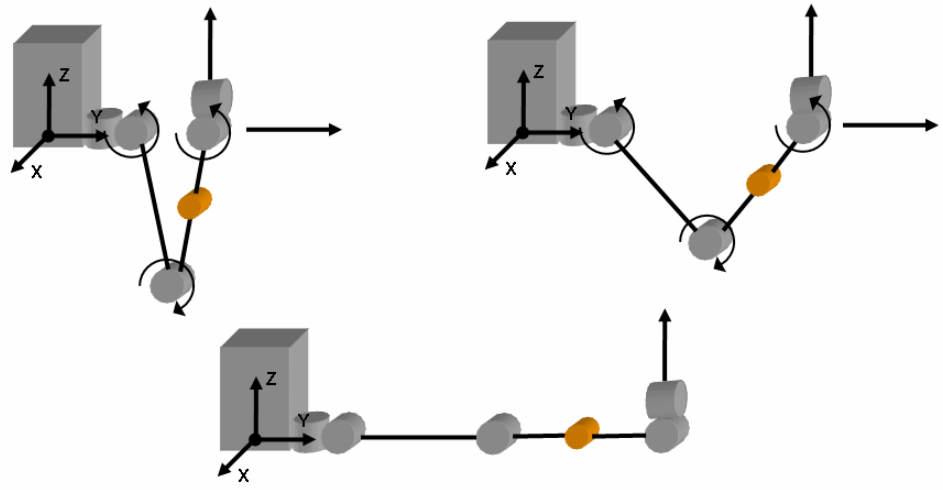

Figure 8-10: Multiple DoF arm – Translation of the telescope

The Multiple DoF arm was compared with a classical linear stage. An existing application of linear stage with a stroke in the same order of magnitude as FIRI can be found on the ISS. This is the Mobile Transporter of the Mobile Servicing System; see RD[59].

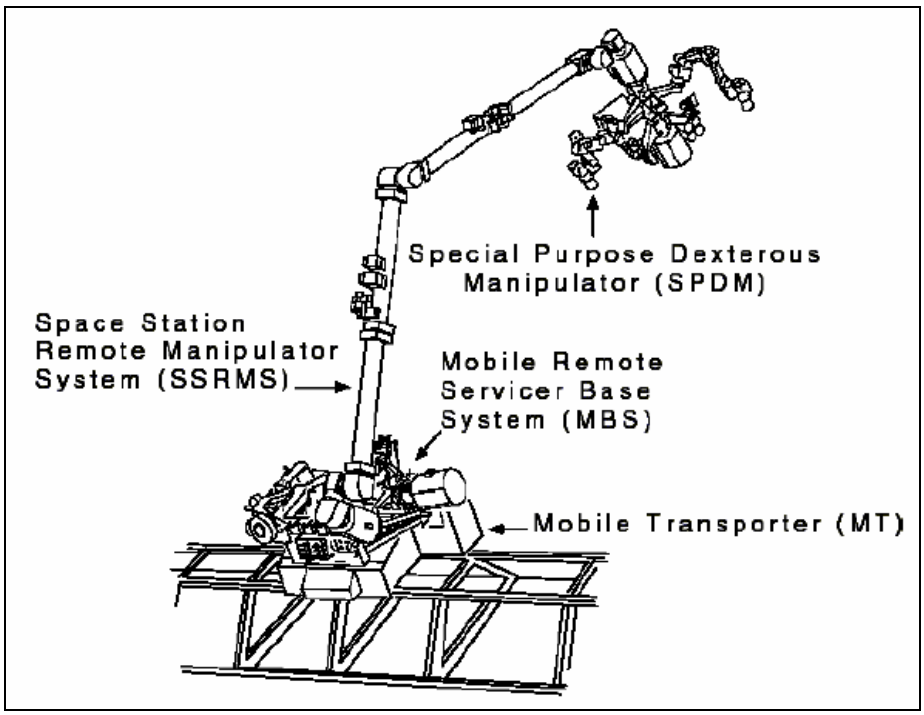

Figure 8-11: Mobile Servicing System of the ISS

	Pro	Cons
Multiple DoF Arm	Reuse of deployment hinges for translation Lower inertia when telescopes inwards Compensation of constant, short term and long term errors Lightweight solution Technology available in Europe (ERA) No need for hold down for telescope carrier during launch 5 DoF repositioning/re-pointing of telescope Harness routing	Telescope stowed at tip Complex sensor and control electronics implementation High power consumption CoG variation along Z Low Stiffness / accuracy High backlash: +/- 2 arcmin; see RD[72]
Linear stage	Stiff and safe support for telescope all along specified stroke Low power consumption	Need for additional telescope tip/tilt mechanism for telescope pointing to compensate MAI effects Use of rails Harness routing

Table 8-3: Linear stage @ Multiple DoF arm

Based on a qualitative trade-off, the linear stage configuration was selected.

8.3.2.4 Boom type #1: Tethers Vs Rigid boom

The objective was to assess the tether technology in order to achieve the telescope translation motion. The use of tethers requires a spinning spacecraft. Tethers would be implemented between the Service Module and the two telescopes. One or several tethers could be used in order to increase the control and the steerability of the "floating" telescope as shown in Figure 8-12:

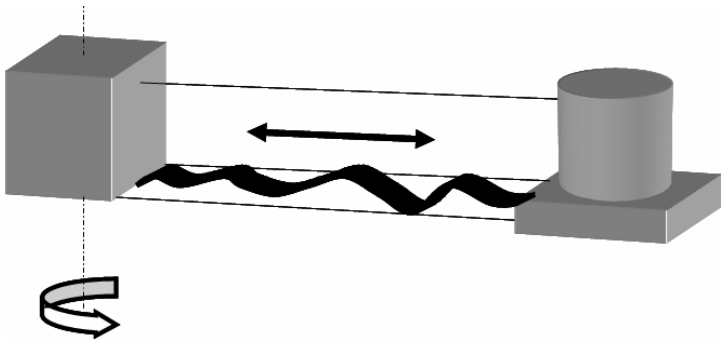

Figure 8-12: Tethers option

Table 8-4 compares the tethers with a traditional configuration based on a rigid boom.

	Pro	Cons
Tethers	Low mass Low volume Low number of components	Low control of motion of the telescope Harness routing Telescope pointing accuracy and stability Alignment the optical chain between the telescope and the Service Module Requires spinning spacecraft; spinning rate too low
Rigid boom	Stiff support for telescope all along specified stroke Full control of telescope motion	High mass High volume High complexity

Table 8-4: Moving telescope Vs fixed telescope

Based on a qualitative trade-off, the rigid boom configuration was selected.

8.3.2.5 Telescope kinematics #1: Moving telescope Vs Fixed telescope

is the trade-off was to identify the most promising approach between a moving telescope on a fixed boom with respect to the Service Module and a Telescope fixed at the tip of a boom in relative motion with respect to the Service Module (Table 8-5).

	Pro	Cons
Moving telescope	Reduced moving mass Better control of telescope motion Stowed configuration for telescope	Exposed mechanism Higher power consumption in telescope carrier
Fixed telescope	Protected mechanism in the service module Easy mechanical synchronisation	Non symmetrical configuration Kinematics / interferences between the two booms No rigid interface with spacecraft Higher volume in stowed configuration at boom root Stowed configuration for telescope

Table 8-5: Moving telescope Vs fixed telescope

Based on a qualitative trade-off, the moving telescope configuration was selected.

8.3.2.6 Boom type #2: Telescopic tubes Vs Truss Vs Multiple segments

This trade-off was to identify the most promising boom configuration for the deployment and potentially the motion of the telescope reusing the deployment approach inherent to some boom designs. Existing boom design and architecture found in the literature are shown in Table 8-6.

	Pro	Cons
Telescopic Tubes	Packaging ratio Optimised structural shape Low mass 1 dimension deployment	No rail integration and deployment possible as non constant cross section over boom length 1 dimension deployment – stowed configuration for telescopes
Telescopic Truss	Packaging ratio 1 dimension deployment	High complexity Poor deployment control Implementation of rail difficult 1 dimension deployment – stowed configuration for telescopes
Multiple segments	Low complexity Low mass High deployed stiffness Dimension deployment – stowed configuration for telescopes Easy integration of rails Robust	High volume in stowed configuration 2 dimension deployment

Table 8-6: Telescopic tubes Vs Truss Vs Multiple segments

Based on a qualitative trade-off, the multiple segments configuration has been selected. According to the available fairing envelope, the boom can be stowed in two segments articulated with two motorised hinge lines, one at the root and one at the middle of the boom.

8.3.2.7 Boom deployment: One shot Vs Retractable/telescopic boom

This trade-off was to investigate the functionality offered by the boom designs assessed in the previous paragraph in order to achieve the deployment of the boom and the telescope motion using the same functional elements Table 8-7.

	Pro	Cons
One shot	Low moving mass Stiff support	Need of additional drive and guiding units for telescope
Retractable boom	Combined deployment and telescope motion No need for specific drive and guiding units for the telescope High packaging ratio	High number of elements / complexity Low stiffness when deployed Stowed configuration of telescope Harness routing Control of dynamics of telescope motion Accommodation of guiding elements (rail) Uniformity of rail (bending, thermo-mechanical behaviour…)

Table 8-7: One shot Vs Retractable/telescopic boom

Based on a qualitative trade-off, the one shot deployment configuration has been selected.

8.3.2.8 Telescope carrier - Guiding unit: Magnetic bearing Vs Rolling elements bearing

This trade-off was between a set of active magnetic bearings with electromagnets on the moving part acting against rails made of magnetic material all along the boom and ball bearing rollers fitted on the mobile part acting against steel rails all along to boom Table 8-8.

	Pro	Cons
Magnetic bearing	Contact less / no friction No lubrication No wear Not sensitive to low temperature Low sensitiveness to rail defects Dynamic control of motion + damping of vibrations Possible correction of rails defects Can be active (no power)	EMC problems with payload No rigid support Control of functional gap versus temperature and physical tolerances High power consumption Complex implementation Need dedicated drive electronics / close loop controller Reliability / failure tolerance
Rolling element bearing	Rigid support for telescope Known kinematics No power consumption	Need for lubrication Complexity for backlash free device Micro vibration due to motion / Noisy motion / Wear Rail manufacturing and assembly Discontinuity in rail connections

Table 8-8: Magnetic bearing Vs Rolling elements bearing

Based on a qualitative trade-off, the rolling elements bearing technology has been selected.

8.3.2.9 Telescope carrier – Drive unit: Linear motor Vs Rotary actuator/rack Vs Cable

This trade-off is between the Linear Motor technology and a configuration implementing a rotary actuator fixed on the mobile part of the linear stage fitted with a gear box and, a pinion acting against a rack fixed on the deployed booms. It will also be compared to a configuration implementing an actuator located in the service module driving a closed loop of a cable routed along the deployed boom, attached to the mobile part of the linear stage and tensioned with a pulley fixed at the tip of the boom (Table 8-9).

	Pro	Cons
Linear motor	Contact less / no friction No lubrication No sensitive to low temperature Can be combined with magnetic bearings (integrated guiding and driving system)	Need power for holding torque / Requires constant power EMC problems with payload Need magnet all along boom length Control of functional gap
Rotary actuator + rack	Simple and robust design Well known technology	Need rack on boom length / High mass Compensation for backlash in gear drive High MAI tolerances required
Rotary actuator + running cable	Drive unit in service module	Deployment of cable Cable technology Control of tension of cable to avoid backlash Accommodation of cable during operation and during launch

Table 8-9: Linear motor Vs Rotary actuator/rack Vs Cable

Based on a qualitative trade-off, the drive unit based on rotary actuators associated with racks fixed on the booms has been selected.

8.3.2.10 Telescope motion profile: Constant speed Vs "stop and go"

The objective was to assess which is the most suitable motion profile of the linear stage in order to achieve the mission objectives (Table 8-10)

	Pro	Cons
Constant speed	? (not at mechanism level)	Very low speed very difficult to achieve with low noise Constant power need Dynamic re-pointing required Constant heat source EMC
"Stop and go"	Easy fine re-pointing No noise due to motion	Holding torque required

Table 8-10: Constant speed Vs "stop and go"

Based on a qualitative trade-off, a motion profile of the linear stage a “stop and go” is preferred from a mechanisms point of view.

8.3.3 Baseline Design

Figure 8-13 and Figure 8-14 present a summary of the result of the trade-off activities performed in order to identify the most promising baseline design for the telescope deployment and motion:

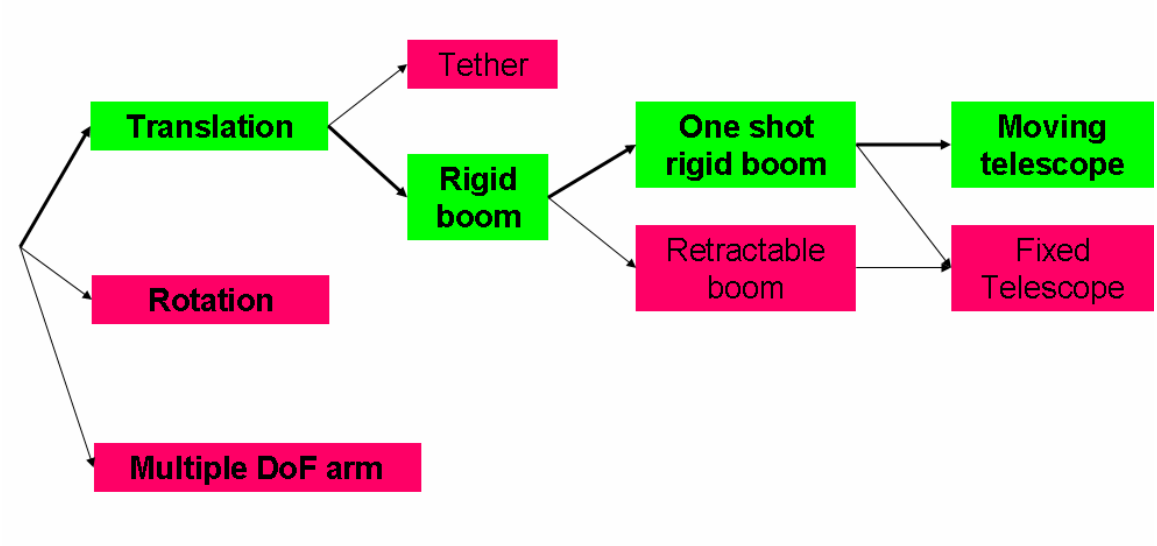

Figure 8-13: Results of telescope deployment and motion trade-offs 1/3
(In red: Not selected; in green: Selected)

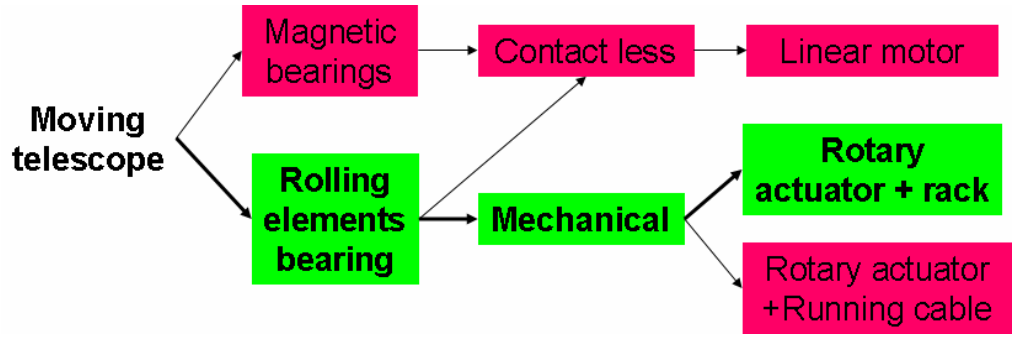

Figure 8-14: Results of telescope deployment and motion trade-offs 2/3

The assembly of the rolling elements bearing (guiding unit) and rotary actuator + rack (drive unit) located on a structure carrying the telescope and other ancillary equipments is the *telescope carrier*.

The assembly of the telescope carrier with the boom structure and support of the telescope carrier (guiding unit) is called *linear stage*.

Figure 8-15 shows the selected chain following trade-off.

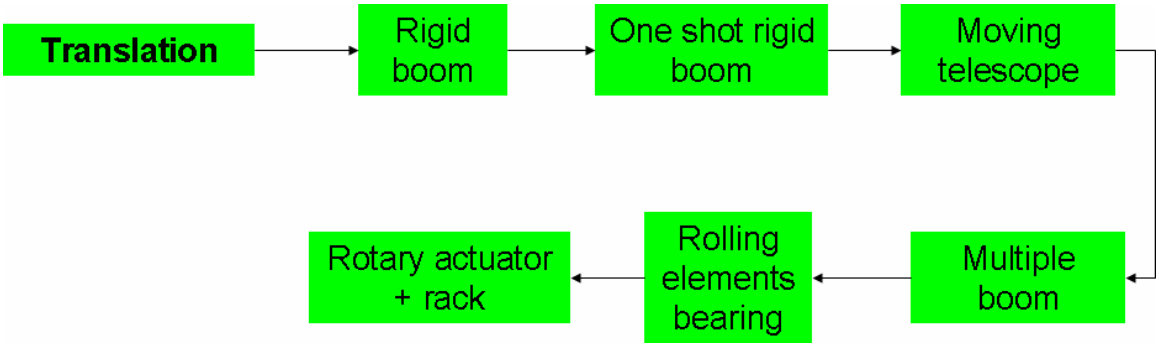

Figure 8-15: Results of telescope deployment and motion trade-offs 3/3

8.3.4 List of Equipment

Following the trade-off activities at mechanisms level but also in other disciplines, the following list of equipments have been generated for the Service Module mechanisms (Table 8-11):

Location	Item identification
• Boom :	Motorised hinge line with latching
• Boom :	Guiding rails + supports to boom
• Boom :	Rack + supports to boom
• Boom :	Boom HDRM + supports
• Hub :	Sun Shield HDRM + deployment foil 1
• Hub :	Antenna HDRM
• Hub :	Antenna Deployment and Pointing Mechanism
• Hub :	Jettison Mechanism
• Telescopes :	Telescope carrier structure
• Telescopes :	Telescope carrier bearing assembly
• Telescopes :	Telescope carrier anti backlash / compliant system
• Telescopes :	Telescope carrier drive unit assembly
• Telescopes :	Telescope carrier HDRM
• Telescopes :	Telescope carrier position sensor
• Telescopes :	Sun Shield HDRM + deployment foil 1
• Telescopes :	Sun Shield HDRM + deployment foil 2
• Telescopes :	Telescope 5 DoF positioning mechanism
• Telescopes :	Telescope HDRM

Table 8-11: List of equipment for Service Module mechanisms

8.3.4.1 Motorised hinge lines with latching

The main functions of the motorised hinges are to deploy the boom segments from stowed configuration, control the deployment dynamics and kinematics and, latch with high accuracy and stiffness.

8.3.4.1.1 Main requirements:

The main set of requirements for motorised hinge line is:

- One shot deployment
- Operational temperature: - 40 °C to +80 °C
- Deployed position accuracy and stability: < 0.01 degree
- Deployment hinge stiffness: > 2.0E+06 N.m/rad.

8.3.4.1.2 Proposed design

The proposed hinge design is based on an existing development named Antenna Deployment and Blocking (ADB) Mechanism developed in the frame of the Large Deployable Antenna (LDA) activity in 2003 under the ARTES-5 programme; see RD[62].

Each boom is equipped with two different hinges, one at the root and one at the middle as each boom is divided into two segments.

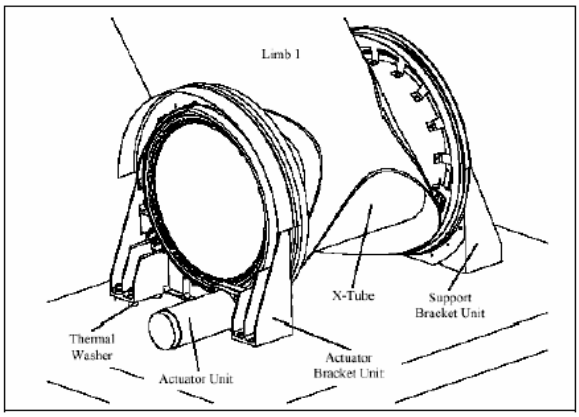

Figure 8-16: ADB – Root hinge - HTS AG

Figure 8-17: ADB – inter segment hinge - HTS AG

Main characteristics:

- Motorised (stepper motor) for coarse deployment control and regulation
- Thin section angular contact ball bearings (high stiffness)
- Heritage: ESA / Large Deployable Antenna (LDA)
- Current status: TRL5

Modifications required:

- High accuracy and stability mechanical latching
- To be scaled for higher loads (TBC)
- Implementation of position sensor for monitoring and control of deployment kinematics

Accommodation issue:

- Telescopes shall be stowed with telescope at boom root to ease the deployment control and regulation
- To be interfaced with specific boom segments cross section.

8.3.4.2 Boom Hold Down and Release Mechanism (HDRM)

The main function of the HDRM is to maintain and secure the booms in stowed configuration during launch and to release them once in orbit to enable the deployment.

8.3.4.2.1 Main requirements:

The main set of requirements for the boom HDRM is:

- Operational temperature - 25 °C to +40 °C
- Max. loads:
  - Force out of plane: 6000 N Based on existing design
  - Force in plane: 7500 N Based on existing design
  - Moment in plane: 200 N.m Based on existing design
  - Moment out of plane: 300 N.m Based on existing design

8.3.4.2.2 Proposed design

The proposed HDRM design is based on an existing development named Antenna Hold Down and Release Mechanism (AHD) developed in the frame of the Large Deployable Antenna (LDA) activity in 2003 under the ARTES-5 programme; see RD[62] and RD[73]. This equipment is able to hold and release two boom segments at the same time.

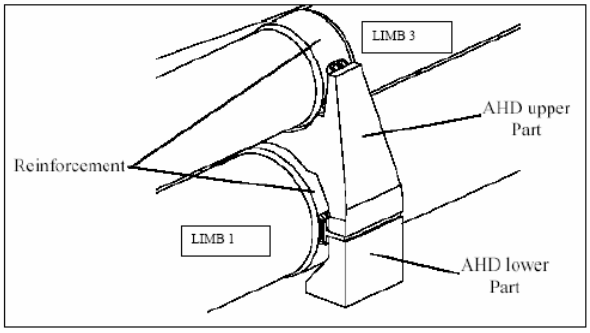

Figure 8-18: AHD – With two segments stowed– Magna Steyr

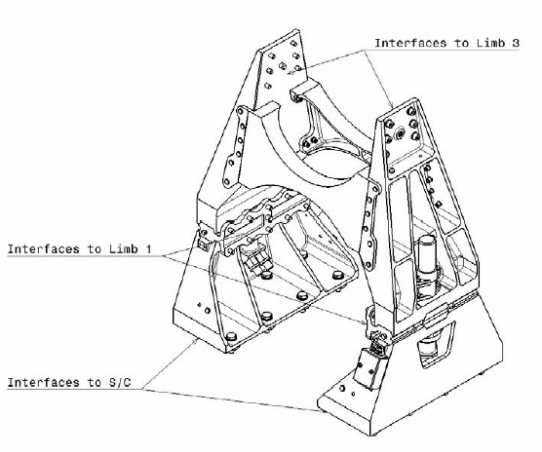

Figure 8-19: AHD – Without segments – Magna Steyr

Main characteristics:

- Pyro separation nuts
- High stowed stiffness
- 2 booms held together
- Heritage: ESA / Large Deployable Antenna (LDA)
- Current status: TRL5.

Modifications required:

- To be scaled for higher loads
- To be modified according to FIRI configuration.

Main accommodation issue:

- Not compliant design to cope with thermo-mechanical loads during launch
- To be interfaced with specific boom segments cross section.

8.3.4.3 Linear stage – Guiding unit – Rails

The main function of the rails is to provide a rigid and smooth support to the telescope carrier on the deployed booms.

8.3.4.3.1 Definition:

- 2 parallel guiding rods (hollow tube: 40 mm outer diameter)
- Material: 440C steel (1.5 Kg /m with attachments to boom)
- Lubrication: Hardened steel + thin dense chrome + overlaid by silver coating (preliminary – Same design as MIPAS).

8.3.4.3.2 Main issues:

- Alignment and manufacturing tolerances TBD
- Requirements on surface finishing relaxed as no continuous motion
- Flexible mount on boom required with hard point at hinge line location
- Thermo-mechanical distortions in combination with the boom materials
- Rails connections when boom deployed for translation motion continuity
- Lubrication selection / processes / generation of debris / particulate contamination
- Manufacturing, Assembly, Integration and testing.

8.3.4.4 Linear stage - Telescope carrier - Guiding unit

The main function of the telescope carrier guiding unit is to provide a mechanical support to the boom (rails) with only one degree of liberty (translation).

8.3.4.4.1 Definition

The definition of the telescope carrier guiding unit lies in the assembly of qualified off the shelve components available in Europe.

The proposed design is based on the configuration of a linear stage developed for the MIPAS instrument onboard Envisat; see RD[63]:

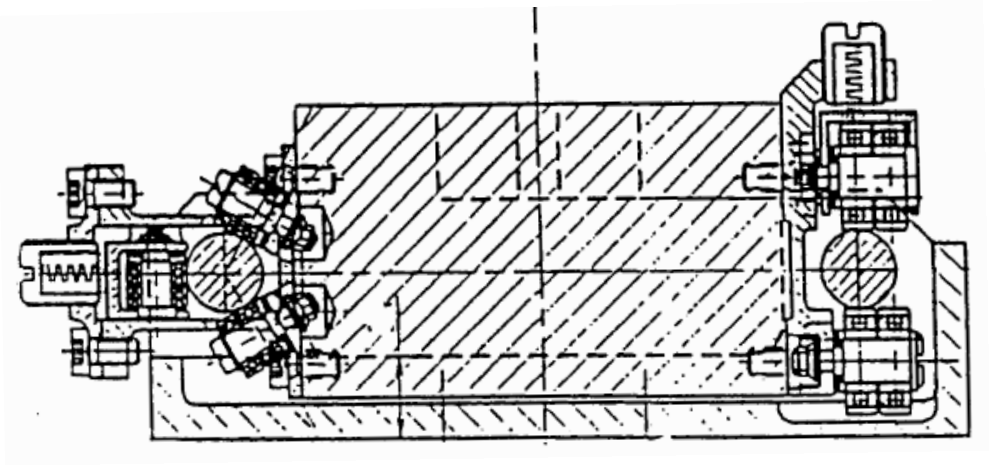

Figure 8-20: Option considered during MIPAS (Envisat) development

- No background in Europe for long strokes as specified for FIRI (max. 40cm)
- Rigid support structure required to interface and accommodate with payload unit equipments (telescope, power sub systems…)
- 3 pairs of preloaded ball bearing rollers assembly: Iso static mount, no backlash
- Each pair composed of 2 sets of 2 angular contact ball bearing rollers mounted back to back and preloaded with belleville washers
- 1 pair mounted on a compliant support (flexible blades) to ensure constant preload and backlash free configuration all along the stroke against rails to cope with misalignment and parallelism errors (stroke and stiffness TBD)
- Dry lubrication: Sputtered MoS2 ball bearings with PGM cages.

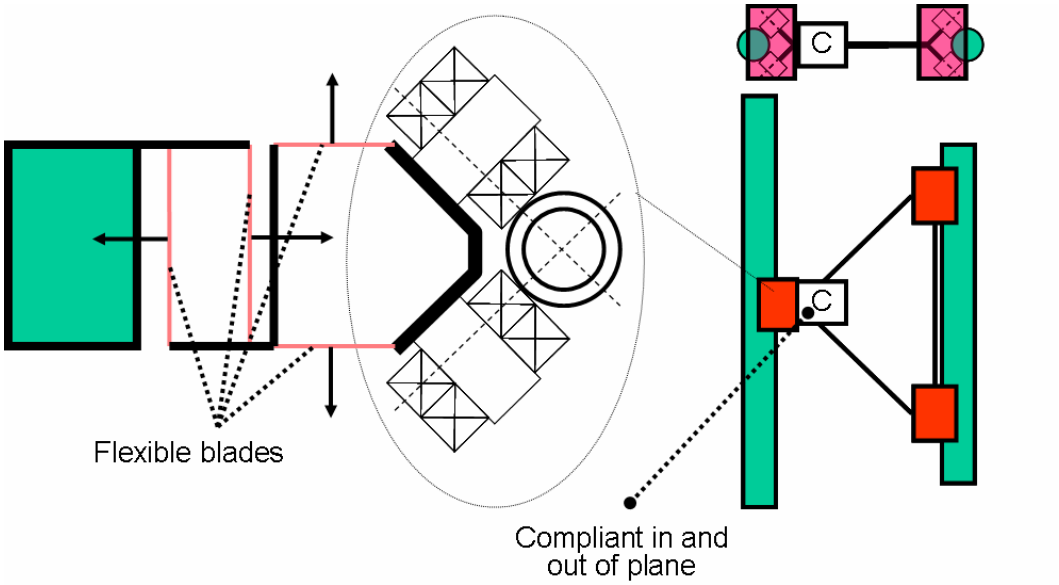

Figure 8-21: Linear stage – Telescope carrier – Guiding Unit

8.3.4.4.2 Main issues:

- Need for bearings assembly unloading during launch or specific coating/counter part material on rails to avoid degradation of bearings to rail contacts and cold welding
- To be launched in stroke area not used during the observation mode (if possible)
- Need for specific HDRM during launch.

8.3.4.5 Linear stage – Telescope carrier - Drive unit

The main function of the drive unit is to provide the actuation of the telescope carrier over the specified stroke of 15 metres according to specified motion profile during the observation mode.

8.3.4.5.1 Definition

The definition of the telescope carrier drive unit lies in the assembly of qualified off the shelve components available in Europe.

Actuator:

- Pinion fitted with anti backlash system (two stages pinion teeth assembly with calibrated torsion bar); Hardened (plasma-nitrided) 722M24 / Dry lubrication: Sputtered MoS2
- Brush less DC motor: higher efficiency, better speed/acceleration profile control, position sensing needed for actuator drive
- Anti backlash and irreversible gear box assembly (Reduction ratio TBD by design).

Rack:

- Through-hardened 440C
- Dry lubrication: Sputtered MoS2.

Position sensors:

- Contactless
- Need for absolute position signal for the telescope position sensing
- Laser measurement system with target on telescope for coarse position sensing
- Position sensor for actuator drive.

8.3.4.6 Sun shield mechanism

The main function of the Sun Shield Mechanism is to hold down, release, deploy and latch in deployed position the sun shield to be fitted on the telescopes and on the Service Module. Sun shield mechanisms and mechanical design will be the same for the telescopes and Service Module applications except for the number of foils.

8.3.4.6.1 Main requirements:

The main set of requirements for the Sun Shield Mechanism is:

- Operational temperature - 40 °C to +65 °C
- Number shields: 1 or 2 foils (separation distance 70 cm)
- Shape foil 1: 5.2 m diameter
- Shape foil 2: 4 m diameter (only for telescopes)

8.3.4.6.2 Proposed design

The proposed hinge design is based on an on-going development for the deployment of an 11 metre diameter Sun Shield for the GAIA mission as shown below. This design can be fully retrofitted on FIRI:

Figure 8-22: GAIA Sun Shield in stowed and deployed configuration

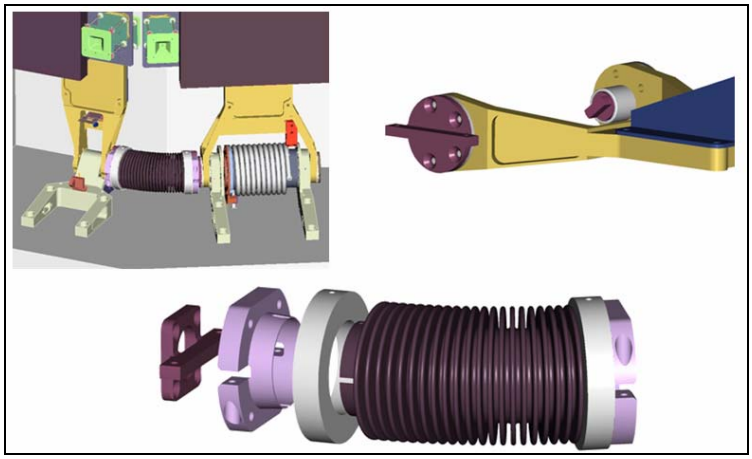

Figure 8-23: GAIA Sun Shield hinge mechanism

Main characteristics:

- Spring actuated hinges with mechanical latching
- Deployment regulation with damper and mechanical synchronisation
- Need for thermo-mechanical loads compensation between backbone structure and foils
- Need for 1 hold down point per rigid frame
- 4 rigid frame tightening 4 foils proposed then deployed octagonal shape
- No flatness tolerance for the deployed foils
- Heritage: ESA / GAIA
- Current status: TRL4

Modifications required:

- To be scaled for FIRI shield area
- To be designed for stowed configuration
- Implementation of deployment synchronisation of the 2 foils with parallelogram.

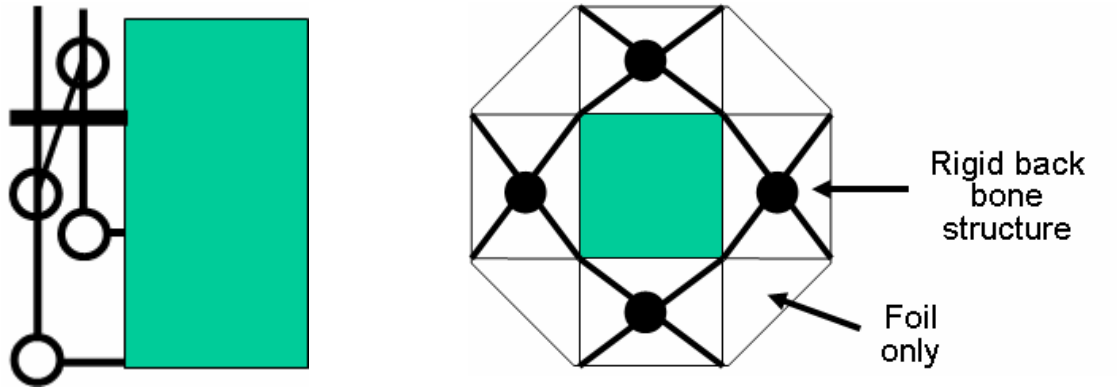

Figure 8-24: Proposed design for Sun Shield mechanism

8.3.4.7 Table Telescope positioning mechanism

The main function of the Telescope Positioning mechanism (in non-cryogenic environment) is to provide a 5 DoF motion capability to the telescope in order to compensate sources of errors for the location of the telescope with respect to the service module (translations) and pointing (in plane rotations) as per the specified Field of View.

8.3.4.7.1 Definition of the need

The need of a 5 DoF fine repositioning of the telescope whatever the position of the telescope is on the boom length comes from the preliminary assessment of the errors in location (translations) of the telescope due to the following identified contributors:

- *Constant induced errors*: Sphere of 35 mm radius at boom tip
  - Hinges accuracy
  - Locking device accuracy
  - Hinges manufacturing errors
  - Deployment repeatability
  - Zero to 1g effects
  - Hinge assembly errors.

  Note: this does not include boom manufacturing tolerances
- Short term errors: TBD
  - Telescope motion Negligible, no motion during acquisition
  - AOCS / damping Structure
  - Thermal distortions Structure

- Long term errors:
  - Ageing (CRFP) Structure
  - Moisture desorption (CRFP) Structure

The minimum achievable telescope location error is defined as a sphere of 35 mm diameter taking into account only constant induced errors which is much higher than what could be allowed by the optical system (10 mm diameter). It is deemed very difficult to achieve such telescope location tolerance only by design, therefore it has been decided to introduce an active mechanism.

8.3.4.7.2 Main requirements

The main set of requirements for the telescope positioning mechanism is:

- Location: Between telescope and telescope carrier
- Pointing range (optics): 3 degrees half cone
- Pointing accuracy: 0.5 arcmin.
- Pointing resolution: 0.2 arcmin.
- Translation range (3D): ± 50 mm
- Frequency bandwidth: < 0.01 Hz
- Payload mass: ~500 Kg
- Operational temperature: - 40°C to + 80°C

8.3.4.7.3 Proposed design

It is proposed to use a hexapod as the one currently in use for the Sage III experiment on board the ISS, see RD[65]:

Figure 8-25: Hexapod - Sage III / ISS - AAS / ADS / ESTL

8.3.4.8 Antenna pointing mechanism

The main function of the Antenna pointing mechanism is to re-point the high gain antenna to earth in order to transmit science data between observations without repointing the spacecraft. The mechanism shall then provide power and data transmission via a slip ring assembly.

8.3.4.8.1 Main requirements

The main set of requirements for antenna pointing mechanism is:

- Maximal spinning rate: 3.1 revolutions per hour
- Maximal mission duration: 5 years
- Number of cycles: 136000
- Angular range: TBD
- Pointing accuracy: TBD
- Pointing resolution: TBD
- Antenna diameter: TBD m
- Operational temperature: - 40°C to + 80°C

8.3.4.8.2 Proposed design

The design is based on the Advanced Scan Mechanism including Power and Data Transmission for a future large conical scanner currently under development at Contraves Space AG (CH).

Modifications will be required in order to meet the FIRI requirements. In addition, the current development doesn't include a re-pointing mechanism of the reflector antenna in order to ensure data transmission for all the specified targets. This 2 DoF pointing mechanism is currently available off the shelf.

8.3.5 Option

For the Service Module, the main option to the proposed baseline design is the Multiple DoF arm which shall be further investigated in order to assess the capabilities of such design to provide satisfactory support of the telescope in terms of stiffness, accuracy and backlash.

8.3.6 Summary

Table 8-12 presents the overall mass budget of mechanisms for the Service Module:

Element 1		Service Module		MASS [kg]			
Unit	Part of:	Unit Name Click on button above to **insert new unit**	Quantity	Mass per quantity excl. margin	Maturity Level	Margin	Total Mass incl. margin
1	Boom	Motorised hinge line with latching	4	15.0	To be modified	10	66.0
2	Boom	Guiding rails + supports to boom	60	1.5	To be developed	20	108.0
3	Boom	Rack + supports to boom	30	2.9	To be developed	20	104.4
4	Boom	Boom HDRM + supports	4	20.0	To be developed	20	96.0
5	Hub	Sun Shield HDRM + deployment foil 1	1	50.0	To be modified	10	55.0
6	Hub	Sun Shield HDRM + deployment foil 2	0	0.0	To be modified	10	0.0
7	Hub	Antenna HDRM	1	4.0	To be modified	10	4.4
8	Hub	Antenna Deployment and Pointing Mechanism	1	15.0	To be developed	20	18.0
9	Hub	Jettison Mechanism	2	20.0	To be developed	20	48.0
10	Telescopes	Telescope carrier structure	2	15.0	To be developed	20	36.0
11	Telescopes	Telescope carrier bearing assembly	6	2.0	To be developed	20	14.4
12	Telescopes	Telescope carrier anti backlash / compliant system	2	2.0	To be developed	20	4.8
13	Telescopes	Telescope carrier drive unit assembly	2	5.0	To be developed	20	12.0
14	Telescopes	Telescope carrier HDRM	4	2.0	To be developed	20	9.6
15	Telescopes	Telescope carrier position sensor	2	2.0	To be modified	10	4.4
16	Telescopes	Sun Shield HDRM + deployment foil 1	2	50.0	To be modified	10	110.0
17	Telescopes	Sun Shield HDRM + deployment foil 2	2	40.0	To be modified	10	88.0
18	Telescopes	Telescope 5 DoF mechanism	2	40.0	To be developed	20	96.0
19	Telescopes	Telescope HDRM	8	5.0	To be developed	20	48.0
-	Do not use	Click on button below to insert new unit		0.0	To be developed	20	0.0
SUBSYSTEM TOTAL			**18**	**794.0**		**16.2**	**923.0**

Table 8-12: Mass budget – Mechanisms – Service Module

The total mass of mechanisms for FIRI is estimated to be: 1247 Kg. Further analysis should concentrate on optimisation, to reduce the mechanisms mass.

Volume, power consumption and risk assessment can be found in the mechanisms workbook.

8.3.7 Open Points

The following aspects of the FIRI missions could not been investigated during the course of the CDF Study:

- Stowed configuration definition with hold down points definition
- Drive of linear stage
- Telescope carrier position sensing definition
- Definition of the jettison mechanism for structural support of booms and telescope during launch
- Definition of the deployment sequence
- Definition of the Antenna pointing Mechanism
- Joint and mechanism between the two boom segments.

8.4 Power

8.4.1 Requirements and Design Drivers

8.4.1.1 General requirements

The main functional requirements of the power subsystem are:

- To supply power to all the onboard equipment for the mission duration wherever they are located in the telescopes, the boom or the hub.
- To include individual protections to isolate a failure and to avoid propagation to others units
- To have switching capabilities on all power lines
- To control all the pyros devices (selecting, arming and firing functions).

In order to enable the mission feasibility, the EPS designs will be mainly driven by the mass parameters. As a second major criterion, the technologies with a higher TRL will be naturally preferred.

In line with the level of definition of FIRI, a power margin of at least 20% shall be considered at bus level.

L2 Lagrange point has been selected for the operations of the FIRI spacecraft meaning that after the LEOP completion, no eclipse periods will take place.

The spacecraft shall have also the capability to point in any direction with a maximum angle of 45 degrees wrt. to the opposite of the sun direction.

8.4.1.2 Power requirements

The power profiles of each unit have been assessed and declined in each mission mode (Launch, Initialisation, Cruise, Orbit Insertion/ Orbit Maintenance, Stand By/Comms, Observation, Retargeting Mode and Safe Mode).

These data have been compiled at element and subsystem level for the three main critical modes (Table 8-13) excluding the contribution of the power system units themselves.

Telescopes (Both telescopes)							
		Stand By / Comms		Observation		Retargeting Mode	
Max Continuous Power	S/S	Max Continuous Power	Peak Power (incl. transients)	Max Continuous Power	Peak Power (incl. transients)	Max Continuous Power	Peak Power (incl. transients)
Cryostat+JT coolers	Thermal	40 W	80 W	40 W	80 W	40 W	80 W
Telescopes Mechanisms	mechanisms	0 W	0 W	0 W	0 W	0 W	0 W
DHS	Data Handling	30 W	45 W	30 W	45 W	30 W	45 W
Wireless Tranceiver	Communications	0 W	0 W	5 W	8 W	3 W	5 W
Total		**70 W**	**125 W**	**75 W**	**133 W**	**73 W**	**130 W**
Maturity Margin	20%	14 W	25 W	15 W	27 W	15 W	26 W
Total		**84 W**	**150 W**	**90 W**	**159 W**	**88 W**	**155 W**

Central Module							
		Stand By / Comms		Observation		Retargeting Mode	
Max Continuous Power	S/S	Max Continuous Power	Peak Power (incl. transients)	Max Continuous Power	Peak Power (incl. transients)	Max Continuous Power	Peak Power (incl. transients)
Service Module	Thermal	100 W	200 W	241 W	481 W	149 W	297 W
Instrument	Thermal	70 W	140 W	70 W	140 W	70 W	140 W
Array + SQUID Read Out	instruments	0 W	0 W	0 W	0 W	0 W	0 W
FPGA	instruments	0 W	0 W	10 W	20 W	0 W	0 W
AOCS	AOCS	20 W	20 W	100 W	200 W	100 W	200 W
Central Module Mechanisms	mechanisms	40 W	80 W	175 W	263 W	0 W	0 W
Communications	Communications	89 W	135 W	15 W	23 W	16 W	24 W
DHS Service Module	Data Handling	36 W	56 W	56 W	56 W	49 W	56 W
DHS Instrument	Data Handling	132 W	132 W	132 W	132 W	80 W	132 W
Metrology	Optics	0 W	0 W	59 W	89 W	59 W	89 W
Total		**487 W**	**762 W**	**857 W**	**1402 W**	**522 W**	**937 W**
Maturity Margin	20%	97 W	152 W	171 W	280 W	104 W	187 W
Total		**584 W**	**915 W**	**1029 W**	**1683 W**	**627 W**	**1125 W**

Table 8-13: Power Requirements

Each telescope requires only a 100W range power supply capability while the Central Module (Hub) will need a power supply in the kilowatt range.

The FPGA of Instruments in Table 8-13 stands for the warm electronicsdriving the SQUIDS.

8.4.2 Centralized / Decentralized EPS Trade-Off

8.4.2.1 Concepts overview

The 30 meters distance needed between the two telescopes and their translation capability are the main drawbacks of a classical, centralized power architecture. Several manners to accommodate a power transmission functionality along the boom from the Hub to the telescopes are proposed and briefly described (chapter 8.4.2.4). All of them imply deeper investigations and costly developments.

An alternative to this technological issue is the consideration of decentralized and autonomous power systems in each telescope and in the Hub.

This trade-off is not limited to the power aspects but has to be tackled at system level. For instance, the ability to accommodate a power harness is a major parameter in the selection of the telescope motion mechanisms.

Moreover, accommodation of data harness along the boom is linked with the capability to transmit the power along the boom. This difficulty can here also be avoided by selecting a

decentralized data handling architecture. As a result of the commonalities between the power and data transmission technological issues, the trade is rationally reduced to the two following possibilities:

- a full power/data centralized option,
- a full power/data decentralized approach.

The content of this chapter is limited to the power issues of the centralized/decentralized avionic trade-off. The system level considerations and the justification of the baseline selection are reported in a dedicated chapter.

In both cases, an EPS has been designed and assessed.

- Centralized Power Architecture
  A regulated bus obtained by the mean of a S4R is the architecture expected to have the best performance: the constant sun illumination conditions, the limited changes of the sun attitude during the operational phase and the absence of eclipses are increasing the attractiveness of this topology. Moreover, the lack of BCR in this architecture enables to get a regulated bus with a light weighted PCU. The battery and BDRs will only be required for contingency purposes, in LEOP and to complement the solar array capability for the peak power occurrences.
  In order to reduce the number of power lines along the two booms, the power distribution functions for the telescopes units are moved in the telescopes themselves.
- Decentralized Power Architecture
  Each telescope EPS requires a dedicated solar array able to fulfil all the internal power needs.
  A battery module is also required for the deployment phase of the telescopes (See deployment sequence in 8.4.2.3)
  The necessity to have a battery onboard should result as well in competitive performance of a S4R regulation concept.
  Note: In a later development stage, this choice should be reassessed based on more consolidated inputs.
  For mass and volume optimization, in each spacecraft element, the PCU and PDU have been combined in a single box named PCDU.

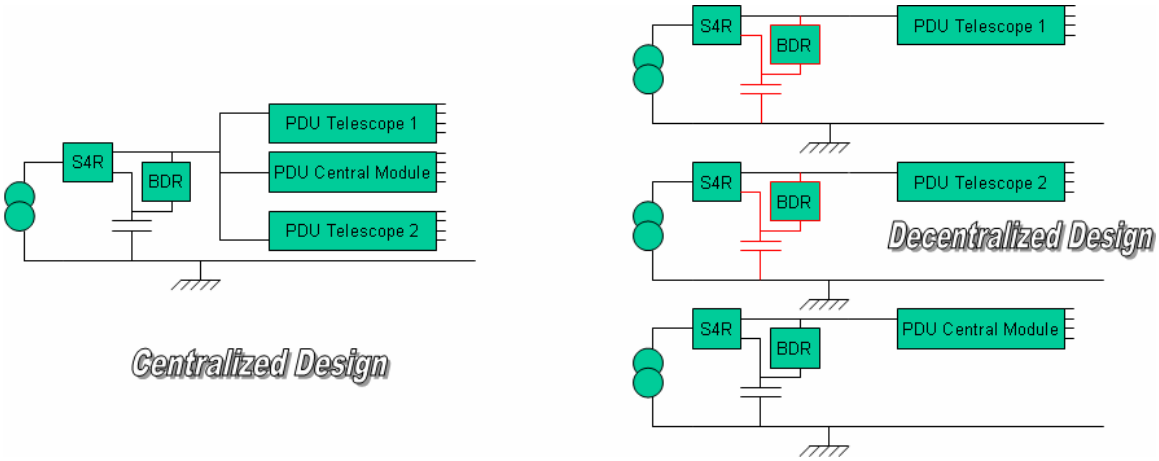

Figure 8-26: Centralized / Decentralized EPS Architectures

Each autonomous power system shall be single point failure tolerant. In the decentralized approach, the loss of one telescope power system is not acceptable: it would indeed imply the abortion of the mission.

8.4.2.2 Solar array

AsGa MJ cells are preferred due to their highest photovoltaic conversion rate resulting in a smallest required total area and their better resistance to radiations. Nowadays, 27% has been achieved by European AsGa TJ cells (currently in qualification) in AM0 conditions. According to the ESA photovoltaic generator roadmap, cells with a 30% conversion efficiency capability can be expected to be available for FIRI.

Taking into account the L2 location of the spacecraft, its operational attitude, the hottest computed thermal conditions, the packing factor and all the parameters contributing to the degradation of the performances, a panel of one square meter is expected to generate 163 W (EOL) as a minimum.

45° inclination
=
Worst Case Illumination

Used for extra string requirement

Solar Array		
Efficiency Solar Array Cells AM0	30.00	%
Temperature Solar Array	**100.00**	degC
dP/dT	-0.23	%/C
Solar Illumination	1300.00	W/m2
Coverglass	0.995	
Mismatch + Calibration	0.970	
UV + Micrometeorites	0.990	
Random failure	0.980	
Radiation	0.920	
Packing Factor	0.850	
SA Diodes	0.976	
Performances SA		
In Sun Pointed Conditions	**231**	**W/m2**
Angle of Incidence SA	45.00	degrees
In Operations	**163**	**W/m2**
SA Body Mounted	2.70	kg/m2
SA Deployable	4.00	kg/m2
Nb Cells per string	28.00	(28 for 50V)
Area One string	**0.11**	**m2**

Table 8-14: EOL Solar Array Performances

For the centralized EPS option, only one SA connected to the Hub PCU is required. This SA has to be sized to provide enough power to supply the units in the telescopes and in the Hub accounting for the voltage drop along the booms (The boom harness will be limited to a 10% voltage drop) and the efficiency of the power system.

A total area of 7.56 m^2 is required to fulfil the mission need including all margins and degradation figures corresponding to a 22.4 kg mass in case of body mounted solar cells.

The decentralized EPS option requires a total area in the same order of magnitude (7.69 m^2) but spread between the telescopes (0.39 m^2 each) and the Hub (6.90 m^2).

Centralized Option

Bus Power Requirement (incl Harness Losses)		
Peak	1894.91	W
Average	1150.12	W
Assumption	**1150.12**	W
S3R/S4R Efficiency	0.97	
Surface Required SA	**7.20**	**m2**
extra redundant SA required	**0.36**	**m2**
Total Surface Required SA	**7.56**	**m2**
Assuming an angle of Incidence of	45.00	degrees during the sizing case
Mass SA		with maturity Margin
Body mounted	20.42 kg	**22.46** kg
SA Deployable	30.26 kg	33.28 kg

Decentralized Option

Bus Power Requirement (incl Harness Losses)	One Telescope	Central Module		
Peak	81.09	1716.51	W	
Average	45.90	1049.14	W	
Assumption	**45.90**	**1049.14**	W	
S3R/S4R Efficiency	0.97			**Total Area Required**
Surface Required SA	**0.29**	**6.57**	m2	
extra redundant SA required	**0.11**	**0.33**	m2	
Total Surface Required SA	**0.39**	**6.90**	m2	**7.69 m2**
Assuming an angle of Incidence of	45.00	degrees during the sizing case		
Mass SA			with maturity Margin	
Body mounted	1.06	18.63	**1.17**	**20.49**
SA Rigid Panel	1.57	27.60	**1.73**	30.36
Total Area Required	7.69	m2		
Total Mass Required	23.95	kg		

Table 8-15: Centralized / Decentralized Solar Array Designs

8.4.2.3 Deployment sequence

FIRI is a challenging spacecraft for the number of mechanisms involved with a critical and extended deployment sequence. The power system will need to cope with this long deployment phase with a partially stowed PVA and to control and fire the numerous pyros mechanisms installed.

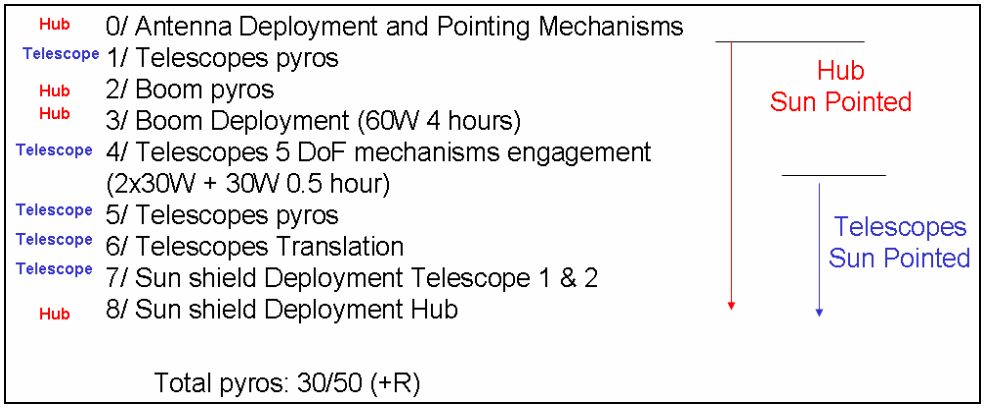

Table 8-16: Deployment Sequence

After the release from the launcher, the stowed spacecraft is placed on a sun pointed attitude (+/-10degres) in order to optimize the power generation on the 2.8m2 body mounted SA on the Hub.

The deployment sequence is then initiated out of any eclipse periods. The succession of events is detailed on Table 8-16. The SAs are full deployed only after the completion at the step 4.

The 2.8m^2 body mounted solar panel will then generate more than 700 W sufficient to supply all the users.

According to the mechanisms involved, around 30/50 pyro activation lines should be installed spread over the telescopes, the booms and the Hub. The locations of the pyros are highlighted in the first row on the Table 8-16.

In the decentralized option, some pyros mounted on the telescopes will need to be commanded and fired while the telescopes SA will not be yet released. This lack of power source justifies the need of battery modules in the telescopes power systems.

8.4.2.4 Power transmission along the booms

This issue concerns only the centralized power architecture option. Depending on the type of articulation mechanisms selected to allow and control the translations of the telescopes, several methods to accommodate the power transmission should be feasible (Figure 8-27):

- The selection of a robotic arm instead of a boom would enable to take advantage of the ISS ERA development where harness is also accommodated.
- Magnetic transmission: An inverter in the Hub will generate an electro-magnetic field along the boom. The energy is then collected in the telescopes through inductors and converted back in DC. This solution is attractive due to the contact less aspect but has also major drawbacks:
  - DC/AC and AC/DC inverters,
  - Influence on the spacecraft units of the generated magnetic field
  - Weight of the inductors/transformers
  - Lowest TRL despite terrestrial applications (e.g. electrical toothbrush, magnetic speed train)
- Fix harness with brush. This principle is similar to the catenaries used in electrical trains or to the power supply of most of the existing subways. The fix harness mounted on the deployment arm could be a gold plate allowing the telescopes to connect via a dedicated unit (e.g. metallic brush). The simplicity of this design has to be traded with the mechanical contact issue that has to be tolerant to the large thermal range and to the mission lifetime and telescope translation cycles requirements.
- Flexible harness. A wide range of possibilities fall in this category: stretched wire cable festoon systems or any various others systems relying on pulleys or springs. Usage of flexible harness in space was until now limited to small distance (e.g. ERA). The various mechanisms required and the development costs are expected to strongly affect the attractiveness of this concept.

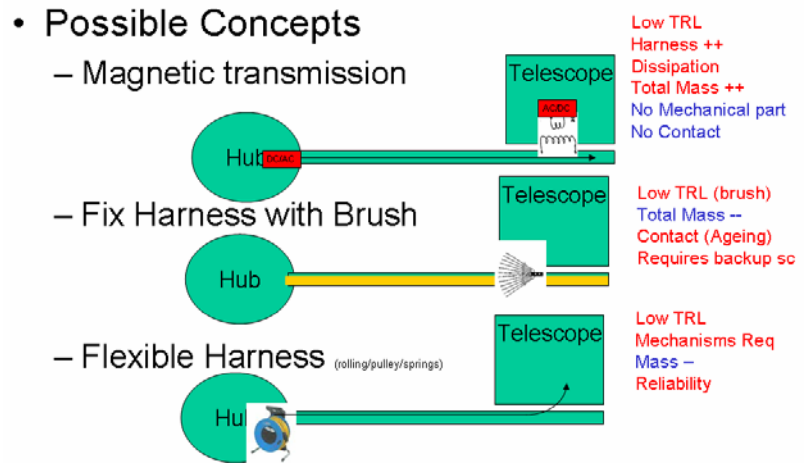

Figure 8-27: Power Transmission along the boom Concepts

None of those concepts show significant advantages and confidence. Moreover, the power transmission will need to be single point failure tolerant involving additional complexity (mechanisms reliability, redundant units and lines…).

As a minimum, four power lines will need to be accommodated (1N+1R positive lines, 1N+1R return lines).

Based on space qualified wire features, on the ESA rating rules, on the reliability issue and the peak power requirements, the harness between the Hub and one telescope is computed with the two following design drivers:

- The voltage drop shall remain lower than 10%
- The harness mass shall be minimized

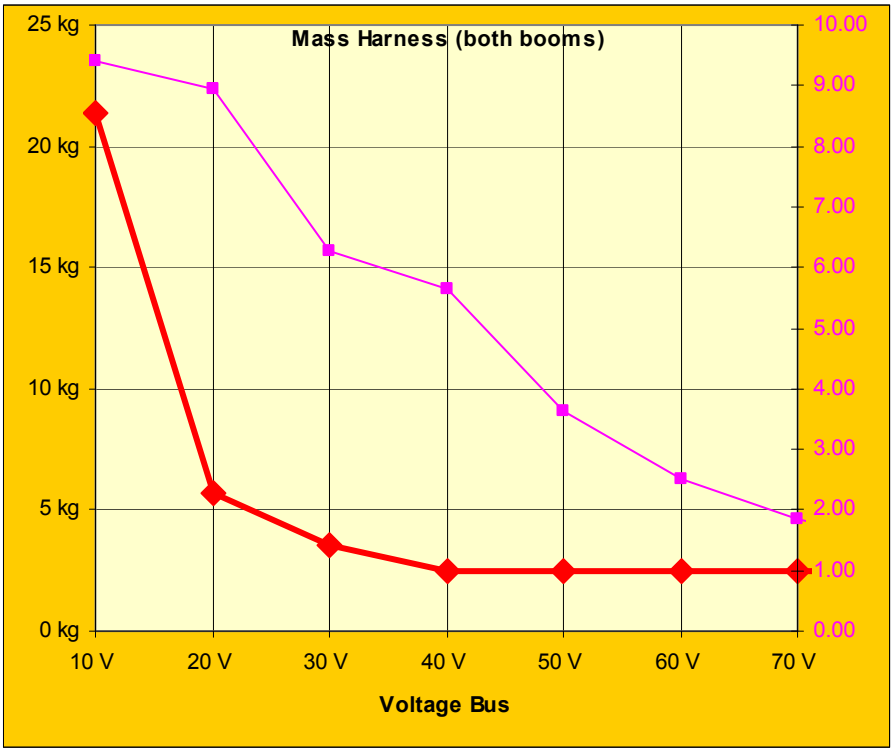

Figure 8-28: Harness Mass Evolution with Bus Voltage

The Figure 8-28 illustrates the sensibility of the harness mass with the selection of the bus voltage considering several AWG wires. The selection of a 50V bus appears to be a good compromise between the harness mass, the users power interface voltage requirements and the total voltage drop. Nevertheless, the 28V bus is also valid. With the decentralised power option there is no harness between the hub and booms and therefore the 28 V bus is an even more valid option.

Note: The associated mechanisms, connectors and attachment points are not included in those mass figures.

8.4.2.5 Power conditioning

All the electrical power units are designed based on the modular power system approach detailed in RD[77]. The use of modular power system functions (extrapolated from existing PCBs) would

have a significant impact in term of non recurrent costs but also on the total mass. The following units have been assessed (Table 8-17):

- Centralized EPS:
  - Hub PCDU (including 20 PCBs with a total mass of 15.6 kg)
  - Telescopes PDUs (including 6 PCBs with a total mass of 4.57 kg)
- Decentralized EPS:
  - Hub PCDU (including 19 PCBs with a total mass of 14.73 kg)
  - Telescopes PCDUs (including 8 PCBs with a total mass of 6.19 kg)

Centralized Option						
Hub EPS						
			With Rounded Up Nb of PCBs			
	(redundancy included)		Nb Terma PCB R	Mass unit		
Pyro Outputs	50		4	0.5	2	
S4R Capability	1937		8	0.45	3.6	
Nb LCL/FCL	100		4	0.55	2.2	
BDR Capability	514	W	2	0.55	1.1	
CM			2	0.35	0.7	
Total Modules			**20**			
Backplane			1		1.55	
Structure	40%					
			Total		**15.60**	**kg**
Telescope EPS (One Telescope)						
			With Rounded Up Nb of PCBs			
	(redundancy included)		Nb Terma PCB R	Mass unit		
Pyro Outputs	20		2	0.5	1	
Nb LCL/FCL	50		2	0.55	1.1	
CM			2	0.35	0.7	
Total Modules			**6**			
Backplane			1		0.46	
Structure	40%					
			Total		**4.57**	**kg**
Decentralized Option						
Telescope EPS (One Telescope)						
			With Rounded Up Nb of PCBs			
	(redundancy included)		Nb Terma PCB R	Mass unit		
Pyro Outputs	20		2	0.5	1	
S4R Capability	101		1	0.45	0.45	
Nb LCL/FCL	50		2	0.55	1.1	
BDR Capability	300	W	1	0.55	0.55	
CM			2	0.35	0.7	
Total Modules			**8**			
Backplane			1		0.62	
Structure	40%					
			Total		**6.19**	**kg**
Hub EPS						
			With Rounded Up Nb of PCBs			
	(redundancy included)		Nb Terma PCB R	Mass unit		
Pyro Outputs	50		4	0.5	2	
S4R Capability	1767		8	0.45	3.6	
Nb LCL/FCL	100		4	0.55	2.2	
BDR Capability	300	W	1	0.55	0.55	
CM			2	0.35	0.7	
Total Modules			**19**			
Backplane			1		1.47	
Structure	40%					
			Total		**14.73**	**kg**

Table 8-17: Centralized / Decentralized PCU/PCDU sizing.

8.4.2.6 Battery modules

Both options required battery modules for the following purposes:

- LEOP phases (including pyro firings),
- Safe/Contingency Modes,
- High peak/transient power periods to complement the PVA power generation.

Rechargeable Li-Ion battery cells are the best candidates. The small space qualified ABSL cells enable to design a mass and volume optimized module perfectly adapted to the energy and power requirements.

The computed battery modules are:

- Centralized EPS:
  - Hub Battery Module: 9.9 kg
- Decentralized EPS
  - Hub Battery Module: 8.3 kg
  - Telescopes Batery Module: 3.0 kg each.

The battery are based on Off the Shelf battery cells and are thus quite conservative regarding the FIRI timeline and the performances enhancements in the ESA battery technological roadmap.

Limited mass saving not accounted here (10/20%) might be possible.

8.4.2.7 Equipment lists

The EPS equipment list has been computed for both options (See Table 8-18).

Centralized Option

Unit Name	Location	Nb Units	Mass Unit (kg)	Total Mass (kg)
PCDU Hub	Hub	1	17.16	17.16
Solar Array Hub	Hub	1	22.46	22.46
Harness Boom	Boom	2	1.24	2.48
Battery Hub	Hub	1	9.87	9.87
PDU Telescop	Telescop	2	5.03	10.05
Total				**62.03 kg**

Decentralized Option

Unit Name	Location	Nb Units	Mass Unit (kg)	Total Mass (kg)
PCDU Hub	Hub	1	16.20	16.20
Solar Array Hub	Hub	1	20.49	20.49
Battery Hub	Hub	1	8.31	8.31
Solar Array Telescop	Telescop	2	1.73	3.46
PCDU Telescop	Telescop	2	6.80	13.61
Battery Telescop	Telescop	2	3.00	6.00
Total				**68.07 kg**

Table 8-18: Centralized / Decentralized Equipment Lists

The centralized option appears to be lighter but does not take into account the mechanical mounting of the harness along the booms.

8.4.2.8 Trade-off conclusion

Power system wise, the centralized power system option shows slight advantages:

- the overall EPS mass is 4 kg lighter
- The 7-8 m^2 can be accommodated on the Hub and on the nearby boom structures without additional substrate
- The overall EPS has less units and will required less TM/TC allocation in the link budget

Nevertheless, at system level, the decentralized option is more attractive and is baselined:

- No additional harness routing requirement on the (already) critical telescope deployment mechanisms,
- Attractiveness of the wireless decentralized architecture.

8.4.3 Baseline Design

The solar arrays are displayed on the Figure 8-29.

Four rigid structures (without deployment mechanisms) of 0.35m2 each are required to accommodate the telescopes PVAs (structure mass accounted in the EPS Equipment list). Those panels locations are selected not to be shadowed by the booms during any operational attitude (+/- 45 degrees).

According to the Hub configuration, 2.8m^2 are available on the back side of the Hub for accommodating a PVA. Since 6.90 m^2 (See Table 8-15) are required, the lightest solution is to mount the additional cells on the sun side of the booms nearby the Hub.

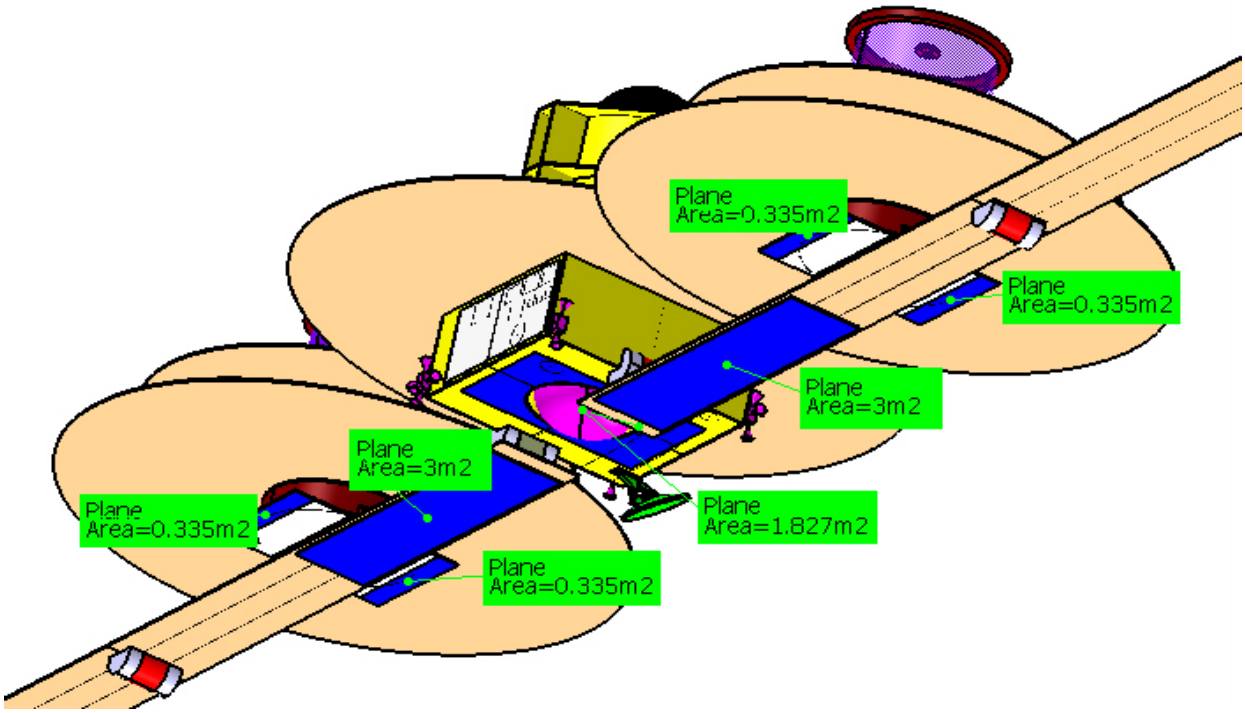

Figure 8-29: Solar Array Baseline

8.4.4 Options

A possible option expected to have performances in line with the selected baseline is to replace the Hub PVA mounted at the booms by solar cells body mounted on the lateral sides of the Hub.

Nevertheless, the total benefit will not exceed a few kilograms but might simplify the overall design.

8.5 Data Handling

8.5.1 Requirements and Design Drivers

The following requirements drive the design of the SVM Data Handling:

- SVM DH shall support the attitude control during all mission phases
- SVM DH shall support the control of the telescopes position on the booms and their pointing at each uv-point
- SVM DH shall include a central TC handler that receives all ground telecommands, analyses the packets and forwards them to the final destination. DH shall handle both the telecommands directed to the SVM and to the FIRI Payload
- SVM DH shall collect Housekeeping telemetry (TM) data including payload, generate TM packets and route them to different virtual channels on the downlink to earth or to different packet stores in the mass memory. Essential TM cyclically stored without software intervention is also included
- • Thermal control: SVM DH maintains the spacecraft temperature inside definite limits by reading thermal sensors and controlling heaters
- SVM DH shall maintain a time reference which value will be acquired and inserted into telemetry packets or distributed to the spacecraft units requiring it
- The SVM DH shall provide sufficient onboard data storage capability, to store Housekeeping data when adequate communications with ground is not possible
- SVM DH shall include functions to monitor and report the FIRI Spacecraft health status, functions to reconfigure faulty elements and functions for restoring the Spacecraft to a nominal state or to a safe state depending on the mission phase
- The FIRI spacecraft shall perform autonomously nominal operations when ground intervention is not possible. The FIRI spacecraft shall remain safe for a period of at least 2 days, without ground intervention

The selection of the technologies and the architecture is driven by three main factors:

- The Technology Readiness Level 5 should be achieved by 2015
- The SVM Data Handling shall be tolerant to any single point failure
- The cost shall be kept at a minimum.

8.5.2 Assumptions and Trade-Offs

Typically the DH design provides an external redundant serial bus (MIL 1553 or CAN Bus) to provide an efficient means of communications for the control and monitoring of the principal platform and payload equipments. Platform or payload units can be also provided with dedicated RS422 serial links.

For the purpose of this design it has been assumed that the majority of connections will be via MIL STD 1553 bus. A more detailed trade-off between serial bus and dedicated point to point connections shall be performed early during FIRI project.

8.5.3 Baseline Design

The SVM Data Handling is implemented in two different boxes: the Mass Memory and the On Board Computer (OBC).

8.5.3.1 SVM Mass memory

The MM shall be able to simultaneously record data and to playback the stored data in formatted CCSDS standard to the transponder assembly. The trade-off considerations are the same as for the payload memory. The selected MM design is derived from the Cryosat Mass Memory. Memory Modules 128 Gbits each are sufficient for the Housekeeping, AOCS and GNC data (less than 4 kbps for up to 48 hours and a BoL/EoL ratio of 1/2). Each Memory Module is self standing and can be independently powered, operated and commanded.

The data interface with the SVM OBC is achieved via a redundant MIL-STD-1553 bus interface with Remote Terminal capabilities (this type of device is controlled by a bus controller). One SpaceWire link connects the Telemetry Formatter to the Transponder.

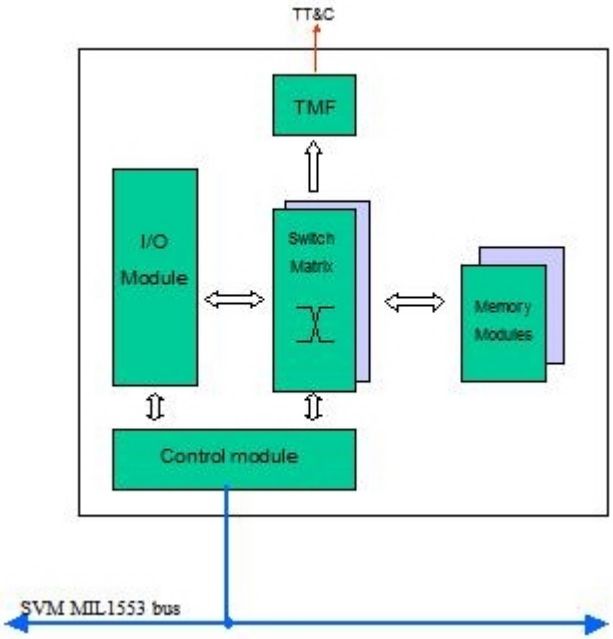

Figure 8-30: SVM Data Handling schematic

8.5.4 SVM Computer (OBC)

There is a number of established suppliers of OBC units, all of which offer internally redundant and fault tolerant designs. Each supplier has adopted generally similar internal unit architectures, based on core processor functions plus modular memory and external interface functions. This modular approach allows easy adaptation of their generic designs to meet the specific requirements of each programme.

The SVM OBC provides a redundant MIL 1553 bus to connect the Payload Computer, the SVM Mass Memory, the PCDU and a number of the individual AOCS equipments like FEEPs, Gyros and The Fine Guidance Sensor equipment.

The OBC includes a Telecommand Decoder that comprises both the Packet Telecommand Decoder function and the Command Pulse Distribution Unit (CPDU) function. The CPDU is hard-wired and issues direct commands without any software involvement as part of the autonomous recovery sequences. The CPDU receives packets either from the Telecommand Decoder, the Reconfiguration Module (RM) or the active Processor. The Packet Telecommand Decoder receives data from the Transponder, which are organised according to the ESA Packet Utilisation Standard (PUS).

The OBC also provides a Direct Telecommand function, which allows high priority commands to be received, interpreted and distributed by the OBC via purely hardware means without the needs for processor intervention. These Direct Telecommands are available internally for OBC configuration switching and externally for direct control of the principal FIRI spacecraft equipments.

The Telemetry Encoder function is built according to the ESA Packet Telemetry Standard. TM data is packetized according to the ESA Packet Utilisation Standard (PUS). Usually the capability is implemented to transmit a group of selected housekeeping parameters also in case of unavailability of all on-board computers to allow ground control to assess the status of essential spacecraft items.

The OBC is equipped with nominal and redundant microprocessors; these are typically the ERC32 (SPARC RISC) single chip processor or the LEON2 processor. Performances are at least 15MIPS for the ERC32 and 86 MIPS for LEON2.

The watchdog supervises the processor and the software. It has to be refreshed within a programmable time window to prevent from expiring and alarm triggering.

The timing and synchronisation function include the Local On-board Time (OBT) based on a hardware counter and the generation of a spacecraft synchronisation clock.

The reconfiguration function is handled by two hot redundant Reconfiguration Modules (RM) that process incoming alarms and generate CPDU packets for execution by the CPDU. Different packets can be generated for different alarm situations and for different hardware configurations. Each RM provides both internal and external alarm inputs. Typical internal alarms could be initiated by the software, Processor module hardware alarms or Power converter undervoltage detection.

A Safe Guard Memory (SGM) is normally provided as part of RM and operated in hot redundancy. The software reads from and writes into the SGM via the RM/Processor communication interface. Writing can be done in parallel such that the data are stored simultaneously in both SGMs.

All the commands and housekeeping from and of the telescopes pass through the IPPM. In cases where adjustment of telescope positions are required, the IPPM receives information from the SVM.

Figure 8-31 depicts a typical SVM OBC with the features previously described.

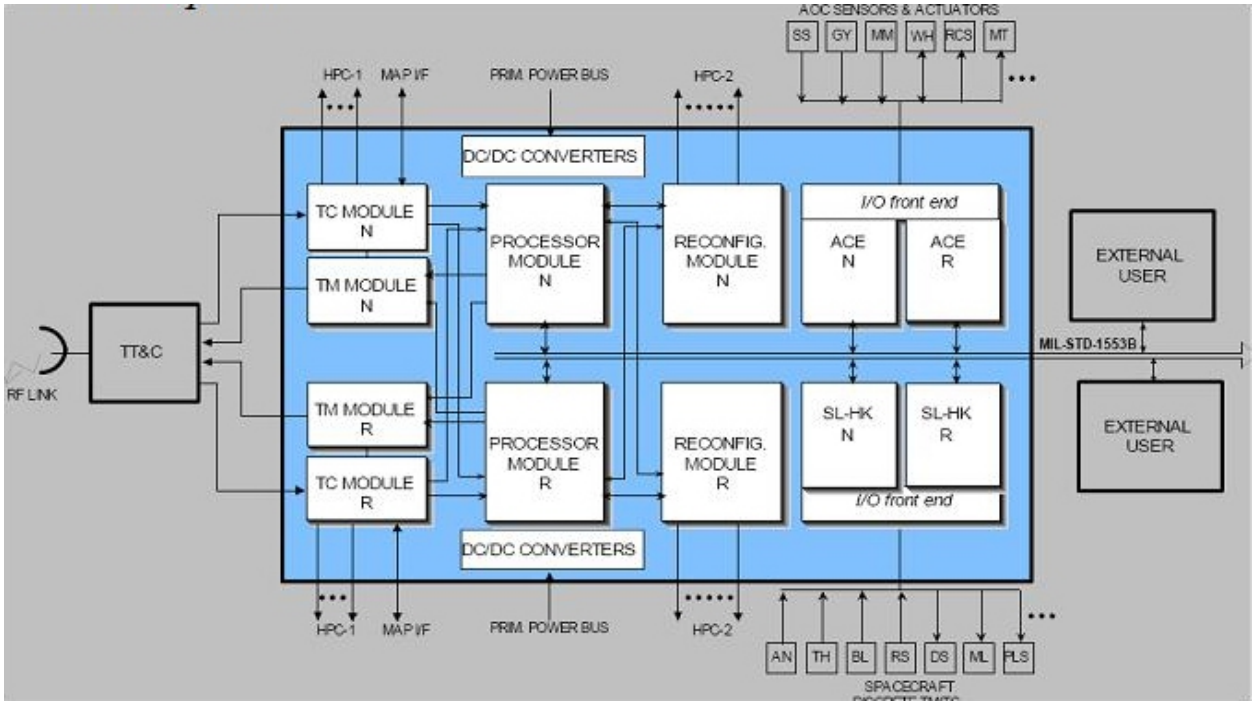

Figure 8-31: Typical SVM OBC

Integrated SVM and Payload Data handling system:

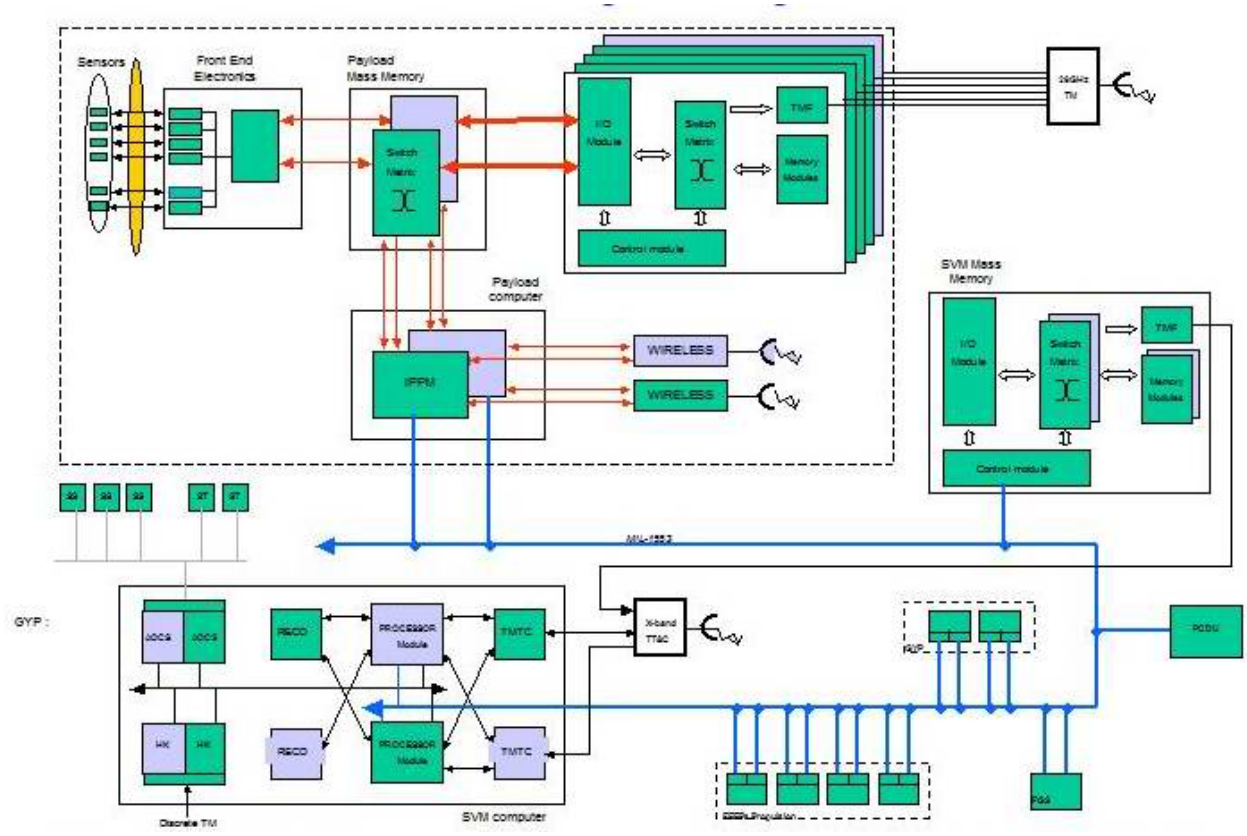

Figure 8-32: SVM Data Handling architecture

8.5.5 Summary

The tables below give the summary of the Service Module characteristics:

	Service Module		MASS [kg]		
	Unit Name	Quantity	Mass per quantity excl. margin	Margin	Total Mass incl. margin
Part of:	Click on button above to **insert new unit**				
Hub	SVM computer	1	19.3	10	21.2
Hub	SVM Mass Memory	1	6.4	5	6.7

Table 8-19: SVM unit mass

	Service Module		DIMENSIONS [m]		
	Unit Name	Quantity	Dim1 Length	Dim2 Width or D	Dim3 Height
Part of:	Click on button above to **insert new unit**				
Hub	SVM computer	1	480.0	240.0	302.0
Hub	SVM Mass Memory	1	360.0	302.0	240.0

Table 8-20: SVM unit dimensions

8.6 Telecommunications

8.6.1 Requirements and Design Drivers

- TT&C communications during all mission phases, any mode and near any attitude are required
- Design should be kept as simple as possible in order to maximize the mission duration and reduce cost
- The TT&C subsystem will provide two-way ranging and Doppler capabilities
- A high-rate science data downlink capable of sending 150 Gbit/day is required
- Impact on science observations should be minimised (i.e. minimise contact time with groundstation)
- Data rates for the telecommand uplink and housekeeping telemetry downlink shall be at least 4 kbps
- Omni directional capability for safety and LEOP shall be provided
- The TT&C subsystem shall show full redundancy except for the high gain antenna
- The operational orbit distance is 1.6 million km
- Earth-pointing is not guaranteed during the whole mission
- Launch date in the 2020 – 2025 timeframe.

8.6.2 Assumptions and Trade-Offs

8.6.2.1 Frequency band selection

8.6.2.1.1 X-band 8450 – 8500 MHz

- Maximum occupied bandwidth

The occupied bandwidth in the band allocated to Category A Space Research missions (i.e. 8450-8500 MHz) is limited to a maximum of 10 MHz. The maximum transmitted symbol rate in a system implementing GMSK modulation (with parameter BT_b = 0.25 as recommended in ECSS-05-50A: RF and Modulation Standard) and with a maximum 99% occupied bandwidth of 10 MHz can be calculated as:

$$eff_{99\%} = \frac{symbolrate(sps)}{BW_{99\%}(Hz)} \rightarrow symbolrate = 10MHz \cdot 1.16b/s/Hz = 11.6Msps$$

In the above calculation, a 99% spectral efficiency of 1.16 b/s/Hz has been assumed for GMSK (BT_b = 0.25). So, a symbol rate of 11.6 Msps can be considered the maximum theoretical symbol rate that can be achieved in the 8450-8500 MHz assuming GMSK with BT_b = 0.25. In order to have some margin due to spectral re-growth from non-linear amplification, we recommend a **maximum symbol rate of 10Msps**.

- Maximum information bit-rate in X-band

Assuming that the maximum occupied bandwidth is available, we can calculate the maximum information bit rate, depending on the coding scheme selected. Two standard coding schemes have been selected as candidates thanks to their bandwidth expansion, correcting performance and ESA ground station support. As a third option, we can assume Turbo ½ coding scheme, standardised in CCSDS but currently (i.e. mid 2006) not supported by the ESA ground station network.

Coding scheme	BW expansion	Symbol rate	Information bit rate
(255, 223) R-S and basic convolutional rate ½	*2.28*	*10 Msps*	*4.36 Mbps*[4]
(255, 223) R-S and punctured convolutional rate ¾	*1.52*	*10 Msps*	*6.54 Mbps*
Turbo code 1/2	*2.0*	*10 Msps*	*5 Mbps*

Table 8-21: Candidate coding schemes

Using standard ESA coding[5], the bandwidth limitation in the 8450 – 8500 MHz band imposes a maximum downlink data rate of about 6.54 Mbps. This does not meet the downlink data rate requirements for FIRI. Note that this limitation is irrespective of any link budget issues.

Note that analysis is based on the current standards. In the future, more spectral efficient modulation schemes (e.g. 8- or 16-APSK) might be available, allowing the transmission of more information within the 10 MHz bandwidth at the expense of a higher required transmit power. Nevertheless, even with these schemes, reaching the data rates in the order of tens of Mbps in a 10 MHz band does not seem to be likely.

8.6.2.1.2 Ka-band 25.5 – 27 GHz

In order to comply with the data requirement for the FIRI mission, a move to a higher frequency band is necessary. In particular, the 25.5 – 27 GHz band (commonly called the '26 GHz band') which has been allocated to Space Research and Earth Exploration Satellites Services, is considered to be the best candidate for the FIRI mission. Typically, this band is available for those missions which cannot meet their very high data rate requirements in the tight X-band. At present, no bandwidth restrictions exist in this frequency band nor are there recommended modulation and coding.

8.6.2.1.3 Ka-band 31.8 – 32.3 GHz

This frequency bands seems an attractive candidate as well since plenty of bandwidth is still available in this band and contrary to the 26 GHz band, it is supported by at least one ESA

[4] This is approximately the downlink rate for the GAIA mission, which is operating is the 8450 – 8500 MHz band.

[5] In principle a link without coding can be proposed: this would allow the theoretical 10 Mbps figure to be reached at the expense of increased power needs on-board. However, as this would lead to an very power inefficient design, this option does not seem realistic.

groundstation, i.e. the Cebreros groundstation. However, this frequency band is strictly reserved for Deep Space missions (i.e. missions going further than $2x10^6$ km) and hence cannot be used by missions going (only) to L2. This option is discarded.

In conclusion, the selected frequency band for the high-rate science data downlink is the 25.5 – 27 GHz Ka-band. For the telecommand and housekeeping telemetry links, the normal X-bands are retained (7190 – 7235 MHz for uplink and 8450 – 8500 MHz for downlink).

8.6.2.2 Ground station selection

Due to the high science data-rate requirement and assuming we want to limit the burden on-board the FIRI spacecraft, a large ground antenna is preferred. Possible ESA groundstations include: New Norcia (Australia) and Cebreros (Spain) which both host a large 35-meter diameter antenna.

However, it is stressed that at present, the ESA ground station network does not support reception of the 26 GHz frequency. Nevertheless, it is reasonable to assume that the Cebreros 35-meter groundstation will be upgraded to support the 26 GHz band should FIRI make the explicit request and be willing to contribute financially. Also the third ESA 35m Groundstation, which is expected to be built along the American longitude and scheduled to be operational in 2011, is supposed to support reception at 26 GHz or at least can be easily upgraded to do so. For more details concerning the groundstation availability, (refer to Chapter 10 on Ground Segment and Operations).

The visibility of the Cebreros G/S from the selected orbit is adequate and throughout the mission, daily passes with varying duration are guaranteed. Assuming a minimum elevation angle of 10 deg, mean pass duration of about 10h is obtained. Relaxing the minimum elevation angle to 20 deg, mean pass duration decreases to about 8.5h, this is still considered largely sufficient to comply with the science data return requirements.

+++++++++ Ground station: 1 ++++++++	
Name: Cebreros	
Number of passes:	1581
Mean pass duration [h]:	8.438
Coverage percentage:	35.272
Mean dur btw. passes [h]:	15.481
Max pass duration [h]:	10.717
Max no-pass duration [h]:	19.400

Table 8-22: Cebreros details for FIRI

For more details concerning the Cebreros visibility statistics, (refer to Chapter 4 on Mission Analysis).

In conclusion, the 35-meter Cebreros G/S is selected as the baseline.

Figure 8-33: Cebreros 35-meter groundstation

8.6.3 Baseline Design

8.6.3.1 Overall TT&C concept

The figure below pictures the overall TT&C concept. It is based on a one-way, high rate downlink in the 25.5 – 27 GHz band for science payload telemetry and a two-way, low rate link in the X-band for TC/HK TM and navigation, both to the 35-meter Cebreros groundstation.

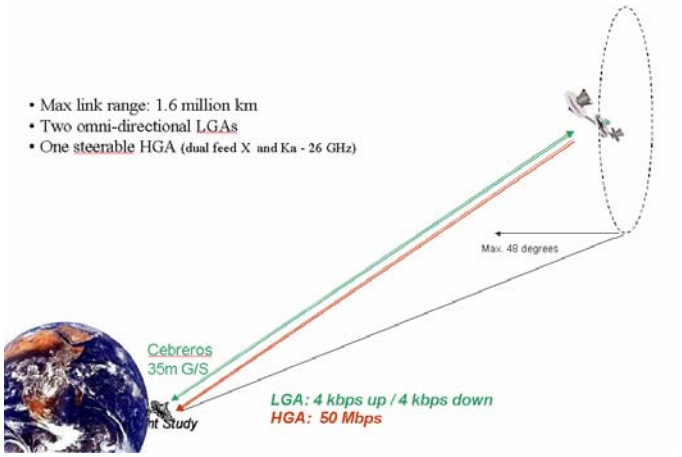

Figure 8-34: Overall TT&C concept

During operations, the FIRI spacecraft will be in an orbit around L2 at a mean distance of about 1.6 million km from Earth.

8.6.3.2 On-board TT&C subsystem

The on-board TT&C subsystem is based on:

- Two redundant X-band transponders for receiving telecommands, sending housekeeping telemetry and supporting two-way ranging and Doppler measurements.
- Two redundant 26 GHz telemetry transmitters for sending science payload telemetry
- Two redundant 26 GHz band TWTA's
- One steerable HGA with dual feed X/26 GHz
- Two omni-directional LGA's
- Radio Frequency Distribution Unit (RFDU)

The architecture of the on-board TT&C subsystem is shown in Figure 8-35:

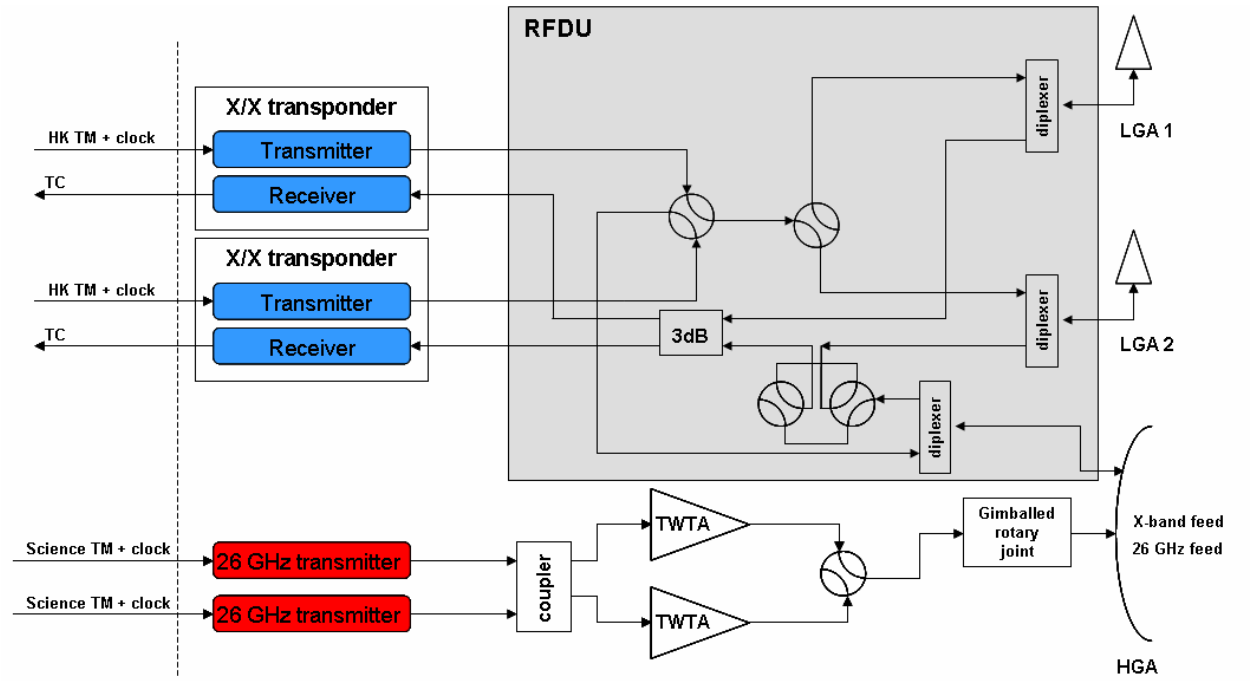

Figure 8-35: Architecture of on-board TT&C subsystem

As can be seen, the high rate science payload telemetry downlink is almost completely decoupled from the classical TT&C function, which is mainly provided by the two redundant X-band transponders. The downlink at 26 GHz is only available via a steerable HGA. The X-band up- and downlinks are available via the two LGA's which provide quasi omni-directional coverage during the LEOP phase and in emergency or safe mode situations. Although not strictly needed, it is pointed out that this architecture also allows the X-band links via the HGA.

8.6.4 Link Budget

8.6.4.1 Modulation and coding

The selected modulation schemes have been chosen from ECSS standard [RD-1] considering that this is a CCSDS category-A mission. The used modulation schemes are:

- Telecommand uplink: NRZ/PSK/PM (sine), modulation index 1.0
- Housekeeping telemetry downlink: NRZ/PSK/PM (sine), modulation index 1.25
- Science payload telemetry downlink: SRRC-OQPSK with roll-off 0.5.

Note however that at present, no recommended modulation and coding schemes exists for the baselined 26 GHz band. Nevertheless, it is assumed that for this band as well, the standardisation bodies such as CCSDS and ECSS will likely recommend a modulation scheme which imposes efficient use of the available bandwidth, such as GMSK or SRRC-OQPSK. Since digital implementation of GMSK at several tens of Mbps might be difficult, SRRC-OQPSK with roll-off = 0.5 has been selected as the baseline modulation scheme for the science payload telemetry downlink.

For downlink telemetry, the coding scheme selected is the CCSDS standard Turbo code with rate ½ (see [RD-2]) which guarantees a Frame Error Rate of 10^{-5} at Eb/N0 = 1.2 dB. The implementation of Turbo Codes with rate ½ allows the required Eb/N0 to be reduced by a factor 0.7 withy respect to current standard concatenated coding scheme.

Although Turbo codes are currently not supported by the ESA Deep Space Network, the DSN is planned to be upgraded in the near future to support Turbo codes such that it is reasonable to assume their availability by 2020.

	TC uplink	**HK TM downlink**	**Payload TM Downlink**
Modulation	PCM/PSK/PM (sine)	PCM/PSK/PM (sine)	SRRC-OQPSK, roll-off = 0.5
Forward Error Coding	-	(CC(1/2,7),RS(255,223)) with I = 5	Turbo 1/2
Link quality	BER ≤ 10^{-5}	FER ≤ 10^{-5}	FER ≤ 10^{-5}
Synchronisation	ASM	ASM	ASM

Table 8-23: Selected modulation and coding schemes

The performance characteristics of the selected combination of modulation and coding scheme are summarised in the table below.

Modulation	**Coding**	**Required Eb/No**
SRRC-OQPSK with roll-off = 0.5	Turbo 1/2	1.2 dB

Table 8-24: Performance characteristic of modulation/coding scheme

One point of concern might be the limitation of the symbol rate in the groundstation IFMS. Currently, this limit is at 10 Msps, however there are plans to upgrade the IFMS to support symbol-rates up 50 Msps. Whether this is enough for FIRI remains TBD.

8.6.4.2 Groundstation

The main characteristics of Cebreros in the X-band are:

Transmission		Reception	
Frequency band	**EIRP**	**Frequency band**	**Effective G/T @ 20° elevation**
7190 - 7235 MHz	107 dBW	8400-8500 MHz	50.8 dB/K

Table 8-25: Characteristics of Cebreros groundstation in X-band

The reception characteristics at 26 GHz frequency are currently not known and are estimated for this study. Increasing the frequency from near 8.475 GHz to around 26.25 GHz increases the antenna gain by:

$$20 * \log\left(\frac{26.25}{8.475}\right) = 9.8dB$$

Sadly, this large gain cannot be fully reflected in the link budget as one has to take into account also the factors that decrease the G/T of the groundstation when moving to 26 GHz and which are discussed in the paragraphs below.

- Increased atmospheric sky noise temperature

Figure 8-36 below gives the simulated atmospheric sky noise temperature at 26 GHz and at Cebreros and this for different elevation angles and as a function of the percentage of time this noise temperature is exceeded. From this figure, a value of 120 K for the atmospheric sky noise temperature, corresponding to 20 degrees elevation angle and 99% availability is derived. Note that the minimum elevation angle of 20 degrees for this study is different from the standard value of 10 degrees. Reason for this are the large atmospheric losses which are incurred at to these low elevation and which have to be taken into account in the link budget. Sizing the link budget at Ka-band for these low but rare elevation angles can easily lead to an overdesigned TT&C subsystem. To avoid this and as we have plenty of G/S visibility, a minimum elevation angle of 20 degrees is preferred.

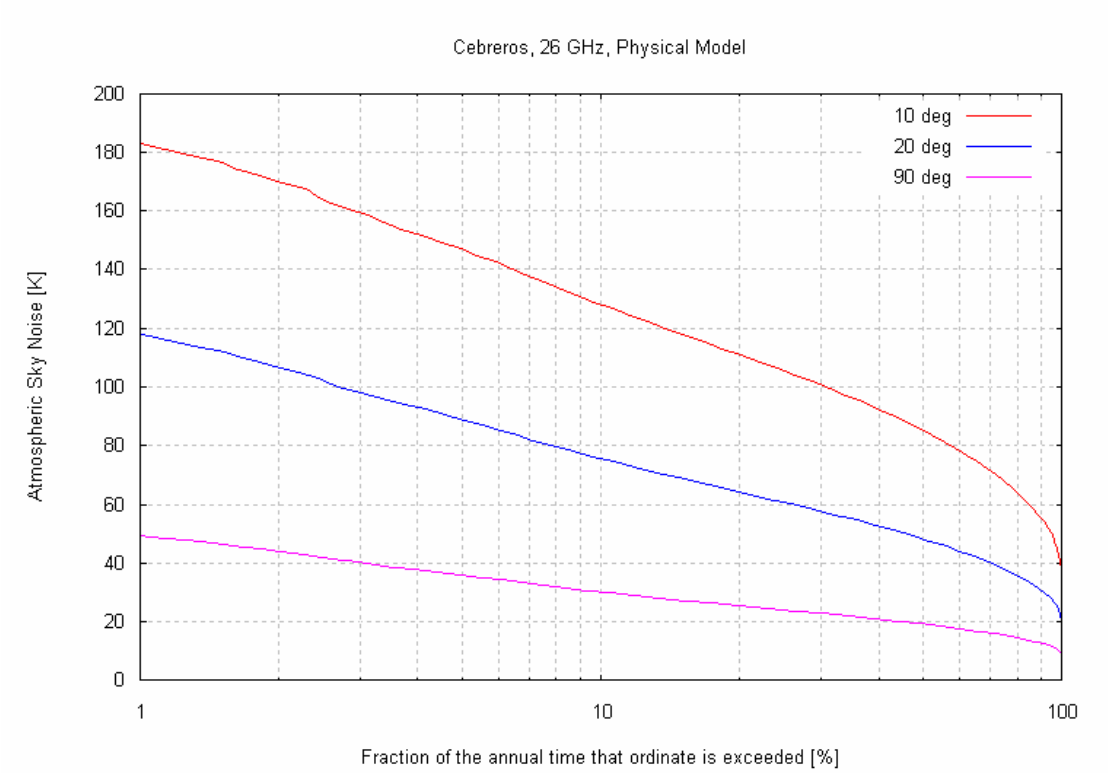

Figure 8-36: Simulated sky-noise temperature at Cebreros at 26 GHz

- Increased receiver noise temperature

The receiver noise temperature is assumed to be 60 degrees, corresponding to a noise figure of 0.82 dB.

- Increased pointing losses

Pointing losses have been set to a worst-case value of 1 dB. This is roughly related to a three times decrease in beamwidth when going from around 8 GHz to 26 GHz. As pointing losses for Cebreros in X-band are about 0.3 dB (and we assume the same absolute pointing accuracy), we end up with about 1 dB pointing loss.

- Estimated Cebreros G/T at 26 GHz

Bringing all the above values together allows us to estimate the G/T of the 35-meter Cebreros at frequencies around 26 GHz, see Table 8-26. This value is considered accurate enough for the sake of this study of the FIRI mission. Furthermore, it is noted that this value is more or less in line with the actual G/T of Cebreros at 32 GHz, i.e. 55.8 dB/K (10 degrees elevation angle but 90 % availability)

Reception	
Frequency band	**Effective G/T @ 20° elevation**
25.5 – 27 GHz MHz	53.7 dB/K

Table 8-26: Estimated Cebreros G/T at 26 GHz

8.6.4.3 Atmospheric attenuation

Figure 8-37 shows the total (including rain) atmospheric attenuation at 26 GHz and this for different elevation angles and as a function of the percentage of time this attenuation is exceeded. From this figure it is clear that 10 degrees elevation angle is a real worst-case for the 26 GHz Ka-band with attenuations reaching up to 6 dB. As in the end these very low elevation angles are rather rare but can become the sizing case for the link budget, this can easily lead to an overdesign of the TT&C subsystem. Moreover, as we have plenty of visibility from Cebreros, a minimum elevation angle of 20 degrees is definitely a more optimum value.

- In conclusion, the atmospheric attenuation which will be taken into account is 3.5 dB, corresponding to 20 degrees elevation and 99 % availability. If however 90 % availability is acceptable, an additional gain of about 2 dB can be appreciated.

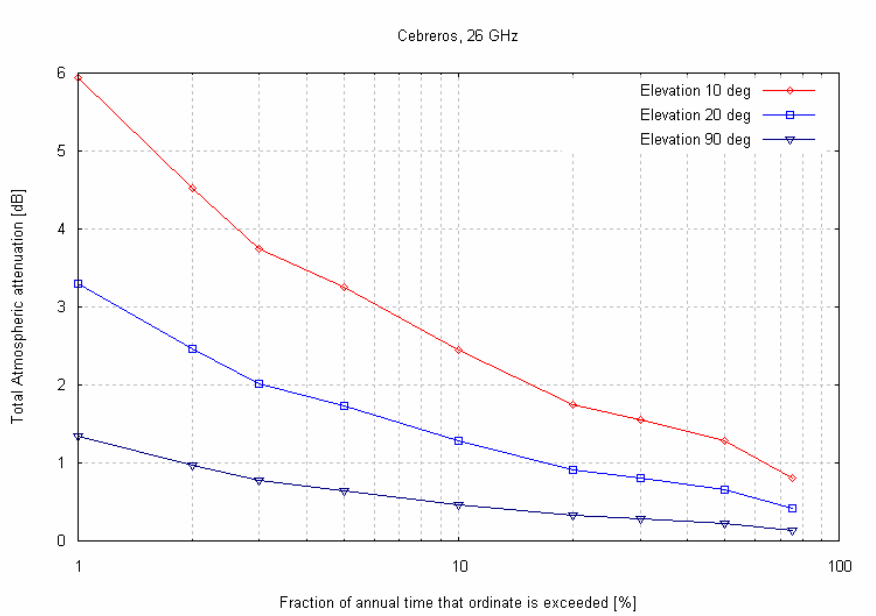

Figure 8-37: Simulated atmospheric attenuation at 26 GHz

8.6.4.4 Science payload downlink budget summary

Table 8-27 gives the summary link budget based on a data-rate of 50 Mbps. Assuming an overhead of 15 % due to packet headers/tails, attached synchronisation markers and re-transmissions, this comes down to a effective data rate of 42.5 Mbps available for science return. This gives us the *capability to downlink 153 Gbit of science data per hour*. Assuming daily communication with the ground station during 3 hours is available; this leads to an overall science return of 459Gbit/day (considering calibration per u-v point; less calibration could reduce the data rate significantly).

Input	Value	Comment
Spacecraft EIRP	50.51 dBW	
Path loss	- 244.93 dB	1.6 million km
Atmospheric & Ionospheric loss	- 4.00 dB	3.5 atmospheric and 0.5 ionospheric

Groundstation G/T	53.47 dB/K	Estimated 35-m Cebreros including pointing losses
Demodulator losses	- 1.00 dB	Assumption
Data-rate	76.99 dBHz	50 Mbps
EbN0	5.11 dB	
Required EbN0	1.2 dB	FER < 10^{-5}
Link margin	3.91 dB	> 3 dB

Table 8-27: Science payload downlink budget

8.6.4.5 On-board transmit parameters

The spacecraft EIRP is to be provided by the combined effort of the transmitted RF power and the antenna gain. Finding the optimum combination of power and gain is the subject of a careful optimisation exercise with the goal of minimising the overall mass and power. In addition, selecting a small antenna is also beneficial not to add tight requirements on attitude control and pointing accuracy. On the other hand, a high RF power has direct impact on the solar array size, battery size and the thermal control subsystem etc.

Figure 8-38 shows the relation between on-board RF transmit power and antenna diameter resulting in a spacecraft EIRP = 50.51dB, enabling a downlink data-rate of 50 Mbps.[6]

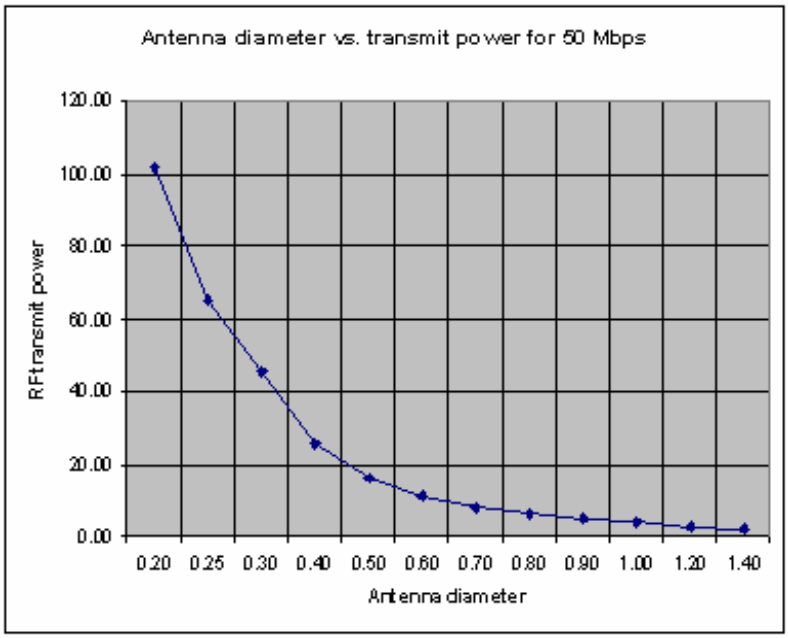

Figure 8-38: Relation between RF power and antenna size for EIRP = 50.51 dB

Based on the above curve, the selected baseline configuration yielding the required EIRP for FIRI is:

[6] The plot takes into account 1 dB pointing losses and 1.5 dB transmit losses.

Input	Value	Comment
RF Power	13.01 dBW	20 W RF power at amplifier output
Total transmit losses	-1.5 dB	
Antenna gain	40.00 dB	0.45 m dish with 65% efficiency
Pointing losses	-1.00 dB	Pointing accuracy < 0.45 deg
EIRP	50.51 dB	

Table 8-28: Ka-band transmit chain characteristics

The mass of the antenna including support structures is estimated at 5 kg, while the power consumption of a 20 W amplifier is estimated to be 40 W (assuming 50 % overall efficiency)

The selected antenna diameter and the transmit frequency allow calculating the beamwidth of the antenna and subsequently the pointing requirement. As in the link budget a maximum of 1 dB pointing losses have been taken into account, one can read from Figure 8-39 that this leads to a required pointing accuracy of better than 0.45 deg.

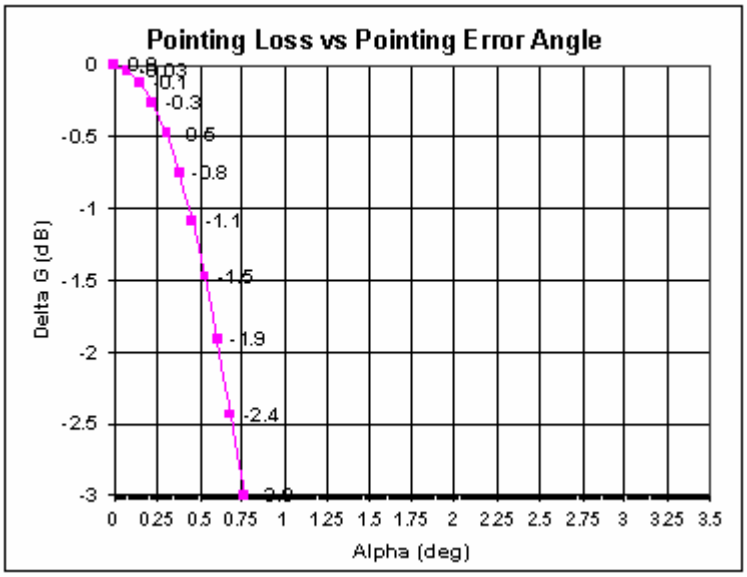

Figure 8-39: Pointing loss versus pointing error

8.6.4.6 Telecommand/Housekeeping telemetry link budgets summary

Table 8-29 and Table 8-30 below give the summary link budget based on a data-rate of 4 kbps in the uplink and 4 kbps in the downlink.

Input	Value	Comment
G/S EIRP	99 dBW	Cebreros
Path loss	- 233.71 dB	1.6 million km
Atmospheric loss	- 1.0 dB	

Input	Value	Comment
Spacecraft Rx antenna gain	1 dB	At +- 60 from boresight
Total Rx losses	- 6.5 dB	
Spacecraft G/T	- 32.77 dB/K	
Modulation losses	- 4.12 dB	Modulation index 1.0, no ranging
Implementation losses	- 1.5 dB	Assumption
Data-rate	36.02 dBHz	4 kbps
EbN0	18.34 dB	
Required EbN0	9.6 dB	BER < 10^{-5}, no coding
Link margin	8.74 dB	> 3 dB

Table 8-29: Telecommand uplink budget

Input	Value	Comment
Spacecraft Tx power	7 dBW	5 W
Total Tx circuit losses	-3 dB	Conservative value
Spacecraft antenna gain	2 dB	At +- 60 from boresight
Path loss	- 235.11 dB	1.6 million km
Atmospheric loss	- 1.0 dB	
Groundstation G/T	50.85 dB/K	35-m Cebreros including pointing losses
Modulation losses	- 2.83 dB	Modulation index 1.25, no ranging
Demodulator losses	- 1.0 dB	Assumption
Data-rate	36.03 dBHz	4 kbps
EbN0	9.39 dB	
Required EbN0	2.8 dB	FER < 10^{-5}, standard ESA coding
Link margin	6.59 dB	> 3 dB

Table 8-30: Housekeeping telemetry downlink budget

Both link budgets show a comfortable margin > 3 dB. The tables above show the link budgets in absence of a ranging signal. It has been verified that also in the presence of a ranging signal, the link margin in both up- and downlink stays > 3 dB (for ranging modulation indices 0.7 and 0.5 in up and down respectively).

8.6.5 List of Equipment

8.6.5.1 Mass breakdown

A summary of communications equipment with their masses can be seen in Table 8-31. Total mass with margin is 37.9 kg; in addition harness mass is estimated at 2 kg.

Element 1		Service Module		MASS [kg]			
Unit		Unit Name	Quantity	Mass per quantity excl. margin	Maturity Level	Margin	Total Mass incl. margin
		Click on button above to **insert new unit**					
1	Hub	X/X transponder	2.00	3.80	Fully developed	5	8.0
2	Hub	X-band SSPA	2.00	0.80	Fully developed	5	1.7
3	Hub	26 GHz transmitter	2.00	2.00	To be developed	20	4.8
4	Hub	26 GHz TWTA	2.00	2.00	To be developed	20	4.8
5	Hub	HGA	1.00	5.00	To be developed	20	6.0
6	Hub	LGA	2.00	0.30	Fully developed	5	0.6
7	Hub	RFDU	1.00	4.00	To be developed	20	4.8
8	Hub	Wireless transceiver	2.00	1.00	To be developed	20	2.4
9	Telescopes	Wireless transceiver	4.00	1.00	To be developed	20	4.8
-				0.0	To be developed	20	0.0
SUBSYSTEM TOTAL			**9**	**32.8**		**15.5**	**37.9**

Table 8-31: TT&C subsystem mass breakdown

8.6.5.2 Power breakdown

The table below shows a power breakdown for the TT&C subsystem. Total power consumption during the daily communications slots with the groundstation is 85 W. During normal TT&C, power consumption is limited to 55 W. The two X-band receivers are always ON which leads to a constant power consumption of 20 W.

Unit	Receive only	TT&C transmit &receive	Science data transmit	Comment
X-band TRSP1	10 W	25 W	10 W	From H/P
X-band TRSP2	10 W	10 W	10 W	
SSPA1	-	20 W	-	25% efficiency
SSPA2	-	-	-	
26 GHz Transmitter1	-	-	25 W	
26 GHZ Transmitter2	-	-	-	
26 GHz TWTA1	-	-	40 W	50% efficiency
26 GHz TWTA2	-	-	-	
Total	20 W	55 W	85 W	

Table 8-32: TT&C subsystem power breakdown

8.6.6 Options

8.6.6.1 Use of X-band

As an alternative to the baseline 26 GHz Ka-band, selecting the classical X-band for science payload data return would offer the following advantages:

- *Increased groundstation support:* currently, no single ESA groundstation supports reception of signals in the 26 GHz band while in X-band, both New Norcia and Cebreros 35-meter antennas are available. The 35-meter Cebreros groundstation can be upgraded to support 26 GHz but most likely FIRI will be requested to contribute financially. (For details see Chapter 10 on Ground Segment and Operations)
- *Smaller development cost thanks to heritage:* the TT&C subsystem of GAIA can be re-used if X-band is chosen as the baseline frequency band. (e.g. transponders and phased-array antenna)

Going back to the X-band also brings the following disadvantages:

- *Reduced science data return:* the (hard) 10 MHz occupied bandwidth restriction in the X-band limits the data-rate to about 4.3 Mbps (cfr. GAIA). Coming from 40 Mbps, this represents almost a reduction of factor 10.
- *Higher operation costs:* to compensate for the smaller downlink rates, longer contact times with the 35-m ground station can be proposed. Indeed, although in the baseline only 4h per day is assumed, we derive from the visibility analysis that about 8 hours per day are available (pending on ESA DSN load). However, this leads to a 100% increase in operation costs and this during the nominal three mission years plus possible three years extension. Despite this effort, the total science return would still be reduced by 80 % with respect to the baseline option.
- *Higher energy consumption:* instead of 4 hours per day, the on-board transmit equipment would be ON for twice as much of the time. Again, this represents a large increase in energy consumption which will ripple down in the design and mass budgets of other subsystem such as power and thermal control.

In the end, trade-off the higher development/upgrade cost for the 26 GHz-band versus the increased operation cost and the significant reduction in science return in the X-band have led to the conclusion that the X-band is discarded.

8.6.6.2 Phased-array antenna

Instead of relying on a steerable dish antenna, another possibility is to have a phased-array antenna: the big advantage in this case is that there are no moving parts which can create vibrations and disturb the science measurements. It is for the same reason that the GAIA mission baselines a phased-array as well. Nevertheless, little technology heritage can be reused from GAIA: embarking a 26 GHz phased-array antenna on FIRI would require a new development due to the new frequency band and very high EIRP (about 20 dB more than GAIA). For this reason, the phased-array antenna option was discarded in this study.

8.7 Thermal

Parts of the Service Module are all the elements that do not require a thermal control at cryogenic level:

- Room temperature compartment of the two telescopes
- Room temperature compartments of the central hub
- Deployable booms.

8.7.1 Requirements and Design Drivers

8.7.1.1 Room temperature compartments

Both telescopes and Hub compartments are used to allocate electronics and more in general dissipative units. These elements have temperature requirements far from cryogenic values. In particular it has been assumed that all of them should stay within:

- -5/+10 °C for the full mission.

This can be achieved by using radiative surfaces to spread out the power dissipated by the units when operating and heating power to keep them at their minimum temperature when in stand-by or OFF mode.

8.7.1.2 Booms

The booms are the Spacecraft part where the two telescopes move to scan different portions of the sky. Since data are transferred to the cryogenic compartment of the Hub by multiple reflections based on precise alignments it is important to limit as much as possible bending phenomena along the booms and thus thermal gradients between up and low parts.

8.7.2 Assumptions and Trade-Offs

8.7.2.1 Telescopes room temperature compartments

The telescopes room temperature compartments are placed below the Sunshield.

Even if Sun impinged the radiators are assumed to be placed on the Sun pointing surface. This for several reasons:

- To have a full view to the deep space.
- To avoid interactions with the Sunshields and thus possible spots at higher temperature on them that can consequently interact with the telescopes radiators.
- To limit the heating power in cold cases due to the contribution of the solar flux even if in this way the radiators will have larger surface areas.

8.7.2.2 Hub room temperature compartment

Also this compartment is placed under the Sunshield. This is a box having a base area of about 5.5 m2 and high of 0.9 m.

Due to the fact that the Sun pointing surface needs to allocate body mounted solar arrays the radiators of this compartment have to be placed on the lateral panels.

The propellant tank partially outside the service module is covered by 20 layers MLI.

8.7.2.3 Booms

It has been assumed the nodes representing the booms in the thermal model being only radiatively linked. With this assumption it is possible to get the max reachable temperature gradients that correspond to the ones that can be observed when using a low conductivity material to realize the boom. This is a worst case.

8.7.3 Baseline Design

Room temperature compartments are wrapped in standard 20 layers Kapton/VDA MLI blankets.

Radiators are white painted and heaters are installed on dissipative unit to cope with cold cases occurring when in stand-by or OFF mode.

To design the radiators and the heating power three modes have been taken into consideration:

- Stand-by/Communication mode
- Observation mode
- Retargeting mode

Booms are aluminium finished having this a low emissivity needed to limit radiative interaction with the surrounding. The booms are also shielded from the direct impingement of the solar flux. These shields can also be used to place solar arrays.

8.7.3.1 Telescopes room temperature compartments

As already said these compartments are allocated under the primary Sunshields. Radiators and heating powers have been computed according to the power dissipation values provided by the different subsystems as shown in the following table according to the three different modes considered.

		Stand By / Comms		Observation		Retargeting Mode	
Max Continuous Power	Max Continuous Power	Max Continuous Power	Peak Power (incl. transients)	Max Continuous Power	Peak Power (incl. transients)	Max Continuous Power	Peak Power (incl. transients)
Tot dissipation for rad. Design [W]		340.00	530.00	90.00	155.00	341.50	532.25

Table 8-33: Power dissipation vs. mode for both telescopes

Retargeting mode is the one used to design the radiators being the one where max power dissipation occurs.

Assuming a max temperature of the radiators of 10 °C the total radiative surface needed to cope with this dissipation is 2.51 m^2, thus 1.25 m^2 per telescope.

Heating power has been calculated assuming a min temperature of the radiators of -5 °C.

According to the dissipative values shown above, only during observation mode heating power needs to be provided. A value of about 232 W has been calculated (116 W per telescope for 45º).

These results are achieved placing the radiators Sun pointing.

If a lateral position is assumed there is no direct impingement from the Sun and radiative exchanges occur between the radiative surfaces and Sunshields plus deep space.

In this way a total radiative surface of about 1.77 m^2 is found (lower than what found assuming the radiators facing the Sun) but about 152 W are needed to cope with the cold case.

8.7.3.2 Hub room temperature compartment

Same exercise has been done to compute radiative surface and heating power for the Hub.

In this case the radiative surface needed to be placed on the lateral panels because the Sun pointing one was used to allocate solar arrays.

The power dissipation in the different modes is as follows:

		Stand By / Comms		Observation		Retargeting Mode	
Max Continuous Power	Max Continuous Power	Max Continuous Power	Peak Power (incl. transients)	Max Continuous Power	Peak Power (incl. transients)	Max Continuous Power	Peak Power (incl. transients)
Tot dissipation for rad. Design [W]		485.06	976.50	735.50	1132.50	592.20	1005.00

Table 8-34: Power dissipation vs. mode for the Hub

Breakdown power dissipation is presented in Table 8-13 for the central module (Hub).

Retargeting mode is the one where the max dissipation occurs. As consequence this value is used to design the radiator. A value of 2.8 m^2 is found.

Heating power is needed only during Stand-by/Communication mode. A value of about 107 W is calculated (considering no solar impingement).

The radiator is split in two panels to be placed on the ±Y faces of the compartment (±X are the axis along which the telescopes can move and Z axis is the one where the telescopes look along).

These two radiative surfaces should also be placed in a non central way due to the presence of the thrusters. This is to avoid possible impingements and consequent degradation of the radiators' optical properties.

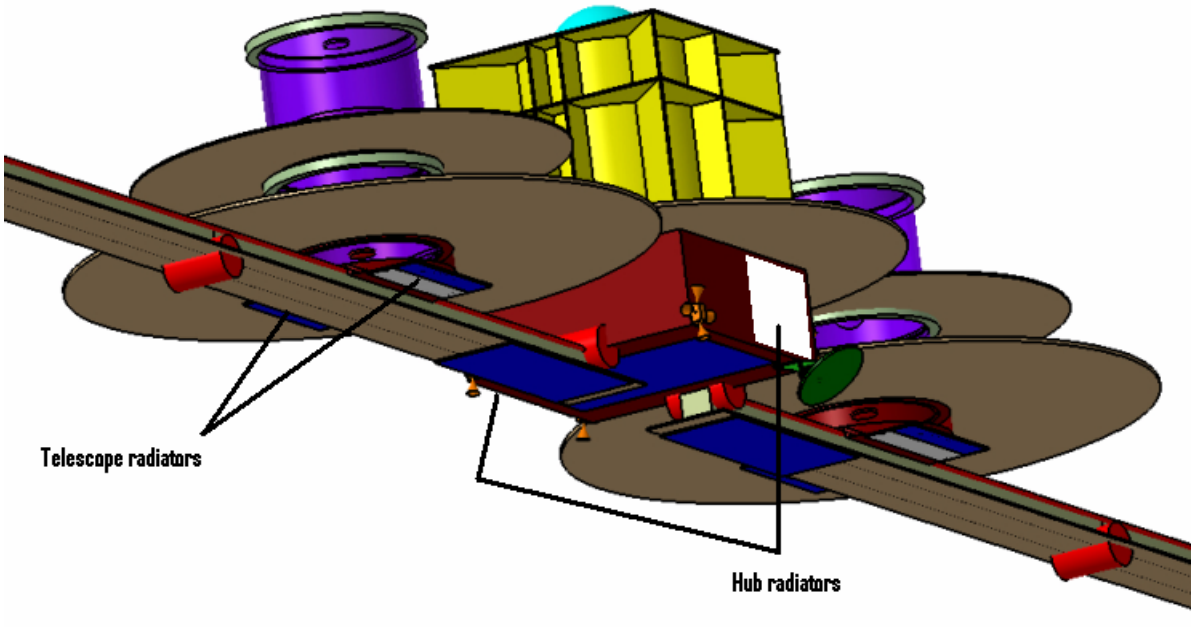

Figure 8-40: S/C configuration layout and radiators allocations

8.7.3.3 Booms

The booms are aluminium finished to limit radiative interactions with the surrounding.

Thanks to the thermal model outputs curves showing the temperature gradients along their length axis have been determined.

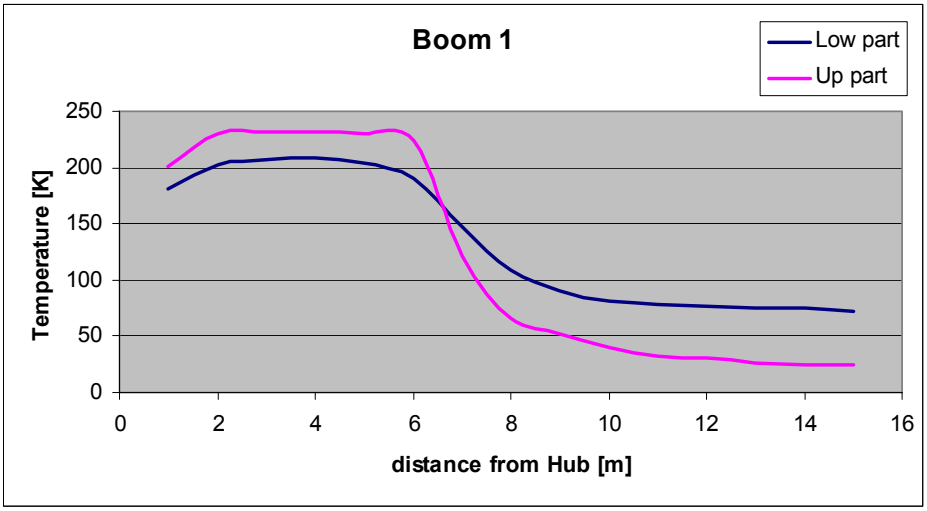

Figure 8-41: Temperature evolutions of the boom up and lower parts as function of the distance from the Hub

From Figure 8-41 it is possible to observe the temperature evolution along the boom for both upper and lower parts.

Picks are observed in correspondence of the telescope position due to the high interaction with the Sunshield. The up part is hotter seeing it the Sunshield directly. These picks move when the telescope moves along the boom. Far from the Hub and telescope it is possible to observe an inversion of the temperature. This because now the up part is free to radiate toward deep space while the low part interact also with the boom Sunshield which is on one of its sides impinged by the solar flux.

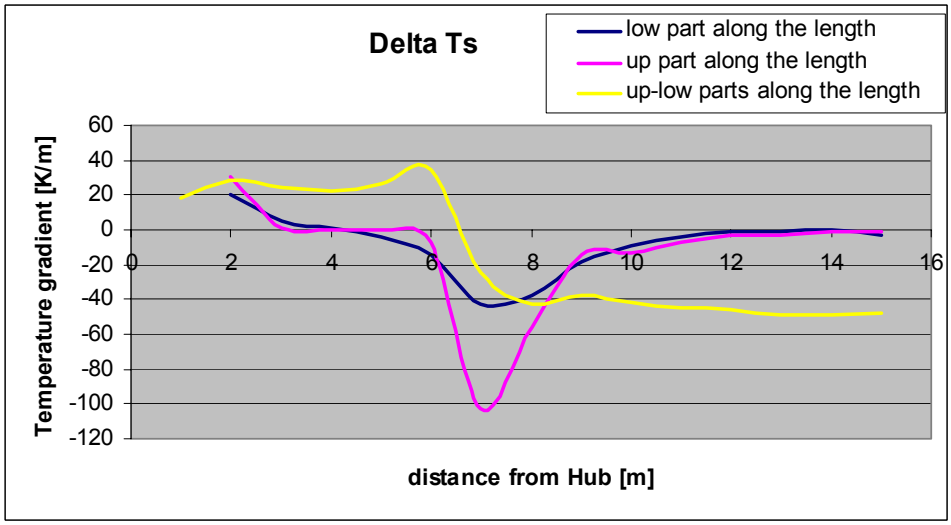

Figure 8-42: Temperature gradients along the boom length of low, up part and up-low parts

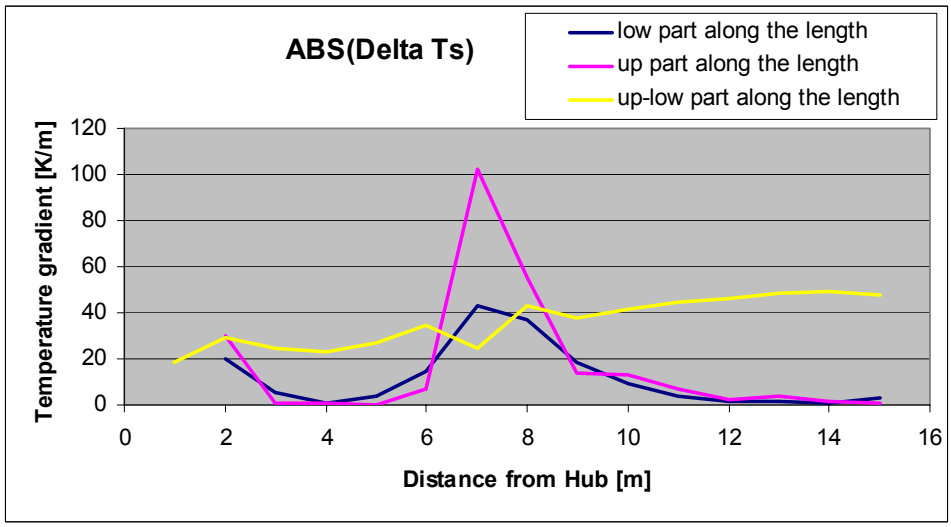

Figure 8-43: Absolute temperature gradients along the boom length of low, up part and up-low parts

In these two pictures the temperature gradients of the nodes representing the up part of the boom $T_{up}(X_2)–T_{up}(X_1)$, its low part $T_{low}(X_2)–T_{low}(X_1)$ and the delta up-low parts $T_{up}(X_i)-T_{low}(X_i)$ are shown as well as the absolute values.

It is possible to observe a max delta temperature of 100 K for the up part, of 45 K for the low part and 50 K between up and low part. These results are implemented for the thermo-mechanical analysis performed in 8.2.3.2.1.

8.7.4 List of Equipment

In the following pictures the different units used for the thermal control of the Service Module are listed together with the correspondent mass.

Element 1		Service Module		MASS [kg]			
Unit	Part of:	Unit Name Click on button above to **insert new unit**	Quantity	Mass per quantity excl. margin	Maturity Level	Margin	Total Mass incl. margin
1	Boom	SVM-Booms Sunshield	1	20.3	To be modified	10	22.3
2	Boom	SVM-Boom finishing	1	3.5	Fully developed	5	3.7
3	Hub	SVM-MLI	1	9.6	Fully developed	5	10.1
4	Hub	SVM-Miscellaneous (paints+washers+fillers)	1	2.0	Fully developed	5	2.1
5	Hub	SVM-Heaters	1	1.5	Fully developed	5	1.6
6	Hub	SVM-WP radiator	1	15.4	Fully developed	5	16.2
7	Hub	SVM-Linear compressor (for coolers on the PLM)	1	20.0	To be developed	20	24.0
8	Telescopes	Telescope1-Sunshields	1	29.1	To be modified	10	32.0
9	Telescopes	Telescope2-Sunshields	1	29.1	To be modified	10	32.0
10	Hub	PLM-Sunshield	1	23.6	To be modified	10	26.0
11	Telescopes	Telescopes - Heaters for room temperature compartments	1	1.3	Fully developed	5	1.3
12	Telescopes	Telescopes - WP radiators	1	13.8	Fully developed	5	14.5
13	Telescopes	Telescopes - MLI on room temperature compartments	1	1.5	Fully developed	5	1.6
14	Hub	MLI on propellant tank	1	2.0	Fully developed	5	2.1
-	Do not use	Click on button below to insert new unit		0.0	To be developed	20	0.0
		SUBSYSTEM TOTAL	**14**	**172.6**		**9.7**	**189.3**

Table 8-35: Service Module mass budget

8.8 Guidance Navigation and Control

8.8.1 Requirements and Design Drivers

The FIRI spacecraft is a spinner spacecraft (S/C), with also the opportunity to be 3 axis stabilised, with stringent pointing requirements imposed by the science instruments. The S/C rotates so that the instrument can analyse the full uv plane of the target. The construction of the S/C is such that the spinning axis is the major axis. A three-dimensional model of the S/C as used in the GNC analysis is shown in Figure 8-44.

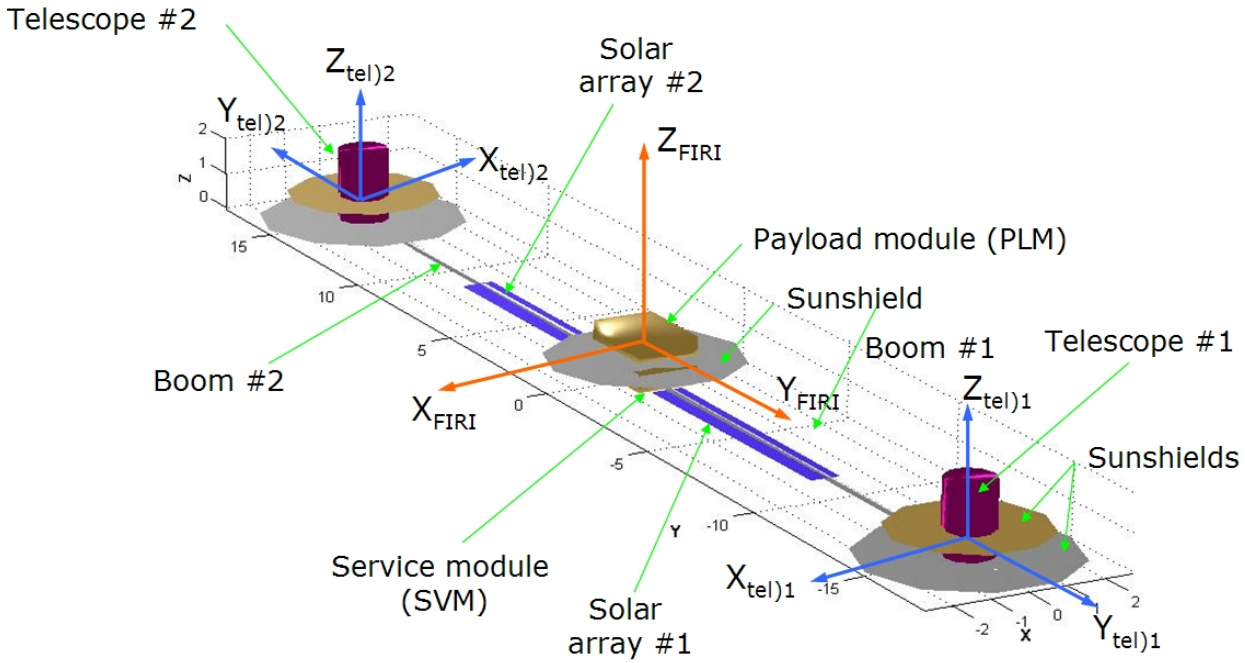

Figure 8-44: Solid model of the FIRI S/C generated from the data of the last CDF session and used in the GNC subsystem design.

8.8.1.1 Requirements

The requirements of the GNC system are:

- The S/C spins about the body Z axis (Z_{FIRI} in Figure 8-44.)
- The inter-telescope distance (ITD) varies from 8 to 30 m.
- The angular rate of the S/C during the observation of one target varies according to the profiles given in Figure 8-45.
- Changes in the spin angular rate should be performed with as little perturbations as possible. (Minimize oscillations of the deployable structures.)
- The AME of 17 mas is driving the design of the optics. The optical system design thus includes a fine star tracker subsystem.
- APE of 13 mas

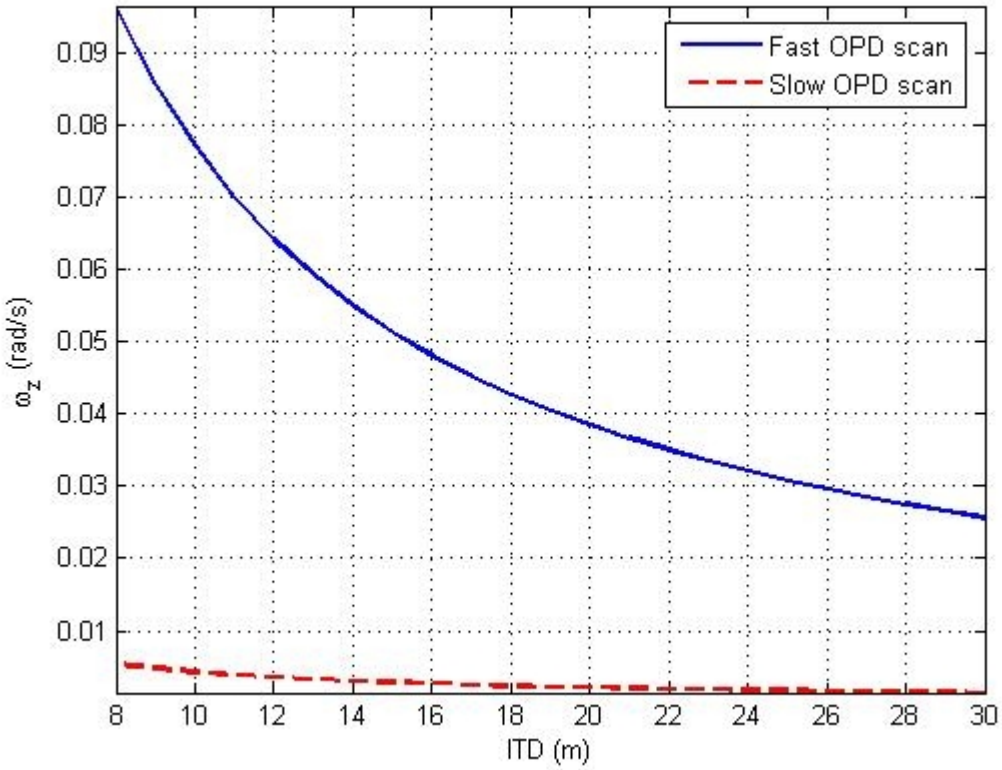

Figure 8-45: Variation of the angular rate about the Z axis of the FIRI S/C versus ITD.

The pointing errors of the FIRI mission are summarized in Table 8-36.

Error Source	Class	X	Y	Z		Comments
Calibration error residual	C	2.1	2.1	2.1	D/A	{Telescope, STR} frames calibration
STR bias	C	2.4	2.4	15.9	D	Worst case (one STR)
STR thermal mechanical stability	LT	0.5	0.5	0.5	A	Highly stable mounting structure
Telescope thermal mechanical stability	LT	1.0	1.0	1.0	A	Highly stable mounting structure
Structural thermal distortion	LT	4.5	4.5	9.0	C	Between {Telescope, STR} frames
Control error	R	0.5	0.5	1.0	C	To be evaluated
STR NEA						
Bearing noise						
RW quantisation						
Controller delay						
External disturbances						
High frequency error	H	0.5	0.5	0.5	A	
RW microvibrations						
Mechanical cooler		0	0	0		
Moving mechanisms						
Total	C	3.2	3.2	16.0		A: allocated R: random
Total	LT	4.6	4.6	9.1		D: datasheet H: harmonic
Total	R	0.7	0.7	1.1		C: calcualted T: transient
Total	H	0.5	0.5	0.5		LT: long term RSS: root sum squared
APE		8.7	8.7	26.3	C+LT+RSS(R+H+T)	
AME		7.8	7.8	25.1	C+LT+residual	

Pointing Error Summary	X	Y	Z	Comments
APE	8.6	8.6	TBD	13" half cone angle (68%)
AME	0.33	0.33	TBD	0.5" half cone angle (68%)
RPE	TBD	TBD	TBD	

All units are arcseconds unless specified otherwise
The 17mas AME is addressed by the optical sub-system

Table 8-36: Pointing error summary presented together with the error budgeting

It can be seen that the AME requirement has not been met, however, this will be covered by the fine guidance system of the Optics (See Optics Chapter for more details).

8.8.1.2 Design Drivers

The requirements that the ITD is varied between 8 and 30 m lead to a design which has variable moments of inertia along the body X and Z axes. The moments of inertia for the two configurations are presented in Table 8-37 and Table 8-38.

I (kg m^2)	X	Y	Z
X	261,111	-5,173	0
Y	-5,173	50,591	0
Z	0	0	309,481

Table 8-37: Moments of inertia of the FIRI S/C for ITD = 30m

I (kg m^2)	X	Y	Z
X	21,582	-5,173	0
Y	-5,173	50,591	0
Z	0	0	69,953

Table 8-38: Moments of inertia of the FIRI S/C for ITD = 8m

In order to vary the spin rate of the S/C during the observation phase it has been proposed that reaction wheels (RWs) are used in order to reduce propellant use as much as possible and introduce as little perturbation as possible in the structure of the S/C. It is to be noted that at the same time as the angular rate varies the moment of inertia of the S/C also varies.

8.8.2 Assumptions and Trade-Offs

The total mass of the S/C is 4,671 kg and the centre of mass (CoM) of the S/C is at (0, 0, 0.55)m from the –Z face of the service module. The moments of inertia are computed with the data from Chapter 7.2 The X and Z moments of inertia have a parabolic variation with the distance between the CoMs of the telescopes and the CoM of the S/C. This variation has been plotted in Figure 8-46.

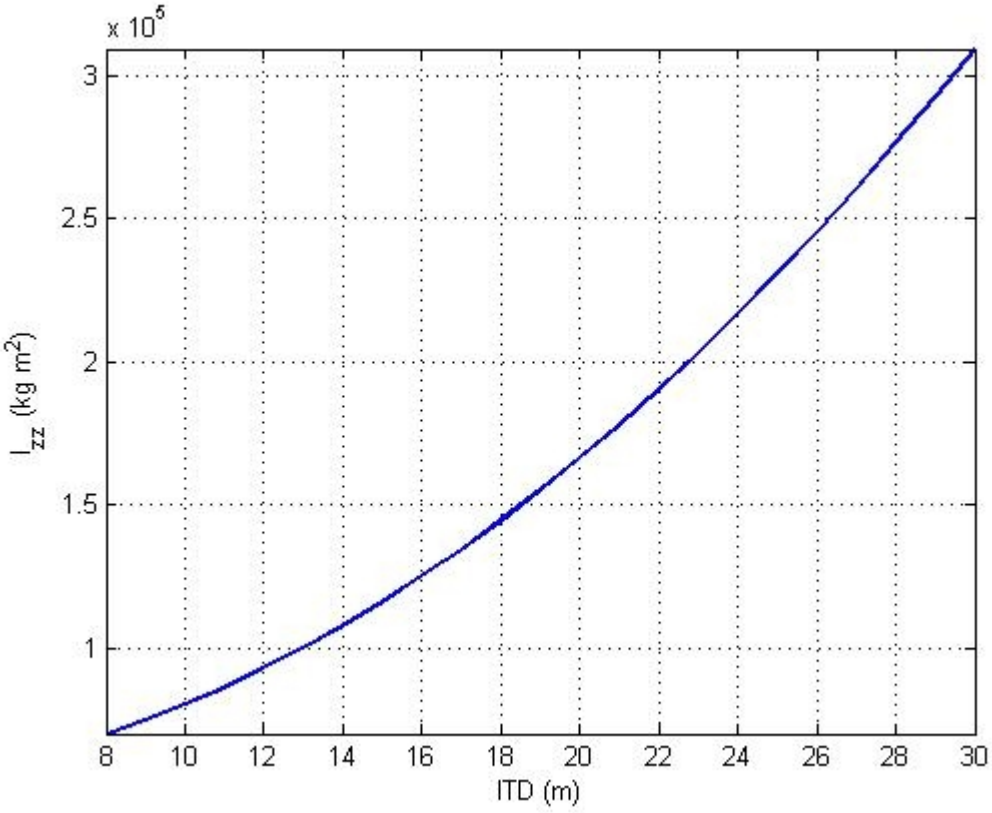

Figure 8-46: Variation of the FIRI S/C Oz moment of inertia with the ITD. The moment of inertia has a parabolic variation according to the parallel axis rule.

To begin the operational phase of the mission the spacecraft has to be spun up from a three-axis stabilized configuration which was used for commissioning it. The spin-up manoeuvre from rest to an angular rate of 96mrad/s, corresponding to l_{ITD} = 8m, is I_{tot} = 3356 Ns. For a spin-up manoeuvre from rest to an angular rate of 25.5 mrad/s corresponding to l_{ITD} = 30 m, is I_{tot} = 3952 Ns.

Two strategies for varying the angular rate during a uv plane scan have been analyzed. One strategy has the telescope at an initial ITD of eight meters. They are moved outwards to a final ITD of 30 m. The second strategy is just the opposite. The telescopes are placed initially at the maximum ITD of 30 m and are brought "in" to the final ITD at eight meters.

Computation of the angular momenta needed to perform the manoeuvre with the fast scan angular rate variation shows that the second strategy, of starting at maximum ITD is beneficial and can be implemented using RWs. Using this strategy results in the angular momentum accumulated in the RW at the end of a uv plane scan to be -51.1 Nms. The assumption made in computing the angular momenta needed for each manoeuvre was that the scanning of the uv plane is performed in 22 steps, i.e. from 30 m to 29 m to 28 m and so on to eight meters. A plot of the angular momentum against the number of steps is presented in Figure 8-47. Note that the angular momentum capability of the RW has to be 94.2 Nms (=99.4 – 5.2 Nms) which is equal to the angular momentum accumulated between steps one and 15.

The time needed to vary the angular momentum only according to the strategy shown in Figure 8-47 is 1421s (=23.7min). This time does not account for the duration of the actual observation.

Another requirement on the GNC subsystem was to provide the re-pointing capability of the S/C. For re-pointing it is proposed that the S/C is kept spinning. The strategy of de-spinning the S/C for re-pointing has been investigated but it is prohibitive in terms of the propellant needed for spinning the S/C up and down.

The following assumptions have been made for the re-pointing manoeuvre: I_{zz} = 3.1e5 kgm^2, I_{yy} = 0.52e5 kgm^2, ω_z = 2.554e-2 rad/s, T_{rep} = 4 Nm. The torque is applied with the GNC subsystem thrusters. The manoeuvre is actually a tilt of the angular momentum with 22.5º vector by applying T_{rep}. It is performed in t_{rep} = 103s (14% of the rotation period) and the total impulse is I_{tot} = 103.05Ns for each 22.5º slew.

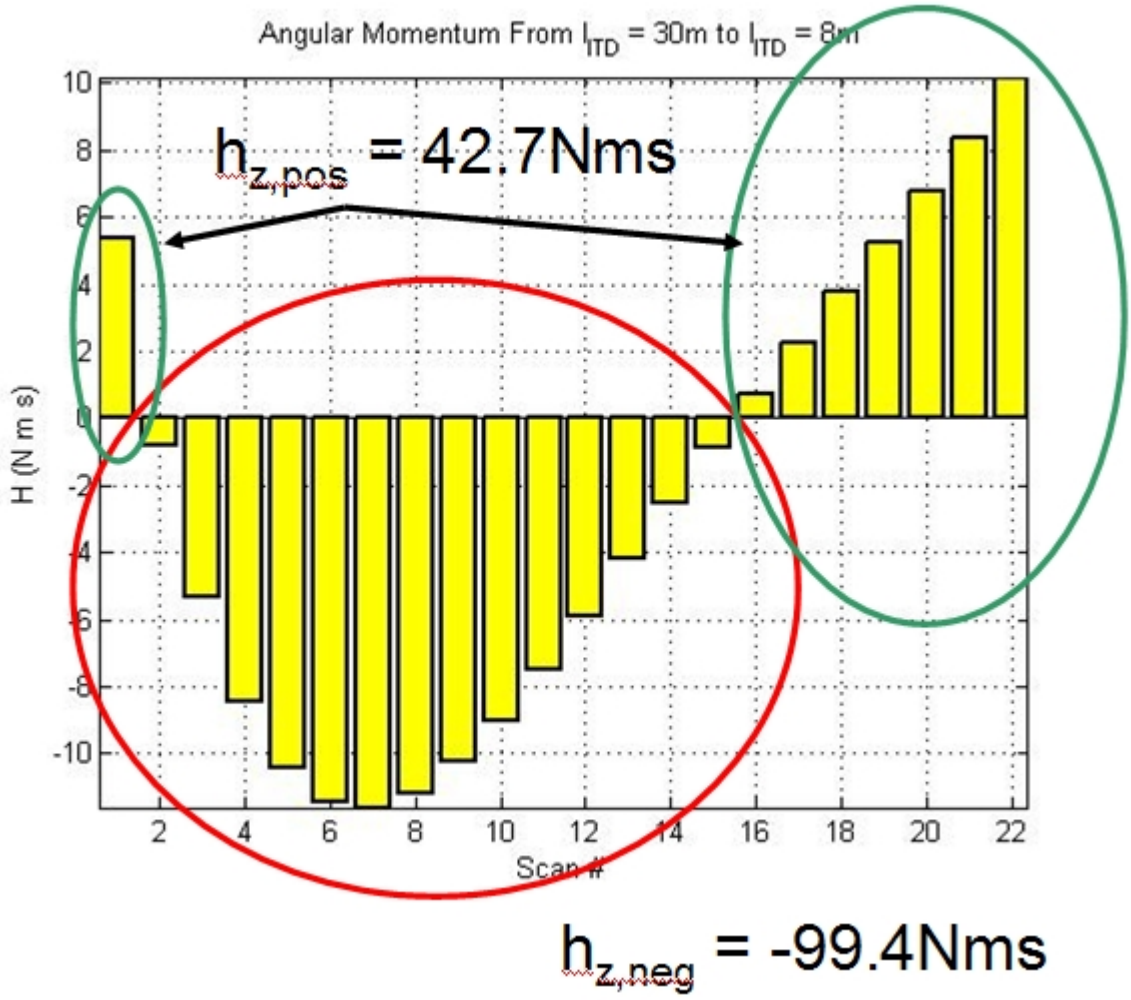

Figure 8-47: Variation of the angular momentum applied by the RW for scanning the uv plane.

Last but not least the GNC subsystem has to reject the perturbations due to the environment. Since the mission is orbiting the L2 point of the Sun-Earth system the gravity gradient is extremely small and the atmospheric drag is null. Thus the only perturbation to be rejected is the solar radiation pressure (SRP). The SRP force produces a torque on the S/C. The following assumptions have been employed for the computation of the SRP torque: p_{SRP} = 4.5e-6 N/m^2, C_r = 1.75 (reflectivity coefficient ranges from 0 to 2, with 0 transparent), A_{cross} = 84m^2 (cross sectional area). With this assumptions and for SRP torque rejection during 24hrs (one uv-plane scan) the angular momentum accumulated in the RWs is h_{SRP} = 25 Nms. To offload the wheels, with a thrusters with a moment arm of l_{RCS} = 2 m the needed total impulse is I_{tot} = 12.5Ns.

8.8.3 Baseline Design

The baseline design of the GNC subsystem is a classical configuration with RWs and thrusters, Sun sensors and rate sensors plus a couple of large RW. The large RWs are installed coaxially and each of them has a angular momentum capability of 100 Nms. One large RW is able to provide the manoeuvre capability. The second large RW is installed as a backup and it can be also used to provide additional torque and angular momentum capability in case they are needed.

The RWs of the "classical" GNC system are installed in a typical tetrahedral configuration. A proposed RW configuration is shown in Figure 8-48.

It is proposed that magnetic bearing RWs from Teldix are used. The advantages of the magnetic bearing RWs are that they produce little vibration compared to the ball bearing RWs and that they can be tilted to cancel any parasitic torques resulting from their coaxial installation.

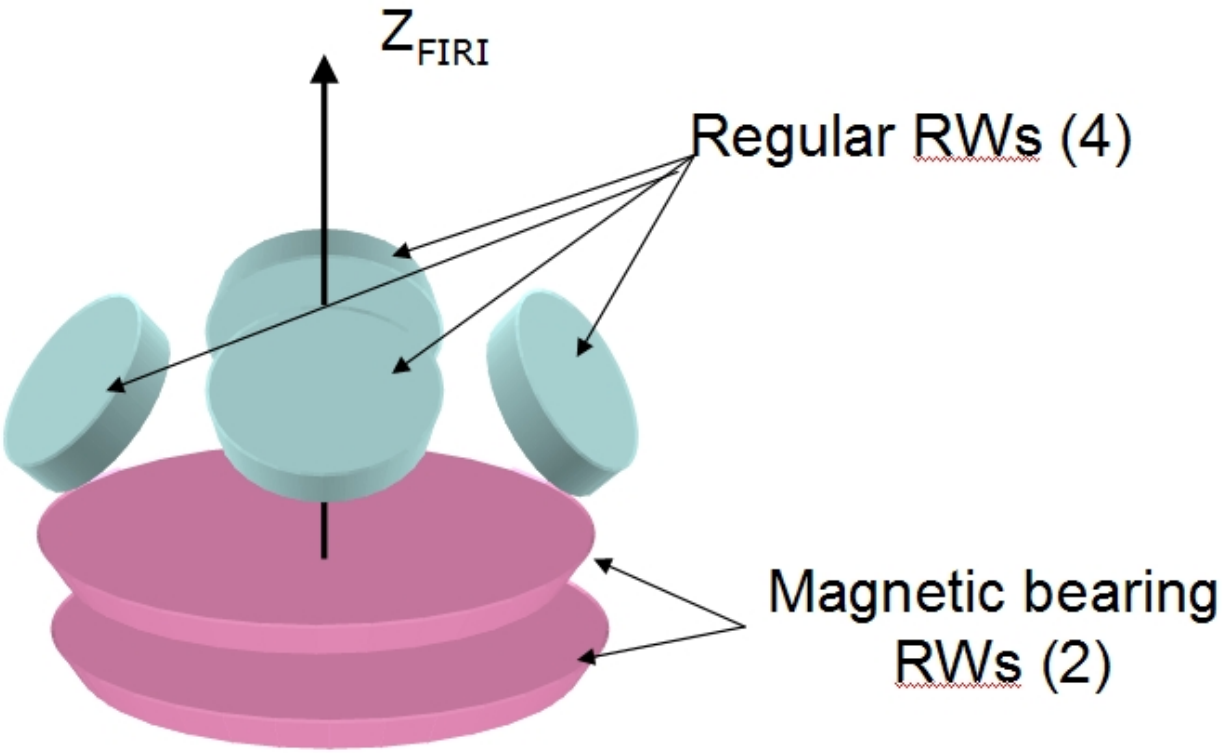

Figure 8-48: Proposed reaction wheel arrangement. The "regular" reaction wheels are used for rejecting perturbations. The large magnetic bearing reaction wheels provide the manoeuvring torque during the uv plane scanning

8.8.4 List of Equipment

The list of equipment is given in Table 8-39.

Equipment name	No.	Mass/unit (Kg)	Power/unit (W)	Potential Supplier
Sun Acquisition Sensor (SAS)	3	0.23	0	TPD/TNO (NL)
Autonomous Star Tracker (AST)	3	1.50	10	Sodern (FR)
Star Tracker Electronics Box (ASTE)	1	2.0	8	Sodern (FR)
Inertial Reference Unit (IRU)	2	4.1	15	Honeywell (US)
Attitude Anomaly Detector (AAD)	2	0.15	0	TPD/TNO (NL)

Equipment name	No.	Mass/unit (Kg)	Power/unit (W)	Potential Supplier
Magnetic Bearing Reaction wheels	2	12	50	Teldix (DE)
Ball Bearing Reaction Wheels (RW)	4	4.85	60	Teldix (DE)
AOCS Interface Unit (AIU)	Inc. in CDMU			
Failure Detection Correction Electronics (FDCE)	Inc. in CDMU			

Table 8-39: FIRI GNC subsystem equipment

8.8.5 Conclusions

The major critical point is the use of dual magnetic bearing RWs to perform scan manoeuvres:

- Pros
  - Magnetic bearings provide long life for the rotating machinery used at a high duty cycle and very low vibrations
  - Dual configuration can provide relatively large torques in directions other than the spin axis
  - The RWs can be gimballed to cancel any parasitic torques resulting from their coaxial installation.
- Cons
  - Development of the relatively complex guidance and control algorithms has to be started early
  - The magnetic bearing RWs are new technology with low TRL at the present time.

The alternative to using magnetic bearing RWs are control moment gyros (CMGs).

Further analysis on micro-vibrations for all different types of wheels should be performed.

It is recommended that a multidisciplinary simulation and analysis tool is developed early in the program. The tool should combine structural dynamics (FEA) with propellant sloshing (CFD) and controlled optics. The tool should be used to investigate the influence of the control strategies on the performance of the S/C.

This Page Intentionally Blank

9 RADIATION ANALYSIS

9.1 Radiation Analysis

The radiation analysis is performed using the SPace ENVironment Information System (SPENVIS) tool (RD[78]) as at the moment there is not the possibility of running the code for an interplanetary orbit. In SPENVIS the L2-orbit is simulated as a circular orbit an altitude of 90,000 km and called 'Near-Earth Interplanetary orbit'. The launch date is assumed to be January 1st 2020.

In this orbit there is hardly any trapped radiation, the radiation is instead coming from the solar wind itself. The solar proton fluencies are calculated with a model from JPL.

From this analysis the radiation dose in Silicon as a function of the spherical Aluminium shielding thickness is computed using SHIELDOSE-2. The results for five years mission duration can be found in Figure 9-1.

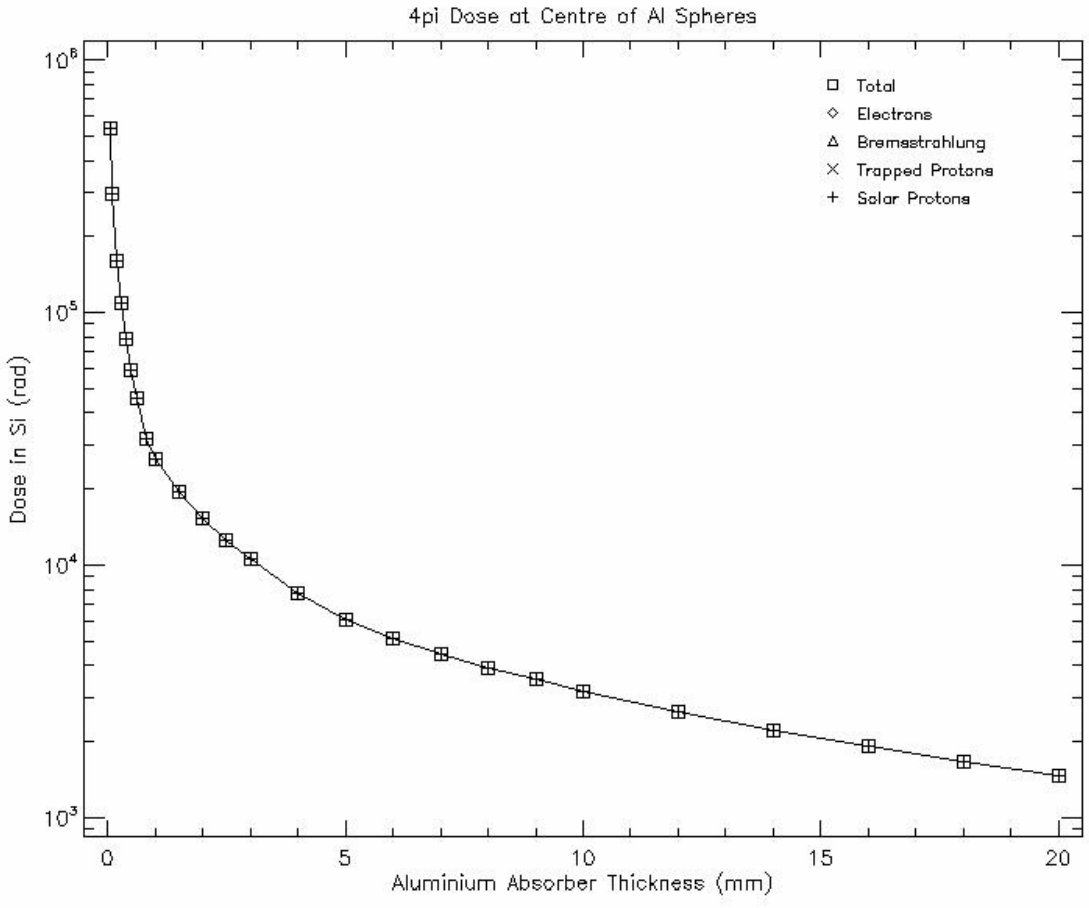

Figure 9-1: Radiation Dose as a Function of Aluminium Absorber Thickness (L2 Orbit, Mission Duration Five Years)

For such an orbit and a mission lifetime of 5 years, the total dose is below 100 kRad for a 0.3 mm shielding and below 15 kRad for a 2 mm shielding.

This Page Intentionally Blank

10 GROUND SEGMENT & OPERATIONS

The ground segment and operations infrastructure for the Mission Operations Centre (MOC) of the Far Infrared Interferometer (FIRI) mission will be set up by ESA/ESOC, and will be based on the extension of the existing ground segment infrastructure, customised to meet the FIRI specific requirements. The concept for the establishment of the FIRI ground segment will be the maximum sharing and reuse of facilities and tools made available for former Observatory missions, (Herschel/Planck, GAIA) if applicable.

10.1 Requirements and Design Drivers

The design of the Ground Segment and the Operations Concept for the FIRI mission are driven by the compliance with the mission requirements and the constrained mission cost envelope. When and where possible the technical facilities and tools and the manpower expertise gained with Herschel/Planck and GAIA will be reused/transferred by/to the FIRI mission.

Due to the characteristics of the mission, and the high amount of data generated by the science payload, the satellite will communicate with the ground station in X-band for TT&C up and downlink and in the 26 GHz Ka-band for science data downlink. The ground station chosen in the baseline design for communications with the spacecraft (TT&C and science TM) has been the ESA Deep Space Antenna (DSA) in Cebreros (Spain). The Cebreros Ground Station will have to be upgraded in order to be able to receive the 26 GHz Ka-band signal, which will be a major design/cost driver (since a mission around L2 is not considered a deep space mission, the 32GHz Ka-band can not be used for communications. However, this cost could be shared with other missions. The antenna in Cebreros already has the capability for 32 GHz Ka-band reception).

Currently ESA is considering the construction of a third DSA at American longitudes, which would represent an option to Cebreros. In case the third antenna is approved it would be ready by 2012, not representing a problem for FIRI. The best solution would be the inclusion of the 26 GHz Ka-band in the initial design.

The Intermediate Frequency Modem System (IFMS) equipment would also need to be upgraded in order to be able to deal with the relatively high downlink data rate foreseen for FIRI.

Another aspect to be taken into account during the early design phases is the foreseen load of the ESA Deep Space Antennas according to the ESA mission model, such that a correct allocation can be done.

Nominal spacecraft control during most of the cruise and the observation phase will be “off-line”. Only one ground station will be allocated for communications with the spacecraft during these phases. The required daily visibility duration will be about 5 hours. This implies that FIRI is assumed to provide on-board capabilities (enough degree of spacecraft autonomy required) such that the satellite is able to perform corrective actions in case of on-board anomalies and the ground segment does not need to monitor the spacecraft in real time. Consequently, anomalies will be detected on ground with a typical delay of approximately 1 day.

10.2 Assumptions and Trade-Offs

The main assumptions considered for the design of the ground segment for FIRI are the following:

- It is assumed that two other Observatory missions will be flying or in preparation, sharing the Observatory missions facilities (mainly software as MCS, Simulator, and the dedicated control room) and manpower (mainly in the areas of Quality Assurance, Project Control, Ground Segment Management, Operations Management). However FIRI will have separate core teams for Flight Control and Flight Dynamics. SPACONS sharing will be considered if possible.
- It is assumed that the FIRI operations can be performed by a team that is organisationally as close as possible/practical to the GAIA Mission Operations and Satellite Control teams.
- A launch date in the interval 2020-2025 is assumed. In the baseline design a launch in 2024 has been considered.
- The following durations for the different mission phases have been considered:
  - LEOP: 1 week (TBC considering that the deployment is complete and is performed during LEOP)
  - Transfer to L2 operational orbit: approximately 3 months
  - Commissioning and Verification Phase: 2 months
  - Nominal routine operations: 5 years
  - Extended operations: None foreseen.
- The spacecraft will be launched by an Ariane 5 from Kourou.
- The LEOP ground station network will be composed by: Kourou (15 m), Maspalomas (15 m) or Cebreros (35 m), and Perth (15 m) or New Norcia (35 m).
- No dedicated backup station will be considered for the routine mission. (S/C emergency cases will be supported by the network as per priority rules).
- The minimum HKTM data rate will be 4 kbps.
- It is assumed that all payload HKTM is included in the same virtual channel as the satellite HKTM and is therefore directly available to ESOC.
- Science data acquisition from Cebreros (26 GHz Ka-band) is the ESOC baseline.
- There is no requirement on latency of delivery of science data from the Ground Station to the SOC.
- A reliability of 95% is assumed for all downlinked science data.
- The composition of the Flight Control Team during mission preparations and mission operations will be determined by the criticality of the operations and the possibilities of sharing the team with other Observatory missions.
- The provision, installation and validation of a mini-Mission Control System (mini-MCS) in the main ground station is part of the baseline.
- Use of the corresponding version of the SCOS2000 Mission Control System is assumed. The cost for the MCS development will include the Mission Planning System.

It is assumed that some automation will be available including: Initial Pass Operations/Establishing of Ground Station Link and some limited reporting capabilities.

- An Operations Automation System will be used for automating certain routine operations activities.
- Hardware usage will be shared/re-used with WFI where possible (e.g. back-up system for the DDS).
- Always in routine phases under ground station visibility (approximately 8 hrs/day) operations will be performed in Near Real Time.
- Off-line operations are performed during the periods when no ground station visibility is available.
- Anomalies will only be detected on ground with a delay, which as a minimum correspond to the light travel time, but typically will rather be in the order of one day, thus quick reaction will not be supported.
- SPACON positions will be manned one 8 hours shift per day (7 days/week)
- It has to be considered that not all the duration of a ground station pass can be dedicated to science downlink.
- Spacecraft TM and TC service will be compliant with the ECSS Standards.

10.3 Baseline Design

The ESA/ESOC ground segment will consists of:

- The Ground Stations and the Communications Network
- The Mission Control Centre (infrastructure and computer hardware)
- The Flight Control System (data processing and Flight Dynamics Software)
- Infrastructure (Mission Control System, Simulator, etc)
- A Ground Operations Automation System

The FIRI ground segment shall provide 26 GHz Ka-band payload data acquisition during the commissioning, nominal observation and extended phases.

The FIRI ground segment shall provide:

- A satellite monitoring and control chain, which includes:
  - A X-band Housekeeping TM acquisition and processing functional chain
  - A X-band TC generation and uplink functional chain
  - Offline performance analysis functions.
- An orbit and attitude monitoring and control functional chain
- An overall Mission Planning function
- An OBSM facility
- Data archiving

10.3.1 Ground Station and Communications Network

The ground stations network to be used for FIRI during LEOP will be composed of the 15 metre antennas in Kourou, Villafranca and Perth (these two last antennas could be substituted by the 35

metres antennas in Cebreros and New Norcia). This network almost guarantees 24 hours coverage of the spacecraft during this critical period.

For the transfer phase and the nominal observation and extended phases the 35 metres antenna in Cebreros is the baseline. In order to receive 26 GHz Ka-band science telemetry, the antenna has to be upgraded. The possible third ESA Deep Space Antenna will be located at American longitudes (either in Chile, Argentina or Canada) and will be operative by 2012, and could be considered as an option for the FIRI mission design. As for Cebreros, 26 GHz Ka-band reception would be required and it would be optimal to include this capability in the initial ground station design.

A preliminary analysis of the ESA Deep Space Network load has been performed in order to assess the ground station availability.

New Norcia:

Rosetta. Long daily passes needed during 2015, due to near comet operations. This activity would be compatible with a 4 hours daily visibility window for a spacecraft in L2, as Rosetta will be approaching the perihelion of its trajectory.

Herschel/Planck. No interference with FIRI, although both mission will have Lissajous orbits around L2, as the end of both missions is foreseen by 2012. Each mission needs a 3 hours daily visibility window and both communicate with the ground station in X-band.

Solar Orbiter. SolO requires the upgrade of the ground station to 32 GHz Ka-band reception, making the Rx 26 GHz upgrade technically very challenging (although not impossible). Launch of SolO is foreseen during the first trimester 2017. SolO would be compatible with FIRI in the same ground station if the installation of the Rx 26 GHz band would be feasible (on top of the Rx 32 GHz) as both missions takes place in opposite hemispheres of the Earth with respect to the Sun.

Cebreros:

GAIA. The spacecraft will be in a Lissajous Orbit around L2. The nominal mission end is foreseen during the second half of 2017.GAIA will need the complete duration of the daily visibility window for science data downlink. Seasonally, daily visibility has to be even completed with New Norcia. In order to minimise the conflict with FIRI, the daily coverage of GAIA could be split between CEB and NNO, although this is not foreseen in the ESA mission model, or the conflict disappears if FIRI is launched after GAIA end of mission.

Bepi Colombo. The launch of Bepi Colombo is planned during the first quarter 2013. The projected extended end of mission occurs during the second quarter 2021. Daily passes are required, but Bepi Colombo is an inner solar system mission and will not conflict with FIRI. Bepi Colombo will require the upgrade of Cebreros for Ka-band transmission.

There are likely to be one or two more science missions, either planetary or astronomy missions, that are likely to take up significant ground station time and depending on selected mission, this could be in conflict with FIRI.

Third DSA:

Exomars. This mission will need daily passes from June 2011 to June 2015 (extended mission). No conflict is foreseen with FIRI as both missions do not coincide in time. The current Exomars design does not include an orbiter, which alleviates the communications scenario.

Mars Sample Return. The launch will take place in 2015, with an expected mission duration of 4 years. A detailed visibility study should be performed during the overlapping periods, as the visibility patterns of an L2 and a Mars mission coincide seasonally. A shared visibility slot will be most probably possible.

LISA. This mission will be launched in 2017. A detailed visibility study has to be carried out.

The Ground Facilities Control Centre monitors and remotely controls all the ESTRACK ground tracking stations, using information provided by Flight Dynamics and the scheduling office. They are also responsible for the TM/TC links to and from the ground stations and any data retrieval of stored science from the TMPs or the ranging IFMS, CORTEX and MPTS equipment.

A station computer monitors and controls (locally, automatic or remotely from the MOC) all equipment on the station. It provides different backup modes (TM quicklook, backup commanding). A Front-End controller unit controls the antenna subsystem.

All ESA stations interface to the MOC at ESOC in Darmstadt via the OPSNET communications network. OPSNET is a closed Wide Area Network for data (telecommand, telemetry, tracking data, station monitoring and control data) and voice.

It is assumed that the communication system will support the LEOP and routine data exchanges between the Control Centre in Darmstadt and the Ground Stations identified in this section.

10.3.2 The Mission Control Centre

The FIRI mission will be operated from ESA/ESOC and it will be controlled from the Mission Operations Centre (MOC), which consists of the Main Control Room (MCR) augmented by the Flight Dynamics Room (FDR) and Dedicated Control Rooms (DCR's) and Project Support Rooms (PSR's). The MCR will be used for mission control during LEOP and possibly the Commissioning Phase in case of serious anomaly. During transfer to L2, and the observation phase the mission control will be conducted from a Dedicated Control Room possibly shared with other Observatory missions.

The control centre is equipped with workstations giving access to the different computer systems used for different tasks of operational data processing. The control centre will be staffed by SPACONS possibly shared with other observatory missions with support from operations engineering staff, experts in S/C control, flight dynamics and network control, available on a part time basis for the full mission duration. Space and equipment for scientists, project and industry experts and public relations will be provided close to the MOC as required, during the critical phases of the mission.

10.3.3 Computer Facilities

The computer configuration used in the MOC for the FIRI mission will be derived from existing structures. The computer system basically consists of:

- A computer system used for the Flight Operations Plan generation in a form directly usable by the mission-dedicated computer
- A mission dedicated computer system (including workstations hosting SCOS2000) used for real time telemetry processing and for command preparation and telemetry and command log archiving, and also for non real time mission planning and mission evaluation
- Workstations hosting the Flight Dynamics System
- The simulation computer, providing an image of the S/C system during ground segment verification, for staff training and during operations
- A computer system for ground operations automation.

All computer systems in the control centre will be redundant with common access to data storage facilities and peripherals. Preferably workstations of a similar type will be used for all related computing, to maximise flexibility and to minimise maintenance costs. The workstations allowing privileged user access to the Flight Control System will be located in the different control rooms as necessary.

10.3.4 The Flight Control Software System

The Flight Control System will be based in infrastructure development (SCOS2000), using a distributed architecture for all spacecraft monitoring and control activities. The Flight Control System includes the following facilities:

- Telemetry reception facilities for acquisition, quality checking, filing and distribution
- Telemetry analysis facilities for status/limit checking, trend evaluation
- Telecommand processing facilities for the generation of commands for control, master schedule updates, and on-board software maintenance. The facilities will provide also uplink and verification capabilities
- Monitoring of instrument housekeeping telemetry for certain parameters which affect spacecraft safety and command acceptance and execution verification
- Separation and forwarding of payload telemetry to Science Data Processing Centres
- Checking, reformatting, scheduling command request for payload.

Within the SCOS2000 system, mission specific software will be developed wherever necessary.

10.4 Mission Operations Concept

10.4.1 Overview

The operations support activities for FIRI will be conducted according to the following general concept:

- All operations will be conducted by ESOC according to procedures laid down in the Flight Operations Plan (FOP)

- The FIRI mission operations will be conducted with one shift of spacecraft controllers, with analysts and engineers working nominal hours. Except for the first period after launch (LEOP duration 1 week), where 24 hours operations per day will be conducted
- All FIRI operations will be conducted by uplink of a master schedule of commands for later execution on the spacecraft. This schedule will contain all commands necessary to undertake the spacecraft and instruments operations in a predictable fashion. A limited number of time tagged commands will be used for spacecraft safety operations. The master schedule will be prepared by a Mission Planning System.

10.4.2 Spacecraft Monitoring and Control

The FIRI spacecraft subsystems performance will be monitored in near real time following each used contact period. All housekeeping data, as recorded in the spacecraft memory, will be processed and analysed for exceptional events and trends (e.g. power, temperatures, etc.). The following assumptions have been made:

- Near real time housekeeping telemetry will be processed in the MOC in real time as it arrives from the ground stations
- All playback telemetry is assumed to pass through the on-board memory and to be dumped in the same time sequence in which it has been recorded; HK data shall be available to the operator in real time as it is dumped during the pass
- All real-time TM will be downlinked directly during coverage
- Auxiliary data (attitude and orbit history and derived parameters) will be made available to authorised personnel via the DDS from the MCS
- Data structures will comply with CCSDS recommendations
- Level 1a and 1b processing of science telemetry packets will not be performed at ESOC, but by the Science Teams.

In addition to near real time HK data processing for spacecraft monitoring, standard facilities will be used for long term performance evaluation and HKTM, TC history and system message archiving.

The command activity comprises the following:

- One command queue will be provided in the MOC: for uplink of the master schedule, integrating the instruments and platform commands. In addition there will be a facility for (manual) uplink of real time commands
- Off-line requests for changing science operations will be submitted by the Science Teams as a complete and consistent input to the MPS. The response time to such changes will nominally be TBD
- The MOC will be the only source of commands to the FIRI spacecraft
- The MOC will provide pre-transmission validation and verification of correct command uplink by the ground station, and verification of correct execution of command in the master schedule, using verification TM packets
- A history of all commands submitted for uplink will be available in the MOC (and made available to the Science/Project Teams on the data server).

It will be possible to manipulate the master schedule using the standard PUS services.

10.4.3 Orbit and Attitude Control

Orbit and attitude determination and control will be performed by the team of specialists, which has prepared the related software facilities.

The operational support to be provided by Flight Dynamics to the FIRI mission will consist of the following major items:

- Launch and Early Orbit Phase LEOP support. This will include LEOP set-up and testing, ground station predictions; early orbit assessment; preparation of manoeuvres if necessary; monitoring of attitude acquisition and deployment
- Orbit determination and auxiliary data product generation. A forward propagation of the orbit will be used to obtain antenna pointing information for the ground stations (in the form of Spacecraft Trajectory Data Messages STDM's), and other auxiliary data such as station pass profiles, eclipse times, prediction of maintenance manoeuvre times, input to MPS, etc. Orbit determination will be performed during all mission phases using coherent Doppler tracking data from up to three ground stations (depending on the mission phase). Orbit determination includes tracking data pre-processing, the calibration of all engines and thrusters used for orbit correction and ground controlled attitude manoeuvres that are not pure torques.
- Transfer Orbit manoeuvre optimisation consisting on the preparation and maintenance of high precision orbit prediction software with and without future planned manoeuvres. The complete sequence of manoeuvres from the rocket separation until insertion into the Lissajous orbit will be optimised to minimise propellant consumption and taking into account all operational conditions. Following each manoeuvre, the remaining sequence will be re-optimised on the basis of the current manoeuvre performance.
- Preparation and evaluation of Lissajous orbit maintenance manoeuvres. The time sizes and directions of the orbit maintenance manoeuvres will be optimised to guarantee payload operations for up to 6 years with a minimum of interruption.
- Periodic monitoring of telemetered positions, velocities and attitudes and their rates. This will be largely automated
- Periodic monitoring of sensor outputs (FGS, star tracker, sun sensor, gyros), also largely automated
- Generation of the values of any onboard parameters that need routinely updating onboard, related to attitude and orbit
- The payload pointing will be pre-programmed according to the scanning law
- Manoeuvre monitoring in near real time of all manoeuvres performed in the presence of an Earth communications link. Deviation from expected performance might cause a long manoeuvre to be terminated by ground command
- Calibration of thrusters and sensors by comparing planned and achieved results. The output of the calibration process will be used for planning of subsequent manoeuvres. All sensor data will be calibrated on ground and the related parameters in the on-board attitude system will be updated

Auxiliary data as orbit, attitude, spin rate, manoeuvre histories, will be provided to the scientists. Flight Dynamics data needed for mission planning purposes, such as ground station visibility times, will also be provided by the FD team.

This Page Intentionally Blank

11 TECHNICAL RISK ASSESSMENT

11.1 Risk Approach

The Risk analysis has been performed to identify and assess the main risk issues affecting the development and the future utilization in a flight mission of the FIRI.

The risks for the Project and the risks for the mission were analysed with the aim of identifying and handling the risks which may cause serious cost, schedule, technical and science value impacts on the whole project.

For the Project related Risks, the Severity Categories are provided in Table 11-1.

They have been applied in compliance with the Risk assessment approach used by D-SCI and ranging from the Severity Level n 5 – Maximum to the Severity level n 1 - minimum.

While for the Mission related Risks, 4 Severity Categories have been applied.

- Severity level 4 – Critical = loss of Satellite, loss of capability to perform the scientific mission, Loss of scientific data return.
- Severity level 3 – Major = Major degradation of the system/mission
- Severity level 2 – Significant = Significant reduction of the science data return.
- Severity Level 1 – Minimum = Minimum or negligible impact.

SCORE	Severity	Cost	Programmatics & Schedule	Technical	Science
5	Maximum	Cost increase beyond estimated CaC	The delay compromise the possibility to launch in the cosmic vision time frame	Loss of Space Craft / Loss of Mission	None of top level goals are achieved. No scientific data return
4	Critical	No increase beyond the estimated CaC however contingency margin is lost	Delay >TBD_1 months	Loss of capability to perform the mission	Critical reduction (50-90%) of the science return
3	Major	No increase beyond the estimated CaC however major part of the contingency margin is lost	Delay >TBD_2 months	Major degradation of the system/mission	Major reduction of the science return 20-50%

SCORE	Severity	Cost	Programmatics & Schedule	Technical	Science
2	Significant	No increase on the estimated CaC, however significant part of the contingency margin is lost	Delay >TBD_3 months	Degradation of the system/mission (e.g. is still able to control the consequences)	Significant reduction (10-20%) of the science return
1	Minimum	No increase on the estimated CaC, however contingency margin starts to be used	Minimum consequences	Minimum consequences	Minimum consequences

Table 11-1: Risks for the Project

The Severity Categories have been applied to the FIRI Design and through the analysis of each Subsystem the main Items of the design affected by specific risks for the project and for the mission have been identified.

Ranking of the identified risks and identification of the likelihood associated with their occurrence has then been used to identify the factors that will influence the FIRI project: Facilities, Technologies, Suppliers, Design Maturity, Tests.

11.2 Assumptions and Trade-Offs

The Items of the FIRI Subsystems causing the more significant Project related risks have been identified and the relevant risk reduction actions have been highlighted as shown in Table 11-2

Subsystems	Sev. for Proj.	Sev. for Proj.	Sev. for Proj.	Likeli .of the undes. event	S x L	Proposed Solution	Likelihood after mitigation	S x L	Remark
	5 Max	4 Crit	3 Major						
AOCS - MSRW			3	C/B	3C/B	Technology for MSRW partially qualified for space application.	B	3B	Technology avail in Europe.
Metrology			3	C	3C	Technology from Darwin can provide heritage	B	3B	
Thermal -Cryos	5			E	5E	Cryogenic development/testing and verification to gain the expected confidence level for achieving the results, will require development of dedicated standards.	D	5D	
COMM S. Wireless trans-vr			3	C	4C	The technology is already under development and consolidation.	B	4B	

Subsystems	Sev. for Proj.	Sev. for Proj.	Sev. for Proj.	Likeli .of the undes. event	S x L	Proposed Solution	Likelihood after mitigation	S x L	Remark
	5 Max	4 Crit	3 Major						
Optics	5			D	5D	Ensure right Thermal environment tests in 5K Develop Functional Test Bed and use of the EQM to start test campaign. Develop specific manufacturing approach. Accuracy of manufacturing polishing (for very smooth surface) and integration. -Functional Test Bed. Heritage from other programs: Gaia, Hershel	C	5C	
Detector - Bolometer	5			E	5E	The Bolometer is the Critical item, It has technology issues that can seriously jeopardize the project. Tests at the required low Watt values (10^{-8}-10^{-20}W) are critical Develop dedicated facilities and Far I/R filters	E/D	5E/D	Technology and tests to be developed will need high effort to ensure the Bolometer is qualified for the launch of FIRI. Photoconductor sensors can be a back-up solution
Mechanisms	5			D	4D	Ensure technology availability for precise mechanisms. Ensure right thermal environment tests in 5K Develop very low dissipation mechanisms. Develop testing on lubrication. For sun shields, there will be heritage from Gaia. Select Cryo compatible materials.	C	4C	
Structure -Boom			3	C	3C	Develop Big Test facility or subscale model for the Boom.	B	3B	

Table 11-2: FIRI Items versus Severity for the Project

The same approach has been used to identify the more significant Mission related risks as shown in Table 11-3 and Table 11-4.

Subsystems	Sev for the Mission	Sev for the Mission	Sev for the Mission	Likelih of the undes event	S x L	Proposed Solution	Likelihood after mitigation	S x L	Remarks
	4 Crit	3Maj.	2Sign.						
AOCS		3		C	3C	Redundancy concept will be implemented. Additional issues: vibrations to be evaluated during development	B	3B	
Metrology		3		C	3C	Design to mitigate consequences of failures in the Metrology system and redundancy implementation wherever possible (will depend on design implementation characteristics).	B	3B	Adequate Manufacturing/ Tests processes will be implemented
Thermal - Cryos	4			D	4D	Safe Life and (where feasible) redundancy concept will be implemented.	C	4D	Adequate Manufacturing/ Tests processes will be implemented

Table 11-3: FIRI Items to severity for the mission (a).

Subsystems	Sev for the Mission	Sev for the Mission	Sev for the Mission	Likelih of the undes event	S x L	Proposed Solution	Likelihood after mitigation	S x L	Remarks
Comm Wireless transceivers	4			C	4C	Redundancy concept will be implemented	B	4B	
Optics	4			D	4D	Design for minimum risk will be applied.	C	4C	Adequate Manuf/ Test processes will be performed
Detector	4			D	4D	Redundancy concept will be implemented	C	4C	If photocond. is chosen impact on technical and science results
Mechanisms	4			D	4D	Fail Safe/Safe Life approach. Redundant actuators (e.g. double windings motors) Design to prevent overloads on mechanisms during launch. Proper design/manufacture	C	4C	Adequate Manuf/ Test processes will be implemented.

Subsystems	Sev for the Mission	Sev for the Mission	Sev for the Mission	Likelih of the undes event	S x L	Proposed Solution	Likelihood after mitigation	S x L	Remarks
Structure(Boom)			2	C	2C	Safe Life approach. Adequate testing on Boom.	B	2B	Adequate manufacturing to guarantee stiffness, planarity, flatness Adequate Tests will be performed.

Table 11-4: FIRI Items versus severity for the mission (b).

11.3 Results

The analysis of the data obtained from the two set of tables for Project and Mission Risks leads to the identification of the Risks scenarios and the Risk Mitigation actions that will have to be pursued.

The main factors that will affect the success of the FIRI project are relevant to the following aspects:

Tests as per Table 11-5 and Table 11-6

Manufacturing as per Table 11-7

Technology as per Table 11-7 and Table 11-8

Suppliers as per Table 11-9.

Risk Scenario for Project	Items affected	Item related scenario	Impacted area	SxL	Risk Reduction Actions	SxL after risk red action implementation	Remark
Thermal environment tests at 5K is critical	Optics	Items not still tested at 5K	C & P	5D	Identify specific issues for testing in 5 K env and Develop test procedures and approach for 5K environment.	5C	
Thermal environment tests at 5K is critical	Mechanisms	Items not still tested at 5K	C&P	5D	Identify specific issues for testing in 5 K env and Develop test procedures and approach for 5K environment	5C	
Thermal environment tests at 5K is critical	Cryosystem	Items not still tested at 5K	All	5E		5D	

Table 11-5: Risks associated with thermal environment test

Risk Scenario for Project	Items affected	Item related scenario	Impacted area	SxL	Risk Reduction Actions	SxL after risk red action implementation	Remark
Tests to validate Bolometer technology	Detectors Bolometer	Tests at the required low Watt values (10^{-8}-10^{-20}W) are critical	C/T/S	5E	Develop dedicated Test facilities and Far I/R filters	5E/D	Back-up Photoconductor sensors instead of Bolometers
Test facility non available	Boom	Big Test facility or subscale model for the Boom needs to be developed	C&P	3D	Assess feasibility of Big Test facility w.r.t subscale model for the Boom. Develop one of the two approaches according to the choice selected.	3C	
Tests for lube in mechanism need to be developed	Mechanisms lubrication	Lubrication system and tests to be defined	C&P		Identification of the adequate lubrication system and develop dedicated testing		
Tests to validate the FIRI Technology	All	FIRI has several technologies that are critical to the development and the validation	All	5E	Develop Functional Test Bed and use of the EQMs to start test campaign.	5D	

Table 11-6: Risks associated with other Tests issues

Risk Scenario for Project	Items affected	Item related scenario	Impacted area	SxL	Risk Reduction Actions	SxL after risk red action implementation	Remark
Manuf issues (manuf technology)	Optics Entrance Pupil Mirror	Primary Mirror has size challenging for manufacturing and coating	All	5D	Identify early the potential manufacturer with the required manufacturing technology	5C	The technology is known but due to the size of the optics and the polishing/coating technique has to be properly adapted for FIRI design.. Use Hershel and Gaia heritage.
Technology availability	Mechanisms: -Guiding Rails -Rack +supp.Boom -Field Separator - Int. metr. Alignemt -Pupil Conditioner	Technology availability for precise mechanisms to be developed.	All	5D	Study and develop adequate technology	5C	
Technology	**Cryosystem**	Technology/testing/verification issues	All	5E	Cryogenic development/testing and verification to gain the expected confidence level for achieving the results, will require development of dedicated standards	5D	

Table 11-7: Manufacturing and technology risks

Risk Scenario for Project	Items affected	Item related scenario	Impacted area	SxL	Risk Reduction Actions	SxL after risk red action implementation	Remark
Technology availability	Detector-Bolometer	Bolometers with the required performances are not available	ALL	5E	The technology is critical, the estimated times are: 7 to 8 years to reach TRL4 (single pixel) and additional 5 years to reach TRL5,(instrument) TRL 5 in 2019	5E	Available Bolom. Is at TRL 3. To reach TRL 5, 13 years are needed: i.e. TRL5 will be available in 2019/2020. **Solutions** A very tough schedule for the Bolometer development and test

Risk Scenario for Project	Items affected	Item related scenario	Impacted area	SxL	Risk Reduction Actions	SxL after risk red action implementation	Remark
							campaign or Back-up solution can be to use Photoconductor Sensors.
Technology issues	Comms. – Wireless transceivers	Some technology issues can be met on the wireless implementation	C/S/T	3C	Maintain vigilance on the wireless implementation	3B	
Technology issues	Optics Beam Splitter	Current Mylar technology or equivalent not enough developed	All	4D	Mylar Technology or equivalent to be properly developed and consolidated	4C	

Table 11-8: Technology risks

Risk Scenario for Project	Items affected	Item related scenario	Impacted area	SxL	Risk Reduction Actions	SxL after risk red action implementation	Remark
Single Supplier	Comms	XX Transponder	C&P	3C	Identify early alternative suppliers	3B	
Single Supplier Company ::European -Teldix acquired by Rockwell	AOCS	Magnetic Suspension Reaction Wheels	C&P	3C/B	Technology available in Europe Start contract for MSRW early in the project	3B	Potential future issues as the company has been acquired by Rockwell
Non European Supplier However technology available in Europe	Detector fringe sensor	MCT Detector is from a non European supplier	All	5D	Identify early alternative suppliers	5C	The Fringe sensors will need delta qualification anyway. Available FS are space qualified at 150K the FIRI FS will be required for 40/50K

Table 11-9: Risks associated with Suppliers.

11.4 Risk Estimate, Back-Up Solution

The Cryosystem and the Detectors are the main problematic Items.

The development of dedicated standards will help in mitigating the risks to the project associated with the Cryosystem technology, test and verification issues.

The Detector (Bolometer) is the more critical item, with the available bolometer only at TRL 3. To reach TRL 5 will take13 years, so the expected TRL5 will be available in 2019/2020.

A possible solution is to implement a very tough schedule for the Bolometer development and test campaign, otherwise a back-up solution can be to use Photoconductor Sensors. With photoconductors the performance will be different (as they work in a different range w.r.t. Bolometer) and some technology and qualification issues will have to be taken into account.

The Optics present manufacturing issues, the technology is known but due to the size of the optics and the polishing and coating issues, adequate techniques have to be properly adapted for FIRI design.

It is suggested to use Gaia and Hershel heritage and to identify early in the project the potential manufacturer with the required manufacturing technology.

Mechanisms, the technology for precise and low dissipation mechanisms has to be developed and adequate manufacturing and test processes will need to be implemented. There is also the need to identify the adequate lubrication system and to develop dedicated testing.

FIRI has several technologies that are critical for the development and validation and there will be the need to develop a Functional Test Bed and use the EQMs to start the test campaign.

Additional issues to be considered:

For AOCS, Fringe Sensors, Communication system, the supplier will have to be identified early in the project and the potential risk for single supplier or non-European suppliers taken into account.

The big size of the Boom will require the development of a big test facility or a subscale model for testing it.

Max 5			Optics←-----	*Cryosystem* ←- **Optics** *(Bolometer)* ←-	**Cryosystem** **Detector**
4		*Comm* ← *Wireless* ←	**Comm.** **Wireless** *Mechanisms* ←	**Mechanisms**	
3		*AOCS* ← *Metrology* ← *Structure* ←	**AOCS** **Metrology** **Structure**		
2					
1					
	A Minimum	**B Low**	**C Medium**	**D High**	**E Maximum**

Table 11-10: Summary of risks related to subsystems

Table 11-11 shows Risk Scenarios – test /technology /manufacturing / suppliers and possible decrease of likelihood of risk if corrective actions are taken.

Max 5			Test5K←---- fringe sensor←--	**Test5K** *Test bed*←---. **FRING SENS** *Test5K*←------ *TestTechn Bolom?*<------	**Test Bed** **Test5K cryos.** **TESTechnology Bolom**
4			*Techno./Test*←	**(Technolg.-Test)**	
3		*Techno Issues*←---- *Supplier*←--	*Test facility avail*←---------- Techno Issues **(Supplier)** *Techno Issues*←--	**(Test F. Avail)** **(Techno Issues)**	
2					
1					
	A Minimum	**B Low**	**C Medium**	**D High**	**E Maximum**

Table 11-11: Risk scenarios and decrease in risk if action taken

12 CONCLUSIONS

The study has shown that the technical implementation of the FIRI science objectives results in a mission class compatible with the Ariane5 ECA launcher but incompatible with Soyuz Fregat launcher due to the mass and size of the resulting satellite. As the full lift capacity of the launcher is not used, there are margins for a potential dual mission launch.

The orbit that meets the science needs, the communication requirements and allowable mass with Ariane 5 is a Halo Lissajous orbit around the Lagrangian point L2 at 800 000 km amplitude. The attractive Earth trailing orbit with its advantages to offer an orbit without any propulsion requirement except for the attitude control was rejected because of the low data transfer rate due to its drift with regards to the Earth.

The proposed design includes a Service Module and a Payload Module. The Payload Module includes two boom mounted telescopes and the beam combiner which is located in a Hub, together with their associated structures, thermal control, mechanisms, calibration devices and optics. The Service Module contains the other parts of the HUB, the sun shields and the two booms on which the telescopes are moving.

Trade-offs at systems level (concerning mainly power system, DHS, optics, mechanism, thermal) were performed during the study. Among these trade-offs, choices have been made and the requested technology development (if any) identified and for some cases, potential back-up solutions.

The power system is distributed between the elements; therefore each telescope and the hub have their own power system. Coupled with this, the data handling system is based on wireless systems. This technical solution allows any harness along the booms to be avoided.

Standard deployable booms have been selected with one folding, which fits into the medium fairing of Ariane 5 when stowed. The exact number of hold-down and release mechanism points has not been determined, which might have a mass impact. In case of later needs, the boom could be designed to fold into more parts to fit into a shorter but larger fairing.

An important driver of the mission design is the cryo-environment of the payload needed for the performances. The sorption cooler and the sorption cooler associated with solid H-cooler provide the required 5 K temperature for the optics of the telescopes and of the hub respectively. An ADR module inside the cryo-compartment provides the 50 mK required for the detector. The performances are also highly demanding for the detectors and for the optics.

The design, with the exception of the cost estimate, is compliant with the requirements (see Systems Chapter 5.5) and includes robust margins and allows further optimisation like structure. Further studies shall be done in later phases for the optical design of the beam combiner, fringe tracking system, FPA and tolerancing analysis of the complete optics. The sensitivity of the payload shall be simulated or calculated in order to state the compliance with the requirements. In further design phases, straylight and contamination issues shall be analysed. The calibration strategy shall also be analysed in more detail in order to confirm the generated data rate. The alignment of the optics is another important point to be analysed.

This mission is a very challenging based on development of some important technologies (low thermal dissipation mechanism under cryo environment, detectors with very low NEP, cryo systems and structures, optics). A dedicated document presents the Technology Development

Plan (see CDF-49(C)). The study has shown that a launch in 2024 is feasible and the technologies could be in TRL5 level in 2015 except for the detectors which will reach this level in 2018.

Finally, a stand-alone model has been created to simulate the observation strategy providing to the Customer a tool allowing simulation of observation strategy.

13 REFERENCES

RD[1] Science drivers for FIRI TRS, Technical Note, A. Lyngvi, (IN MISCELLANEOUS)

RD[2] Hechler, M.: GAIA Consolidated Report on Mission Analysis Issue 2.0, GAIA-ESC-RP-0001, ESA/ESOC/OPS/GFA, March 2006

RD[3] Hechler, N., Yañez : Herschel-Planck Consolidated Report on Mission Analysis, PT-MA-RP-0010-OPS-GMA, ESA/ESOC/OPS/GFA, January 2006

RD[4] Hechler, M.:GAIA/FIRST Mission Analysis: Ariane and the Orbits Around L2, Mission Analysis Working Paper 393, ESA/ESOC/OPS/GFA, November 1997

RD[5] Encyclopaedia of Astronomy and Astrophysics, Copyright © Nature Publishing group edition 2001

RD[6] Fourier Transforms in Spectroscopy. J. Kauppinen, J. Partanen, Copyright © 2001 Wiley-VCH Verlag GmbH

RD[7] Introduction to Fourier Optics, Joseph W. Goodman, second edition, Copyright © The McGraw-Hill Companies

RD[8] Specifities of Interferometric Beam Combination Techniques for Direct Imaging, L.Abe, SPIE proceedings vol 5491, Bellingham, New Frontiers in Stellar Interferometry, WA, 2004

RD[9] Double-Fourier spatio-spectral interferometry : combining high spectral and high spatial resolution in the near infrared, J.M. Mariotti, S.T. Ridgway, Astro.&Astrophys., 195, 350-363, 1988

RD[10] Development of Multi-Fourier Transform interferometer: Fundamental, I. S. Ohta, Applied Optics, Vol. 45, Issue 12, pp. 2576-2585 (April 2006)

RD[11] Optical interferometry in astronomy, J. D. Monnier, Report on Progress in Physics, 66, 789-857, 2003

RD[12] Visibility, optical tolerances and error budget, CHARA Technical report, n.2, 15th April 1994

RD[13] Strehl ratio and coherence loss in long baseline interferometry, CHARA Technical Report, No. 6, 15 December 1994,

RD[14] The wide-field imaging interferometry testbed 1 : purpose, testbed design, data and synthesis algorithms, D.Leisawitz, Bradley J. Frey, Douglas B. Leviton, et al., Interferometry in Space, Proceedings of SPIE vol.4852, 2003

RD[15] Visibility retrieval in Michelson wide-field stellar interferometry, I. Montilla, J. Sellos, S.F. Pereira, J.J.M. Braat, Modern Optics, vol.53, No.4, December 2005, pp. 437-460

RD[16] Pupil-plane recombination for a non-monolithic array, J.M. Mariotti, Amplitude and Intensity Spatial Interferometry, Proceedings of SPIE vol.1237, USA-Tucson AZ, 14th February 1990

RD[17] Michelson versus Fizeau type beam combination: Is there a difference? , Michel Faucherre, Bernard Delabre, Philippe Dierickx and Fritz Merkie, Amplitude and Intensity

Spatial Interferometry, Proceedings of SPIE vol.1237, USA-Tucson AZ, 14th February 1990

RD[18] Challenges in optics for Extremeley Large Telescope Instrumentation, P. Spano, F.M. Zerbi, C.J. Norrie, et al., Astron.Nachr, n.88,789-811 (2006)

RD[19] Optical Coating Technology, P.W. Baumeister, SPIE Press, vol. No. PM137, 2004

RD[20] Michelson Stellar Interferometry, W.J.Tango, R.Q.Twiss, Progress in Optics XVII, editor E.Wolf, p.240, 1980

RD[21] Diffraction and Line Shape of Fourier transform spectrometers, J.Genest, P.Tremblay, Applied Optics, vol.42 No.22, August 2003

RD[22] Detection and correction of instrumental line-shape distortions in Fourier spectroscopy, M.Ahro, J.Kauppinen, I.Salomaa, Applied Optics, vol.39 No.33, November 2000

RD[23] Perspective of long baseline optical interferometry, Bulletin of Astronomical Society of India, S.K.Saha, S.Morel, vol.28, 2000

RD[24] The FIRST-SPIRE Spectrometer A novel Imaging FTS for the Sub-Millimeter, Bruce. M. Swinyard, Peter Ade, Matthew J. Griffin, Kjetil Dohlen, Jean-Paul Baluteau, Dominique Pouliquen, Didier Ferand, Pascal Dargent, Guy Michel, Jerome Martignac, Louis Rodriguez, Donald Jennings, Martin Caldwell, Anthony Richards, Peter Hamilton, David Naylor, uv, Optical, and IR Space Telescopes and Instruments, SPIE Proceedings vol.4013, Munich, 27-31 March 2000

RD[25] High-precision early mission narrow-angle science with the Space Interferometry Mission, Stuart Shaklan, Mark H. Milman, Xiaopei Pan, Interferometry in Space, SPIE proceedings, editor M.Shao, Waikoloa, HI, USA, 26 August 2002

RD[26] Overview of SIM Wide Angle Astrometric Calibration Strategies, L. Sievers, R.P. Korechoff, M.H. Milman, et al., Interferometry in Space, SPIE proceedings, editor M.Shao, Waikoloa, HI, USA, 26 August 2002

RD[27] Cyrogenical optical performance of the ASTRO-F SiC telescope, H.Kaneda, T.Onaka, T.Nakagawa, K.Enya, H.Murakami, R.Yamashiro, T.Ezaki, Y.Numao, Y.Sugiyama, Applied Optics, vol.44 No.32, 10 November 2005

RD[28] Optical aperture synthesis A comparison of techniques for wide-field interferometric imaging, Casper van der Avoort, PhD thesis, University of Delft, May 9th 2006, http://www.library.tudelft.nl/dissertations

RD[29] The Space Infrared Interferometric Telescope (SPIRIT): mission study results, David Leisawitz, Charles Baker, Amy Barger, Dominic Benford, et al., Space Telescopes and Instrumentation I: Optical, Infrared, and Millimeter, Proceedings of SPIE, vol.6265, USA-Orlando FL, 24th May 2006

RD[30] Offset-Parabolic Antennas : A review, A.W.Rudge, N.A.Adatia, Proceedings of the IEEE, vol.66, n.12, December 1978

RD[31] "*Sensitivity Calculations for FIRI*", Technical Note, SCI-A/2006.108/AL, A. Lyngvi, Issue 1, 11 May 2006

RD[32] "*Detector Needs for Long Wavelength Astrophysics*", A Report by the Infrared, Submillimeter, and Millimeter Detector Working Group, June 2002, Edited by E. Young, http://www.sofia.usra.edu/det_workshop/report/ISMDWG_final.pdf, (accessed September 4, 2006)

RD[33] "*ESPRIT base line design document* ", SRON-G/ESPRIT/BD/2005-002, Issue 1, prepared by F. P. Helmich, W. Wild, H. J. van Langevelde, et al., 18 April 2005

RD[34] "*Direct Detectors for FIR/submm Light: Overview of Existing & Emerging Concepts*", A. Poglitsch, IR Group Science Retreat, Ringberg, Nov 2002, http://www.mpe-garching.mpg.de/ir/irretreat2005/poglitsch.pdf#search=%22Direct%20Detectors%20for%20FIR%2Fsubmm%20Light%3A%22 (accessed September4, 2006)

RD[35] "*Superconducting Detectors and Mixers for Millimeter and Submillimeter Astrophysics*", J. Zmuidzinas & P. L. Richards, Proc. IEEE, Vol. 92, No. 10, p. 1517, Oct. 2004.

RD[36] "*Report on Trends in FIR/submm Detector Technology*", TOS-EEO/2002.36/BL/BL, B. Leone, Issue 1, 14 May 2002

RD[37] "*The Photoconductor Array Camera & Spectrometer (PACS)for the Far Infrared and Submillimetre Telescope (FIRST)*", A. Poglitsch, C. Waelkens, and N. Geis, Proc. SPIE 4013, 221 (2000)

RD[38] "*Herschel PhotodetectorPhotodetectorArray Camera & SpectrometerArray Camera & Spectrometer*", A. Poglitsch, http://www.rssd.esa.int/herschel/Publ/2006/AAS207_PACS_science.pdf#search=%22Herschel%20Photodetector%20Array%20Camera%20%26%20Spectrometer%22 (accessed September 18, 2006)

RD[39] "*Investigation and Development of Imaging Radiometers using Superconducting Transition Edge Sensor Arrays for Ground and Space Sub-millimeter Telescopes*", A. N. Vystavkin, Presentation to ESA, Noordwijk, May 2005

RD[40] "*Arrays of TES Direct Detectors for Supersensitive Imaging Radiometers of 1.0 – 0.2 mm Waveband Region*", A. N. Vystavkin, S. V. Shitov, A. G. Kovalenko, et al., WOLTE-7 Proceedings WPP 264, Noordwijk, 21 – 23 June 2006

RD[41] "*SCUBA-2 arrays to system interfaces*", W. Duncan, *et al.*, Nuclear Instruments and Methods in Physics Research A 520 (2004) 427–430

RD[42] "*SCUBA-2, A Submillimetre Bolometer Array Camera for the JCMT*", A Status Review for the Long Range Plan Mid-Term Review Panel, Mike Fich, University of Waterloo, http://www.casca.ca/lrp/SCUBA2_LRPMTR.pdf#search=%22SCUBA-2%20a%20submillimetre%20bolometer%20array%20camera%20for%20the%20JCMT%22 (accessed September 18, 2006)

RD[43] "*The EBEX Experiment*", P. Oxley, P. Ade, C. Baccigalupi, et al, arXiv:astro-ph/0501111 v1 6 Jan 2005

RD[44] "*Open-loop Frequency Division Multiplexing (FDM) scheme for low impedance detectors using SQUID amplifiers that allows long cryogenic cable harnesses suitable for space applications*", P. Mauskopf, WOLTE-7 Presentation, Noordwijk, 23 June 2006

RD[45] "*Far Infrared/ Submillimeter Imager-Polarimeter Using Distributed Antenna-Coupled Transition Edge Sensors*", P. K. Day, *et al*., Millimeter and Submillimeter Detectors for Astronomy II, edited by Jonas Zmuidzinas, Wayne S. Holland, Stafford Withington, Proceedings of SPIE Vol. 5498 (SPIE, Bellingham, WA, 2004)

RD[46] "*Voltage-Biased TES Bolometers for the Far-Infrared to Millmeter Wavelegth Range*", A. T. Lee, S. Cho, J. Gildemeister, et al., http://www.sofia.usra.edu/det_workshop/papers/session5/5-04lee_edjw020717.pdf#search=%22VOLTAGE-BIASED%20TES%20BOLOMETERS%20FOR%20THE%20FARINFRARED%22 (accessed September 18, 2006)

RD[47] "*NbN Hot Electron Bolometer Mixers with Superior Performance for Space Applications*", J. R. Gao, *et al.*, Proc. WOLTE-6, June 2004

RD[48] "*Cold-Electron Nanobolometer. Cascade Quasiparticle Amplifier*", L. Kuzmin, Cardiff Meeting, Cardiff, 2003

RD[49] "*Hot Electron Bolometer Multipixel Heterodyne Receiver*", ESA Contract16940, Technical Note 2, "*Feasibility of Individual Technical Components*", March 2006

RD[50] "*Fabrication of large NbSi bolometer arrays for CMB applications*", M. Ukibe, B. Belier, Ph. Camus, C. Dobrea, et al., http://crtbt.grenoble.cnrs.fr/astro/publications/LTD11_FabMatrix_preprint.pdf#search=%22Fabrication%20of%20large%20NbSi%20bolometer%20arrays%20for%20CMB%20applications%22 (accessed September 18, 2006)

RD[51] "*Fabrication of prototype imaging arrays for SCUBA-2*", G. C. Hilton, *et al.*, Preprint submitted to Elsevier Science, October 2005

RD[52] "*Frequency-Domain-Multiplexed Read-Out of EURECA*", J. van der Kuur, WOLTE-7 Proceedings WPP 264, Noordwijk, 21 – 23 June 2006

RD[53] "*Conceptual Design Study for an Imaging Far Infrared Spectrometer for SPICA*", Study Report April 2005, Edited by B. Swinyard, http://www.mpe-garching.mpg.de/ir/irretreat2005/ESI.pdf#search=%22Conceptual%20Design%20Study%20for%20an%20Imaging%20Far%20Infrared%20Spectrometer%20for%20SPICA%22 (accessed September 4, 2006)

RD[54] A waveguide-coupled millimetre-wave TES bolometer suitable for 2-D arrays, Angiola Orlando, Marcel P. Bruijn, Henk F.C. Hoevers, et al., Nuclear Instruments and Methods in Physics Research A 559 (2006) 534–535

RD[55] Background-limited membrane-isolated TES bolometers for far-IR/submillimeter direct-detection spectroscopy, M. Kenyon, P.K. Day, C.M. Bradford, J.J. Bock, H.G. Leduc, Nuclear Instruments and Methods in Physics Research A 559 (2006) 456–458

RD[56] http://www.esa.int/esaHS/ESAQEI0VMOC_iss_0.html

RD[57] http://www.nasa.gov/mission_pages/station/structure/elements/subsystems.html

RD[58] International space station robotic systems operations – a human factors perspective
Nancy J. Currie, NASA – Johnson Space Center, Houston, Texas
Brian Peacock, National Space Biomedical Research Institute, Houston, Texas

RD[59] http://www.space.gc.ca/asc/eng/missions/sts-111/mobile_backgrounder.asp
http://www.nasa.gov/mission_pages/station/structure/elements/mss.html

RD[60] The Extendable and Retractable Mast (ERM)
M. Schmid (Dornier System GmbH), M. Aguire (ESA/ESTEC)

RD[61] Family of deployable / retractable structures for space application
J. Unda; J. Weisz; J. Rivacoba; I. Ruiz Urien Sener

RD[62] Large Deployable Reflector Study
Presentation of system activities and arm component development
G.Lorenzo Scialino(1), P. Pellegrino(1), V. Lubrano (1) ,A. Cherniavsky (2), M. Domingo Oslé(3) , A. Neukom (4), S.Oschkera (5), E.Gabellini(6) , Jan Michel Lautier (7) , Paul Hodgetts (8) , J.Santiago-Prowald (7)
(1) ALENIA SPAZIO, (2) NPO EGS, (3) SENER, (4) HTS, (5) MAGNA STEYR,(6) SAMTECH, (7) ESTEC, Noordwijk, Holland, (8) AOES/ESA

RD[63] Double Linear Scanning Mechanism for MIPAS interferometer
Robert Birmer, Ralf Maurer. Dornier Satellitensysteme GmbH

RD[64] MIPAS – An Envisat Instrument for Atmospheric Chemistry and Climate Research
M. Endemann, P. Garé, J. Langen, H. Nett & C.J. Readings
ESA Directorate for Applications Programmes, ESTEC, Noordwijk, The Netherlands

RD[65] Hexapod / SAGE III roller screws lifetime and lubrication tests
Piero Pochettino*, Marino Ballesio*, Daniele Gallieni**, Steve Gill***
* ALENIA AEROSPAZIO – Space Division; ** ADS International s.r.l.; *** AEA Technology / ESTL

RD[66] SPIRE Design Description
Douglas Griffin ; Matt Griffin ; Bruce Swinyard

RD[67] Cryogenic Scan Mirror Mechanism. Cryogenic Scan Mirror Mechanism for SIRTF/MIPS
Robert M. Warden and Gerald B. Heim

RD[68] The SPIRE Beam Steering Mirror: a cryogenic 2 axis mechanism for the Herschel Space Observatory. I.Paina, B.Stobie, G.S.Wright, T.A.Paul, C.R.Cunningham
UK Astronomy Technology Centre, Royal Observatory Edinburgh, Edinburgh, EH9 3HJ.

RD[69] The Development of a Cryogenic Optical Delay Line for DARWIN
T. C. van den Dool, F. Kamphues, B.C. Braam
TNO Science & Industry, Stieltjesweg 1, 2628 CK, Delft, The Netherlands

RD[70] Voice-coil actuators in space.N. Wavre & ThouveninETEL SA, Motiers, Switzerland

RD[71] Cryogenic Delay Line for Long-Baseline Interferometry in the Far-Infrared
P.R. Lawson, M.R. Swain, P.J. Dumont, J.D. Moore, and R.F. Smythe
Jet Propulsion Laboratory

RD[72] Robotic calibration issues Accuracy, repeatability and calibration
Kevin L. Conrad, Panayiotis S. Shiakolas shiakolas@uta.edu, T. C. Yih

RD[73] Arm hinge deployment and blocking mechanism for large deployable reflector antenna
Stefan Oschkera
MAGNA STEYR

RD[74] Leon 2 IP Core Document, http://microelectronics.esa.int/core/corepage.html

RD[75] Data sheet of PSI tank 80451-1, http://www.psi-pci.com/Data_Sheets_Library/DS451.pdf

RD[76] Data for EADS 10 N Hydrazine thruster, http://cs.space.eads.net/sp/SpacecraftPropulsion/MonopropellantThrusters.html#ModelCHT10

RD[77] Future Power Systems, Terma A/S, J. Laursen, H. Jensen, ESTEC Presentation 19th Sept 2003

RD[78] Space Environment Information System (SPENVIS), http://www.spenvis.oma.be/

RD[79] ECSS-E-50-05A, Radio Frequency And Modulation Standard, published 24 Jan 2003

RD[80] CCSDS 101.0-B-6. Telemetry Channel Coding Standard. Blue Book. Issue 6. October 2002.

RD[81] PSS-04-104, Ranging Standard, March 1991

RD[82] CCSDS 102.0-B-5. Packet Telemetry Standard. Blue Book. Issue 5. November 2000.

RD[83] CCSDS 201.0-B-3. Telecommand Part 1—Channel Service. Blue Book. Issue 3. June 2000.

RD[84] CCSDS 202.1-B-2. Telecommand Part 2.1—Command Operation Procedures. Blue Book. Issue 2. June 2001.

RD[85] CCSDS 203.0-B-2. Telecommand Part 3—Data Management Service. Blue Book. Issue 2. June 2001.

RD[86] ECSS-E-70-41A, Telemetry And Telecommand Packet Utilization, published 30 January 2003

RD[87] CCSDS 211.0-B-2. Proximity-1 Space Link Protocol—Data Link Layer. Blue Book. Issue 2. April 2003

RD[88] CCSDS 211.1-B-1. Proximity-1 Space Link Protocol—Physical Layer. Blue Book. Issue 1. April 2003

RD[89] CCSDS 211.2-B-1. Proximity-1 Space Link Protocol—Coding and Synchronization Sublayer. Blue Book. Issue 1. April 2003.

RD[90] FIRI Mission Concept – Memo by A. Lyngvi dated March 2 2006..

RD[91] GAIA Mission Assumptions Document, GAIA-GS-1001-OPS-OSA, J.L. Pellón-Bailón, Issue 2.0, February 2005.

RD[92] FIRI Internal Final Presentations, CDF Team, Drafts, June 2006.

14 ACRONYMS

Acronym	Definition
ADB	Antenna Deployment and Blocking Mechanism
ADRM	Antenna Deployment and Release Mechanism
ADR	Adiabatic Demagnetisation Refrigerator
AHD	Antenna Hold Down and Release Mechanism
AOCS	Attitude and Orbit Control System
APE	Actual Pointing Error
Arcmin	Arc minute. 1 arcmin = 1/60 degrees
Arcsec	Arc second. 1 arcsecond = 1/60 arcmin = 1/3600 degrees
AsGa	Gallium Arsenide
ASM	Attached Synchronisation Marker
AU	Astronomical Unit
AWG	Astronomy Working Group
AWG	American Wire Gauge
BC	Beam Combiner
BCR	Battery Charge Regulator
BDR	Battery Discharge Regulator
BER	Bit Error Rate
BIB	Blocked Impurity Band
CC	Concave
CCSDS	Consultative Committee for Space Data Systems
CDF	Concurrent Design Facility
CEB	Cebreros Ground Station
CEB	Cold Electron Bolometer
CHT	Catalytic Hydrazine Thrusters
CoM	Centere of mass
CORTEX	Command Ranging and Telemetry Unit
CPDU	Command Pulse Distribution Unit
CVP	Commissioning and Verification Phase
CX	Convex

Acronym	Definition
DC	Direct Current
DCR	Dedicated Control Room
DDS	Data Distribution System
DMM	Design Maturity Margin
DoD	Depth Of Discharge
DoF	Degree of Freedom
DSA	Deep Space Antenna
DSM	Deep Space Manoeuvre
DSN	Deep Space Network
ECA	Etage Cryogénique A
ECSS	European Cooperation for Space Standardization
EIRP	Effective isotropically-radiated power
EOL	End Of Life
EPE	External Project Environment
EPS	Electrical Power System
ERA	European Robotic Arm
ESA	European Space Agency
ESOC	European Space Operations Centre
ESTRACK	ESA Tracking Stations Network
EU	European Union
FCT	Flight Control Team
FD/FDS	Flight Dynamics/Flight Dynamics System
FDM	Frequency Domain Multiplexing
FDR	Flight Dynamics Room
FER	Frame Error Rate
FFT	Fast Fourrier Transforms
FGS	Fine Guidance Sensor
FIR	Far Infra-Red
FIRI	Far InfraRed Interferometer
FOP	Flight Operation Plan
FPA	Focal Plane Array

Acronym	Definition
FPA	Fine Pointing Assembly
FSU	Fringe Sensor Unit
FTS	Fourier Transform Spectrometer
G/S	Ground Station
GMSK	Gaussian Minimum Shift Keying
GNC	Guidance, navigation, and control
GTO	Geostationary Transfer Orbit
H/W	Hardware
H2	Hydrogen
HDRM	Hold Down and Release Mechanism
He	Helium
HEB	Hot Electron Bolometer (mixer)
HEO	Highly Eccentric Orbit
HGA	High Gain Antenna
HK	House keeping data
HKTM	House keeping Telemetry
ICU	Interferometer Controller Unit
IFMS	Intermediate Frequency and Modem System
IFOV	Interferometric Field Of View
ILS	Instrument Line Shape
IPPM	Integrated Payload Processing Module
IR	Infrared
ISL	Inter-satellite link
ISO	Infrared Space Observatory
ISS	International Space Station
ITD	Inter-Telescope Distance
JPL	NASA Jet Propulsion Laboratory
JT	Joule Thompson
JWST	James Web Space Telescope
KID	Kinetic Inductance Detector
L2	Second Lagrangian Equilibrium Point (Sun-Earth System)

Acronym	Definition
LAN	Local Area Network
LCT	Light Collecting Telescopes
LDA	Large Deployable Antenna
LEO	Low Earth Orbit
LEOP	Launch and Early Orbit Phase
LGA	Low Gain Antenna
Mbps	Mega bits per second
MCR	Main Control Room
MCS	Mission Control System
MGA	Medium Gain Antenna
MIPAS	Michelson Interferometer for Passive Atmospheric Sounding
MJ	Multi Junctions
MLI	Multi Layer Insulation
MM	Mass Memory
MOC	Mission Operations Centre
MPS	Mission Planning Centre
MPTS	Multipurpose Tracking System
NASA	National Aeronautics and Space Administration
NEP	Noise Equivalent Power
NER	Noise Equivalent Radiance
NNO	New Norcia Ground Station
NRT	Near Real Time
NSSDC	National Space Science Data Centre
OBC	On-Board Computer
OBSM	On-Board Software Maintenance
OBT	On-Board Time
ODL	Optical Delay Line
OPD	Optical Path Difference
OPSNET	Operational Network
PACS	Photoconductor Array Camera and Spectrometer
PCU	Power Conditioning Unit

Acronym	Definition
PDU	Power Distribution Unit
PLM	Payload Module
PSR	Project Support Room
PUS	Packet Utilisation Standard
PV	Photovoltaic
RD	Reference Document
RFDU	Radio Frequency Distribution Unit
RM	Reconfiguration Module
RMS	Root Mean Square
RW	Reaction wheel
S/C	Spacecraft
S/W	Software
S4R	Sequential switching & serial shunt regulator
SA	Solar Array
SADM	Solar Array Drive Mechanism
SCOS	Spacecraft Control System
SED	Single Event Detection / Definition
SGM	Safe Guard Memory
SIM	Space Interferometry Mission
SIS	Superconductor-Insulator-Superconductor (junction mixer)
SNR	Signal to Noise Ratio
SPACON	SPAcecraft CONtroller
SPENVIS	SPace ENVironment Information System
SPIRE	Spectral and Photometric Imaging Receiver
SPT	South Pole Telescope
SQUID	Superconducting Quantum Interference Device
SRP	Solar radiation pressure
SRRC-OQPSK	Square-Root Raised Cosine Offset Quadrature Phase Shift Keying
SSEA	Sun-Spacecraft-Earth Angle
SSPA	Solid State Power Amplifier
STDM	Spacecraft Trajectory Data Messages

Acronym	Definition
STJ SQPC	Superconducting Tunnel Junction Single Quasiparticle Photon Counter
SVM	Service Module
TBC	To Be Confirmed
TBD	To Be Defined
TC	Telecommand
TDM	Time Domain Multiplexing
TDP	Technology Development Plan
TES	Transition Edge Sensor
TJ	Triple Junction
TM	Telemetry
TRL	Technology Readiness Level
TRS	Technology Reference Study
TT&C	Tracking, Telemetry and Command
TWTA	Travelling Wave Tube Amplifier
US	United States
VDA	Vapour Deposited Aluminium
VIS	Visible spectrum
WAN	Wide Area Network
WFE	Wave Front Error
WB	Workbook
WSB	Weak Stability Boundary
XEUS	X-Ray Evolving Universe Spectrometer